J. Condensed Matter Nucl. Sci. 12 (2013) 1–12

Research Article

How the Flawed Journal Review Process Impedes Paradigm Shifting Discoveries

P.A. Mosier-Boss *

Research Laboratory of Electronics, Massachusetts Institute of Technology, Cambridge, MA 02139, USA

L.P. Forsley †

JWK International Corporation, Annandale, VA 22003, USA

F.E. Gordon ‡

Research and Applied Sciences Department, US Navy SPAWAR Systems Center Pacific, Retired, San Diego, CA 92152, USA

Abstract

The purpose of scientific journals is to review papers for scientific validity and to disseminate new theoretical and experimental results. This requires that the editors and reviewers be impartial. Our attempt to publish novel experimental results in a renowned physics journal shows that in some cases editors and reviewers are not impartial; they are biased and closed-minded. Although our subject matter was technical, its rejection was not: it was emotionally charged. It was an agenda-laden rejection of legitimate experiments that were conducted in US DoD and DoE laboratories. This paper describes the flawed journal review process, detailing our own case and citing others. Such behavior on the part of editors and reviewers has a stifling effect on innovation and the diffusion of knowledge.
 ISSN 2227-3123

Keywords: Discovery, Flawed journal review, Nuclear diagnostics, Review process, Scientific breakthrough, Scientific policy

1. Introduction

In 1989, Drs. Martin Fleischmann and Stanley Pons published a peer-reviewed claim that their palladium/deuterium (Pd/D) electrochemical cells were generating more excess heat than could be accounted for by conventional chemistry. [1] Over the ensuing years, researchers accumulated additional evidence that nuclear processes occur within metal

*E-mail: pboss@san.rr.com
†Research Associate, Nuclear Engineering Teaching Laboratory University of Texas, Austin, TX 78712. USA.
‡Head, Research and Applied Sciences Department

 ISSN 2227-3123

lattices. Successful replications of these novel "Low Energy Nuclear Reaction" (LENR) results have been published in several peer-reviewed journals.

However, potential government sponsors have stated that these peer-reviewed publications are meaningless because the research was not published in either Nature or Science, as if these two were the only legitimate arbiters of scientific truth. Those journals are considered to be prestigious because of their high impact factors[a] of 36.280 for Nature [2] and 31.201 for Science [3] in 2011 [4]. By comparison, the Journal of the American Chemical Society, the flagship of the world's largest scientific society which has published successful cold fusion replications, had an impact factor of 9.907 in 2011 [5]. Replications have also been published in prestigious overseas journals such as the Japanese J. Applied Physics. This is published by the Japanese Applied Physics Society, and it is thus roughly equivalent to Science, published by the AAAS. We, and others, have attempted to publish papers in Nature, but our submissions were returned with the admonishment, "This subject area is of no interest to our readers." In fact, Nature has published a number of papers on experiments that failed to replicate the Fleischmann–Pons results, such as the one written by Lewis et al. [6], as well as negative commentaries on the field [7,8]. In light of criticisms of not having published our results in higher-tiered journals, we attempted to publish a LENR-based paper in a higher-tier physics journal. In this communication, we document and discuss the outcome of our experience as a case study to illustrate the larger problem.

Unfortunately, the problem of publishing controversial papers is hardly a new phenomenon. In their book entitled *Responsible Conduct of Research,* Shamoo and Resnick [9] stated:

> *History provides us with many examples of important theories that were resisted and ridiculed by [reviewers of] established researchers, such as Gregory Mendel's laws of inheritance, Barbara McLintock's gene jumping hypothesis, Peter Mitchell's chemiosmostic theory, and Alfred Wegener's continental drift hypothesis.*

Campanario [10] documented instances where 24 scientists encountered resistance by scientific journal editors or referees when they tried to publish manuscripts on discoveries that later earned them the Nobel Prize. Recently, Nature published an editorial on the subject of peer rejection [11]. Nature acknowledged that they had rejected papers on Cerenkov radiation; Hideki Yukawa's meson; the work on photosynthesis by Johann Deisenhofer, Robert Huber and Hartmut Michel; and the initial rejection (but eventual acceptance) of Stephen Hawking's black-hole radiation. The editorial concluded:

> *… rejected authors who are convinced of the groundbreaking value of their controversial conclusions should persist. A final rejection on the grounds of questionable significance may mean that one journal has closed its door on you, but that is no reason to be cowed into silence. Remember, as you seek a different home for your work, that you are in wonderful company.*

2. Our Rejection Experience

The journal wherein we submitted our observations publishes short, important papers from all branches of physics. Although its impact factor was 7.37 in 2011, it is considered to be among the most prestigious publications in any scientific discipline. In December 2009, we submitted a paper *comparing* fast neutron-induced triple tracks in a Solid State Nuclear Track Detector (CR-39) that we observed as a result of our LENR experiments with those generated by a DT fusion generator. Previously, we had published a paper in a "lower-tier" journal, *Naturwissenschaften* [12] discussing our first observation of energetic neutrons in a deuterated palladium lattice (Pd/D), in addition to three other papers using CR-39 to detect energetic particles [13–15].

[a]The impact factor of a journal is a measure of the frequency with which the "average article" in a journal has been cited in a particular year or period.

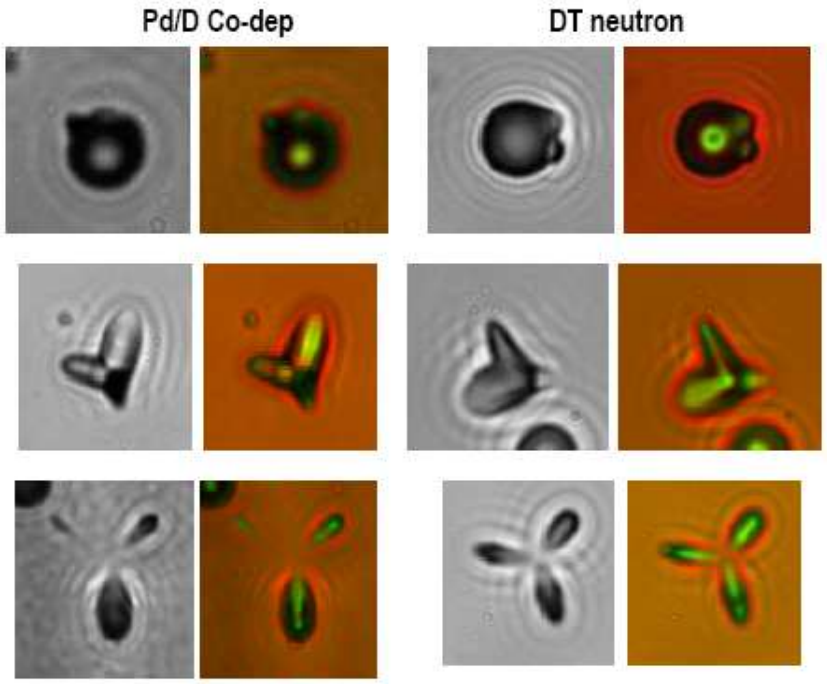

Figure 1. Comparison of DT fusion induced tracks. Palladium deuterium co-deposition tracks are in the two left columns and DoE accelerator driven DT fusion neutron generator tracks are in the right two columns. The black and white pictures are CR-39 microphotographs. The false color photographs are a composite of two microphotographs, one focused at the bottom of the track with one focused on the surface. This allows both the extent of the track and its "origin" to be more clearly observed. Triple tracks are caused by a nearly 10 MeV neutron striking a carbon atom in the CR-39, shattering it into three energetic alpha particles that create an ionization trail in the CR-39. The CR-39 is etched for several hours, enlarging the trail until it is visible with a microscope as a track. *If you cannot tell the difference, there is no difference.*

2.1. Our claim: solid-state nuclear track detector — CR-39 and neutron detection

Our submission described our experiments with CR-39 neutron detection. CR-39 is a solid-state nuclear track detector (SSNTD) that is commonly used to detect neutrons and charged particles in inertial confinement fusion (ICF) *aka* "laser fusion" [16]. When an energetic, charged particle traverses a solid-state nuclear track detector it creates an ionization track [17,18]. When the detector is etched, the tracks are enlarged until they are visible with the aid of a microscope. However, neutrons only leave tracks under certain conditions. The neutron must either elastically scatter off or undergo an inelastic nuclear reaction with, the hydrogen, carbon, or oxygen atoms within the CR-39 [19].

The most easily identified neutron interaction is a "triple track" that occurs when a neutron with over 9.6 MeV shatters a carbon atom in the detector resulting in a three pronged star [19–23]. Figure 1 shows representative triple tracks observed in CR-39 detectors that were used in Pd/D co-deposition experiments as well as their corresponding accelerator-driven DT fusion neutron generated triple track. The tracks are clearly indistinguishable.

2.2. The reviews

When the paper was first internally reviewed by the Journal, we were told that the paper was too long and that we needed to shorten it. However, we could include additional material in an electronic supplement. We complied with this request and resubmitted the paper along with the names of three potential referees, one of whom was a CR-39 expert.

2.2.1. *Reviewer A*

Our paper was rejected in February 2010 after being reviewed by three referees. The editor commented:

> *Referee A sent but a short report of no value to either of us. He or she did go over your manuscript and offered emendations in electronic form. We enclosed the marked manuscript in case it will be of use to you elsewhere.*

The emendations made by the referee clearly showed that he/she was knowledgeable on the use of CR-39 and interpreting the tracks. We had discussed the origins of asymmetric triple tracks, suggesting,

> *They could also be due to reactions of the type* $^{12}C(n,\alpha)^{9}Be$ *or* $^{16}O(n,\ \alpha)^{13}C$*. The track caused by these reactions typically has one prong with a larger cone angle than the other which are attributed to the alpha particle and the recoiling residual nucleus, respectively.*

To this Referee A commented,

> *This is due to the fact that cone angle decreases with increasing ionization rate. The* ^{9}Be *recoil has a higher ionization rate and thus a smaller cone angle.*

We asked the Journal's editor if we could have Referee A's comments. The editor steadfastly refused to send them to us. It is unheard of for editors to deny referee's comments to authors. In contrast, this editor had no qualms sending us the reports of the other two referees.

2.2.2. *Reviewer B: Authors should be glad they're not dead*

Referee B's report stated:

> *The authors claim to produce a source that emits approximately a few Hz, perhaps 10 Hz, 14 MeV DT neutrons. This is a formidable source. The rate of 2.5 MeV DD neutron source should be considerably (many order of magnitudes) stronger. Such a strong source of 2.5 and 14 MeV neutrons should be easily detectable with live electronical [sic] neutron detector. The fact that the authors did not make an attempt to measure these neutrons with the more reliable neutron detectors speaks volume of the less than adequate research effort.*
>
> *The authors are the best living evidence that this high intensity neutron source did not exist. We note from the outset that a full body neutron dose of 500 REM (5 Sv) will cause severe radiation sickness. A slightly larger dose will cause death within a few weeks. Such a full body dose is produced by* 10^{10} *2.5 MeV DD neutrons or* 2×10^{9} *14 MeV DT neutrons.*
>
> *The authors reported a "DT fusion flux of 1.25–2.5 n/cm*^{2}*/s" which leads to a full body dose of* 2×10^{7} *secondary DT neutrons per hour. The flux of the primary DD fusion will thus be many orders of magnitude above and beyond the lethal dose. A person spending one hour (in fact considerably less than one hour) in the vicinity of the apparatus will suffer severe radiation sickness and will die shortly afterward.*

The author should be thankful for not discovering DT fusion and in any case there is no place for such a low quality research in the pages of …[this Journal]… or for that matter in any scientific publication that adheres to a minimum standard of quality.

2.2.2.1 Our response to Reviewer B: No lethal neutron flux reported

The Journal did not give us the opportunity to refute the comments made by reviewer B. We will take that opportunity now. Reviewer B erroneously states the DD fusion rate should be many orders of magnitude greater than the DT fusion rate. In fact, the fusion cross-section over a wide variety of ion energies is 100 times greater for DT fusion than DD fusion [16]. The referee advocated the 'dead graduate student' argument first publicized by John Huizenga [24], the head of the 1989 ERAB panel charged with investigating cold fusion claims. In the submitted paper we measured the integrated DT neutron flux as 1.25–2.5 n/cm^2/s. The CR-39 detectors are 4 cm^2 in area. So the total number of neutrons per hour, at most, is 3.6×10^4 and not 2×10^7, as the referee stated. It is not clear how the referee calculated over 500 times our reported value.

An integrated neutron radiation dose of 6 Gy is considered lethal [25]. This is equivalent to 6000 REM.[b] For neutrons with energies between 10 and 30 MeV, the integrated number of neutrons per square centimeter equivalent to a dose of 1 REM is 1.4×10^7 n/cm^2 [26]. For the entire Pd/D co-deposition experiment (typically two weeks), the total number of neutrons per square centimeter is 3.024×10^6 n/cm^2. This is equivalent to a total dose of 0.216 REM, which is far below the lethal limit for neutron exposure. Even if we use the referee's erroneous value of 2×10^7 n/cm^2/hr, a neutron dose over a two-week period of 480 REM is still far below the lethal limit of 6000 REM.

2.2.3. *Reviewer C*

Referee C commented:

The authors report the observation of "triple tracks" in a relatively new type of detector material, which is claimed to be proof for DT fusion events within the material.

At some points in the paper it becomes clear that the observed tracks in the detectors are "indicative" or "consistent with" DT fusion reactions. Such phrases, along with controversy discussions about the method that can be found in literature, make clear that the used method is far from being a solid proof for such reactions. They try to argue with heaps of supplementary material does not replace the need to establish the new method in peer-refereed journals. On the other hand, I am wondering why particles, be it alphas or neutrons, cannot be detected with conventional, well established, detection methods, at least in order to show the applicability of the new detection method relative to something else. In the end, I am not convinced that the observed "tracks" or "bubbles" are a unique signature of 3 alpha breakup of ^{12}C, such as claimed by the authors.

All these are technical details, (which the general …[this Journal]… reader will have no chance to comprehend from the present manuscript,) whereas the biggest question to this paper is what the reader is supposed to conclude from it. Multiple times the authors assume the source for the claimed detected neutrons to be DT fusion. However, quite artificially, the source for this DT fusion is left open until the conclusion. Even there,

[b]A gray (Gy) is a unit of absorbed dose, specific energy (imparted) and of kerma. One Gy is equivalent to 100 RAD (Radiation Absorbed Dose). REM is damage produced by 1 RAD in body tissue where REM = $Q \times$ RAD. Q is the quality factor which accounts for the difference in the amount of biological damage caused by the different types of radiation. For gamma and beta radiation, 1 RAD = 1 REM. For neutrons, 1 RAD = 10 REM.

one finds speaking of "hot" fusion DD reactions - without mention what hot means. Presumably, it means the energy necessary to actually fuse to deuterium nuclei. Unfortunately, the authors do not give any hint where this necessary energy would come from.

It is quite simple: in order to get fusion you have to overcome a Coulomb barrier. The authors themselves admit in the conclusion that the mechanism for the DD reaction is "not yet fully understood". Not surprising, since nothing I read explains where the necessary energy would come from. Instead, even more reactions are mentioned in the end (Oppenheimer-Phillips stripping) which now shall account for the observed tracks - without explanation. After that some mentioning of oscillations of atoms within the material, again with absolutely no firm connection to the observations. I am left with the impression that nobody has a clue where the energetic tritons (intermediate reaction products) would come from.

2.2.3.1 Our Response to Reviewer C: CR-39 was the appropriate method

Again the Journal did not give us the opportunity to refute the comments made by reviewer C. We will take that opportunity now. CR-39 is not a new detector material. Cartwright et al [17] were the first to demonstrate that CR-39 could be used to detect nuclear particles in 1978. There are hundreds of papers in the literature describing the use and development of CR-39 for neutron dosimetry. Countries involved in this research include Italy [27], Egypt [28,29], India [30], Japan [31], Hungary [20] , as well as the United States [16,17,19,32]. Landauer uses CR-39 in their Neutrak® dosimeter for neutron detection [33]. In the supplementary material that we provided to the Journal, we discussed the use of CR-39 in neutron detection. In the text of the submitted manuscript, we wrote:

Inertial confinement fusion (ICF) experiments with DT targets generate 14.1 MeV neutrons and routinely observe three outgoing particle tracks from a single point in SSNTDs. This is diagnostic of the $^{12}C(n,n')3\alpha$ carbon breakup reaction in the detector with an energy threshold $\geq$ 9.6 MeV [20–23]. Furthermore, these features, which are characteristic of the carbon breakup reaction, make it easy to differentiate this reaction from neutron recoils, charged particle tracks and background events.

Therefore, CR-39 is an established technique for identifying tracks resulting from $\geq$ 9.6 MeV neutrons.

The referee asked, "why the particles, be it alphas or neutrons, cannot be detected with conventional, well established detection methods?" Presumably he/she is referring to real-time measurements. Detection of neutrons is non-trivial. Because neutrons have no charge, there is no direct method to detect them. Consequently, indirect methods must be used in which the neutrons are allowed to interact with other atomic nuclei. The response of that interaction is then measured. The most common means of detecting neutrons in real-time are based upon either neutron capture or elastic scattering. In neutron capture, the target nucleus captures the neutron to create an unstable nucleus that spontaneously loses energy by emitting either ionizing particles or gamma/X-rays. These radioactive decay products are then detected. However, the cross-section for neutron capture is very low at high neutron energies. As a result, this method requires the use of moderators to slow the neutrons down so that capture can occur. A detector based upon neutron capture will generally be unable to determine the energy of the neutrons. In the elastic scattering method, the neutron scatters off nuclei causing the struck nucleus to recoil. The recoiling nucleus can ionize and excite additional atoms through collisions producing detectable electrical charges and/or scintillation light. These types of detectors do not require a moderator so that the energy of the neutrons can be determined. However, these detectors also respond to gamma/X-rays and require a peak shape discriminator.

Other problems with real-time neutron detectors are that they are often temperature sensitive and subject to low-level electronic noise from the local environment causing false signals. Typically long acquisition times are used to improve

the signal to noise ratio. If neutron production is sporadic and/or at a low level, the resultant signal may be averaged away. There is also a problem with the solid angle of detection. Neutrons are emitted from a source in all directions. In our experiments, we reported a maximum DT fusion flux of 2.5 n/cm^2/s. In 4π, this flux is 0.2 n/cm^2/s. It would be very difficult to measure such a low flux using real-time detectors. The CR-39 detectors used in these experiments were able to detect this low flux because they are integrating detectors, meaning events are recorded accumulatively. Nothing is averaged away. Also, these detectors were placed in direct contact with the cathode, which nearly eliminates solid angle detection issues. Thus, CR-39 was the correct choice to detect energetic neutrons in these experiments.

The referee's comment about using conventional, well-established methods to detect the alphas from the carbon break-up reaction shows that he/she does not understand the problem. We stated a $\geq$9.6 MeV neutron could cause a carbon atom to shatter into three alpha particles. The carbon atom that shatters to form the triple track in the CR-39 detector is part of the molecular structure of the detector. The resultant alpha particles have energies on the order of 1 MeV. These experiments were conducted in aqueous media. Linear energy transfer (LET) curves show that, in water, 1 MeV alphas have a range of 5.9 μm in water and 4.7 μm in CR-39. Consequently a real-time particle detector would only be able to detect alpha particles that were generated at the surface of the plastic detector. Alphas formed from the carbon break-up reaction occurring deeper inside the detector would not be able to get out. In the submitted manuscript, we indicated that we observed 5–10 triple tracks on both the front and back surfaces of the CR-39 detector. This translates into 15–30 alpha particles generated on the entire surface of the detector (4 cm ^{2}). For a two-week experiment, this translates into a maximum alpha flux from the carbon breakup of 6.2 $\times 10^{-6}$ α/cm^2/s. Real-time particle detectors cannot detect this low alpha flux *in-situ*. Therefore, CR-39 is the only detector capable of detecting these alphas.

3. Discussion

The journal required us to provide a mechanism by which the triple tracks were formed. Yet, the purpose of the paper was only to compare DT fusion tracks from a DoE accelerator with tracks generated by Pd/D co-deposition. Granted, we mentioned that energetic tritons and 2.45 MeV neutrons had been previously detected in the Pd/D system [34]. One source for these tritons and neutrons are conventional hot fusion reactions. The energetic triton can react with another deuterium inside the Pd lattice producing a 14.1 MeV neutron as a secondary reaction. We noted the process of forming energetic tritons was unknown, but theories were under development. There was no difference in the tracks, meaning that they are one and the same, resulting from the same reaction: a $>$9.6 MeV neutron that shattered a carbon atom in the detector into three alpha particles.

The submitted paper was intended to stimulate interest in the phenomenon, leading to further investigation. Yet, neither referees B nor C commented on the data presented in the paper (Fig. 1). Instead, the reviewers relied upon their erroneous calculations of the neutron flux and integrated dose. They castigated the research with uninformed comments regarding the diagnostic used, although CR-39 is commonly used for both alpha particle and neutron detection. Unfortunately, given the nature of the review process, we had no opportunity to address erroneous or fallacious reviewer comments. One would have thought that the journal's editors would have found something awry, given the difference between the comments by reviewer A and those by reviewers B and C, as well as the vehemence of the latter two reviews. These responses, as well as the actions of the editors, were unprofessional.

Even more disturbing was the lack of curiosity and the unwarranted, surprisingly emotional responses by two of the reviewers. We reported on the unexpected observation of DT fusion neutrons in a palladium lattice. We explained how the detector worked, and displayed equivalent tracks from a known DT fusion source. Two of the reviewers ignored the data and denigrated the work while the journal editors blindly accepted these flawed evaluations.

Reviewers B and C clearly demonstrated their unfamiliarity with, and ignorance of, neutron detection and solid-state nuclear track detectors. This contrasts with reviewer A whose comments upon our paper in the emendated manuscript

clearly indicated that he/she was familiar with CR-39 and understood its use.

Previously published physics papers have discussed CR-39 as an energetic particle diagnostic. Kinoshita [35] employed CR-39 in high-energy physics experiments. Clark [36] used CR-39 for studying proton transport in magnetized plasmas. Li et al. [37] also used it for diagnosing laser plasma interactions. Contrary to Reviewer B, CR-39 has been in use for decades. The fact that the editor selected and then stood with reviewers who were ignorant of standard practices in fast neutron detection indicates editorial failure, as it is incumbent upon editors to select competent reviewers.

The journal refused to provide us with the report of reviewer A as it was of "no value to either of us". It is unheard of for an editor to refuse to provide all responses to the authors, regardless of whether the editor thinks the responses have merit or will do the authors any good. This is unethical. The attitude of both the editor and Reviewers B and C demonstrate an unwillingness to examine observations contrary to accepted beliefs.

Shamoo and Resnick [9] further commented upon how the review of controversial data should be handled:

> *To provide objective and reliable assessments of controversial research, journal editors and review panel leaders should be willing to do what it takes to "open the doors" to new and novel work. If they close these doors, then they are exerting a form of censorship that is not especially helpful to science or society. What it takes to open the door to controversial research may vary from case to case, but we suggest that editors and review panel leaders should always try to understand controversial research within its context. For instance, if an editor recognizes that a paper is likely to be controversial, then he or she should not automatically reject the paper based on the one negative review; before rejecting it, he or she should seek other reviews and give the paper a sympathetic reading.*

It would appear that the editors of the Journal in question inverted Shamoo's suggestion: upon receiving *one positive review* they sought negative reviews in order to reject the paper. Again, this suggests an *a priori* agenda against the subject. Shamoo and Resnick [9] also recognize this as problematic:

> *As a result of this controversy, it has been difficult to conduct peer-reviewed work on cold fusion, because mainstream physics journals select reviewers with strong biases against cold fusion.*

4. Conclusions

One immediate and long lasting effect of journals refusing to publish papers on as yet controversial observations is the elimination of a field of research and the diminution of scientists and engineers working in it. Without peer-reviewed publications, university faculty are precluded from funding as well as students, as no student will pursue an unrecognized field where jobs do not exist. Scientists are unable to find funds or management support. Entrepreneurs are limited because it is not likely that corporate angels or venture capitalists will risk funds on a technology, which is denigrated by leading scientists and subject to ridicule. In 1991, Nobel Laureate Julian Schwinger [38] aptly summarized the problem when he wrote:

> *"The pressure for conformity is enormous. I have experienced it in editors' rejection of submitted papers, based on venomous criticism of anonymous referees. The replacement of impartial reviewing by censorship will be the death of science."*

Indeed, this whole situation is a "Catch-22" [39]; a situation named for the war novel in which a pilot who claims he is crazy so he wouldn't have to fly missions, but by refusing to fly missions he proved he was sane! Our Catch-22 is that both DoE and DoD have unequivocally stated that until "first-tier" journals, like Science and Nature, publish papers in this field, they will not fund programs. But, editors of these journals have stated they would not publish papers without DoE acceptance of the phenomena: *a Catch-22*.

US008419919B1

(12) **United States Patent**
Boss et al.

(10) **Patent No.: US 8,419,919 B1**
(45) **Date of Patent: Apr. 16, 2013**

(54) **SYSTEM AND METHOD FOR GENERATING PARTICLES**

(75) Inventors: **Pamela A. Boss**, San Diego, CA (US); **Frank E. Gordon**, San Diego, CA (US); **Stanislaw Szpak**, Poway, CA (US); **Lawrence Parker Galloway Forsley**, San Diego, CA (US)

(73) Assignees: **JWK International Corporation**, Annandale, VA (US); **The United States of America as represented by the Secretary of the Navy**, Washington, DC (US)

(*) Notice: Subject to any disclaimer, the term of this patent is extended or adjusted under 35 U.S.C. 154(b) by 1036 days.

(21) Appl. No.: **11/859,499**

(22) Filed: **Sep. 21, 2007**

Related U.S. Application Data

(60) Provisional application No. 60/919,190, filed on Mar. 14, 2007.

(51) **Int. Cl.**
C25D 5/48 (2006.01)
C25C 1/20 (2006.01)

(52) **U.S. Cl.**
USPC **205/220**; 205/102; 205/265; 205/627

(58) **Field of Classification Search** 204/229.4, 204/660, 663; 205/339, 340, 565, 627, 102, 205/220, 265, 441
See application file for complete search history.

(56) **References Cited**

U.S. PATENT DOCUMENTS

6,248,221 B1 6/2001 Davis et al.
6,379,512 B1 * 4/2002 Brown et al. 204/245
6,444,337 B1 9/2002 Iyer
6,562,243 B2 * 5/2003 Sherman 205/745
2001/0019594 A1 9/2001 Swartz
2002/0009173 A1 1/2002 Swartz
2002/0018538 A1 2/2002 Swartz
2002/0021777 A1 2/2002 Swartz
2003/0112916 A1 6/2003 Keeney et al.
2003/0213696 A1 11/2003 Danfik
2005/0045482 A1 3/2005 Storms
2005/0129160 A1 6/2005 Indech
(Continued)

OTHER PUBLICATIONS

J. O'M. Bockris, R. Sundaresan, Z. Minevski, D. Letts. "Triggering of heat and sub-surface changes in Pd-D Systems." The Fourth International Conference on Cold Fusion. Transactions of Fusion Technology, Dec. 1994. vol. 25, No. 4T. p. 267.*
(Continued)

Primary Examiner — Keith Hendricks
Assistant Examiner — Steven A. Friday
(74) *Attorney, Agent, or Firm* — Ryan J. Friedl; Kyle Eppele

(57) **ABSTRACT**

A method may include the steps of supplying current to the electrodes of an electrochemical cell according to a first charging profile, wherein the electrochemical cell has an anode, cathode, and electrolytic solution; maintaining a generally constant current between the electrodes; exposing the cell to an external field either during or after the termination of the deposition of deuterium absorbing metal on the cathode; and supplying current to the electrodes according to a second charging profile during the exposure of the cell to the external field. The electrolytic solution may include a metallic salt including palladium, and a supporting electrolyte, each dissolved in heavy water. The cathode may comprise a second metal that does not substantially absorb deuterium, such as gold. The external field may be a magnetic field.

7 Claims, 10 Drawing Sheets

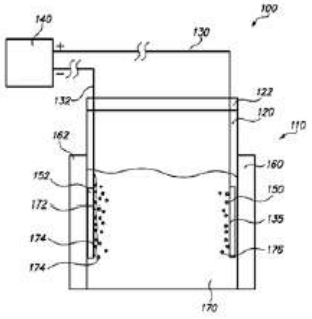

Figure 2. US Patent 8,419,919.

4.1. Prestigious journals publish fraudulent results

Prestigious journals are not infallible. There have been many disputes in the history of science; Nature and Science have not always been on the winning side. It is not reasonable for government agencies to require publication in these journals as proof that a phenomenon is real. Nature and several other high tier journals have also accepted papers that were later retracted. The most egregious failure of the editors and reviewers to deal with fraudulent physics papers was that of then Bell Laboratory's researcher, Jan Hendrik Schoen [40]. Schoen [41] published 36 papers, all of which were retracted, including seven from Nature, nine from Science and six from the Physical Review journal. In this case, there was a "rush to judgment" to publish the expected. As noted above, they have also failed to publish the unexpected, as they did when they rejected 24 papers that later won the Nobel prize [10].

4.2. The end of knowledge?

The impact of impeded discovery was recently featured in the cover story of the The Economist magazine, "The Great Innovation Debate" [42]. They noted, "If the rate at which we innovate, and spread that innovation, slows down, so too, other things being equal, will be our growth rate." One of the ways in which scientific discoveries become innovative technologies is through patents. Over six years ago the method producing the results cited in this paper were submitted to the US Patent Office. Normally, patents are granted in less than half that time. Because of the difficulty in publishing our results neither the US Patent Office nor other US agencies gave credence to these results, until now. US Patent 8,419,919, "System and Method for Generating Particles" was issued on April 16, 2013 (Fig. 2).

The journal review process prevents conscientious scientists from reaching beyond what is known or expected, ignoring the fact that most scientific and technical breakthroughs arise from the unexpected. These are the paradigm shifts that make progress in our technological civilization possible. Government agencies that refuse to fund research because the results have not been published in specific journals put their nations at risk of technological surprise. The dysfunctional research funding and review processes we have described here has dire consequences.

Acknowledgements

We acknowledge the financial support for the original paper, whose adverse review necessitated this correspondence, from the Defense Threat Reduction Agency, DTRA; JWK International Corporation; and the Department of Energy (DoE), National Nuclear Security Agency (NNSA) under Contract No. DE-AC52-06NA25946. We also appreciate the assistance of Dr. Gary Phillips, Georgetown University, for his fruitful discussions and insight into the origin of "triple tracks", as well Dr. Johan Frenje, MIT, the University of Rochester, Laboratory for Laser Energetics, and the Lawrence Livermore National Laboratory National Ignition Facility, for confirming the assignment of triple tracks to DT fusion events [43]. We appreciate the editing assistance of Ms. Amy Rankin, Global Energy Corporation and Jed Rothwell, librarian of LENR-CANR.org. Partial support for this paper was provided by JWK International Corporation.

References

[1] M. Fleischmann, S. Pons and M. Hawkins, Electrochemically induced nuclear fusion of deuterium, *J. Electroanal. Chem.* **261** (1989) 301 and errata in Vol. 263.
[2] http://en.wikipedia.org/wiki/Nature_(journal).
[3] http://en.wikipedia.org/wiki/Science_(journal).
[4] http://thomsonreuters.com/products_services/science/free/essays/impact_factor/
[5] http://pubs.acs.org/journal/jacsat
[6] N.S. Lewis et al., Searches for low-temperature nuclear fusion of deuterium in palladium, *Nature* **340** (1989) 525.

[7] J. Maddox, Farewell (not fond) to cold fusion, *Nature* **344** (1990) 365.
[8] D. Lindley, "The embarrassment of cold fusion", *Nature* **344** 375 (1990).
[9] A.E. Shamoo and D.B. Resnik, *Responsible Conduct of Research*, Oxford University Press, Oxford, 2002.
[10] J.M. Campanario, Rejecting and resisting Nobel class discoveries: accounts by Nobel Laureates, *Scientometrics* **81** (2009) 549–565.
[11] http://www.nature.com/nature/journal/v425/n6959/full/425645a.html
[12] P.A. Mosier-Boss et al., Triple tracks in CR-39 as the result of Pd-D co-deposition: evidence of energetic neutrons, *Naturwissenschaften* **96** (2009) 135–142.
[13] S. Szpak, et al. "Further evidence of nuclear reactions in the Pd/D lattice: emission of charged particles", *Naturwissenschaften* **94** 511-514 (2007).
[14] P.A. Mosier-Boss et al., Use of CR-39 in Pd/D co-deposition experiments, *Eur. Phys. J. Appl. Phys.* **40** (2007) 293–303.
[15] P.A. Mosier-Boss et al., Characterization of tracks in CR-39 detectors obtained as a result of Pd/D co-deposition, *Eur. Phys. J. Appl. Phys.* **46** (2009) 30901, p1–p12.
[16] F.H. Séguin et al., Spectrometry of charged particles from inertial-confinement-fusion plasmas, *Rev. Sci. Instr.* **74** (2003) 975–996.
[17] B.G. Cartwright et al., A nuclear-track-recording polymer of unique sensitivity and resolution, *Nucl. Instr. Meth.* **153** (1978) 457–460.
[18] S.A. Durrani, Nuclear tracks today: strengths, weaknesses, challenges, *Radiation Measurements* **43** (2008) S26–S33.
[19] J.A. Frenje et al., Absolute measurements of neutron yields from DD and DT implosions at the OMEGA laser facility using CR-39 track detectors, *Rev. Sci. Instr.* **73** (2002) 2597–2606.
[20] J.K. Pálfalvi, Cosmic ray studies on the ISS using SSNTD, BRADOS projects, 2001–2003, *Radiation Measurements*. **40** (2005) 428–432.
[21] S.A.R. Al-Najjar, "Fast-neutron spectrometry using the triple-α reaction in the CR-39 detector, *International Journal of Radiation Applications and Instrumentation. Part D, Nuclear Tracks and Radiation Measurements.* **12** 611-615 (1986).
[22] A.M. Abdel-Moneima and A. Abdel-Naby. A study of fast neutron beam geometry and energy distribution using triple-α reactions, *Radiation Measurements* **37** (2003) 15–19.
[23] L. Saj-Bohus et al., Neutron-induced complex reaction analysis with 3D nuclear track simulation, *Radiation Measurements.* **40** (2005) 442–447.
[24] ERAB, "Cold fusion research: a report of the energy research advisory board to the United States Department of Energy", DOE/S-0073 DE90 005611 (1989).
[25] http://www.osha.gov/pls/oshaweb/owadisp.show_document?p_table=STANDARDS&p_id=10098
[26] http://www.thelivingmoon.com/45jack_files/03files/ERW_Neutron_Bomb.html
[27] E. Vilela et al., Optimization of CR-39 for fast neutron dosimetry applications, *Radiation Measurements* **31** (1999) 437.
[28] A.R. El-Sersy, et al. "Determination of CR-39 detection efficiency for fast neutron registration and the absolute neutron dosimetry", *Nuclear Instrumentation and Method in Physics Research B* **215**, 443 (2004).
[29] A.R. El-Sersy, Study of absolute fast neutron dosimetry using CR-39 track detectors, *Nucl.. Instr. Meth. Phys. Res. A* **618** (2010) 234.
[30] V. Kumar et al., Optimization of CR-39 as neutron dosimeter, *Independent J. Pure and Appl. Phys.* **48** (2010) 466.
[31] T. Tsuruta et al., Experimental, study of CR-39 etched track detector for fast neutron dosimetry, *J. Nucl. Sci. Technol.* **29** (1992) 1108.
[32] G.W. Phillips et al., Neutron spectrometry using CR-39 track etch detectors, *Radiation Protection Dosimetry* **120** (2006) 457–460.
[33] http://www.landauerinc.com/uploadedFiles/Healthcare_and_Education/Products/Dosimeters/Neutrak%20Specifications.pdf
[34] A.G. Lipson et al., Evidence for low-intensity D-D reaction as a result of exothermic deuterium desorption from Au/Pd/PdO:D Heterostructures, *Fusion Technol.* **38** (2000) 238–252.
[35] E.L. Clark et al., Measurement of energetic proton transport through magnetized plasma from intense laser interactions with solids, *Phyl Rev. Lett.* **84** (2000) 670–674.
[36] K. Kinoshita et al., Search for Highly Ionizing Particles in e + e - Annihilations at Sqr(s) = 50–52 GeV, *Phy. Rev. Let.* **60** (1988) 1610.

[37] C.K. Li et al., Measuring E and B Fields in Laser-Produced Plasmas with Monoenergetic Proton Radiography, *Phy. Rev. Lett*. **97** (2006} 135003.
[38] http://www.lenr-canr.org/acrobat/SchwingerJcoldfusiona.pdf
[39] J. Heller, *Catch-22*, Simon & Shuster (1961).
[40] E.S. Reich, *Plastic Fantastic: How the Biggest Fraud in Physics Shook the Scientific World*. Palgrave Macmilian (2009).
[41] http://en.wikipedia.org/wiki/Jan_Hendrik_Schön
[42] "The Great Innovation Debate", *The Economis*t, January 12, 2013 p 11
[43] C. Barras, Neutron Tracks Revive Hopes for Cold Fusion, *New Scientist*, March 23, 2009.

J. Condensed Matter Nucl. Sci. 12 (2013) 13–17

Research Article

Using Bakeout to Eliminate Heat from H/D Exchange During Hydrogen Isotope Loading of Pd-impregnated Alumina Powder

Olga Dmitriyeva*† and Garret Moddel

Department of Electrical, Computer, and Energy Engineering, University of Colorado, Boulder, CO 80309-0425, USA

Richard Cantwell and Matt McConnell

Coolescence LLC, 2450 Central Ave Ste F, Boulder, CO 80301, USA

Abstract

Earlier studies [1,2] have shown that a hydrogen–deuterium (H/D) exchange chemical reaction initiated in Pd-impregnated material can account for at least some of the excess heat observed during gas-loading experiments. We report on using *in-situ* material bakeout for an extended time to assess and eliminate the chemical heat contribution.
 ISSN 2227-3123

Keywords: Excess heat, Gas-loading, H/D Exchange, LENR, Pd

1. Introduction

Multiple studies on deuterium loading of Pd nanomaterials demonstrated consistent and repeatable anomalous heat production [3–7]. Low-energy nuclear reaction (LENR) has been offered as an explanation for this heat production. Excess heat production in such systems was observed only in the presence of deuterium, but not hydrogen – an isotope effect. We replicated and analyzed the results of deuterium/hydrogen gas loading experiments. In the study reported here, we show that a conventional heat generation process could account for these observations. Also, we proposed a method that would help to assess this chemical heat contribution.

These anomalous effects were demonstrated in nano-Pd-on-oxide materials, which are well-known catalytic systems. Catalysis is a surface phenomena, and hence an efficient catalyst must have a large surface area, implying that the active particles must be small. Small metal particles can be unstable and prone to sintering in order to reduce surface area. Therefore, most heterogeneous catalysts consist of particles inside the pores of inert substrates such as alumina, silica,

*E-mail: olga.dmitriyeva@colorado.edu
†Also at: Coolescence LLC, 2450 Central Ave Ste F, Boulder, CO 80301, USA.

 ISSN 2227-3123

titania magnesia, zinc oxide, zirconia, zeolite and others. Thus, Pd-impregnated alumina appears to be a suitable system to promote chemical reactions in the presence of hydrogen isotopes. However, the question of isotope selectivity of such a reaction still remained: why was the excess heat observed during deuterium loading but not hydrogen? An explanation was proposed by Kidwell et al. [6], suggesting hydrogen/deuterium (H/D) exchange as a heat generation mechanism in Pd-impregnated systems. Replacement of a hydrogen atom by deuterium in a water molecule or a hydroxyl group on oxide support is an exothermic reaction. However, if the same material is exposed to hydrogen, no exchange takes place and no heat is released.

In our previous work [2], we tested the isotope dependence of heat generation in Pd-impregnated alumina and showed that Pd nanoparticles catalyze H/D exchange chemical reactions. One of the necessary reactants is a gas atom (deuterium or hydrogen), while the other reactant is a particular water isotope trapped in the material due to its hydroscopic nature. We called the water isotope fuel. This fuel can be supplied to the material in two ways: (1) material can be enriched with a particular water isotope during the fabrication or (2) by subsequent exposures to deuterium or hydrogen gas. We used both methods to enrich Pd-impregnated alumina powder with the water isotope of our choice. By subjecting the hydrogenated material to deuterium gas we produced an exothermic H/D exchange reaction and the system generated excess heat. While subjecting the deuterated material to hydrogen gas, we found that the system absorbed heat from the environment This can be explained by a reverse H/D exchange. Expected gas products of the reaction were consistent with those observed using a residual gas analyzer (RGA).

In this paper we present an approach that allowed us to control the amount of water absorbed in the material, while measuring generated heat to quantify the contribution of the H/D exchange reaction. The detailed description is given in Section 3:

Section 3.1 discusses TGA and RGA data that show the traces of water trapped in the material. Section 3.2 provides the results of H/D and reverse H/D exchange in Pd-impregnated alumina powder. Section 3.3 discusses the method of depleting material from water by baking it out in-situ at 390˚C in vacuum for at least 35 h. Section 3.4 demonstrates reactivation of the H/D exchange and heat production in the material following reabsorption of water. Section 3.5 includes experimental data on material reabsorbing water from air. The amount absorbed is quantified.

2. Experiment

2.1. Material fabrication

We used 80–200 mesh Al_2O_3 powder (Fisher Scientific P/N: CAS 1344-28-1) that was baked in vacuum at 350˚C for 12 h before processing. Powder samples containing 2.0% by weight of Pd were fabricated by the incipient wetness method [8] of impregnating hot H_2PdCl_2solution into alumina, forming a slurry. This slurry was then dried in air at room temperature without calcination. Prior to loading into an experimental apparatus, the sample was baked in a vacuum oven at 120˚C for 24 h. However, some water is still trapped in the material even after prebake (discussed in Sections 3 and 3.1). During the loading process the sample was exposed to air for about 5 min, during which there was a chance for more water vapor to be absorbed. This fabrication method produces nanoscale Pd clusters on the surface of the alumina support, which was confirmed by TEM analysis.

2.2. Experimental setup

Figure 1 shows a block diagram of the experimental setup. The system was enclosed in an isothermal chamber (an HP 5890A gas chromatograph oven). The temperature of the oven can be set between 40˚C and 400˚C. The maximum oven temperature used in our experiments was 390˚C. A removable stainless steel vessel was placed inside the oven and connected to the gas line. The vessel contained 6 g of material. Hydrogen, deuterium or nitrogen could be supplied through the gas line. H_2 and D_2 were supplied through an oxygen-removing hydrogen purifier. The D_2 gas was 99.9%

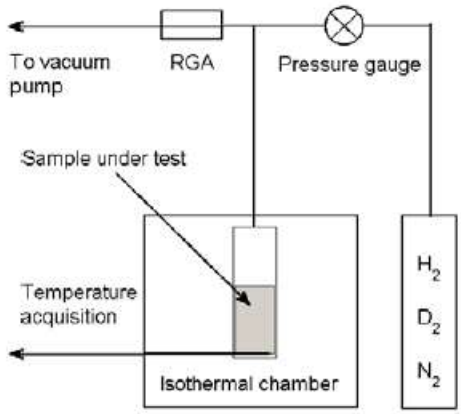

Figure 1. Schematic representation of the experimental apparatus. The sample vessel is enclosed in the oven. Hydrogen, deuterium, or nitrogen can be supplied to the vessel through the gas line.

pure and the H_2 gas was 99.99% pure. Nitrogen was used to fill the system while the vessels were exchanged and new material was loaded.

A typical run consisted of (1) pressurization by hydrogen or deuterium, (2) a period of 2 h when system remained under pressure, (3) an evacuation for 4 h. The system was pressurized up to 1.6×10^5 Pa (1200 torr). Evacuation of the system was done using a turbo-molecular pump down to 10^{-4} Pa (10^{-6} torr). Heat released or consumed by the system during gas load/unload cycles resulted in temperature changes that were measured by RTD sensors (Omega RTD-NPT-72-E-MTP-HT), located in the bottom of the vessels. A residual gas analyzer (SRS RGA200) was connected to the system. Temperature changes that exceeded oven's background temperature fluctuations were associated with exothermic or endothermic heat generated in the system.

System control, and temperature, pressure and RGA data acquisition were done using LabView software.

3. Results

3.1. Material characterization

Thermogravimetric analysis (TGA) of our material showed ~10% of weight loss as the temperature was ramped up to 1000°C. Half of this weight was lost by the material before the temperature reached 400°C. RGA data showed that water (mass 18) was a major chemical released during the bakeout.

3.2. Heat generation

In previous work [2], we demonstrated (1) deuterium producing excess heat production in Pd-impregnated alumina previously exposed to the air, (2) excess heat tapering off with repeated runs, (3) subsequent exposure to hydrogen changing the reaction from exothermic to endothermic. The results were explained by the H/D and reverse H/D exchange chemical reactions activated by Pd nano-catalysts. Exchange reaction products were also observed using the RGA.

Figure 2, part I, shows the excess heat produced in 26 runs, where the reaction gas was switched from deuterium (first 16 runs – exothermic process) to hydrogen (subsequent 10 runs – endothermic process). The amount of heat was calculated as a difference between the energy released or absorbed by the system during pressurization and evacuation.

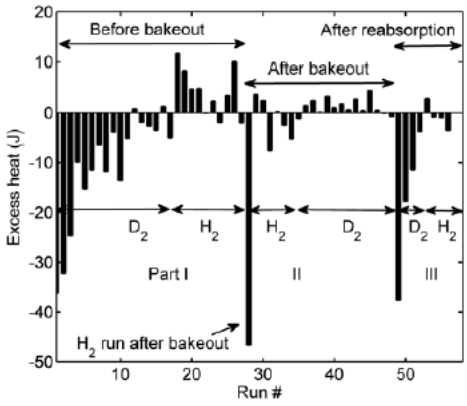

Figure 2. Heat generated by the material during deuterium and hydrogen pressurizations.

3.3. High-temperature treatment

The system bakeout was carried out by ramping the temperature in 50˚C increments up to 390˚C for a total time of about 35 h. The bakeout was carried out in situ, so that the material was not exposed to atmosphere between the bakeout and subsequent testing. Figure 2, part II, shows the result of the following hydrogen and deuterium pressurizations. The first H_2 exposure resulted in an increased amount of released heat. We suggest it is due to chemical reaction of the gas with the bakeout products. However, the temperature measurements of the subsequent 20 runs showed a significant decrease in the amount of heat generated by the system, with no difference between deuterium and hydrogen runs. For the subsequent runs RGA testing showed no evidence of H/D exchange reactions.

3.4. Reactivation of excess heat generation

After unloading from the apparatus the material was placed on the lab scale to monitor the reabsorption of the moisture from air. On average our materials reabsorbed about 6% water by its weight. Due to a delay in the transfer of the material to the scale, the percentage of absorbed water may be slightly underestimated. Twenty-four hours later the material was loaded back to the apparatus and pressurized with deuterium. Figure 2, part III, shows reactivation of the excess heat generation in the presence of deuterium. H/D exchange was evident from RGA data.

3.5. Calculations

Assuming that water is a fuel for the exothermic H/D exchange reaction we can calculate the amount of energy available. 6% by weight of reabsorbed water is equal to 0.36 g. The enthalpy of the exchange reaction is 8.3 kJ/mol [9], which would result in 166 J of released heat. Based on the data presented in Fig. 2, part 1, we estimate that 165 J was generated.

4. Discussion and Conclusions

It is important to be able to assess the chemical heat contribution when reporting on LENR in Pd-impregnated oxide powders. In our previous work, we demonstrated that water isotopes trapped in a powdered Pd-impregnated alumina

catalyst act as a fuel to support H/D exchange chemical reactions. These reactions were shown to be either exothermic or endothermic. In this paper we describe a technique that allows control of the H/D chemical reaction. Extended bakeout is necessary to remove the residual water from the absorptive powdered material. It is important to avoid any air exposure between the elevated temperature treatment and gas-loading steps, to insure that material does not reabsorb water from the air. We found that an in-situ bakeout at 390˚C for at least 35 h is sufficient. The reactivation of the H/D exchange to its initial level after water reabsorption from air suggests that the Pd catalyst did not undergo any significant physical or chemical transformation during the high temperature treatment. Thus, *in-situ* bakeout of the material in vacuum for an extended period of time prior to the contact with hydrogen or deuterium is an effective method to insure that chemical heat due to the H/D exchange is not present during gas-loading experiments.

References

[1] D. Kidwell, D. Knies, A. Moser and D. Domingues, Yes, Virginia there is heat, but it is most likely of chemical origin, *Proc. 15th Int. Conf. on Condensed Matter Nuclear Science*, 2009, pp. 100–109.

[2] O. Dmitriyeva, R. Cantwell, M. McConnel and G. Moddel, Origin of excess heat generated during loading Pd-impregnated alumina powder with deuterium and hydrogen, *Thermochimica Acta* **543** (2012) 260–266.

[3] Y. Arata and Y.-C. Zhang, Establishment of the *Solid Fusion* reactor, *J. High Temp Soc*. **34** (2008) 85–93.

[4] Jean-Paul Biberian, Cold Fusion by gas loading: a review, *Pro. 14th Int. Conf. Condensed Matter Nucl. Sci.,* 2008, pp. 370–384.

[5] F. Celani et al., Deuteron electromigration in thin Pd wires coated with nano-particles: evidence for ultra-fast deuterium loading and anomalous, large thermal effects, *Pro. 14th Int. Conf. Condensed Matter Nucl. Sci.,* 2008, pp. 385–399.

[6] A. Kitamura, T. Nohmi, Y.Sasaki, A. Takahashi, R. Seto and Y. Fujita, Anomalous effects in charging of Pd powders with high density hydrogen isotopes, *Phys. Lett. A* **373** (2009) 3109–3112.

[7] T. Hioki, H. Azuma, T.Nishi, A. Itoh, J. Gao, S. Hibi, T. Motohiro and J. Kasagi, Hydrogen/deuterium absorption property of Pd fine particle systems and heat evolution associated with hydrogen/deuterium loading, *Pro. 15th Int. Conf. Condensed Matter Nucl. Sci.,* 2009, pp. 88–93.

[8] Sheng-Yang Huang, Chin-Da Huang, Boh-Tze Chang and C.-T. Yeh, Chemical activity of palladium clusters: sorption of hydrogen, *J. Phys. Chem. B* **110** (2006) 21783–21787.

[9] L.V. Gurvich, I.V. Veyts and C.B. Alcock, *Thermodynamic Properties of Individual Substances*, 4^{th} ed., Hemisphere, New York, 1989.

J. Condensed Matter Nucl. Sci. 12 (2013) 18–40

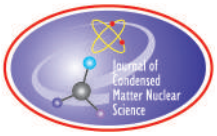

Research Article

Electron Mass Enhancement and the Widom–Larsen Model

Peter L. Hagelstein *

Research Laboratory of Electronics, Massachusetts Institute of Technology, Cambridge, MA 02139, USA

Abstract

Widom and Larsen have put forth a model to describe excess heat and transmutation in LENR experiments. This model is the single most successful theoretical model that the field has seen since it started; it has served as the theoretical justification for a program at NASA; and it has accumulated an enormous number of supporters both within and outside of the condensed matter nuclear science community. The first step in the model involves the proposed accumulation of mass by electrons through Coulomb interactions with electrons and ions in highly-excited coupled plasmon and optical phonon modes. Historically for us this mass increase has been hard to understand, so we were motivated in this study to understand better how this comes about. To study it, we consider simple classical models which show the effect, from which we see that the mass increase can be associated with the electron kinetic energy. The basic results of the simple classical model carry over to the quantum problem in the case of simple wave packet solutions. Since there are no quantum fluctuations of the longitudinal field in the Coulomb gauge, the resulting problem is conventional, and we find no reason to expect MeV electron kinetic energy in a conventional consideration of electrons in metals. We consider the numerical example outlined in a primer on the Widom–Larsen model, and find that multiple GW/cm^2 would be required to support the level of vibrational excitation assumed in the surface layer; this very large power per unit area falls short by orders of magnitude the power level needed to make up the expected energy loss of the mass-enhanced electrons. We note that the mass enhancement of an electron in a transverse field is connected to acceleration, so that the electron radiates. A similar effect is expected in the longitudinal case, and a very large amount of easily detected X-ray radiation would be expected if an MeV-level mass enhancement were present even in a modest number of electrons.
 ISSN 2227-3123

Keywords: Electric field fluctuations, Increased electron mass, LENR theory, Weak interaction models, Widom–Larsen theory

1. Introduction

Excess heat in the Fleischmann–Pons experiment [1,2] has proven to be particularly vexing to theorists. The original experiment involved electrolysis in heavy water with a Pd cathode and a Pt anode, run in a configuration known to load deuterium into the Pd cathode. A very large amount of excess heat is seen in successful experiments, but there is no sign of commensurate chemical products, a situation which led to Fleischmann's conjecture that the energy produced was of nuclear origin. The absence of commensurate energetic nuclear products places the effect outside of conventional

*E-mail: plh@mit.edu

 ISSN 2227-3123

nuclear physics, and in addition prevents us from studying the reaction kinematics directly as we might with any normal nuclear reaction.

During the subsequent 24 years and more, much attention has been focused on figuring out how deuterons might tunnel, and then fuse, in a way that has something to do with the experiments. In spite of the many papers devoted to this approach, at present it has not won over a clear majority of the field. There are issues associated with how the Coulomb barrier might be overcome; why one should not expect to see the normal deuteron–deuteron fusion reaction products if the deuterons managed to get together; and finally the question of what happened to the 24 MeV gamma if helium is formed. Of course, we know now that the problem is even more perplexing; rather than being restricted to gammas, the issue is that as far as we know in the PdD experiments there are no commensurate energetic products of any kind.

The problem associated with overcoming the Coulomb barrier in the case of incoherent reaction schemes is sufficiently difficult that there have been many efforts to look to reaction schemes that do not involve fusion at all. Largely these have simply been ignored within the field (to be fair, nearly all theories have pretty much been ignored by the experimentalists, and the theorists have tended to focus only on their own approaches).

The situation changed considerably with the publication of a model by Widom and Larsen in 2006 [3]. While the theorists in the field have come from diverse backgrounds, this was the first major new theory in more than a decade from a mainstream active particle physicist (Widom), and published initially in a mainstream journal. It was not a fusion-based model, so there was no problem with the Coulomb barrier. In this model, electrons acquire sufficient mass so that electron capture produces the weak interaction mediated reaction [4]

$$W_{\text{electric}} + \text{e+p} \;\rightarrow\; \text{n} + \nu_{\text{e}}.$$

Here W_{electric} is energy contributed from the longitudinal electric field interactions with excitations in the local environment. Normally it is the neutron that undergoes a beta decay via

$$\text{n} \;\rightarrow\; \text{p+e} + \overline{\nu}_{\text{e}} + 0.782\ \text{MeV}.$$

To get the reaction to go in reverse sufficient energy (more than 0.782 MeV) must be supplied; the backward version of the reaction is important in astrophysics, for example in the conversion of electrons and protons to neutrons in a very strong magnetic field [5]. Once a neutron is created, then Widom and Larsen propose that it makes use of long wavelength states (that diffract) in a crystal, and are transferred to other nuclei resulting in energy production and transmutation effects.

Since it first appeared, this model has been remarkably successful. The existence of the model has been communicated to a very large number of people that follow the field but are not in it; a surprisingly large number of people within the scientific community in general are aware of the model, and many think highly of it; and by now there have been many presentations. Mike Melich reported receiving a widely favorable response in an unscientific polling of high-energy physicists at a Lake Louise Winter Institute meeting. This new model has received considerable attention at the New Energy Times web site, which some have suggested advocates for the theory. A success that cannot be similarly claimed by any other model in the field, is that Widom–Larsen has been deemed sufficient to justify an experimental LENR effort at NASA.

When we first encountered the model, our attention was drawn to the very large mass enhancement predicted for electrons, sufficiently large to be able to drive the neutron beta decay reaction backward. Since there are no obvious conventional mechanisms at play in the experiments done so far capable of doing this, we were under the impression that the model sought to take advantage of some new exotic mechanism related to quantum fluctuations of the electromagnetic field. For example, an argument can reasonably be made that quantum fluctuations in the transverse field produces

a mass shift in the electron (as one term among many that appear in perturbation theory), and effect which has been verified both theoretically and experimentally [6]. After some thought, it became clear that if we work in the Coulomb gauge (and most applied physics is done in the Coulomb gauge) there are no quantum fluctuations in the longitudinal field [7]. The largest mass shift obtainable in a terrestrial laboratory is much too small to be relevant for the application under discussion.

This argument was criticized by Widom et al. [8], who suggested that we had omitted Coulomb interactions, and by doing so had thrown out the effects of interest in the Widom–Larsen model. >From our perspective, the issue was never whether Coulomb interactions should be included or not included (and we had included a brief discussion of the longitudinal field in our work), but that there were no quantum fluctuations associated with the Coulomb fields in the Coulomb gauge (while there are quantum fluctuations in the case of transverse fields). This may seem to be a minor technical issue, but it relates to how we might think about the effect, what models we might use, and whether we can use our intuition about the associated physics and applications. If there are no quantum fluctuations of the longitudinal fields in the Coulomb gauge, then the effects under discussion are purely conventional (and there would be no reason to expect mass increases at the MeV level in LENR experiments). In a sense the arguments of Ref. [8], and also of the subsequent primer [4], are helpful in clarifying the issue since the discussion and analysis is conventional.

Some years have passed now, and we have been motivated to return to the problem once again. The Widom–Larsen model has now more supporters by far than any other model in the field, and it is becoming clear that both the theorists and experimentalists in the field probably need to become more familiar with the ideas and the analysis of Widom and coworkers. According to the New Energy Times web site, this model explains LENR, and we should cease thinking about cold fusion altogether. And we can find some guidance in Larsen's slides as to how to think about the effect. For example, in the Lattice Energy LLC slide set from Feb. 14, 2009, we find written: "E-M radiation on metallic hydride surface increases mass of surface plasmon electrons." An arrow points to the reaction

$$(\text{radiation}) + e^- \rightarrow \tilde{e}^-, \tag{1}$$

where $\tilde{e}^-$ is a "heavy-mass surface plasmon-polariton electron."

This, of course, is where our difficulties begin. We simply do not understand how an electron in a metal hydride can develop a mass enhancement as large as needed by the model. However, given the importance of the model, probably it is time to roll up our sleeves and try to understand how this might work. If electrons are going to gain mass, and a lot of mass, then we would like to understand how it works in simple terms if possible. We know that mass is energy, and vice versa, so this will take energy, and the energy has to come from somewhere. We would like to understand where the energy comes from, what form it is in according to a conventional perspective, and we would like to be able to develop intuition generally in terms of the standard microscopic picture that we use for other applied physics effects.

As mentioned above, we are motivated in part by a responsibility to understand what has been argued to be the solution to a problem that has vexed the field for several decades. But there are other motivations as well. For example, applied physics in the areas of atomic physics and solid state physics are mature fields, and an effect in which an electron gains mass at the MeV level does not seem to be in the associated textbooks. One could argue that excess heat in the Fleischmann–Pons experiment is not in the textbooks either, so new textbooks need to be written. On the other hand, it would be nice to understand the new effects in conventional terms if possible in order to connect them to things that we have intuition about already.

So, we proceed with determination to understand the first step of the Widom–Larsen model, which involves the mass increase of the electron.

2. Electron Mass Increase in a Classical Model

Widom and Larsen [3] start from a description in terms of relativistic quantum mechanics, but our starting point is going to be with a much simpler description. Given the very close connection between quantum mechanics and classical mechanics, often it is the case that a quantum system acts very much like its classical equivalent. Our hope is that the same will be the case here, which motivates us to consider here the classical version of the model. One of our goals in this discussion is to familiarize ourselves with the the electron mass increase in a more familiar setting.

Unfortunately, some subtleties arise already. In the original model the effect seemed to be connected to quantum fluctuations of the electromagnetic field. However, as discussed above and in [7] there are no quantum fluctuations in the longitudinal field in the Coulomb gauge. Yet Widom and Larsen have formulas in terms of the associated power spectral density of the electric field, which again seems to point to fluctuations in the longitudinal fields. As there are no quantum fluctuations associated with the longitudinal field itself, all that is left is that there must be fluctuations in the charge density that sources the fields. There is no difficulty in extending this notion to a classical model. We might imagine that other charges move with some degree of randomness, producing random longitudinal electric fields. We are able to analyze the case of an electron in free space interacting with such a field; there are no associated difficulties.

2.1. Nonrelativistic model

We then begin with the simple case of a free electron interacting with a time-dependent longitudinal electric field that we will write as

$$\mathbf{E}(\mathbf{r},t) = -\nabla\Phi(\mathbf{r},t). \tag{2}$$

At this point in the discussion there is no reason not to assume that it is sinusoidal in time and uniform in space. Newton's laws are then

$$\frac{\mathrm{d}}{\mathrm{d}t}\mathbf{r}(t) = \frac{\mathbf{p}(t)}{m}, \qquad \frac{\mathrm{d}}{\mathrm{d}t}\mathbf{p}(t) = q\mathbf{E}(t). \tag{3}$$

We assert a time-dependence of the form

$$\mathbf{E}(t) = \mathbf{E}_0\cos(\omega_0 t) = \mathrm{Re}\{\mathbf{E}_0 \mathrm{e}^{-i\omega_0 t}\} \tag{4}$$

and then solve to get a sinusoidal steady-state solution of the form

$$\mathbf{r}(t) = \mathrm{Re}\left\{-\frac{q\mathbf{E}_0}{m\omega_0^2}\mathrm{e}^{-i\omega_0 t}\right\}, \qquad \mathbf{p}(t) = \mathrm{Re}\left\{i\frac{q\mathbf{E}_0}{\omega_0}\mathrm{e}^{-i\omega_0 t}\right\}. \tag{5}$$

Our goal was to consider things in the simplest possible terms, and it is clear that things cannot get much simpler than this.

In this simple model, the electric field drives the free electron, and the electron moves. The total energy can be computed from the potential plus kinetic energy, but we will focus on the kinetic energy here. We compute

$$E_{\mathrm{K}}(t) = \frac{|\mathbf{p}(t)|^2}{2m} = \frac{q^2|\mathbf{E}_0|^2}{2m\omega_0^2}\sin^2(\omega_0 t). \tag{6}$$

2.2. Electron mass

If the electron is at rest, then the mass contribution to the energy is mc^2. However, here the electron is moving, so we can determine the (rest mass and kinetic) energy of the electron according to

$$m^*(t)c^2 = \sqrt{(mc^2)^2 + c^2|\mathbf{p}(t)|^2} \;\rightarrow\; mc^2 + \frac{|\mathbf{p}(t)|^2}{2m}, \tag{7}$$

where the approximate version is for the nonrelativistic case. The dynamical electron mass satisfies

$$\begin{aligned} m^*(t)c^2 &= \sqrt{(mc^2)^2 + \frac{c^2q^2|\mathbf{E}_0|^2}{\omega_0^2}\sin^2(\omega_0 t)} \\ &= mc^2\sqrt{1 + \frac{q^2|\mathbf{E}_0|^2}{m^2c^2\omega_0^2}\sin^2(\omega_0 t)}. \end{aligned} \tag{8}$$

The associated dynamical mass enhancement factor is then

$$\frac{m^*(t)}{m} = \sqrt{1 + \frac{q^2|\mathbf{E}_0|^2}{m^2c^2\omega_0^2}\sin^2(\omega_0 t)}. \tag{9}$$

2.3. Constant electric field

Given this situation, it seems that the simplest way (consistent with this very simple approach) to develop a large electron mass increase is to accelerate the electron in a uniform field that is constant in time. In this case if we take the momentum to be zero initially, then the momentum evolves as

$$\mathbf{p}(t) = q\mathbf{E}_0 t. \tag{10}$$

We can write for the dynamical mass

$$m^*(t)c^2 = mc^2\sqrt{1 + \frac{q^2|\mathbf{E}_0|^2}{m^2c^2}t^2} \tag{11}$$

with a mass enhancement factor given by

$$\frac{m^*(t)}{m} = \sqrt{1 + \frac{q^2|\mathbf{E}_0|^2}{m^2c^2}t^2}. \tag{12}$$

The thought here is that we can develop a mass enhancement factor that is substantially greater than unity by simply accelerating an electron up to a few MeV using a static electric field accelerator.

2.4. Random electric field

In the event that the electric field is stochastic, then we need to make use of the somewhat more complicated mathematical tools to describe it. The momentum can be related to the field according to

$$\mathbf{p}(t) = \int_{-\infty}^{t} q\mathbf{E}(t')\,\mathrm{d}t'. \tag{13}$$

Assuming that the electric field is wide-sense stationary the momentum autocorrelation function can be defined as

$$\begin{aligned} R_{\mathbf{pp}}(\tau) &= E[\mathbf{p}(t+\tau)\mathbf{p}(t)] \\ &= \int_{-\infty}^{t+\tau} \mathrm{d}t' \int_{-\infty}^{t} \mathrm{d}t'' \left\{ q^2 E[\mathbf{E}(t')\mathbf{E}(t'')] \right\} \\ &= \int_{-\infty}^{t+\tau} \mathrm{d}t' \int_{-\infty}^{t} \mathrm{d}t'' \left\{ q^2 R_{\mathbf{EE}}(t'-t'') \right\}. \end{aligned} \tag{14}$$

The corresponding power spectral density is

$$S_{\mathbf{pp}}(\omega) = \int_{-\infty}^{\infty} R_{\mathbf{pp}}(\tau) \mathrm{e}^{i\omega\tau} \mathrm{d}\tau = \frac{q^2}{\omega^2} S_{\mathbf{EE}}(\omega). \tag{15}$$

We can use this to evaluate the kinetic energy

$$\begin{aligned} E\left[\frac{|\mathbf{p}(t)|^2}{2m} \right] &= \mathrm{Tr}\{R_{\mathbf{pp}}(0)\} \\ &= \mathrm{Tr}\left\{ \int_{-\infty}^{\infty} S_{\mathbf{pp}}(\omega) \frac{\mathrm{d}\omega}{2\pi} \right\} \\ &= \mathrm{Tr}\left\{ \int_{-\infty}^{\infty} \frac{q^2}{\omega^2} S_{\mathbf{EE}}(\omega) \frac{\mathrm{d}\omega}{2\pi} \right\}. \end{aligned} \tag{16}$$

Since we assumed that the electric field is wide-sense stationary, the expectation value of the mass in the nonrelativistic limit is time-independent

$$E[m(t)c^2] \;\rightarrow\; E\left[mc^2 + \frac{|\mathbf{p}(t)|^2}{2m} \right] = mc^2 + \frac{q^2}{2m} \mathrm{Tr}\left\{ \int_{-\infty}^{\infty} \frac{S_{\mathbf{EE}}(\omega)}{\omega^2} \frac{\mathrm{d}\omega}{2\pi} \right\}. \tag{17}$$

The expectation value of the mass increase in the nonrelativistic limit is then

$$E\left[\frac{m(t)}{m} \right] \;\rightarrow\; 1 + \frac{q^2}{2m^2c^2} \mathrm{Tr}\left\{ \int_{-\infty}^{\infty} \frac{S_{\mathbf{EE}}(j\omega)}{\omega^2} \frac{\mathrm{d}\omega}{2\pi} \right\}. \tag{18}$$

The generalization of this to the relativistic case looks to be problematic since we need to evaluate higher-order moments. A way to circumvent this is to work instead with

$$\sqrt{E\left[\frac{m^2(t)}{m^2}\right]} = \sqrt{1+\frac{E[\,|\mathbf{p}(t)|^2]}{m^2c^2}}$$
$$= \sqrt{1+\frac{q^2}{m^2c^2}\mathrm{Tr}\left\{\int_{-\infty}^{\infty}\frac{S_{\mathbf{EE}}(\omega)}{\omega^2}\frac{\mathrm{d}\omega}{2\pi}\right\}}. \quad (19)$$

This is consistent with the relevant equations given by Widom and Larsen [3]. Based on the discussion here, we will require very large random fields to accelerate an electron to the MeV scale. The underlying problem is very little different from the deterministic case, except perhaps that the acceleration will be more efficient in the case of constant or sinusoidal fields. In the stochastic case we would expect cancellation effects since the fields may point in random directions, or reverse sign randomly in a preferred direction.

2.5. Discussion

If the dynamics are nonrelativistic then we can use Newton's laws to understand the motion that results. If the dynamics are relativistic, then the trajectory is more complicated, but we would get the same solution for the momentum. An electron in motion has kinetic energy because it moves. Finally, we can evaluate the mass increase once we know the kinetic energy, since in this way of looking at things the kinetic energy and mass provide two ways of describing the same thing. We find that the mass increase is dynamic (as expected because the momentum is dynamic). The situation in the presence of a stochastic field is very closely related; if anything, we would expect a somewhat weaker mass increase due to cancellation effects.

The mass increase comes about due to a momentum increase, which means in the classical version of the free electron problem, terms containing the electric field only arise because we have solved for the momentum in terms of the electric field. The mass enhancement from this perspective is only due to the contribution of the momentum (a point we will think about again later on).

Perhaps the most useful result here is that we have a picture now which we can understand simply, and that shows us precisely what the mass shift is all about. The mass shifts because the electron acquires kinetic energy when it is accelerated by the electric field. There is no mysterious quantum effect here that conspires to arrange for collective effects to increase the mass of the electron. In essence, knowing the mass increase of the electron in this case is equivalent to knowing its kinetic energy.

Given this, then if the electron mass in free space is increased by ten percent for example, we know that this is because it has gained kinetic energy equal to ten percent of the rest mass.

3. Electron Mass Increase in a Quantum Mechanical Model

At this point in the discussion we are generally pleased that mass shifts similar to what is discussed by Widom and Larsen can be understood simply in the classical case. In turning our attention to the quantum mechanical case, once again there are several issues to be thought about. Perhaps the first is the establishment of a suitable starting place for the discussion, which motivates us to consider a generalized Foldy–Wouthuysen transformation. Although not pursued by Widom and Larsen, it is clear that a sizable mass shift can be developed in the case of a bound electron; this becomes of interest to us in connection with the issue of the electron mass shift in general, but it will lead to a clarification of whether we should focus on the energy or the mass shift (or whether there is a difference). This discussion generally will put us in a better position to think about mass shift for an electron in a metal.

3.1. Electron interacting with a potential and a field

We consider now a Hamiltonian of the form

$$\hat{H} = \boldsymbol{\alpha} \cdot c\hat{\mathbf{p}} + \beta mc^2 - e\boldsymbol{\alpha} \cdot \hat{\mathbf{A}}(\mathbf{r}) + V(\mathbf{r}). \tag{20}$$

If the potential is equal to zero

$$V(\mathbf{r}) \;\rightarrow\; 0, \tag{21}$$

then we can carry out a Foldy–Wouthuysen transformation leading to a rotated Hamiltonian of the form

$$\hat{H}' = \hat{\mathcal{U}}^\dagger \left[\boldsymbol{\alpha} \cdot c\hat{\mathbf{p}} + \beta mc^2 - e\boldsymbol{\alpha} \cdot \hat{\mathbf{A}}(\mathbf{r}) \right] \hat{\mathcal{U}} = \beta \sqrt{(mc^2)^2 + c^2 \left| \hat{\mathbf{p}} - \frac{e}{c}\hat{A} \right|^2}. \tag{22}$$

If we include the potential, things quickly become more complicated; we may write

$$\hat{H}' = \hat{\mathcal{U}}^\dagger \hat{H} \hat{\mathcal{U}} = \beta \sqrt{(mc^2)^2 + c^2 \left| \hat{\mathbf{p}} - \frac{e}{c}\hat{A} \right|^2} + V(\hat{\mathbf{r}}'), \tag{23}$$

where

$$\hat{\mathbf{r}}' = \hat{\mathcal{U}}^\dagger \mathbf{r} \hat{\mathcal{U}}. \tag{24}$$

The transformation of the position coordinate is straightforward, but untangling the results leads to all kinds of terms. From our perspective, we will view the rotated version of the model as

$$\hat{H}' = \beta \sqrt{(mc^2)^2 + c^2 \left| \hat{\mathbf{p}} - \frac{e}{c}\hat{A} \right|^2} + V(\mathbf{r}) + \cdots \tag{25}$$

The idea here is that in the Coulomb gauge the transverse field operator transforms as the momentum operator, but to the potential remains outside the square root. This is consistent with our earlier arguments [7] that it is the transverse fields that contribute to a mass shift, while the longitudinal fields in this way of thinking do not.

Note that in light of the arguments of the previous section, it is still the case that we can think of a mass shift resulting from longitudinal interactions, but this additional analysis will be required (since the mass enhancement is still due to an increase in the kinetic energy, which may depend on the potential).

In light of our earlier work [7], the largest mass shift that can be developed from transverse field fluctuations in the absence of an intense laser field are very small. Correspondingly, either we can absorb them into the mass here and continue, or else we can simply neglect them. In either case there is no reason to carry transverse fields further in this discussion.

3.2. Mass effect due to localization in a bound state

If we seek a sizable mass shift for an electron in a potential, it seems the place to look for it is in the case of a bound electron, and the more strongly bound the better. In the case of a hydrogenic ion, the deeply bound $1s$ electron has a (nonrelativistic) kinetic energy given by

$$\frac{\langle|\hat{\mathbf{p}}|^2\rangle}{2m} = Z^2 I_{\rm H}. \tag{26}$$

The corresponding (nonrelativistic) mass enhancement factor is

$$\frac{m^*}{m} = 1 + \frac{\langle|\hat{\mathbf{p}}|^2\rangle}{2m^2c^2} = 1 + \frac{Z^2 I_{\rm H}}{mc^2} = 1 + \frac{1}{2}(Z\alpha)^2. \tag{27}$$

At large Z the electron has sufficient kinetic energy that relativistic effects are important and one can see the effects of the increase mass on the wavefunction itself.

In this case we can generate a substantial mass increase, however this is under conditions where the electron is tightly bound. The mass increase in this case corresponds to a great deal of energy that can contribute in a weak interaction, but there is also a corresponding potential energy that is twice as large and opposite in sign

$$\langle V\rangle = -2\frac{\langle|\hat{\mathbf{p}}|^2\rangle}{2m} \tag{28}$$

in the nonrelativistic problem.

3.3. Mass and energy

We know that mass and energy are the same thing; however, probably here we need to think about the issue for a bound electron. The mass of the electron and nucleus as a composite in the $1s$ state is reduced by the binding energy $Z^2 I_{\rm H}$, of this we can be sure. Should we think of the electron as having a reduced mass in this case, instead of an increased mass as we have argued above? In the case of a free electron things seemed to be much clearer, since we could identify the mass increase of the electron with the kinetic energy.

But on second thought perhaps things should not have been so clear. For the classical problem of the last section, we might have written for the total energy the sum of the kinetic and potential energy

$$E(t) = \frac{|\mathbf{p}(t)|^2}{2m} + V(\mathbf{r}(t), t). \tag{29}$$

We might have sought to equate mass with the total energy, which might be problematic. For example, in one way of thinking the potential here is not specified to within a constant, so the total energy in such a calculation could be negative. Clearly under these conditions, it would make sense to consider the kinetic energy in connection with the mass increase. On the other hand, it might be the case that the electron is attracted to ions that are moving by slowly. In this case, we know that if the electron is (weakly) bound to these moving ions that the mass of the electron and ions would be reduced by the amount of the binding energy. In such a picture the notion of mass in connection with the potential becomes sensible, but perhaps only when thinking about the total mass of the electron and ions.

3.4. Electron wave packet in free space and uniform field

In the classical version of the problem (in free space with a uniform dynamic external field), once the longitudinal field is given, we can solve for the electron momentum directly in terms of the field, and then solve for the electron mass. In the quantum mechanical version of the problem it would be most elegant to rotate out the uniform field, and end up with a Hamiltonian with an explicit dynamical mass. Unfortunately, as yet we have not found publications where this

kind of unitary transformation is studied (but we would expect it to exist). So instead, we will rely on the less elegant use of wave packet solutions.

For the nonrelativistic case we consider the Schrödinger equation

$$i\hbar\frac{\partial}{\partial t}\psi(\mathbf{r},t) = \left[-\frac{\hbar^2\nabla^2}{2m} - q\mathbf{E}(t)\cdot\mathbf{r}\right]\psi(\mathbf{r},t). \tag{30}$$

We can develop a Gaussian wave packet solution of the form

$$\psi(\mathbf{r},t) = \frac{1}{(\pi L)^{3/4}}\frac{1}{(1+i\hbar t/mL^2)^{3/2}}\,\mathrm{e}^{-i\Theta(t)}\,\mathrm{e}^{i\mathbf{P}(t)\cdot[\mathbf{r}-\mathbf{R}(t)]}\,\mathrm{e}^{-|\mathbf{r}-\mathbf{R}(t)|^2/2L^2(1+i\hbar t/mL^2)}, \tag{31}$$

where $\mathbf{R}(t)$ and $\mathbf{P}(t)$ satisfy the classical equations of motion

$$\frac{\mathrm{d}}{\mathrm{d}t}\mathbf{R}(t) = \frac{\mathbf{P}(t)}{m}, \qquad \frac{\mathrm{d}}{\mathrm{d}t}\mathbf{P}(t) = q\mathbf{E}(t). \tag{32}$$

The phase factor satisfies

$$\hbar\frac{\mathrm{d}}{\mathrm{d}t}\Theta(t) = -\frac{|\mathbf{P}(t)|^2}{2m} - q\mathbf{E}(t)\cdot\mathbf{R}(t). \tag{33}$$

The kinetic energy in this case is

$$\frac{\langle|\hat{\mathbf{p}}|^2\rangle|}{2m} = \frac{|\mathbf{P}(t)|^2}{2m} + \frac{\hbar^2}{4mL^2}. \tag{34}$$

The nonrelativistic mass enhancement is then

$$\frac{\langle m^*(t)\rangle}{m} = 1 + \frac{|\mathbf{P}(t)|^2}{2m^2c^2} + \frac{\hbar^2}{4m^2c^2L^2}. \tag{35}$$

In this case we see that the mass shift includes the classical contribution as well as a contribution due to the original localization of the wave packet. This result demonstrates that for a Gaussian wave packet we can take the classical results over directly to the quantum version of the problem. If we consider a random external electric field, and ignore the localization energy, then the nonrelativistic mass increase for this wave packet solution would be

$$E\left[\frac{\langle m\rangle}{m}\right] \;\rightarrow\; 1 + \frac{q^2}{2m^2c^2}\mathrm{Tr}\left\{\int_{-\infty}^{\infty}\frac{S_{\mathbf{EE}}(j\omega)}{\omega^2}\frac{\mathrm{d}\omega}{2\pi}\right\}. \tag{36}$$

The construction of wave packets in the relativistic case is technically more complicated, but can be done as discussed in Ref. [9]. We would expect to recover a comparable relativistic relations between the mass enhancement and the classical momentum in this case.

3.5. Discussion

This discussion helps us in developing intuition about the electron mass increase generally. We know that the contribution of the transverse fields is small in laboratory experiments that do not involve an intense laser field, and we see that the longitudinal fields rotate differently than transverse fields under a Foldy–Wouthuysen transformation. A modest mass enhancement can be developed for a tightly bound electron, but in this case we need to focus on the total electronic energy (including the potential) rather than on the mass shift, unless we wish to work with the total mass of the composite.

Since the analysis for the quantum version of the problem is more complicated than the classical version, we probably need to think some about the connection between the classical and quantum versions of the problem. A reasonably general unitary transformation capable of rotating out a field uniform in space would be very useful in this context, and would allow for an elegant treatment of the problem. Probably such a rotation exists, in spite of our not having found a relevant publication. Instead we can work with wave packet solutions, which exhibit explicitly the classical relations in the context of the quantum problem. This is very useful because it shows that both the classical and quantum mechanical models describe essentially the same physics of interest to us.

4. Electrons in a Metal

At this point we have developed a sufficient foundation to begin considering the situation of an electron interacting with other electrons in a metal. Widom and Larsen have proposed that there is a mass enhancement in this case, so this motivates us to consider longitudinal Coulomb interactions between a reference electron and other electrons in the metal. >From the arguments of Section 2, the picture that is suggested is one in which the electron in the metal is in some ways like a free electron, and that it experiences longitudinal electric fields due to Coulomb interactions with the very large number of other electrons in the metal. These interactions are random, so if we think classically we end up with a situation very much like the one considered above. In this case we found that the momentum resulting from a stochastic electric field comes into the problem as a mass shift, and we were were able to recover a formula analogous to Widom and Larsen's equation for the mass enhancement.

There are of course issues to be considered in such a picture. For example, the electrons are not free electrons; but instead are either Bloch electrons, or quasi-particles, or perhaps something more complicated depending on the theoretical perspective adopted. In the original version of the problem there appear Coulomb interactions which all of the other electrons in the metal; however, we know that conduction electrons are effective at screening, so that interactions are only significant with a few at a time. We know that large electric fields can be generated with strong plasmon excitation. In this case the plasmon fields are coherent (and not stochastic), which given the discussion above presents no particular difficulty in thinking about or analyzing.

4.1. Conduction in a static field

The simplest model for conduction in a metal is one in which the electrons are treated as classical, are accelerated by a field, and lose momentum by scattering treated as friction. This is the metal version of the uniform constant accelerator field problem from Section 2. In this case we may write

$$\frac{\mathrm{d}\mathbf{p}}{\mathrm{d}t} + \frac{\mathbf{p}}{\tau} = q\mathbf{E}. \tag{37}$$

The momentum in this case is constant

$$\mathbf{p} = \tau q\mathbf{E}. \tag{38}$$

The kinetic energy is then

$$\frac{|\mathbf{p}|^2}{2m'} = \frac{\tau^2 q^2 |\mathbf{E}|^2}{2m'}. \tag{39}$$

The electron mass in a metal in connection with the Bloch picture, the quasi-particle picture, or in connection with experiment, is in general different from the free electron mass. It is usually denoted as m^*, which in the context of the present discussion is a notational headache. Consequently, we will use m' instead in this section. If we decide that the mass enhancement is consistent with this kinetic energy, then we end up with

$$\frac{m^*}{m} = \sqrt{1 + \frac{\tau^2 q^2 |\mathbf{E}|^2}{mm'c^2}}. \tag{40}$$

This mass enhancement in general is small, unless the applied electric fields are enormous (in which case the mass enhancement will still be small but but plasma formation would be expected follow).

The problem is straightforward, but ultimately we would imagine that a better approach might be to use an external high-current accelerator to produce a beam of MeV electrons, and drive them into the metal. At least until they degrade, a situation will be produced in which there will be a large number of electrons with increased mass.

4.2. ARPES and correlation contributions

In textbooks on solid state physics, one can find discussions of the problem of an electron in a periodic potential, which have periodic Bloch solutions. The energy eigenvalues associated with these solutions depend on the wave vector, and people use the results to construct band diagrams. The effective mass tensor of the Bloch states can be determined from the energy bands through

$$\frac{1}{m'_{i,j}} = \frac{1}{\hbar^2} \frac{\partial^2}{\partial k_i \partial k_j} E(\mathbf{k}). \tag{41}$$

In the case of insulators and semiconductors, once an energy band has been established (fitted to experimental data), one can use it to determine the effective mass for modeling.

In the case of metals, there are electron-electron and electron-ion interactions which are present beyond the effects of a periodic potential. The importance of these additional effects became particularly evident once angular-resolved photoelectron spectroscopy (ARPES) began to be used to study electron bands in metals [10–12]. Although electronic band structures in metals had been calculated for decades, there had not been a good way to extract an electron band directly from a set of experimental measurements. Once data was taken in the case of simple metals, and band diagrams began to be constructed, it became evident that the experimental results differed considerably from the theoretical band diagrams. This motivated the theorists to bring to bear more powerful theoretical tools, which led to the adoption of the G-W formalism and the quasi-particle picture [13,14], and other techniques [15]. Correlation effects (which include exactly the effect described by Widom and Larsen, among others) and phonon exchange are well modeled in this approach, with the result that the band diagrams from quasi-particle models are in good agreement with experiment.

The results can be understood in this case as O(eV) corrections to the band diagram. Effective masses can be developed from the corrected band diagrams which differ from those obtained from Bloch theory. Substantial corrections to the effective masses are found.

4.3. Plasma oscillations

Plasma oscillations are known to occur as organized longitudinal modes in metals, and have been proposed to contribute to the enhancement of the electron mass. It seems useful to consider this briefly here.

Collective oscillations in conduction electrons in metals was described many years ago by Pines and Bohm [16]. The plasma frequency (in MKS) is

$$\omega_{\rm p} = \sqrt{\frac{ne^2}{\epsilon_0 m'}}. \tag{42}$$

It varies from a few eV to more than 10 eV in different metals. Since the electric field varies sinusoidally, the dynamical mass increase can be computed directly from

$$\frac{m^*(t)}{m} = \sqrt{1 + \frac{q^2|\mathbf{E}_0|^2}{(m')^2c^2\omega_{\rm p}^2}\sin^2(\omega_{\rm p}t)} \tag{43}$$

in the case of a long-wavelength plasmon wave. Generally the associated momentum enhancement will be much smaller than the Fermi momentum, so that the incremental kinetic energy of an individual electron is much less than 1 eV (which does not get us close to the regime of interest for a reverse beta decay reaction).

However, the plasmon resonance in metals can be at a sufficiently high energy to result in observable physical effects. One example of interest in the literature is enhanced surface desorption resulting from plasmon excitation (see e.g. Hoheisel, Vollmer, and Träger [17]). In this case, the average electron kinetic energy is small, but the energy exchange with an electron involved in the plasmon excitation occurs near the plasmon energy $\hbar\omega_{\rm p}$.

It is possible to drive plasmon oscillations in a metal sufficiently hard that much higher electron energies are produced using intense laser excitation. An example of this is reported by Fennel et al. [18], in which electron energies up to a few hundred eV were detected at a laser intensity near 10^{14} W/cm^2 incident on metal clusters. Presumably we might expect MeV-level electron acceleration at much higher incident laser intensity.

4.4. Electron–phonon interactions

In [4] a discussion is given as to how energy exchange between moving ions in a metal might interact with electrons in order to contribute to a mass enhancement in the electrons. As might be expected, the interaction between vibrating ions in a metal and conduction electrons has been of interest for a very long time and there is a corresponding extensive literature.

In the earliest of these models, a uniform positive charge distribution up to a fixed radius away from the nucleus is used. The corresponding potential is

$$V(r) = \begin{cases} -\dfrac{Z^*e^2}{4\pi\epsilon_0}\left(\dfrac{3r_s^2 - r^2}{2r_s^3}\right) & r \le r_s, \\ -\dfrac{Z^*e^2}{4\pi\epsilon_0 r}, & r_s \le r. \end{cases} \tag{44}$$

This is consistent with the electron–phonon interaction used by Bardeen [19], and by many other authors up until about 1960. This interaction is much softer than an unscreened ion potential, which was required to obtain agreement with experimental conductivity data. The interaction comes about when the ion is displaced, so that [20]

$$V(\mathbf{r}-\mathbf{R}) = V(\mathbf{r}-\mathbf{R}^{(0)}) + (\mathbf{R}-\mathbf{R}^{(0)}) \cdot \left[\nabla V(\mathbf{r}-\mathbf{R})\right]_{\mathbf{R}_0} + \cdots \tag{45}$$

It was found to provide at least a plausible description for the phonon dispersion relation of Na by Toya [21,22]. Subsequently, people have relied on pseudopotentials for the electron–phonon interaction. In the case of hydrogen, one might imagine that a bare Coulomb potential is appropriate. However, a free-electron picture is used in a description such as in Refs. [21,22] under conditions where the electrons are better described by Bloch waves. As such, an electron–phonon matrix element calculated with free-electron wavefunctions and a Coulomb potential for conduction electrons will greatly overestimate the coupling, as compared to an electron–phonon matrix element computed with Bloch waves.

We would expect electron–phonon coupling (for conduction electrons) in a metal hydride to be much weaker than would result from the picture assumed in Ref. [4]. On the other hand, very energetic electrons would see the full Coulomb field of a proton at close range well inside of the 1*s* radius.

4.5. Discussion

Metals are made up of individual atoms, and most of the electrons in a metal are tightly bound to the nuclei in the lattice. Bloch conduction electrons, even in the case of alkali metals which most closely match a free-electron model, have localized components which are for the purpose of the discussion more like bound electrons than free. Consequently, our focus really should be on the electron energy, rather than on the mass enhancement determined from the rest mass and kinetic energy.

Nevertheless, free-electron models have been very important for describing conduction electrons in metals, and there is no reason not to consider the mass increase associated with the kinetic energy. For electron conduction it is straightforward to determine the momentum and corresponding mass enhancement as above, and we find that the mass enhancement is above unity by only a trivially small amount (expect perhaps in exploding wire experiments, and other fast electron plasma systems).

The analysis of electron-electron interactions in metals is a worthy topic of discussion in its own right. Electron-electron correlations are most readily treated in jellium [23], and come about due to potential contributions (rather than indirectly through the resulting momentum as we have interpreted the Widom–Larsen formalas). These contributions are included in modern GW calculations, and in related models; corrections are at the eV level (and not at the MeV level).

Bulk and surface plasmon modes are well studied in metals, and are interesting for all kinds of reasons in solid state physics and for applications. We would not expect plasmon excitation to result in MeV electrons unless driven by a very intense laser.

5. Mass Enhancement in PdH

In contrast to the possibly discouraging conclusions one might come to in light of the arguments outlined above, we can find in Ref. [4] a discussion of the mass enhancement in PdH where the authors come to a decidedly optimistic conclusion. This motivates us to examine the arguments, given that we would not have expected an optimistic conclusion in this case.

In our view there are a host of issues that could be touched on in connection with this single example. Rather than attempting to deal with even a subset of them, we will follow a simple line of thought. Our first goal is to orient ourselves with an example of an electronic vibration which would correspond to a mass increase sufficiently large to

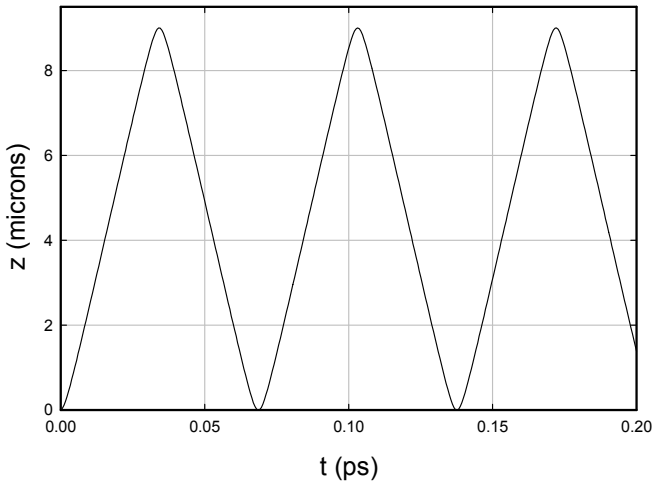

Figure 1. Trajectory of a relativistic electron with $\hbar\omega_0 = 60$ meV and maximum $\beta = 5$.

be relevant for neutron production from a proton. Once we have develop some intuition about the problem, we turn our attention to the practical issues of energy, power, and the transfer of energy from the vibrations to the electrons.

5.1. Model electron oscillation trajectory

It would seem that the place to start is with the end result, specifically the electron oscillations, which are already enormously interesting. Suppose that we consider free-space oscillations with $\beta = 5$, using the frequency consistent with the phonon frequency of 60 meV assumed in [4]. The trajectory that results is illustrated in Fig. 1; we see that the electron in this model travels close to 10 μm and has a roughly saw-tooth appearance since it spends most of the time moving close to c.

In Fig. 2 is shown the derivative of the kinetic energy with respect to time, which we see goes from about -30 to 30 W for one electron. The rate of energy exchange in this case for a single electron is prodigious. This brings out the biggest headache associated with the development of a mass shift through either uniform field that is sinusoidal in time, or random Coulomb fields; that an extremely large amount of power exchange is required to produce or maintain the electron energy.

5.2. Electron energy loss in Pd

However, in the Widom–Larsen model it is proposed that the electrons experience a mass enhancement in a metal hydride, rather than in free space. Energetic electrons lose energy rapidly through collisions and by radiative in solid matter, and it is of interest here to examine the rate of this energy loss. In Fig. 3 is shown the stopping power for energetic electrons in Pd (from the NIST ESTAR online database). From this stopping power we can estimate the rate of energy loss for an electron executing the above trajectory in Pd (the contribution of the H to this energy loss is minor); the results are shown in Fig. 4. We see that energy loss is minimized when the electron has acquired an energy near 1

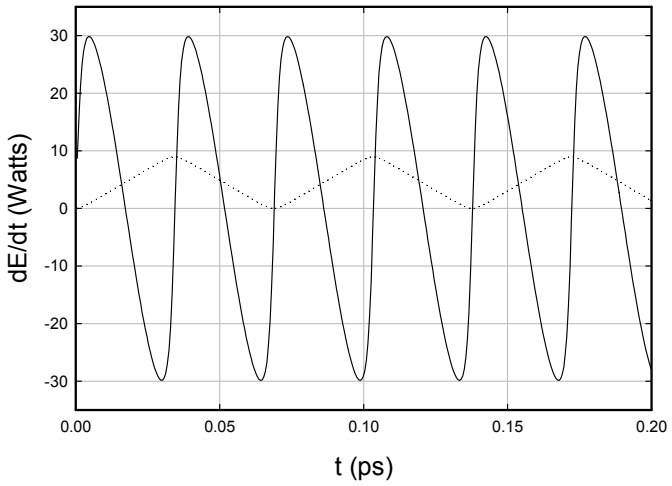

Figure 2. Rate of energy exchange dE/dt in Watts as a function of time (*solid line*); trajectory as in Fig. 1 (*dotted line*).

MeV, so that the electron loses only about 70 mW. The loss is very much larger when the electron energy is much less than 1 MeV.

An addition issue of interest is radiative loss, which would be expected to lead to penetrating X-rays that could be

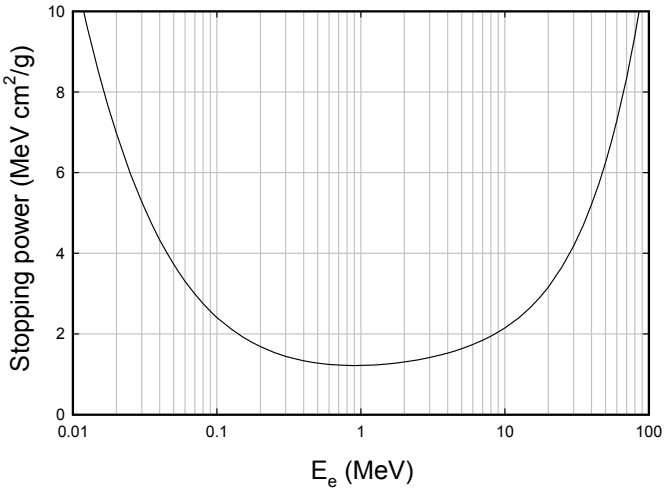

Figure 3. Electron stopping power in Pd.

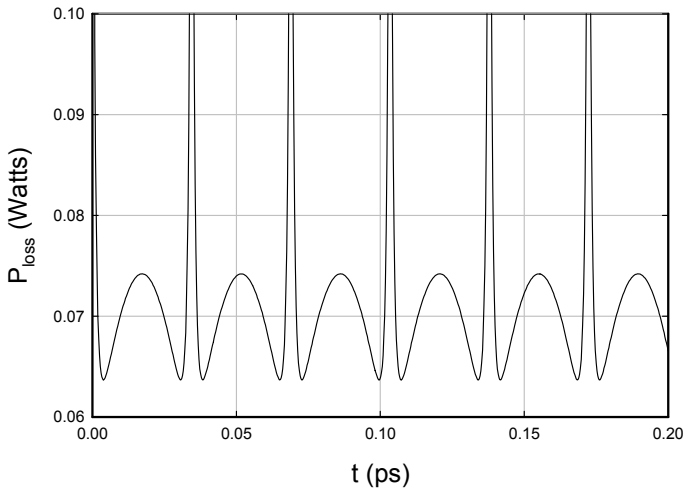

Figure 4. Rate of energy loss due to collisions and radiation for the trajectory above in Pd.

measured readily outside of the cell. For an MeV electron in the vicinity of 1 MeV, the fraction of the total rate of energy loss is about 6% of the total power loss due to collisions and radiation. Hence we would expect the radiated power to be near 4 mW per electron for at the 1 MeV electron minimum. This effect would seem to be useful in this context, as a positive signature for this radiation could be used to prove the existence of the effect.

5.3. Energy and power for phonon–electron coupling

It was suggested in [4] that a very highly excited optical phonon mode might couple with electrons in such a way as to produce MeV-level electron mass shifts. The arguments above suggest that maintaining an electron mass shift at the MeV level will involve substantial energy exchange, so this motivates us to examine the associated energy per unit area and exchanged power per unit area.

For simplicity we will consider a harmonic lattice model. The hydrogen motion is dominant for the optical phonon modes in PdH, so we can develop a reasonable estimate by neglecting the motion of the Pd atoms. In this case we can write for the vibrational energy

$$\sum_j \frac{1}{2} M\omega_0^2 \langle |\mathbf{R}_j|^2 \rangle \;\rightarrow\; N_{\rm H} \frac{1}{2} M\omega_0^2 \langle |\mathbf{R}|^2 \rangle. \tag{46}$$

We can evaluate the average vibrational energy of one hydrogen atom according to

$$\frac{1}{2} M\omega_0^2 \langle |\mathbf{R}|^2 \rangle \;\rightarrow\; 430 \text{ meV} \left(\frac{\langle |\mathbf{R}|^2 \rangle}{1 \text{ Å}^2} \right). \tag{47}$$

The total energy would be twice this in a harmonic lattice model. Note that vibrational amplitude in the bulk at the 1 Å level in this case could be considered to be positively heroic; certainly the vibrations would no longer be in a linear

regime, and the hydrogen atoms would have no difficulty moving from site to site. This is relevant because surface vibrations will couple to near surface layers, so most of the vibrational energy will be away from the surface.

In Ref. [4] an estimate for the number of surface electrons and protons involved is taken to be 10^{16} per cm^2. We can use this to obtain a vibrational energy estimate of

$$\frac{E_{\rm vib}}{\rm area} = 1.4\ \frac{\rm mJ}{\rm cm^2}\ \left(\frac{\langle|\mathbf{R}|^2\rangle}{1\ \text{Å}^2}\right). \tag{48}$$

This perhaps seems like a manageable number; however, since optical phonons lose vibrational energy very rapidly, the power per unit area required to sustain this level of vibrations is roughly

$$\frac{P_{\rm diss}}{\rm area} = \left(\frac{\omega_0}{2\pi\ 10}\right)\frac{E_{\rm vib}}{\rm area} = \frac{10^{10}}{2\pi}\ \frac{\rm W}{\rm cm^2}\ \left(\frac{\langle|\mathbf{R}|^2\rangle}{1\ \text{Å}^2}\right). \tag{49}$$

This is a very high surface power.

Unfortunately, based on the estimates for power loss above, this falls far short of what is required to sustain an electron mass shift large enough to do what is proposed. Let us take the 70 mW power loss number per electron, and turn this into a surface power density using 10^{16} electrons/cm^2 (and for this estimate not worry about how such energetic electrons would manage to remain localized to a few Angstrom surface layer); the result is

$$\frac{P_{\rm loss}}{\rm area} = 70\ {\rm mW}\times 10^{16}\ {\rm cm^{-2}} = 7\times 10^{14}\ \frac{\rm W}{\rm cm^2}. \tag{50}$$

In the electrochemical experiments the power dissipation at the surface is on the general order of 10 W/cm^2, which falls far short of being able to provide sufficient power to the electrons or the hydrogen atoms required by the example of Ref. [4].

5.4. Number of excited electrons

We might expect some of the input electrochemical energy to find its way into exciting optical phonon modes, and there is no question that some of this energy will couple to conduction electrons. In a conventional picture individual electrons would be promoted with an energy increment of one phonon (60 meV in this example). We could begin to estimate how many individual electrons would be excited through this mechanism at a time; we estimate

$$N_{\rm e} = \eta_{\rm p}\eta_{\rm e}\left(\frac{P_{\rm electrochem}}{\hbar\omega_0}\right)\tau_{\rm e}, \tag{51}$$

where $\eta_{\rm p}$ is the fraction of the electrochemical energy going into optical phonon excitation; where $\eta_{\rm e}$ is the fraction of the phonon energy going into electron excitation; and where $\tau_{\rm e}$ is the relaxation time of an excited electron. We can parameterize to obtain

$$N_{\rm e} = 10^5\ \eta_{\rm p}\eta_{\rm e}\left(\frac{P_{\rm electrochem}}{1\ {\rm W}}\right)\left(\frac{\tau_{\rm e}}{1\ {\rm fs}}\right). \tag{52}$$

We conclude from this that we might expect fewer than 1000 electrons to retain the 60 meV phonon energy at any particular time per watt of electrochemical power.

5.5. Discussion

A significant issue in working with the ideas put forth by Widom and Larsen is the clarification of what the mass shift is. For example, if we regard the effect as some benign interaction of the electron with its environment that simply makes the electron heavier, then we would be talking about a new physical picture very different from what is commonly understood as how electrons work in applied physics applications. On the other hand, if we understand the mass shift as connected with the electronic kinetic energy in a free-electron model, then there is nothing new or exotic to be worried about, and we can use standard pictures and analysis to bear.

In this case, independent of how a large mass enhancement is produced, we know that a great deal of energy must be involved. The purpose of the oscillating electron example was to allow us to study this in the case of a simple example where we can quantify every relevant number. The consideration of this example showed us that there is no particular difficulty in specifying a trajectory which has a large associated mass enhancement, but the rate at which energy much be exchanged to maintain it is astronomically large, and if we try to maintain such oscillations in PdH the power loss is prodigious.

If we pursue the numerical example of Ref. [4], we find that even though the example restricts consideration to only the outer monolayer of an idealized metal hydride, the energy involved even in the atomic vibrations are orders of magnitude higher than what is available. The amount of power needed to maintain a sizable mass shift in the number of electrons under consideration are even more orders of magnitude larger. How energetic electrons with MeV level mass increase might remain localized to a surface layer is problematic. Were we to carry out a conventional analysis of electron promotion in a this kind of highly idealized model for the the outer skin of a cathode, we would conclude that fewer than a thousand electrons on average would retain even one phonon of energy per watt of electrochemical power.

6. Mass Enhancement and Radiation

An accelerating charge accelerates, so we would expect an electron which is accelerated sufficiently to develop a mass increase on the order of the rest mass to radiate. For linear motion the radiated power is

$$P_{\rm rad} = \frac{2}{3}\frac{e^2}{4\pi\epsilon_0}\frac{1}{m^2c^3}\left(\frac{{\rm d}p}{{\rm d}t}\right)^2. \tag{53}$$

6.1. Linear oscillations

In the case of our example with a field uniform in space and sinusoidal in time, this becomes

$$P_{\rm rad} = \frac{2}{3}\frac{e^2}{4\pi\epsilon_0}\frac{e^2|\mathbf{E}_0|^2}{m^2c^3}\cos^2(\omega_0 t). \tag{54}$$

It seems useful here to relate the time averaged radiated power to the time average mass shift; we may write

$$\overline{P}_{\rm rad} = \frac{1}{3}\frac{e^2}{4\pi\epsilon_0}\frac{e^2|\mathbf{E}_0|^2}{m^2c^3} \tag{55}$$

and

$$\overline{\left(\frac{m^*(t)}{m}\right)^2} = 1 + \frac{q^2|\mathbf{E}_0|^2}{2m^2c^2\omega_0^2}. \tag{56}$$

We can use this to write for a single electron

$$\overline{P}_{\rm rad} = \frac{2}{3}\frac{e^2}{4\pi\epsilon_0}\frac{\omega_0^2}{c}\left[\overline{\left(\frac{m^*(t)}{m}\right)^2} - 1\right]$$
$$= 0.592\ \mu{\rm W}\left[\overline{\left(\frac{m^*(t)}{m}\right)^2} - 1\right]. \quad (57)$$

Even a modest number of electrons so excited would give a very clear signal that is detectable.

6.2. Discussion

It is possible to develop an exact solution for a Dirac electron in a classical electromagnetic field which exhibit a mass shift due to interactions with the field. From our perspective, the mass shift in this case is due to the electron acquiring considerable kinetic energy. The accelerating electron in this case is known to radiate [24]. Consequently, we would expect generally that when an electron interacts with a dynamic electric field, whether it is transverse or longitudinal, that it will radiate. The only question then is how much radiation is expected. We have estimated here the radiated power in the case of periodic linear oscillations.

Although the radiated power for a single electron is modest (about half a microwatt), in the example considered in Ref. [4] there are 10^{16} electrons/cm^2 with a substantail mass enhancement assumed. In this case the radiated power that could be associated with the electron acceleration is in the range of 10^{10}–10^{11} W/cm^2. This radiation is readily detectable if present, and it could be taken advantage of to verify the presence of enhanced mass electrons.

7. Summary and Conclusions

Widom and Larsen have put forth a new model to account for excess heat and transmutation in LENR experiments. As mentioned in the Introduction this model has proven to be the most successful model since the field started; it has an enormous number of supporters within and without the CMNS community; and it has been judged of sufficient merit to justify an experimental effort at NASA.

The model itself is complicated, with a great many individual pieces. Our focus in this work has only been on issues associated with a single issue in the model; the proposed increase of the electron mass. When we started this study, one of our goals was to understand this issue. Now, after many pages of discussion the conclusion is at best mixed. Inasmuch as the effect under discussion is conventional, we can understand it in terms of relatively simple classical and quantum mechanical models; in this case we would not expect a significant mass enhancement under conditions relevant to experiments in the field. On the other hand, it may be that there remain subtleties associated with the approach, which somehow allows a benign accumulation of mass through a large number of random low-energy Coulomb interactions. If so, then Widom, Larsen, and coworkers have some work left to do in explaining how such a thing might happen.

In our earlier work, the main conclusion relevant to this work was that the longitudinal field comes into the problem conventionally (since there are no quantum fluctuations for longitudinal electric fields in the Coulomb gauge). At the time we considered this to be significant, with the implication that no MeV-level mass increases would be expected due to conventional physics under the experimental conditions of the Fleischmann-Pons experiment and related experiments. As our work was criticized in Ref. [8], it seems that we did not succeed in making the point, or that perhaps there were aspects of the model that we did not understand. In the end, we were motivated to return to the problem once again, determined to understand things better.

We first considered the classical problem, where things are perhaps simplest and clearest. For an external field uniform in space, the electron acquires momentum, which in turn produces an increase in the electron mass. In this problem we are able to take advantage of this relation to express the mass increase in terms of the electric field. This was demonstrated for a constant field, a sinusoidal field, and a random field. Some of the formulas that we ended up with seem to be very close to those given by Widom and Larsen; where in our case we have very simple pictures and models that go with the formulas.

Ultimately we expect the quantum version of the problem to be very close to the classical problem, due to the close connections that exist between classical mechanics and quantum mechanics. We are able to develop a quantum wave packet solution in which the average position and momentum variables satisfy Newton's laws, and which the kinetic energy is related to the expectation value of the momentum very much like in the classical problem (with an additional contribution from the localization of the wave packet). This connection works for constant external longitudinal fields, sinusoidal fields, and fields with random time-dependence on equal footing. In all cases, classical and quantum mechanical, the mass increase of the electron is a result of its kinetic energy, acquired in interactions with the longitudinal fields. We find a modest increase in the electron mass for tightly bound electrons, where we conclude that the electron energy is more important if we focus on the electron (although mass is still relevant if we work with the composite instead of the electron).

In conventional models of electrons in metals, a great deal of work has been done, and there is no MeV-level mass increase of electrons. We can generate an increase in the electron kinetic energy in conduction, in Coulomb interactions, and in the case of plasmons; in all cases the problems are well known. But in no cases do we find MeV energy increases. We did note that in the case of an intense laser interacting with the plasmon mode of a metal cluster that electrons with several hundred eV energies result.

Given the rather dismal expectation for MeV mass enhancement from the conventional models, we turned our attention back to the example described in the primer of Ref. [4]. We find immediately that if we make use of the simple models from earlier in the paper, that an enormous amount of energy exchange would be required to support an electron trajectory that reaches a mass increase of 5 in free space. The power loss that such an energetic electron would sustain in a metal due to scattering and radiating is on the order of 70 mW per electron over most of its cycle. When we considered the proton vibrations in the model, then we find that GW/cm^2 would be required to sustain the assumed motion of a monolayer of protons at the surface assuming the loss occurs at a rate comparable to optical phonon loss rates in metal hydrides. Even though the power level associated with the assumed vibrations is astronomical, it is short by orders of magnitude of what would be needed to sustain the requisite electron mass shift of the small number of surface electrons in the model.

In the interaction of electrons with an electromagnetic traveling wave field, an exact analytic solution is available in which the dressed electron motion is described simply in terms of an effective mass (which is increased by interactions with the field). In a sense, this problem is the reference problem which is then generalized greatly by Widom and Larsen, which motivates us to consider it in similar simple terms. The interaction with the transverse fields causes the electron to execute a complicated trajectory, and to acquire kinetic energy as a result of the field interactions. This situation is similar to the one described in this work, in which the electron gains kinetic energy due to interactions with longitudinal fields. An electron interacting with an intense laser field radiates, and this radiation is well accounted for from a classical model where the radiation is computed by averaging the square of the acceleration over the trajectory. Similarly, an electron accelerated by longitudinal fields is going to radiate, simply because it has a charge that undergoes acceleration. The amount of radiation that would be produced by an electron with a 5-fold mass increase is in the vicinity of a microwatt. The large amount of penetrating X-rays that would result if even a modest number of electrons had this much kinetic energy could be readily measured. The absence of such signals in the few cases where relevant X-ray measurements have been done under conditions where excess heat has been observed would seem to preclude this as an explanation.

Our goal in this study was to understand the electron mass increase in the Widom and Larsen model. In the end, we have considered a variety of scenarios under which an electron mass enhancement can occur, but none of these have anything to do with LENR experiments. We have considered the example in the case of PdH which they have put forth to support the approach, but the example assumes an astronomically large level of vibrational excitation, which falls orders of magnitude short of being able to provide the amount of power needed to maintain the target level of electron kinetic energy required by the model. Electrochemical power at the watt/cm^2 level could support in a conventional analysis the promotion of less than 10^3 electrons/cm^2 at a time with one 60 meV phonon worth of excitation, rather than the several MeV level excitation in 10^{16} electrons/cm^2 discussed in the model. We conclude that we do not understand how Widom and Larsen's model could account for anomalies in LENR experiments. Since accelerated electrons radiate, if electrons were present according to the Widom and Larsen model, there would be a readily detected X-ray signal. The absence of such hard X-ray signals in experiment argues against this model.

We note that we are not alone in noticing issues in connection with the Widom-Larsen model; Vysotskii has earlier commented on a variety of issues with the model [25,26]. Although we had seen Vysotskii's presentation at ICCF17, we had clearly not appreciated the points which he made (points which became clear when a reviewer provided encouragement to look at his papers). One issue is that the large electric fields in the vicinity of a nucleus are localized, and do not persist over a large spatial region; so the use of the large local atomic field strength to estimate the coherent extended plasmon field strength is an overestimate (our arguments are consistent with Vysotskii on this point). Vysotskii makes an argument concerning the development of a mass enhancement without an associated momentum increase in a static electric field; an argument with seems qualitatively inconsistent with our conclusions (since the mass increase in the dressed description in our view arises from the momentum increase). Vysotskii argues that the efficiency of the electron-proton reactions in the Widom–Larsen model will be reduced because energy loss through ionization and radiative losses by orders of magnitude from that claimed by Widom and Larsen; we note here that by implication Vysotskii has already recognized the rapid energy loss of energetic electrons in the Widom–Larsen model. Finally, Vysotskii pointed out the very high surface power requirements implied in the Widom–Larsen model; qualitatively we are in agreement with Vysotskii on this, but the contributing factors are somewhat different, and our estimates are higher than those of Vysotskii.

The biggest issue in the consideration of the part of the Widom–Larsen model from our perspective is the origin of the mass enhancement in the Coulomb gauge when transverse fields are not present. Consequently, our focus initially was on examining how such a mass enhancement could come about, since in the Coulomb gauge there are no quantum fluctuations associated with the longitudinal field. Our conclusion is that when the electron is accelerated, the momentum that results can be described through a mass enhancement (a result that should persist in a dressed picture). Vysotskii for the most part appears to have for the most part presumed this to be the case based on the starting point for his discussion. Widom and Larsen seem to consider the mass enhancement to be associated with mass renormalization, perhaps with the implication that the excess mass is benign in the same sense as the rest mass. However, the formulas which they obtain to evaluate the mass shift in the case of a longitudinal field are very similar to ours, and the mass enhancement in our formulas come about from a momentum increase.

In connection with the last issue, one might assert that mass renormalization in QED itself is modified in the presence of an external longitudinal field. Probably there is literature on this issue that could be dug up which would shed light on things. On the other hand, the issue is in a sense moot, since all of the longitudinal fields in the problems at hand originate from other electrons and ions (there is no significant "external" field if we include all of the relevant electrons and nuclei in our description). Hence if there is a mass renormalization effect due to an external field, then we would expect that if we replaced the external field with a larger description so that no external field were needed, we should be able to make use of conventional mass renormalization. In this case, there would be no physical basis for a benign electron mass shift (i.e. one that is unconnected with an enhanced momentum). Presumably Widom and Larsen will clarify things in their future publications.

References

[1] M. Fleischmann, S. Pons and M. Hawkins, *J. Electroanal Chem.* **201** (1989) 301; errata, **263** (1990) 187.
[2] M. Fleischmann, S. Pons, M.W. Anderson, L.J. Li and M. Hawkins, *J. Electroanal. Chem.* **287** (1990) 293.
[3] A. Widom and L. Larsen, "Ultra low momentum neutron catalyzed nuclear reactions on metallic hydride surfaces," *Eur. Phys. J. C* **46** 107 (2006).
[4] Y.N. Srivastava, A. Widom and L. Larsen, A primer for electroweak induced low-energy nuclear reactions, *Pramana* **75** (2010) 617.
[5] D. Lai and S.L. Shapiro, Cold equation of state in a strong magnetic field: effects of inverse β-decay, *Astrophysical J.* **383** (1991) 745.
[6] J.F. Donoghue, B.R. Holstein and R.W. Robinett, Quantum electrodynamics at finite temperature, *Ann. Phys.* **164** (1985) 233.
[7] P.L. Hagelstein and I.U. Chaudhary, Electron mass shift in nonthermal systems, *J. Phys. B* **41** (2008) 125001.
[8] A. Widom, Y.N. Srivastava and L. Larsen, Errors in the quantum electrodynamic mass analysis of Hagelstein and Chaudhary, LANL ArXiV arXiv:0802.0466 (2008).
[9] J. San Roman, L. Roso and H.R. Reiss, *J. Phys. B: At. Mol. Opt. Phys.* **33** (2000) 1869.
[10] P. Thiry, D. Chandesris, J. Lecante, C. Guillot, H. Pinchaux and Y. Petroff, E vs **k** and inverse lifetime of Cu(110), *Phys. Rev. Lett.* **43** (1979) 82.
[11] F.J. Himpsel, Experimental determination of bulk energy band dispersions, *Applied Optics 19* (1980) 3964.
[12] H.J. Levinson, F. Greuter and E. W. Plummer, *Phys. Rev. B* **27** (1983) 727.
[13] L. Hedin, New method for calculating the one-particle Green's function with application to the electron-gas problem, *Phys. Rev.* **139** (1965) A796.
[14] F. Aryasetiawan and O. Gunnarsson, The GW method, *Rep. Prog. Phys.* **61** (1998) 237.
[15] M. Cazzaniga, GW and beyond approaches to quasiparticle properties in metals, *Phys. Rev. B* **86** (2012) 035120.
[16] D. Pines and D. Bohm, A collective description of electron interactions: II. Collective vs individual particle aspects of the interactions, *Phys. Rev.* **85** (1952) 338.
[17] W. Hoheisel, M. Vollmer and F. Träger, Desorption of metal atoms with laser light: Mechanistic studies, *Phys. Rev. B* **48** (1993) 17463.
[18] Th. Fennel, T. Doppner, J. Passig, Ch. Schaal, J. Tiggesbaümker and K.-H. Meiwes-Broer, Plasmon-Enhanced electron acceleration in intense laser metal–cluster interactions, *Phys. Rev. Lett.* **98** (2007) 143401.
[19] J. Bardeen, Conductivity of monovalent metals, *Phys. Rev.* **52** (1937) 688.
[20] L. Nordheim, Zur Elektronentheorie der Metalle. I, *Annalen der Physik* **6** (1931) 607.
[21] T. Toya, Hartree-Fock method for the interaction of lattice vibrations with electrons in a metal, *J. Res. Institute for Catalysis Hokkaido University* **6** (1958) 161.
[22] T. Toya, Normal vibrations of sodium, *J. Res. Institute for Catalysis Hokkaido University* **6** (1958) 183.
[23] G. Mahan, *Many-particle Physics*, Plenum Press, NY, 1990.
[24] E.S. Sarachik and G.T. Schappert, Classical theory of the scattering of intense laser radiation by free electrons, *Phys. Rev. D* **1** (1970) 2738.
[25] V.I. Vysotskii, On the possibility of application of Widom–Larsen theory for analysis and explanation of Rossi experiments, *Proc. ICCF17* (in press).
[26] V.I. Vysotskii, Critique of the Widom–Larsen theory, *Infinite Energy* **105** (2012) 37.

J. Condensed Matter Nucl. Sci. 12 (2013) 41–53

Research Article

Neutrino Equation of Motion and Neutrino–electron Bound Pairs in LENR

Burke Ritchie *

Lawrence Livermore National Laboratory, Livermore, CA 94550, USA

Abstract

The long-established electron-capture reaction $e^- + p^+ = n + \nu$ may be considered to be a prototype reaction in the nascent field of physics known as low-energy nuclear reactions (LENR) since it involves an interface between electron and atomic physics (EAP) on the left-hand side and nuclear physics on the right-hand side of the reaction. It is a form of inverse beta decay $n = p^+ + e^- + \nu$, which is understood using a conceptual and mathematical methodology (forces mediated by the exchange of bosons known as force carriers and specifically for beta decay the W^- boson as the force carrier for the electroweak force) which is totally foreign to EAP but well-supported by copious nuclear experimental data. Since no such established experimental database exists in LENR, an equation of motion (EOM) is proposed for the neutrino in analogy to Dirac's equation, which is the EOM for the electron. The combined electron and neutrino EOM's support temporary neutrino-electron binding and discover the mass and length scales of a nucleon on an *ab initio* basis. It is believed that the bound pair is a form of W boson, symbolized here by $W_s^{\pm}$ for binding of a neutrino to a positron or electron ($\pm$) and for spin (s) equal to 0 or 1. It is also believed that $W_s^{\pm}$ bosons may be useful as building blocks in constructing models in the LENR regime which may be physically equivalent to quarks and the known $W^{\pm}$ boson in the high-energy regime.
 ISSN 2227-3123

Keywords: Electron, Neutrino, Nucleon, Positron, W-boson

1. Introduction

A small theoretical and experimental community exists in low-energy nuclear reactions (LENR); however it appears that a overwhelming majority of the general theoretical-physics community has reached a consensus that LENR observations cannot be explained by quantum mechanics using Coulombic forces [1]. Remarkably a prototype of a LENR experimental observation, namely electron capture by a nucleus, has long been known,

$$e^- + p^+ = n + \nu, \tag{1}$$

where ν represents a neutrino. Pauli first postulated the existence of the neutrino in beta decay,

*E-mail: ritchie@lstc.com

 ISSN 2227-3123

$$\mathrm{n} = \mathrm{p}^{+} + \mathrm{e}^{-} + \nu \tag{2}$$

and Fermi successfully calculated the rate of beta decay using first-order perturbation theory (Fermi's Golden Rule) with a phenomenological nuclear interaction for the nuclear internal-conversion transition. Modern theory has postulated a fundamental electroweak interaction which causes a nuclear internal conversion from an up to a down quark, which cancels the net unit positive charge of the proton's two up and one down quarks. The electroweak interaction is supported by experimental observation and is understood as a force mediated by the W^{-} boson, which decays immediately into an electron and a neutrino.

A fundamental difference in the mathematical and conceptual methodologies between high-energy physics and electron and atomic physics (EAP) is already obvious from the description I have just given of beta decay such that it is no mystery that never the twain shall meet between the high-energy and low-energy communities, thereby leading to the negative conclusions of particle theorists regarding the validity of LENR experiments. In particle physics forces are mediated by the exchange of bosons or force carriers. Taking this picture to EAP the Coulombic force is mediated by the exchange of photons. The force-carrier formalism is based on perturbation theory with free-particle zeroth-order basis and is therefore largely inapplicable to bound states. The nonperturbative theory appropriate for bound states is lattice quantum chromodynamics (QCD), whose set of difficulties include its totally numerical nature such that there are no analytic test problems available to mitigate numerical uncertainties as in other computationally-intensive fields of physics. Curiously one could not easily, if at all, repeat the highly accurate nonperturbative calculations of atomic, molecular, and condensed-matter physics using the force-carrier formalism, even though remarkably lattice QCD is the primary tool available for elucidating the internal structure of nucleons and of nucleon–nucleon forces generally.

Of greater importance however is the need in high-energy physics to understand the nature of forces as mediated by intermediate particles which are bosons and are known as force carriers. Using this picture we may attempt to formulate the decay of an excited atom which lies above one or more ionization thresholds such that the atom spontaneously emits an electron. The forces are Coulombic such that the intermediate particle is a photon. The photon is unobserved so that it must be considered to be a virtual particle. In beta decay however the intermediate particle, the W^{-} boson, must be considered to be a real since the experimental observation is its decay into an electron and a neutrino. The fragmentation of the W^{-} boson is "immediate" compared to the electroweak up to down quark transition mediated by the W^{-} boson, which requires nearly 15 min.

In practice the lifetime of the force carrier is determined experimentally by the range of the interaction which varies from infinite (photons) to very short ($W^{\pm}$ bosons). The conceptual difference from the nonperturbative calculations of EAP, in which the force can be expressed mathematically without the need to postulate an intermediate particle at all, is striking. Most importantly in the low-energy theory of matter the particles are the *same* before and after a transition, whereas in nuclear theory the particles are different, for example quarks and $W^{\pm}$ bosons initially and quarks, electrons, and neutrinos finally. The vague description of an "immediate" decay of the $W^{\pm}$ intermediate particle into a positron and neutrino or an electron and neutrino is a "black box" with respect to further physical elucidation of the internal structure of the $W^{\pm}$ boson before its fragmentation. The darkness of our knowledge of any possible $W^{\pm}$ boson internal structure is mandated by the binomial logic of particle methodology in which particles are created or destroyed with respect to a particle field which possibly comprises an incomplete physical description of the particle itself.

I discuss this point at length in the appendices of [1] in which I point out that that radiation-free matter does not exist in nature. But yet theoretical physics has evolved, reflecting the separate developments historically of mechanics and electrodynamics, into a radiation-free quantum theory of matter, a matter-free quantum theory of radiation, and a theory of the mutual interaction of radiation and matter. This piecemeal approach leads to an infinite energy for the Lamb shift and other "radiative corrections" of the electron in absence of the use of physical argument and mathematical adjustments to "renormalize" theory in order to obtain a finite result which remarkably agrees with high accuracy with

experimental observation. One may question however if perfect theoretical agreement with a specific set of experiments should be accepted with uncritical acclaim in absence of a theory which explains the source of the infinities and provides a divergence-free result. It is hard to imagine that renormalization theory with its mathematical recipes for the removal of divergent contributions could be a general theory of nature, not withstanding its high degree of accuracy.

Indeed one may say that particle fields for matter-free photons or photon-free electrons represent incomplete physical descriptions of these particles. This is the lesson which we may take away from Lamb's experiments, which definitively demonstrate the existence of permanent radiative shifts in atomic energy levels, namely that radiation-free matter does not exist in nature such that a photon- free material particle field or a particle-free photon field, however neat and pleasing this it is mathematically, is not a complete picture either of the material particle or of the photon. The renormalization scheme itself confirms this view since infinities are removed from radiation-matter calculations by postulating that photons are always present in the structure of a free electron such that when the free-electron radiative shift is added back to bound-electron calculations the unphysical infinities are removed.

In this paper I return to the fully relativistic, Lorentz-invariant potential methodology of relativistic quantum mechanics as a powerful tool available for use in particle theory. As an application I propose a neutrino equation of motion (EOM).

It is shown that a neutrino–positron or neutrino-electron pair can form a mutually bound state with lifetime against breakup into a free neutrino and positron or a free neutrino and electron of the same order as the lifetime of the neutron against beta decay. The temporarily bound pair is given the symbol $W_s^{\pm}$ for a positron-neutrino (+) or electron-neutrino (−) boson where the subscript denotes the two possible spin states 0 or 1. It is possible therefore to postulate that the unstable $W_s^{\pm}$ bosons aggregate to give a physical equivalency for the proton. One such aggregate might be $e^- W_0^+ W_0^+ n\nu \leftrightarrow$ UUD for the two up and one down quarks of the proton. Since the zero-mass, zero-charge neutrinos would not be expected to undergo mutual repulsion or add mass or charge, it is possible that a large number of neutrinos ($n \gg 1$) could be dragged along as internal constituents of the proton, where in a spin unpolarized state the net spin of the aggregate of n neutrinos would be zero such that the net spin and charge of the proton is given by the two $W_s^{\pm}$ bosons and the electron. Then it can be further postulated that electron capture given by Eq. (1) proceeds as follows,

$$e^- W_0^+ W_0^+ n\nu + e^- = e^- W_0^+ W_0^+ W_1^- (n-2)\nu + \nu \tag{3}$$

such that an equivalency exists for the neutron

$$e^- W_0^+ W_0^+ W_1^- (n-2)\nu \quad \leftrightarrow \quad \text{UDD}$$

for the one up and two down quarks of he neutron. The neutron decay is then determined by the decay of W_1^-,

$$e^- W_0^+ W_0^+ W_1^- (n-2)\nu = e^- W_0^+ W_0^+ (n-2)\nu + e^- + \nu \tag{4}$$

such that our postulate for the proton (first term on the right-hand side of Eq. (4)) holds if $(n-2)\nu \cong n\nu$. Neutrino emission in LENR has also been proposed by authors using a "selective resonant" theory [2] in which the rate of tunneling through the deuterium–deuterium Coulomb barrier matches the rate of decay of an excited state of the helium nucleus by the electroweak interaction accompanied by neutrino emission [3].

We close this section by reminding readers of the Lorentz covariance of Dirac's equation even in the presence of the potentials [4] by writing Dirac's equation in manifestly covariant form using the Clifford algebra of 4×4 γ-matrices,

$$(\gamma_0, \vec{\gamma}) \cdot \left(\left(i\hbar \frac{1}{c} \frac{\partial}{\partial t} - \frac{e}{c} \Phi \right), \left(i\hbar \vec{\nabla} + \frac{e}{c} \vec{A} \right) \right) \psi_{\mathrm{D}} (\vec{r}, t) = mc \psi_{\mathrm{D}} (\vec{r}, t) , \tag{5a}$$

$$\left[\gamma_0\left(i\hbar\frac{1}{c}\frac{\partial}{\partial t}-\frac{e}{c}\Phi\right)+\vec{\gamma}\cdot\left(i\hbar\vec{\nabla}+\frac{e}{c}\vec{A}\right)-mc\right]\psi_{\mathrm{D}}(\vec{r},t)=0, \tag{5b}$$

where Eq. (5b) follows on carrying out the 4-vector operations indicated in Eq. (5a), $(\Phi, \vec{A})$ is the electromagnetic 4-potential, and $\psi_{\mathrm{D}}(\vec{r},t)$ is Dirac's 4-component vector wave function. Notice in Eq. (5a) Dirac's equation has been written formally as the scalar product of 4-vectors (scalar product of γ 4-vector and the electron's 4-momentum) operating on $\psi_{\mathrm{D}}(\vec{r},t)$ on the left-hand side equal to the Lorentz constant mc times $\psi_{\mathrm{D}}(\vec{r},t)$ on the right-hand side. Readers are reminded that

$$(\gamma_0,\vec{\gamma})=\left(\begin{pmatrix} I & 0\\ 0 & -I\end{pmatrix},\begin{pmatrix} 0 & \vec{\sigma}\\ -\vec{\sigma} & 0\end{pmatrix}\right),$$

where I is the 2×2 identity matrix, $\vec{\sigma}$ is Pauli's vector,

$$\vec{\sigma}=\hat{i}\begin{pmatrix} 0 & 1\\ 1 & 0\end{pmatrix}+\hat{j}\begin{pmatrix} 0 & -i\\ i & 0\end{pmatrix}+\hat{k}\begin{pmatrix} 1 & 0\\ 0 & -1\end{pmatrix},$$

and

$$\psi_{\mathrm{D}}(\vec{r},t)=\begin{pmatrix}\psi(\vec{r},t)\\ \chi(\vec{r},t)\end{pmatrix}$$

in which $\psi(\vec{r},t)$ and $\chi(\vec{r},t)$ respectively are the "large" and "small" two-component spinors. As pointed out in [4] the transformation properties of the γ-matrices guarantee the Lorentz covariance of Eqs. (5a) and (5b) even in the presence of the 4-potential since the frame transformation is now carried out on the vector difference of the 4-momentum and the 4-potential, namely

$$\left(ih\frac{\partial}{c\partial t}-\frac{e}{c}\Phi,\ ih\vec{\nabla}+\frac{e}{c}\vec{A}\right)$$

rather than on the free-particle 4-momentum by itself, and the vector difference is still a 4-vector such that Lorentz covariance is preserved.

I believe that it is possible to use first-quantized relativistic quantum mechanics and potential theory to understand nuclear reactions such as electron capture, $\mathrm{e}^- + \mathrm{p}^+ = \mathrm{n} + \nu$, which take place in the low-energy regime. This belief is supported by the success of Dirac's equation to give an exact *ab initio* description of the hydrogen atom in absence of radiative corrections and nuclear recoil. It is necessary then to discover neutrino-matter forces on an *ab initio* basis, which has been accomplished here by deriving a neutrino EOM which is compatible with the electromagnetic equation of continuity, in analogy to the electron EOM (Dirac's equation with electromagnetic 4-potential), which is compatible with the material equation of continuity. The latter criterion was essential to Dirac in his program to derive a correct Lorentz-invariant relativistic EOM for the electron. Remarkably the neutrino EOM is used in combination with the electron EOM to find a neutrino-electron or neutrino-positron temporarily bound state which has the mass and length scales of a nucleon and whose lifetime has the time scale of the neutron's lifetime.

2. Neutrino Equation of Motion (EOM)

Since the neutrino is ubiquitous in nuclear reactions it would be useful in the theory of LENR to have an EOM for the neutrino which could be then be combined with the EOM for the electron, which is Dirac's equation, in a theory which

is general enough to make some progress in explaining LENR observations. In their classic text Morse and Feshbach discuss the theorem that the scalar product of 4-vectors is always Lorentz-invariant [5]. Two examples are the Lorentz gauge equation, which is the scalar product of the 4-gradient and the electromagnetic 4-potential,

$$\left(\frac{1}{c}\frac{\partial}{\partial t}, \vec{\nabla}\right) \cdot (\Phi, \vec{A}) = \frac{1}{c}\frac{\partial \Phi}{\partial t} + \vec{\nabla} \cdot \vec{A} = 0, \tag{6}$$

and the equation of continuity, which is the scalar product of the 4-gradient and the 4-current,

$$\left(\frac{1}{c}\frac{\partial}{\partial t}, \vec{\nabla}\right) \cdot (c\rho, \vec{j}) = \frac{1}{c}\frac{\partial \rho}{\partial t} + \vec{\nabla} \cdot \vec{j} = 0. \tag{7}$$

Proceeding heuristically Dirac's equation for a free electron can be inferred from a form of Lorentz gauge equation, in which the electromagnetic 4-potential is replaced by a generalized 4-potential $(\Psi, \vec{X})$ posited for the electron,

$$\left(\frac{1}{c}\frac{\partial}{\partial t}, \vec{\nabla}\right) \cdot (\Psi, \vec{X}) = \frac{1}{c}\frac{\partial \Psi}{\partial t} + \vec{\nabla} \cdot \vec{X} = 0. \tag{8}$$

The scalar and vector potentials can be written in the form of carrier-wave expansions for an assumed dominant frequency component, thusly,

$$\Psi = \chi(\vec{r}, t)\, \mathrm{e}^{-i\omega t} + \psi(\vec{r}, t)\, \mathrm{e}^{i\omega t}, \tag{9a}$$

$$\vec{\mathrm{X}} = \vec{\mathrm{X}}_{-}(\vec{r}, t)\, \mathrm{e}^{-i\omega t} + \vec{\mathrm{X}}_{+}(\vec{r}, t)\, \mathrm{e}^{i\omega t}. \tag{9b}$$

On substituting Eqs. (9a) and (9b) into Eq. (8) and separately setting the coefficients of the exponential factors equal to zero, we obtain

$$\left(i\hbar\frac{\partial}{\partial t} - mc^2\right) \psi(\vec{r}, t) + i\hbar c\vec{\sigma} \cdot \vec{\nabla}\chi\,(\vec{r}, t) = 0, \tag{10a}$$

$$\left(i\hbar\frac{\partial}{\partial t} + mc^2\right) \chi\,(\vec{r}, t) + i\hbar c\vec{\sigma} \cdot \vec{\nabla}\psi\,(\vec{r}, t) = 0, \tag{10b}$$

which are identically Dirac's pair of first-order equations for a free electron on setting

$$\omega = \frac{mc^2}{\hbar},$$

$$\vec{\mathrm{X}}_{+}(\vec{r}, t) = \vec{\sigma}\chi\,(\vec{r}, t),$$

$$\vec{\mathrm{X}}_{-}(\vec{r}, t) = \vec{\sigma}\psi\,(\vec{r}, t),$$

where $\vec{\sigma}$ is Pauli's vector and the wave functions are the Dirac two-component spinors. Dirac's own derivation, which flows from the tradition of matter as opposed to radiant physics [6], follows from his demands that a correct relativistic equation of motion (EOM) for the electron should satisfy the relationship between energy and momentum of special relativity ($E = \gamma mc^2$, for Lorentz factor

$$\gamma = \sqrt{1 + \frac{p^2}{m^2c^2}}$$

subject to the quantization rules

$$E \to i\hbar \frac{\partial}{\partial t}$$

and $\vec{p} \to -i\hbar\vec{\nabla}$) and further should satisfy the equation of continuity given by Eq. (7). The latter demand is satisfied by Dirac's equation, giving a current,

$$\vec{j}(\vec{r}, t) = c[\psi^+(\vec{r}, t)\vec{\sigma}\,\chi\,(\vec{r}, t) + \chi^+(\vec{r}, t)\,\vec{\sigma}\,\psi\,(\vec{r}, t)], \tag{11}$$

where the superscripts denote Hermitian conjugates. Notice that the only identification of Eqs. (10) with the electron is in the mass term since Pauli's vector, originally identified with the electron by Pauli, can be generally identified with any spin-1/2 particle or fermion. This means that the Dirac equation with $m = 0$ can sensibly be considered to be the EOM for a neutrino, although again the free-particle EOM tells us nothing about the property of charge either for the electron or the neutrino.

The neutrino shares its zero-mass and charge neutrality with electro- magnetic radiation. It is therefore assumed that a 4-potential exists for the neutrino such that its EOM can be inferred from the Lorentz invariant found from the scalar product of an electromagnetic 4-momentum and the neutrino's posited 4-potential thusly,

$$\left(\frac{\hbar}{c}\frac{\partial}{\partial t}, \hbar\vec{\nabla} + \frac{e\hbar}{mc^2}\vec{E}, \vec{H}\right) \cdot (\Phi_\nu, \vec{A}_\nu) = \frac{\hbar}{c}\frac{\partial}{\partial t}\Phi_e + \left(\hbar\vec{\nabla} + \frac{e\hbar}{mc^2}\vec{E}, \vec{H}\right) \cdot \vec{A}_\nu = 0 \tag{12}$$

for either electric or magnetic fields $\vec{E}, \vec{H}$. The electromagnetic 4-momentum is found from $\hbar$ times a 4-gradient,

$$\left(\frac{\partial}{c\partial t}, \vec{\nabla} + \frac{e}{mc^2}\vec{E}, \vec{H}\right),$$

whose scalar product with the electromagnetic 4-current,

$$\left(c\left(u + \int_0^t \mathrm{d}t'\,\vec{j} \cdot \vec{E}\right), \vec{S}\right),$$

where

$$u = \frac{1}{8\pi}(\vec{E} \cdot \vec{D} + \vec{H} \cdot \vec{B})$$

is the electromagnetic energy density and $\vec{S} = \frac{c}{4\pi}\vec{E} \times \vec{H}$ is the electromagnetic 3-current, gives the Lorentz-invariant electromagnetic continuity equation,

$$\frac{\partial u}{\partial t} + \vec{\nabla} \cdot \vec{S} + \vec{j} \cdot \vec{E} = 0. \tag{13}$$

This is simply the electromagnetic analog of writing the Lorentz-invariant material continuity equation given by Eq. (7) as the scalar product of the known 4-gradient,

$$(\frac{\partial}{c\partial t}, \vec{\nabla})$$

,
and the known material 4-current, $(c\rho, \vec{j})$. Notice that in the theory developed above the known 4-gradient is simply renormalized by the replacement

$$\vec{\nabla} \rightarrow \vec{\nabla} + \frac{e}{mc^2}\vec{E}, \vec{H},$$

which gives a Lorentz- invariant electromagnetic continuity equation since the scalar product of $\vec{E}$ or $\vec{H}$ with the electromagnetic 3-current, $\vec{S}$, vanishes. As with the electron the neutrino scalar and vector potentials can be written in the form of carrier-wave expansions for an assumed dominant frequency component, thusly,

$$\Phi_\nu = \Phi_{\nu_-} \mathrm{e}^{-i\omega_\nu t} + \Phi_{\nu_+} \mathrm{e}^{i\omega_\nu t}, \tag{14a}$$

$$\vec{A}_\nu = \vec{A}_{\nu-} \mathrm{e}^{-i\omega_\nu t} + \vec{A}_{\nu+} \mathrm{e}^{i\omega_\nu t}, \tag{14b}$$

from which on substituting Eqs. (14a) and (14b) into Eq. (12) and separately setting the coefficients of the exponential factors equal to zero, we obtain,

$$\left(\frac{1}{c}\frac{\partial}{\partial t} + i\frac{\omega_\nu}{c}\right)\Phi_{\nu+} + \left(\vec{\nabla} + \frac{e}{mc^2}\vec{E}, \vec{H}\right) \cdot \vec{A}_{\nu+} = 0, \tag{15a}$$

$$\left(\frac{1}{c}\frac{\partial}{\partial t} - i\frac{\omega_\nu}{c}\right)\Phi_{\nu-} + \left(\vec{\nabla} + \frac{e}{mc^2}\vec{E}, \vec{H}\right) \cdot \vec{A}_{\nu-} = 0. \tag{15b}$$

On setting $\Phi_{\nu+} = \xi_{E,H}$, $\vec{A}_{\nu+} = \vec{\sigma}_\nu \zeta_{E,H}$, $\Phi_{\nu-} = \zeta_{E,H}$, $\vec{A}_{\nu-} = \vec{\sigma}_\nu \xi_{E,H}$, where $\vec{\sigma}_\nu$ is Pauli's vector for the neutrino's spin, we obtain a Dirac form for the neutrino EOM,

$$\frac{\partial \xi_{E,H}}{c\partial t} + i\frac{\omega_\nu}{c}\xi_{E,H} + \vec{\sigma}_\nu \cdot \left(\vec{\nabla} + \frac{e}{mc^2}\vec{E}, \vec{H}\right) \zeta_{E,H} = 0, \tag{16a}$$

$$\frac{\partial \zeta_{E,H}}{c\partial t} - i\frac{\omega_\nu}{c}\zeta_{E,H} + \vec{\sigma}_\nu \cdot \left(\vec{\nabla} + \frac{e}{mc^2}\vec{E}, \vec{H}\right) \xi_{E,H} = 0 \tag{16b}$$

including the interaction of the neutrino with the electron. Writing $\xi_{E,H} = \mathrm{e}^{-i\omega t}\psi_{E,H}$ and $\zeta_{E,H} = \mathrm{e}^{-i\omega t}\chi_{E,H}$ in Eqs. (16a) and (16b) we derive stationary equations for$\psi_{E,H}$ and $\chi_{E,H}$; then we eliminate the equation for $\chi_{E,H}$ in favor of a second-order equation for $\psi_{E,H}$,obtaining equations for the neutrino wave functions which have the Helmholtz form

$$\left\{\nabla^2 + \frac{\omega^2 - \omega_\nu^2}{c^2} + \frac{e}{mc^2}\left[\vec{\nabla} \cdot \vec{E} + 2\vec{E} \cdot \vec{\nabla} + i\vec{\sigma}_\nu \cdot (\vec{\nabla} \times \vec{E}) + \frac{e}{mc^2}E^2\right]\right\}\psi_E = 0, \tag{17a}$$

$$\left\{\nabla^2 + \frac{\omega^2 - \omega_\nu^2}{c^2} + \frac{e}{mc^2}\left[\vec{\nabla} \cdot \vec{H} + 2\vec{H} \cdot \vec{\nabla} + i\vec{\sigma}_\nu \cdot (\vec{\nabla} \times \vec{H}) + \frac{e}{mc^2}H^2\right]\right\}\psi_H = 0, \tag{17b}$$

where we have used the identity, $(\vec{\sigma}_\nu \cdot \vec{A})\,(\vec{\sigma}_\nu \cdot \vec{B}) = \vec{A} \cdot \vec{B} + i\vec{\sigma}_\nu \cdot (\vec{A} \times \vec{B})$. On setting $\omega_\nu = 0$ the 0-mass, charge-neutral neutrino EOM is obtained. On setting $\vec{E} = \vec{H} = 0$ Dirac's 0-mass equation is recovered. The neutrino EOM given by Eq. (17b) has also been interpreted as the EOM for the radiant aspect of the electron, for which it has been used to calculate a divergence-free Lamb shift [11] and the electron's anomalous magnetic moment [12]. The material aspect of the electron is of course described by Dirac's equation, whose physical interpretation regarding the phenomena of matter versus antimatter states and of Zitterbewegung are discussed at length in previous work [13–15].

Notice that the proposed neutrino EOM agrees with observation that (a) the neutrino is a spin-1/2 particle, (b) the neutrino has zero mass (or for

$$\omega_\nu = \frac{m_\nu c^2}{\hbar} > 0$$

a finite mass m_ν to be determined from experiment), and (c) the neutrino interacts with the electron in a scaled electromagnetic interaction which is weaker than the electromagnetic interaction between charged particles such that it is sensible to investigate if the neutrino-matter interaction terms in Eqs. (17a) and (17b) arise from fundamental electroweak forces.

Finally, in order to highlight the structural similarity of the neutrino and electron EOM's, Dirac's equation for an electron in the presence of electro-magnetic fields follows if the 4-gradient in Eq. (8) for $(\Psi, \vec{\mathrm{X}})$ is replaced by the electron's 4-momentum as follows

$$(\gamma mc, -\gamma m\vec{\upsilon}) = \left(i\hbar \frac{\partial}{c\partial t} - \frac{e}{c}\Phi,\ i\hbar\vec{\nabla} + \frac{e}{c}\vec{A} \right), \tag{18}$$

where γ is the Lorentz factor, and the scalar and vector components of the 4-momentum on the left-hand side of Eq. (18) have been replaced by substitution using the classical relativistic expressions for the energy and canonical momentum, $\vec{P}$,

$$E = \gamma mc^2 + e\Phi, \tag{19a}$$

$$\gamma m\vec{\upsilon} = \vec{p} = \vec{P} - \frac{e}{c}\vec{A}, \tag{19b}$$

where the quantized forms of energy and the kinetic momentum have been used,

$$E \to i\hbar \frac{\partial}{\partial t}, \tag{20a}$$

$$\vec{P} \to -i\hbar\vec{\nabla}. \tag{20b}$$

The scalar product of the electron's 4-momentum and the 4-potential posited for the electron is,

$$\left(i\hbar \frac{\partial}{c\partial t} - \frac{e}{c}\Phi,\ i\hbar\vec{\nabla} + \frac{e}{c}\vec{A} \right) \cdot (\Psi, \vec{\mathrm{X}}) = \left(i\hbar \frac{\partial}{c\partial t} - \frac{e}{c}\Phi \right) \Psi + \left(i\hbar\vec{\nabla} + \frac{e}{c}\vec{A} \right) \cdot \vec{\mathrm{X}} = 0. \tag{21}$$

Using the same carrier-wave expansions for $(\Psi, \vec{\mathrm{X}})$ as we used in Eqs. (9) for a free electron we obtain,

$$\left(i\hbar \frac{\partial}{\partial t} - e\Phi - mc^2 \right) \psi(\vec{r}, t) + \vec{\sigma} \cdot (i\hbar c\vec{\nabla} + e\vec{A})\chi\,(\vec{r}, t) = 0, \tag{22a}$$

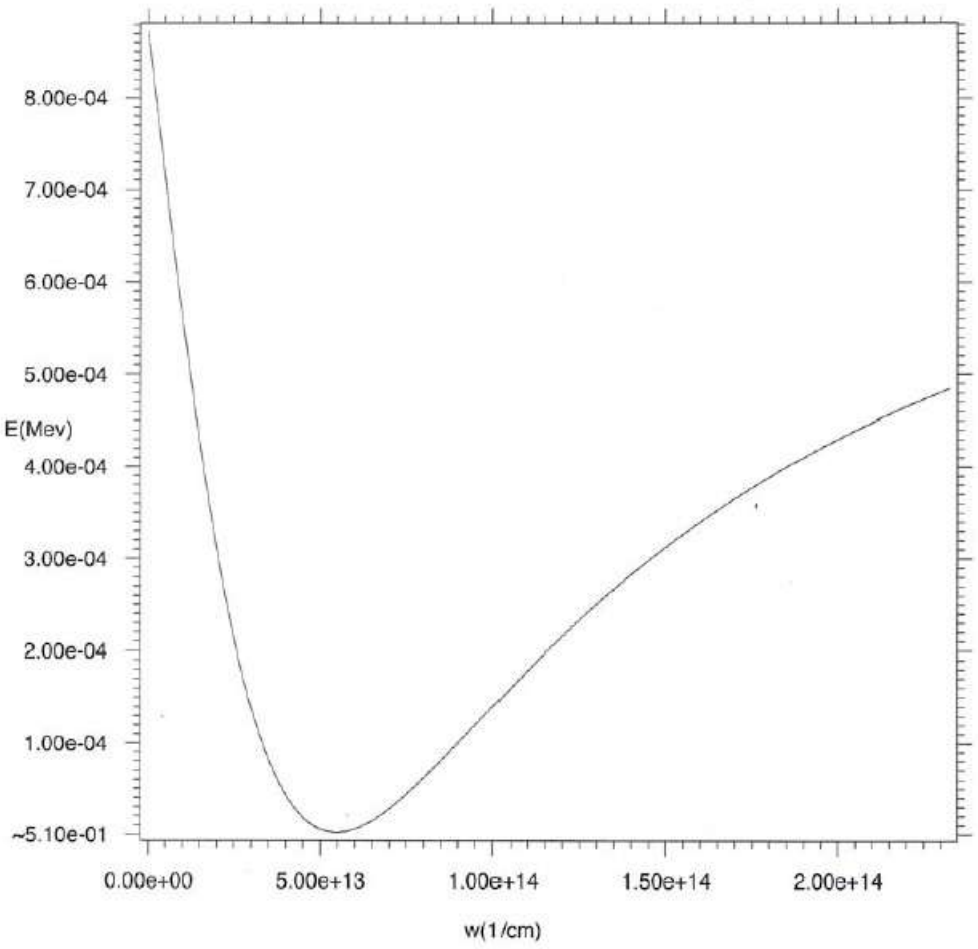

Figure 1. Electron energy versus variational parameter. The ordinate numbers above the origin are the energies in MeV to be added to 0.510 MeV at the origin. The binding energy is the energy difference from 0.511 MeV (positive-energy threshold) to the minimum of the well at 0.510 MeV or about 1 keV.

$$\left(i\hbar\frac{\partial}{\partial t} - e\Phi + mc^2\right)\chi(\vec{r},t) + \vec{\sigma}\cdot(i\hbar c\vec{\nabla} + e\vec{A})\,\psi(\vec{r},t) = 0, \tag{22b}$$

which is identically Dirac's equation on setting $\hbar\omega = mc^2$, $\vec{\mathrm{X}}_+(\vec{r},t) = \vec{\sigma}\,\chi(\vec{r},t)$, and $\vec{\mathrm{X}}_-(\vec{r},t) = \vec{\sigma}\,\psi(\vec{r},t)$. Notice that Eqs. (22a) and (22b) follow from Eq. (8) on renormalizing the 4-gradient as follows

$$\frac{1}{c}\frac{\partial}{\partial t} \to \frac{1}{c}\frac{\partial}{\partial t} - \frac{e}{i\hbar c}\Phi \qquad \text{and} \qquad \vec{\nabla} \to \vec{\nabla} + \frac{e}{i\hbar c}\vec{A}.$$

.

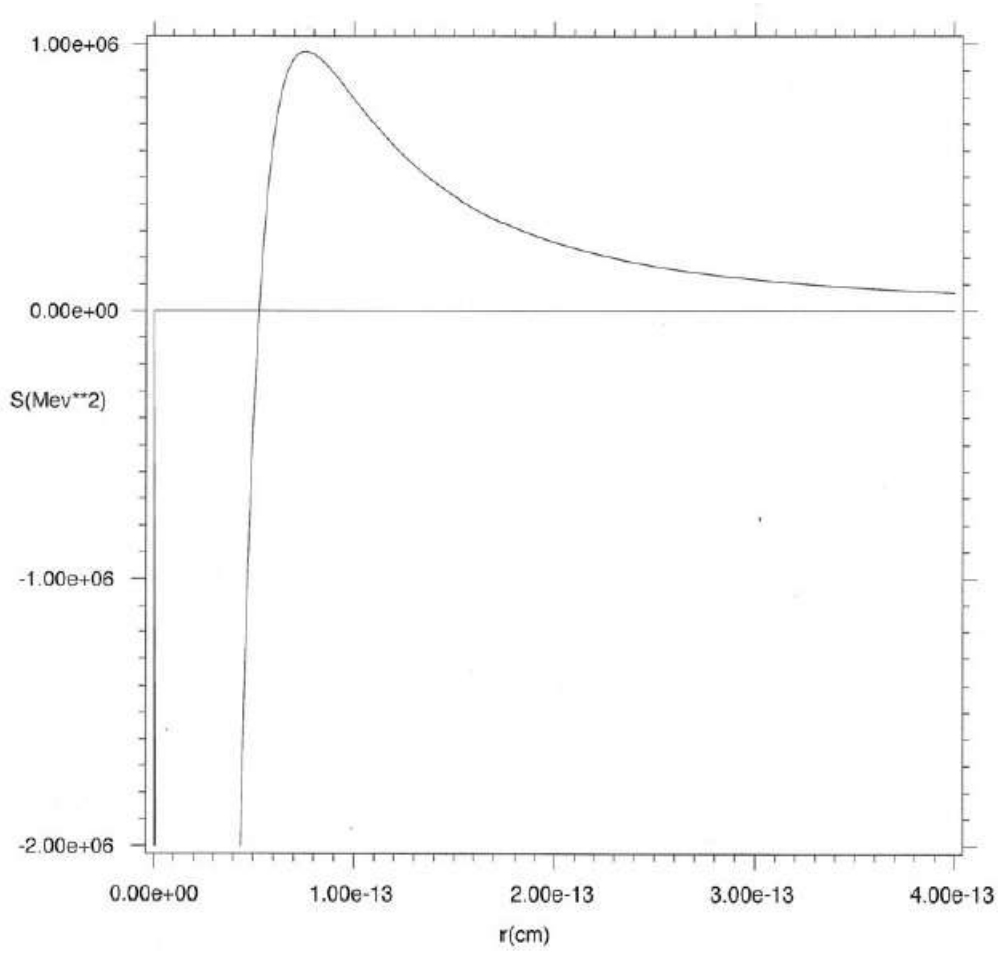

Figure 2. The "potential" function $S(r)$ in Eq. (28a) versus r. The rate of tunneling through the barrier is roughly equal to the reciprocal of the lifetime of the neutron ($\approx$ 15 min) for an energy behind the barrier $E_\nu = 1.7$ MeV.

3. Mutual Binding of the Neutrino and Electron

The EOM's for the neutrino and electron, as discussed in the previous section, are given respectively by Eq. (17a) and by the second-order form of Dirac's equation (Eqs. (22a) and (22b)) for $\Phi = 0$ as follows,

$$\text{neutrino}: \quad E_\nu^2\psi_E + \hbar^2c^2\left\{\nabla^2 + \frac{e}{mc^2}\left[\vec{\nabla}\cdot\vec{E} + 2\vec{E}\cdot\vec{\nabla} + \frac{e}{mc^2}E^2\right]\right\}\psi_E = 0; \tag{23a}$$

$$\text{electron}: \quad (E_e^2 - m^2c^4)\psi + \hbar^2c^2\left\{\nabla^2 - \frac{e}{\hbar c}\left[i\vec{\nabla}\cdot\vec{A} + 2i\vec{A}\cdot\vec{\nabla} + \frac{e}{\hbar c}A^2 - \vec{\sigma}\cdot\vec{H}\right]\right\}\psi = 0, \tag{23b}$$

where in Eq. (17a) $\omega_\nu = m_\nu c^2/\hbar = 0$ (neutrino assumed to have zero mass), $\omega = E_\nu/\hbar$, and only electrostatic interaction terms have been retained in both equations. Eq. (23b) is essentially Pauli's equation, which is Dirac's equation for $\Phi = 0$ and for $E_e^2 \cong m^2c^4 + 2mc^2E_{nr}$, where E_{nr} is an energy in the nonrelativistic regime. Notice that the interaction terms in the neutrino EOM are weaker by a factor of c^{-1} than the electromagnetic interactions of the electron EOM, such that they may possibly be associated with the electroweak interaction. This difference occurs due to the scaling of $e\vec{E}$ as a force (energy divided by length) in the neutrino EOM rather than to the scaling of $e\vec{A}$ as an energy in the electron EOM. The interaction of the neutrino with the electron is given by the electric field arising from the charge density of the electron (or positron), $e\vec{E} = -\vec{\nabla}V$, where

$$V = e^2\left[\frac{1}{r}\int_0^r \mathrm{d}r' r'^2(G_{-1}^2 + F_{-1}^2) + \int_r^\infty \mathrm{d}r' r'(G_{-1}^2 + F_{-1}^2)\right], \tag{24}$$

where the electronic density is that inferred from Dirac's equation using the large and small components of Dirac's wave function for the electron $\psi = G_\kappa(r)\chi_{\kappa\mu}(\theta,\phi)$ and $\chi = iF_\kappa(r)\chi_{-\kappa\mu}(\theta,\phi)$. The interaction of the electron with the neutrino is given solely by the A^2 interaction and the Pauli interaction $\vec{\sigma}\cdot\vec{H}$ since $\vec{\nabla}\cdot\vec{A} = 0$, which is demonstrated below, which means that the $\vec{A}\cdot\vec{\nabla}$ term also gives a zero contribution by parts integration of its expectation value. The A^2contribution is found to be negligible compared to the Pauli contribution. The magnetic field interaction of the electron with the neutrino is calculated from Maxwell's equation,

$$\nabla^2\vec{A} = -\frac{4\pi e}{c}\vec{j}_\nu,, \tag{25}$$

where the current arises from the permanent magnetic moment due to the neutrino's spin, $\vec{j}_\nu = c(\xi_E^+\sigma_\nu\varsigma_E + \varsigma_E^+\sigma_\nu\xi_E)$, which follows from Eqs. (16a) and (16b) due to the Dirac form of the neutrino EOM, such that the spinor analysis for the neutrino is the same as that for the electron, for which $\xi_E = g_\kappa(r)\chi_{\kappa\mu}(\theta,\phi)$ and $\varsigma_E = if_\kappa(r)\chi_{-\kappa\mu}(\theta,\phi)$. The radial parts for the electron are of course different and are given by $G_{-1}(r)$ and $F_{-1}(r)$ for the large and small components, respectively. The cartesian components of the current for $\kappa = -1$ are

$$j_{\nu x} = \frac{c}{2\pi}\hat{y}R, \quad j_{\nu y} = -\frac{c}{2\pi}\hat{x}R, \quad \text{and} \quad j_{\nu z} = 0,$$

where $R = g_{-1}(r)\,f_{-1}(r)$. Finding the divergence of both sides of Eq. (25) the reader may easily verify that $\vec{\nabla}\cdot\vec{A} = 0$ due to the transverse nature of the current. The magnetic field is found by taking the curl of both sides of Eq. (25),

$$\nabla^2\vec{H} = -\frac{4\pi e}{c}\vec{\nabla}\times\vec{j}_\nu. \tag{26}$$

Only the diagonal or z-component of $\vec{H}$ is considered here; the z-component of the curl of the current is given by

$$\left(\vec{\nabla}\times\vec{j}_\nu\right)_z = \frac{c}{2\pi}\left[2\frac{R}{r} + \left(R' - \frac{R}{r}\right)\sin^2\theta\right],$$

where the prime denotes derivative with respect to r. Solving Eq. (26),

$$H_z = \frac{4}{3}e\left[\frac{1}{r}\int_0^r \mathrm{d}r' r'^2\left(R' + 2\frac{R}{r'}\right) + \int_r^\infty \mathrm{d}r' r'\left(R' + 2\frac{R}{r'}\right)\right]. \tag{27}$$

Proceeding heuristically the radial equations (for $\kappa = -1$) are solved variationally using the unnormalized trial forms $G_{-1}(r) = \mathrm{e}^{-wr}$ and $g_{-1}(r) = \mathrm{e}^{-w'r}$ for the "large" components, where $w = 1.15w$'. The "small" components are calculated using the trial forms,

$$f_{-1}(r) = \frac{\hbar c}{m_p c^2} g_{-1}^{'} \quad \text{and} \quad F_{-1}(r) = \frac{\hbar c}{mc^2} G_{-1}^{'}$$

for the neutrino and electron respectively, where m_p is the proton mass, which is the only empirical parameter in the calculation. The electron energy versus the variational parameter w is shown in Fig. 1, in which the minimum energy lies below 0.511 MeV indicating binding to the neutrino with binding energy of about 1 keV. Notice that the minimum energy occurs for w approximately equal to the reciprocal of the proton Compton wavelength, $w \cong m_p c/\hbar$, which is consistent with our choice in the denominator of the variational form for $f_{-1}(r)$ given above. Indeed the scaling of

$$f_{-1}(r) \quad \text{as} \quad f_{-1}(r) = -\frac{\hbar c w'}{m_p c^2} g_{-1}(r) \cong -g_{-1}(r),$$

in which the large denominator $m_p c^2$ is cancelled by the numerator $\hbar c w$ near the minimum of the electron energy versus$w$ (Fig. 1), is consistent with the inverse relationship of particle range and particle mass in particle theory. Once the derivative operation has been carried out on the trial function Eq. (23a) has the standard Schroedinger form,

$$\left[E_\nu^2 + \hbar^2 c^2 \nabla^2 - S(r)\right] \psi_E = 0, \tag{28a}$$

$$S(r) = -\frac{e^2 \hbar^2}{m} \left(\rho_r + \frac{V'}{e^2} w' + \frac{1}{mc^2 e^2} V'^2\right), \tag{28b}$$

where $S(r)$ is plotted versus r in Fig. 2. The first and third terms on the right-hand side of Eq. (28b) are attractive while the second term is repulsive such that a neutrino can bind to an electron or positron behind the potential barrier shown in Fig. 2. Standard WKB theory [16] can be used to estimate the energy levels behind the barrier and the tunneling rate through the barrier, whence

$$I = \int_{r_1}^{r_2} \mathrm{d}r \sqrt{\kappa_\nu^2 - \frac{S(r)}{\hbar^2 c^2}} = \left(n + \frac{1}{2}\right)\pi, \tag{29}$$

where $\kappa_\nu = E_\nu/\hbar c$ and the limits of integration are over the classical region in which the argument under the square-root sign is positive, and

$$R = \frac{\hbar}{m} \frac{\mathrm{e}^{-2\int_{r_2}^{r_3} \mathrm{d}r \sqrt{\frac{S(r)}{\hbar^2 c^2} - \kappa_\nu^2}}}{4\int_{r_1}^{r_2} \mathrm{d}r \left[\kappa_\nu^2 - \frac{S(r)}{\hbar^2 c^2}\right]^{-1/2}} \ \mathrm{s}^{-1}, \tag{30}$$

where the integration limits in the exponential term are over the barrier width For the value of w giving the minimum electron energy in Fig. 1 ($w \cong m_p c/\hbar$) an energy E_ν is chosen for which the reciprocal of the tunneling rate is nearly equal to the lifetime of the neutron. The calculated rate is 8.41×10^{-4} s^{-1}, whose reciprocal gives a lifetime

of 1.19×10^3, which is close to the observed lifetime of nearly fifteen minutes. In Eq. (29) this rate corresponds to 1.7 MeV and a principal quantum number close to $n = 3$. The rate would of course be slower for smaller n and faster for larger n. In atomic units the numerator in Eq. (30) is 1.52×10^{-30} and the integral in the denominator is 1.87×10^{-11}, such that the quotient is 2.34×10^{-20}, which, converted to CGS units by division by the atomic unit of time, 2.42×10^{-17}, gives the the rate cited above.

4. Conclusions

An EOM has been presented for the neutrino which contains an interaction with charged matter. For zero interaction with matter the EOM reduces to the zero-mass Dirac equation, which is the generally accepted EOM for the neutrino. I believe that the postulated bosons, which we denote by the symbol $W_s^{\pm}$ for binding of a neutrino and a positron (+) or of a neutrino and an electron (−) and for spin s equal to 0 or 1, since they discover the mass, length, and lifetime scales of a nucleon, should be useful in future work as building blocks to construct a nucleon with constituents physically equivalent to quarks and intermediate force-carrier bosons.

Acknowledgements

The author is grateful to T. Scott Carman for supporting this work. He is grateful to Professor John Knoblock of the University of Miami and to Dr. Ray Garrett of the University of Tennessee for seminal discussion. This work was performed under the auspices of the Lawrence Livermore National Security, LLC, (LLNS) under Contract No. DE-AC52-07NA27344.

References

[1] B. Ritchie, *J. Condensed Matter Nucl. Sci*. **11** (2013) 101.
[2] Xing Z. Li, Jian Tian, Ming Y. Mei and Chong X. Li, *Phys. Rev. C* **61** (2000) 024610; Xing Z. Li, Bin Liu, Si Chen, Qing Ming Wei and Heinrich Hora, *Laser Part. Beam* **22** (2004) 469.
[3] Xing Z. Li, Qing M. Wei, Bin Liu and Shao L. Ren, *J. Condensed Matter Nucl. Sci.* **I** (2007) 11.
[4] J. D. Bjorken and S. D. Drell, *Relativistic Quantum Mechanics* (McGraw-Hill, New York,1964), p. 18.
[5] P. Morse and H. Feshbach, *Methods of Theoretical Physics* (McGraw-Hill, New York, 1953), p. 208.
[6] The matter tradition of quantum physics also includes the Dirac–Feynman path-integral reformulation of quantum theory starting with the action, which is possibly going in the wrong direction since a wave theory of natural phenomena would be more closely associated with electrodynamics than with mechanics. For example see B. Ritchie, *J. Mod. Optics* **55** (2008) 2003.
[7] C.G. Darwin, *Proc. Roy. Soc.*. **118** (1928) 654–680.
[8] O. Laporte and G. Uhlenbeck, *Phys. Rev.* **37** (1931) 1380–1397.
[9] R. Armour, Jr., *Found. Phys.* **34** (2004) 815–842 and references therein.
[10] B. Ritchie, *Optics Commun.* **262** (2006) 229–233.
[11] B. Ritchie, *Optics Commun.* **280** (2007) 126; *Int. J. Quantum Chem*. **112** (2012) 2632.
[12] B. Ritchie, *Optics Commun.* **281** (2008) 3492.
[13] B. Ritchie and C. Weatherford, *Int. J. Quantum Chem.* **2012**, DOI10.1002/qua.24156.
[14] A.B. Evans, *J. Cond. Matter Nucl. Sci.* **2** (2009) 7; *Found. Phys*. **28** (1998) 291; *Found. Phys*. **21** (1991) 633; *Found. Phys.* **20** (1990) 309; and references therein. This author uses the proper time from classical relativity to implement time-dependent Dirac theory as a 4-space theory. It is found in [10] that a geometric space–time or 4-space solution evolves naturally on solving the time-dependent Dirac equation in 3-space and the scaled time, *ct*. The electronic density is positive definite in our theory.
[15] R. Gerritsma, G. Kirchmair, F. Zaehringer, E. Solano, R. Blatt and C. Roos, *Nature* **463** (2010) 68.
[16] H.A. Bethe and E.E. Salpeter, *Quantum Mechanics of One- and Two-Electron Atoms* (Dover, New York), p. 238.

J. Condensed Matter Nucl. Sci. 12 (2013) 54–68

Research Article

Simulation of Crater Formation on LENR Cathodes Surfaces

Jacques Ruer *

Abstract

Many authors reported the presence of small-size craters on the surface of cathodes after Low-energy Nuclear Reaction (LENR) electrolysis experiments. It is conjectured the craters result from violent reactions, perhaps of nuclear origin. Nagel proposed a correlation between the crater diameter and the energy involved in its formation. Starting from this assumption, it can be estimated that the enthalpy released can raise the temperature of the crater content to about 2000 K. A simple model is used to calculate the crater cooling by conduction and radiation. It gives the order of magnitude of the maximum event duration in order to achieve some melting of the cathode material. The duration of the eruption is estimated from the gas pressure developed within the crater. A value of 6 ns is obtained for a 2 μm diameter, and 600 ns for a 20 μm crater. In large craters, a part of inner material can be molten. Small craters are strongly cooled by the surrounding metal and do not show signs of fusion.
 ISSN 2227-3123

Keywords: Cooling, Craters , Explosion, LENR, Melting

1. Introduction

Several authors observed small-size craters on the surface of metals after electrolysis experiments. They have been reported on different metals, but mostly on palladium cathodes [1–5].

The morphology of these structures is very similar to the craters created by the impact of high-speed objects, like meteorites or bullets [6]. A round shaped void can be seen with the periphery protruding from the original surface. In the case considered here, the dimensions of the craters are small, in the range of a few micrometres to a few tens of micrometres.

The similarity of the shape of these craters with the large ones raises the question of the phenomenon responsible for their formation. It is tempting to assume that local reactions led to the melting and eruption. Elemental analysis in and near the craters suggests that the craters could mark the location of LENR events [2–5]. The relation between the presence of craters and excess heat is not yet fully established [6]. However, craters are frequently seen on cathodes, which gave excess heat. The simple fact that craters could be the sites of creation of at least a fraction of the LENR energy makes it interesting to further investigate the question of the energetics and dynamics of their formation.

This paper presents some estimations of the typical time scales involved for the different phenomena taking place during the formation of craters and discusses the main results.

*E-mail: jsr.ruer@orange.fr

 ISSN 2227-3123

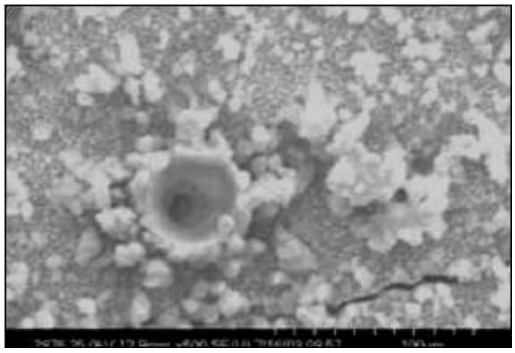

Figure 1. Large crater with a rounded shape. There are evident signs of melting of the ejected material, some of it solidified around the crater rim. The diameter is 50 μm. The original point of the explosion seems to be located several tens of μm below the surface [3].

2. Examples of Craters Observed on Palladium Cathodes of LENR Experiments

Nagel discussed the different types of craters observed [6]. The observed diameters are generally between 2 and 50 μm, and a few are larger. In most cases, the craters exhibit a circular shape. The ratio between the crater depth and diameter ranges between 0.5 and 5.

3. Energy of Crater Formation

Kim [7] calculated the energy required to melt or vaporize the quantity of metal located in a cone having the dimensions of the crater considered. For a crater with a diameter of 50 μm and a depth of 25 μm, the energy calculated is 3.2×10^{-5} J, if we consider that the metal is molten, or 6.5×10^{-4} J if the metal is vaporized. Assuming these energies result from D–D fusion into He^4, they correspond respectively to 8.3×10^6 and 1.7×10^8 nuclear reactions.

Nagel [6] compared the dimensions of craters of very different origins and the energy involved for their formation. A simple correlation can be drawn between the size and the energy. The relationship obtained is reproduced in Fig. 5. Nagel compared the values given by Kim with his own investigations. The orders of magnitude agree quite well. The energy given by the correlation falls between the values calculated assuming melting and vaporization.

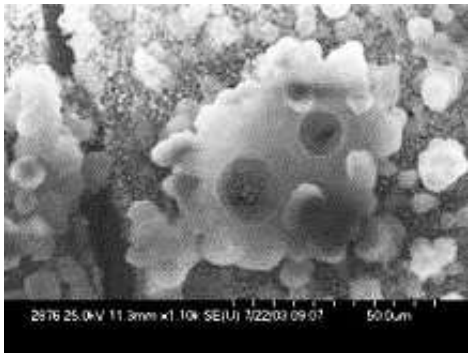

Figure 2. Two adjacent craters, 15 and 10 μm in diameter. The larger one is fully rounded, while a hexagonal shape can still be recognized in the small one. Although both embedded within a common mass of molten material, they do not seem to be obviously correlated [3].

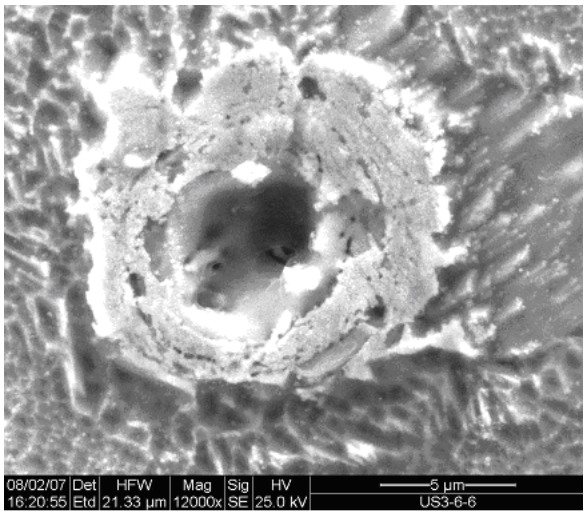

Figure 3. Micrograph showing a 6 µm diameter crater. One can notice the round shape, the concentric rings of ejected material and the deformation of the surrounding metal surface [5].

In the following, we assume that the energy required for cratering is given by the correlation of Fig. 5. The corresponding energy is 10^{-3} J for a crater 100 μm diameter and 50 μm deep, with a volume of 1.31×10^5 μm^3. The energy density is then 7.6×10^9 J m^{-3}, or 640 kJ kg^{-1}. Accordingly, the correlation can be described by the equation:

$$E_i = \alpha_i \cdot V, \tag{1}$$

where E_i is the energy input (J), $\alpha_i = 7.6 \times 10^9$ J m^{-3} (equivalent to 640 kJ kg^{-1}) and V is the crater volume (m^3).

Figure 6 shows the relationship between the temperature and the specific enthalpy of palladium [8]. It can be seen that the enthalpy mentioned above corresponds to a temperature close to 2000 K.

4. Simple Modelling of the Main Phenomena

4.1. Basis of the simulation

The estimation of the energy does not give information about the kinetics of the crater formation. The simple model presented here gives some insight.

The only features, which can be observed, are the craters left after the eruption. The precise sequence of the phenomena cannot be directly observed, but can at most be derived from a simulation.

The only things known at the beginning are as follows:

- Craters are present on the surface, showing that some material is ejected away from the cathode.
- The largest craters have a circular shape and show signs of melting.
- The smallest ones may have a non-circular shape and do not exhibit traces of molten metal.
- According to Nagel and the discussion of the previous paragraph, the energy involved in the crater formation corresponds to the heating of a hot core up to 2000 K before the eruption.

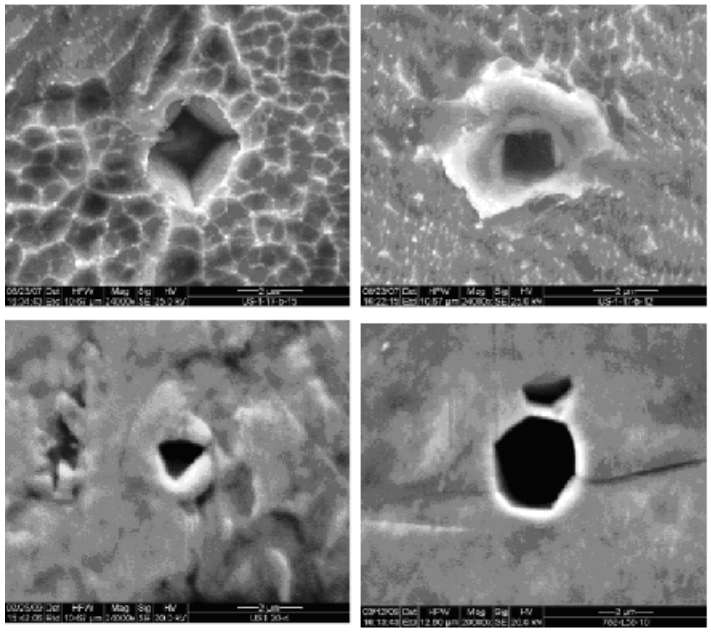

Figure 4. Micrographs of small craters from Super-wave experiments by M. Tsirlin . Published by Nagel [6]. The diameters range from 1µm to 2 µm. There are no signs of melting. The shapes appear to be influenced by the cathode crystal structure.

The simulation must be able to explain these observations. We are going to follow three distinctive steps in order to introduce the main phenomena

- In the first step, we examine the temperature evolution of a hot core before the eruption. This will show that a hot core having small dimensions cools down very fast. The cooling time gives a upper bound of the possible LENR event duration.

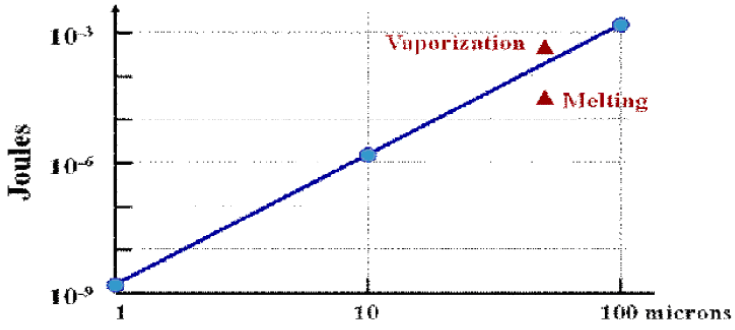

Figure 5. Correlation between the crater diameter and the energy necessary for its formation [6].

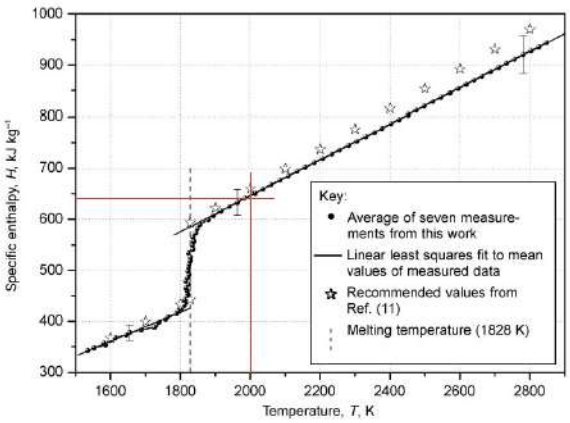

Figure 6. Specific enthalpy of palladium [8] The value α_i from Eq. (1) is indicated. It corresponds to a heating of the metal up to 2000 K.

- The dynamics of the eruption is evaluated. The comparison of the time required for the ejection of the crater content and of the cooling time explains why melting is only observed in large craters
- The fact that most craters are circular suggests that the initial LENR sites are smaller than the craters observed on the surface. The logical consequences of this last assumption are discussed.

At this stage, the model uses very rough assumptions. However, they are enough to find out the orders of magnitude of the different phenomena involved:

(1) Thermal flow between the crater and the surrounding metal
(2) Heat radiated out of the crater considered as a black body
(3) Eruption and ejection of the crater content

4.2. Hot core cooling

A small volume with dimensions of a few micrometres cools down very fast. The purpose of the simulation is to obtain a quantitative figure of the duration during which a hot core can retain a high temperature. Obviously, the duration of the LENR event responsible for the formation of the hot core must be shorter than the cooling time, otherwise the energy is dissipated away while it is released by the LENR event and the hot core temperature remains limited.

4.2.1. *Thermal flow by conduction*

We assume that the energy input is supposed to be confined in a spherical core which has the same volume as the final crater. The energy is in the form of enthalpy within the material contained inside the crater just before the eruption and is given by Eq. (1). The heat is transferred to the surrounding metal by conduction.

In order to simplify the calculation, we consider in a first approach that the hot core is deeply embedded below the surface, as shown in Fig. 7. The reaction does not create a crater on the surface and cooling only results from conduction in the solid metal surrounding the hot core.

Hypotheses:

- The matrix is made of palladium.

Table 1. Palladium properties.

Density	12 023 kg m^{-3}
Melting	1555°C = 1828 K
Boiling	2963°C = 3236 K
Specific heat	245 J kg^{-1} K^{-1}
Thermal conductivity	71 W m^{-1} K^{-1} at 20°C
Velocity of sound	3070 m s^{-1}

- Before the reaction, the base metal is a solid body.
- The reaction takes place uniformly throughout the core, a sphere with a radius, R.
- No eruption takes place.
- The energy input E_i is proportional to the core volume, as per Eq. (1).
- The reaction evolves at a constant pace, during a reaction time τ. This duration is taken as a variable to study its influence.
- The energy is transferred by conduction.
- The heat capacity and the thermal conductivity are constant, taken for pure palladium

The last hypothesis neglects the fact that the metal is loaded with deuterium. This simplification is addressed below. It should not alter the orders of magnitude of the results.

The heat flow is computed according to a spherical model using the Fourier equation of heat conduction, see Fig. 8. Within the core with a radius R, some energy α_i is released per unit volume. It is assumed that this energy evolves at a constant pace during the reaction time τ. Between time $t = 0$ and time $t = \tau$ the reaction creates in the volume $\mathrm{d}V$ a local energy input $\mathrm{d}W$:

$$\frac{\mathrm{d}W}{\mathrm{d}V} = \frac{\alpha_\mathrm{i}}{\tau}\,\mathrm{d}t. \tag{2}$$

The solid taken into account in the model has the properties of pure palladium, as listed in Table 1.

In fact, in LENR experiments, the palladium is loaded with deuterium, so that at least a part of the metal is transformed into hydride PdD_x. The values of x are larger than 0.6 and can be close to 1. The properties of the hydride differ from metallic Pd. In particular, the density is lower, about 10^4 kg m^{-3}. The other properties are not well known.

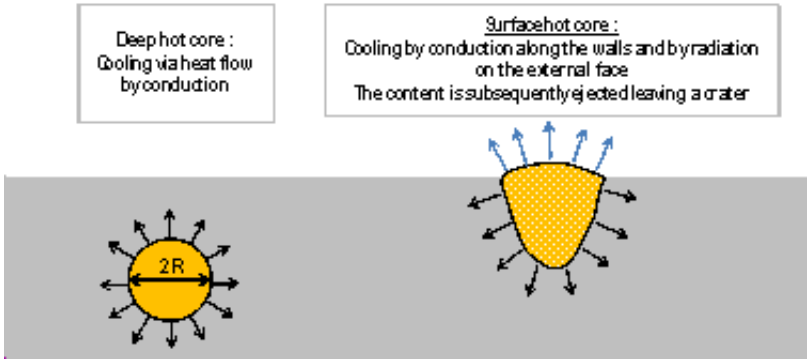

Figure 7. Schematic representation of hot core cooling – The hot core is the volume heated up to 2000 K by the LENR event – defined by Nagel's equation.

In any case, as only the orders of magnitude are calculated, the precise characteristics are not absolutely necessary at this stage, so that pure palladium properties are used for this first approach.

The results of the heat flow model are presented for two different core diameters: 2 and 20 μm. The energy inputs E_i are proportional to the volumes according to Eq. (1). They are, respectively, 2.12×10^{-8} and 2.12×10^{-5} J.

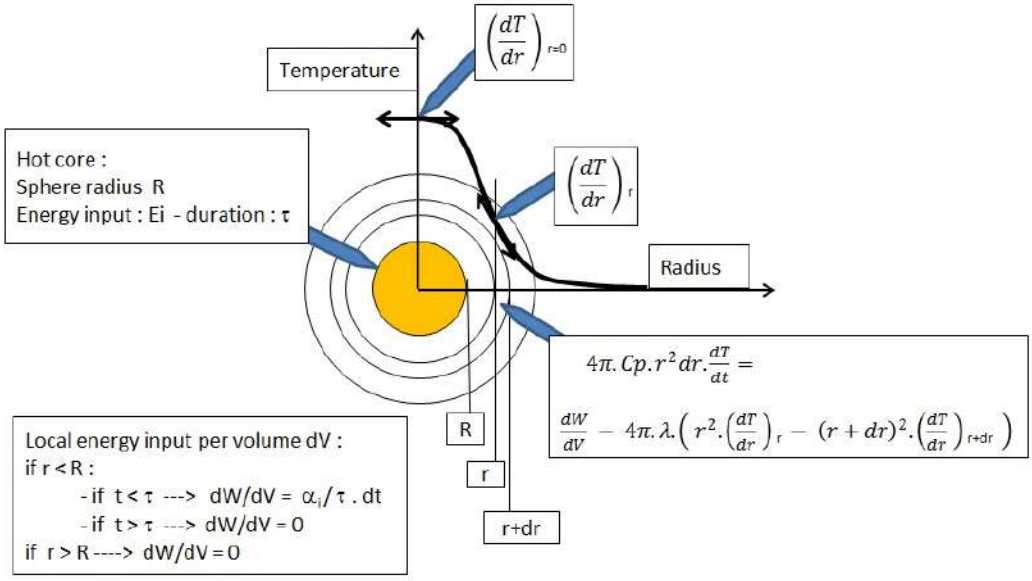

Figure 8. Schematic representation of the heat flow model.

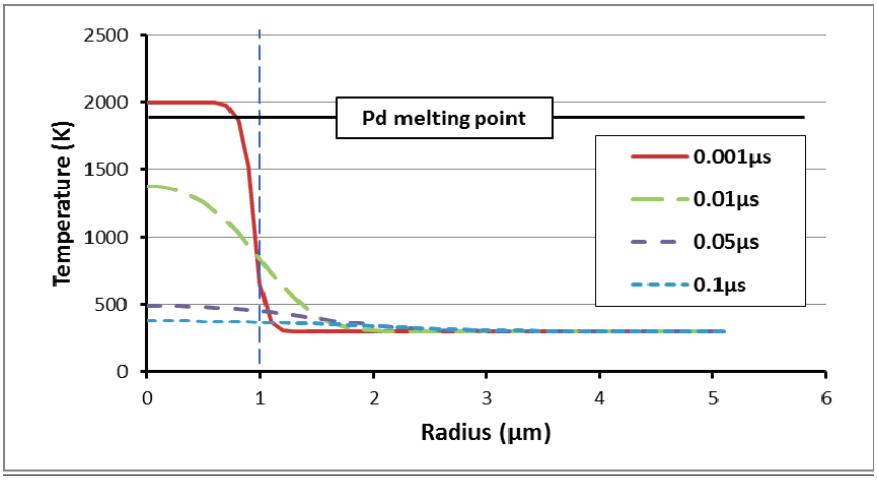

Figure 9. Evolution of the temperature for a 2 μm diameter core – Assumed reaction time is 0.001 μs.

The temperature reaches a maximum at the end of the reaction time τ .

If τ is small, as shown in Fig. 9 for τ = 1 ns and Fig. 11 for τ = 100 ns , the heat loss towards the surrounding metal is still very limited at the end of the reaction. Most of the energy is still confined within the core and the temperature reaches 2000 K in both cases, as can be deduced from Eq. (1) and Fig. 6.

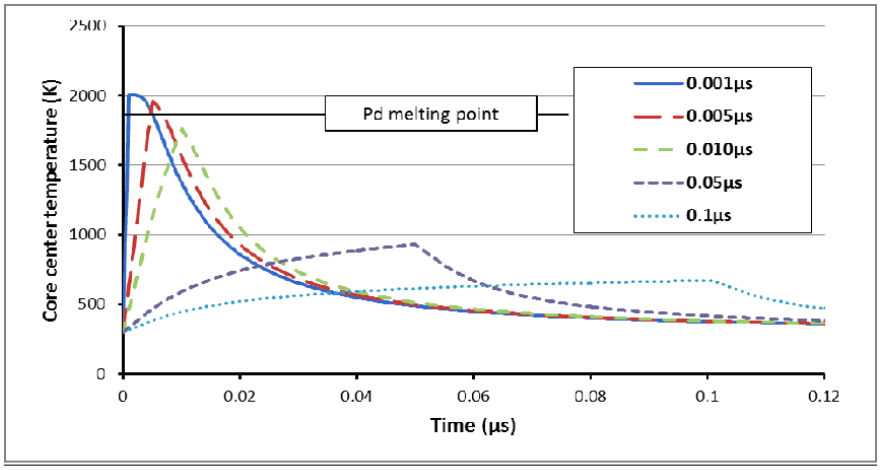

Figure 10. Evolution of the temperature at the centre of a 2 μm core – Influence of the reaction time.

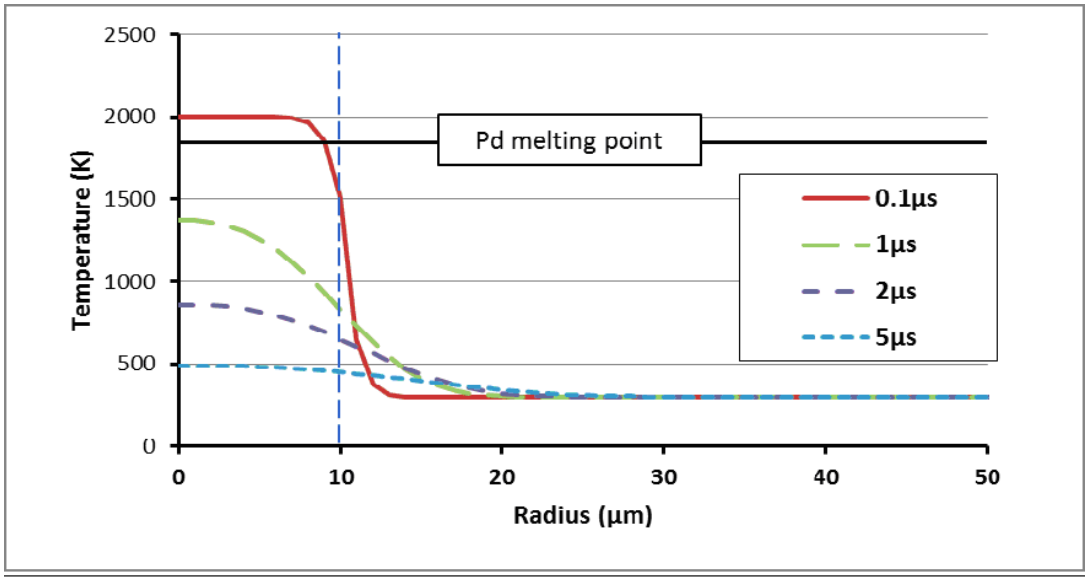

Figure 11. Evolution of the temperature for a 20 μm diameter core – Assumed reaction time is 0.1 μs.

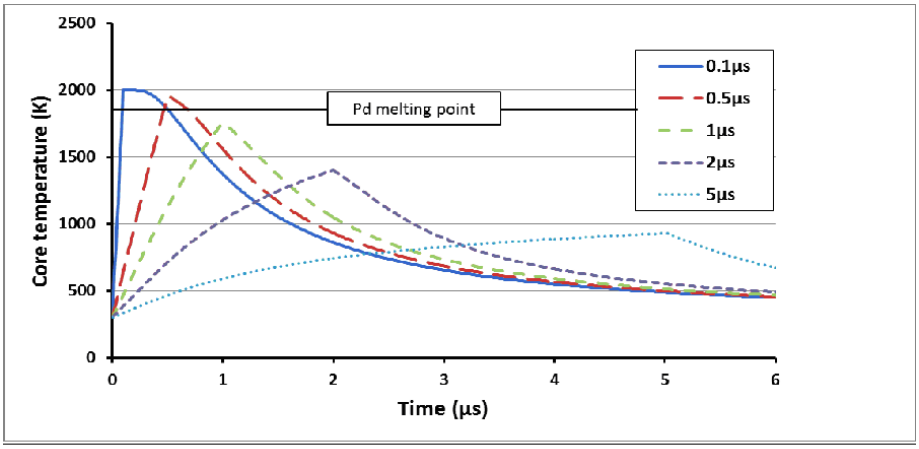

Figure 12. Evolution of the temperature at the centre of a 20 μm core – Influence of the reaction time.

The subsequent cooling by conduction is, however, very rapid. If we define $t_{1/2}$ the time necessary to reduce by half the temperature rise of the core centre, Figs. 10 and 12 show that $t_{1/2}$ is 0.013 μs for the 2 μm core and 1.3 μs for the 20 μm core. We can generalize :

$$t_{1/2} = 3250\, d^2, \tag{3}$$

where d is the hot core diameter.

If we use longer reaction times τ, the maximum temperatures reached at the end of the reaction are markedly lower. Conduction takes away the heat as it evolves. Nagel's correlation does not depend on the time. This can be easily explained by this model if we accept that the reaction time τ is probably very short.

τ is probably less than 6×10^{-9} s for the 2 μm crater and less than 6×10^{-7} s for the 20 μm crater. From that, we can even derive a criteria giving the maximum value of τ as follows :

$$\tau < 1500\, D^2, \tag{4}$$

where τ is the maximum value of the reaction time (s), and D the crater diameter (m).

This relation does not mean that the reaction kinetics depends on the crater dimension. It only indicates what the longest duration can be. It may be faster, with no relation to the size. However, this equation shows that very small craters can only be created by very fast reactions.

4.2.2. *Hot spot cooling by radiation*

When the reaction takes place close to the surface, a crater is formed. The surface exhibits a hot spot at this location and the crater ejects some material.

Let us first consider the energy loss into the environment. Because of the high temperature, the hot spot radiates strongly, so that it is necessary to evaluate how much energy the hot core looses by radiation. To do this we assume that:

- The hot spot is a flat circular disk with the same diameter as the crater (an overestimate).

- The temperature is 2000 K.
- The duration is $t_{1/2}$ as per Eq. (3).
- The hot spot radiates like a black body.

The Stefan–Boltzmann equation gives the quantity of energy E_r lost by radiation:

$$E_r = \frac{\pi}{4} D^2 \sigma T^4 t_{1/2}, \tag{5}$$

where D is the crater diameter, σ the Stefan–Boltzmann constant (5.67×10^{-8} W m^{-2} K^{-4}).

We find $E_r = 3.7 \times 10^{-14}$ J for the 2 μm crater and $E_r = 3.7 \times 10^{-10}$ J for the 20 μm crater. These values are orders of magnitude lower than E_i. We can therefore conclude that radiation cooling is not a relevant factor in this problem.

4.3. Crater eruption

We now have to examine the crater eruption itself. If the material originally located inside the crater is ejected, this is because mechanical forces are acting on it. It can be assumed that the driving force results from the evolution of gases within the crater. The sources of gas may be:

- Metal vapour resulting from the high temperature.
- Hydrogen (deuterium) present in the palladium hydride.
- Nuclear reaction products.

In the above, it is considered that the temperature reached at the beginning of the crater eruption is about 2000 K. This is much below the palladium boiling point (3236 K). Therefore, the palladium vapour pressure is probably low during the eruption itself.

The quantity of nuclear ashes is probably negligible and can be disregarded.

When LENR reactions are observed, the palladium is heavily loaded with deuterium. At high temperature, the hydride is dissociated [9]. The solubility of deuterium is known to decrease as the temperature increases. In our case, during the eruption, the palladium is molten. The gas pressure build-up is difficult to quantify, because the reaction is very rapid. It is unclear how fast the atoms of deuterium present in the liquid phase combine into D_2 molecules, how gas bubbles can germinate, etc.

Facing these difficulties, we are again obliged to use a very simple model in an attempt to find out the main orders of magnitude of the eruption mechanism.

Should the quantity of hydrogen (deuterium) contained in the hydride instantaneously evolve as gas, the local pressure could be estimated as follows:

- Mass of hydride : 10^4 kg m^{-3} $= 8.85 \times 10^4$ mol PdD per cubic meter.
- If the gas is released as monoatomic hydrogen, considered as a perfect gas, the equivalent pressure of the gas would be 1.98×10^3 bar at 0°C. Because the temperature is 2000 K, the gas pressure may be as high as 1.45×10^4 bar.

The actual pressure is difficult to assess. We can nevertheless estimate that the pressure is quite high, possibly ranging between 100 and 20,000 bar.

The mechanism of eruption is probably complicated, but as we are only looking after approximations, the following *ad hoc* model is a first approach:

- The gas pressure P is taken as a variable to study its influence.

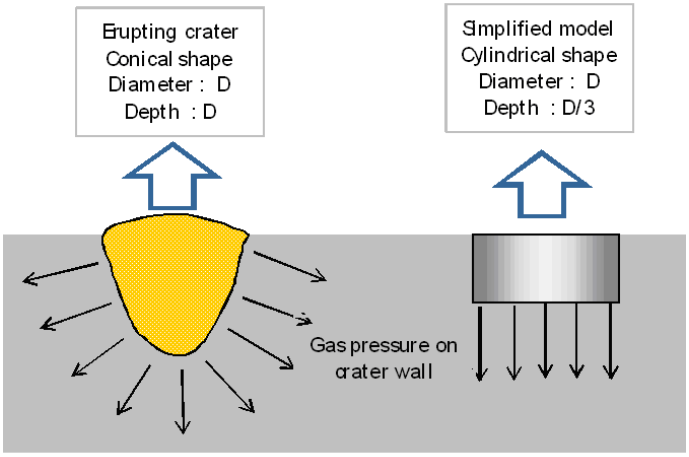

Figure 13. Schematic view of a crater in eruption and simplified modelling. The cylinder in the model has the same volume as the crater.

- The pressure is constant during the eruptive phase and appears instantly.
- The crater having a diameter D is represented by a cylinder perpendicular to the surface, with the same diameter D and a depth $D/3$ to account for the fact that the actual crater has a conical shape, see Fig. 13.
- The gas pressure is exerted on the bottom face of the cylinder and creates a force pushing out the content of the cylinder, as if it were solid.

The eruption duration is defined as the time required to lift the cylinder along a distance equal to its height $D/3$.

We can write the force F exerted at the base of the cylinder:

$$F = \frac{\pi}{4} D^2 P = m\gamma = \frac{\pi}{12} \rho D^3 \gamma, \tag{6}$$

where P is the gas pressure and γ is the acceleration of the cylinder.

The time t_e required to travel the distance $D/3$ during the eruption is:

$$\frac{1}{2}\gamma t_e^2 = \frac{D}{3}. \tag{7}$$

Replacing the value of γ obtained in Eq. (5), we get:

$$t_e^2 = \frac{2}{9}\rho \frac{D^2}{P}. \tag{8}$$

Taking $\rho = 10^4$ kg m^{-3} for the hydride, it gives:

$$t_e = 47.1\, D\, P^{-0.5}. \tag{9}$$

Figure 14 shows the eruption time calculated for different diameters and pressures.

It is instructive to compare the values of t_e with the values of τ given by Eq. (3). Both values are equal when the following equations are satisfied :

$$1500\, D^2 = 47.1\, D\, P^{-0.5}, \tag{10}$$

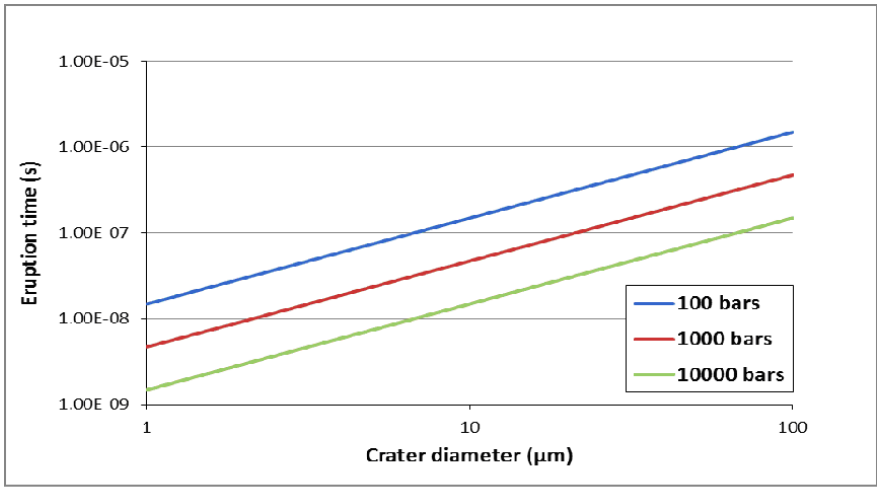

Figure 14. Eruption time calculated for different crater diameters and gas pressures.

$$D = 0.03P^{-0.5}. \tag{11}$$

For example, if the gas pressure is 1000 bar (10^8 Pa), we have $D = 3$ μm.

Craters smaller than this value are cooled down before the eruption is completed. They cannot contain molten material because the metal is quenched by the wall as the eruption proceeds. Larger craters erupt faster than they cool, so that molten material is present in the ejected debris.

5. Discussion of the Results

The correlation established by Nagel gives the energy input for the formation of micro-craters, as seen on the palladium cathodes of LENR experiments.

The simplified modelling approach presented here lacks precision, but gives the orders of magnitude of the time scales of the related phenomena. The event duration ranges from a few nanoseconds to less than a microsecond depending on the crater size.

The cooling of small craters is very fast. It may be so fast that the LENR energy is dissipated by conduction before the temperature reaches the metal melting point. The gas released must however find its way to the outside, tearing off the base metal.

In larger craters, the energy results in the melting of at least a part of the crater content, which is subsequently blown away by the gas, see Fig. 15.

This simple model may explain why the small craters shown in Fig. 4 do not exhibit signs of melting, while the large ones in Figs. 1 and 2 show accumulation of molten metal around the rim.

This model does not give any hint of the LENR mechanism itself. However, the occurrence of such craters, assuming they result from LENR events, invites the following remarks, most of them already pointed out by Nagel [6] :

- LENR reactions are said to be related to some particular behaviour of deuterium atoms incorporated in Pd crystalline structure. The Pd crystals are not rounded, contrary to the large craters. This means that the

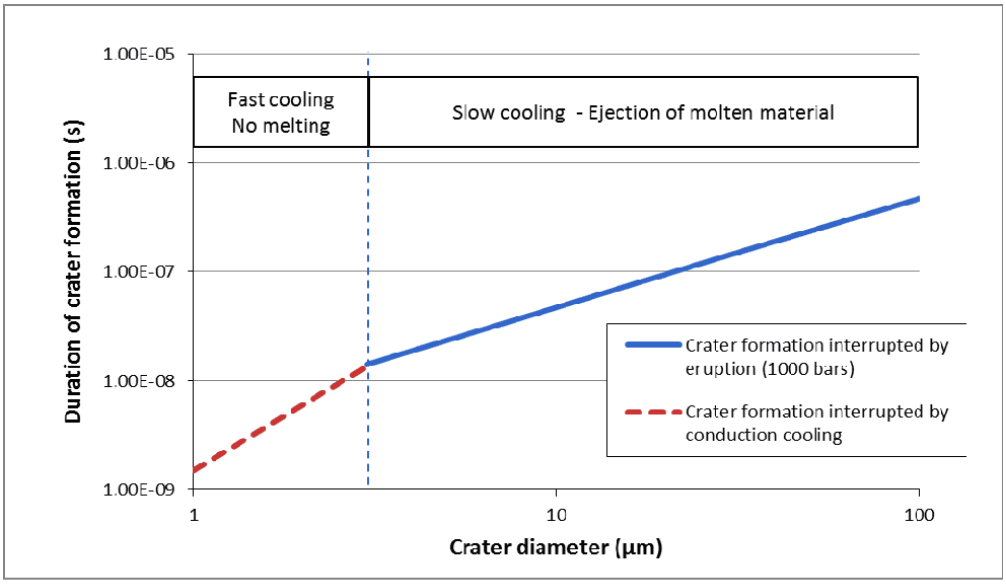

Figure 15. Criteria for the presence of molten material in LENR craters.

dimensions of the LENR sites may be markedly smaller than the final craters.

- Shortly before the reaction starts, the site is obviously at the same temperature as the base metal. The reaction is not initiated because of a high local temperature.
- If all the energy is generated within a site smaller than the crater, the temperature level reached at the end of the nuclear event, before the crater expansion, is considerably higher than the 2000 K value estimated by the crater formation energy correlation (1). Dividing the volume by 10 means a reaction temperature of 20 000 K for example. May be, the multiplication factor is much higher.
- If the LENR site is smaller than the crater, the duration of the nuclear reactions is even shorter than the values given for τ in equation (4)
- The crystalline structure supposed to be the matrix of LENR events is completely destroyed by the high temperature. If LENR reactions occur in such sites, they take place in a medium completely out of equilibrium.
- Such high temperatures developed in a very short time mean huge instantaneous powers. If we consider again the Nagel's correlation, the 50 μm conical crater represent an energy of 10^{-4} J. If the LENR site dimension is a 10 μm large cube, the energy density is 10^{11} J m^{-3}, released in less than 150 ns. The instantaneous power is then larger than 6×10^{17} W m^{-3}. These are really microscopic explosions.
- It is tempting to relate such phenomena to some explosions which have been reported by several researchers [10]. It is however not easy to explain how small size explosions can trigger an explosion in a large volume.
- The LENR energy is probably transferred to the surrounding metal via a shock wave, resulting in the formation of the crater, very much like during an underground explosion.
- A possible sequence of the formation of a crater is proposed in Fig. 16:
  - LENR reactions starts on a given site, initially cold, for some reasons which remain to be explained,
  - The reactions develop very fast within the site and the temperature reaches a very high temperature, maybe in the order of several thousands of Kelvins,

  - A shock wave transfers the energy to the surrounding metal. The temperature decreases gradually. When the event takes place close to the surface, the shock wave reaches the surface. The temperature is close to 2000 K, at least for the large craters,
  - The gases contained in the hot metal create a pressure build-up, which leads to the ejection of the crater content.

- The explosions are probably accompanied by flashes of visible light. In fact, hot spots have already been observed in the infrared domain [3,11]. The direct observation of the cathodes during the experimentation with a monitoring of the images should make it possible to confirm the mechanisms proposed here.
- Many craters have a depth of several μm. If we accept that the LENR reactions at the origin of the crater are located near the bottom, this means that the reactions arise far below the surface, measured according to the atom scale.
- It is even possible that reactions are present at greater depths, not revealed by craters on the outer surface. Szpak et al. detected events underneath the surface during their co-deposition experiments [3]. It would be interesting to check if special metallic features possibly related to deep LENR sites can be observed within the palladium cathodes, which gave excess heat, several tens to hundreds of μm below the surface. This can be done with metallographic techniques on transverse cuts of the cathodes.
- Such investigations should help to understand better the mechanism of formation of the craters themselves, and to confirm or infirm the hypotheses made here.
- It is beyond the objective of this paper and the competencies of the author to draw any conclusion regarding the nature of LENR phenomena, but the above raises many points which should deserve further thoughts.

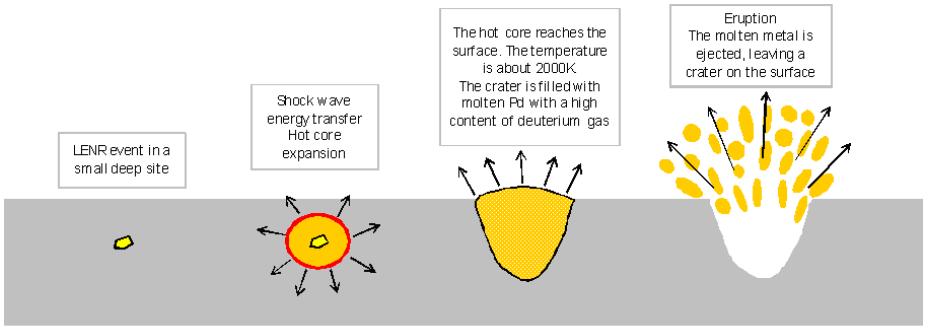

Figure 16. Schematic representation of the formation of a crater.

6. Conclusions

Simple models of heat flow and eruption kinetics give some orders of magnitude of the time scales involved during the formation of the micro-craters observed on palladium cathodes after LENR experiments. The reactions durations are measured in nanoseconds. The model explains the presence or not of molten material around the craters according to their size. The values of time and dimensions mentioned here lead to the conclusion that LENR seem to evolve like microscopic nuclear explosions, at least as far as deuterium loaded palladium cathodes are concerned.

The reactions start in a cold material, so the reactions are not initiated because of a high temperature. Another unexplained phenomenon is responsible for the onset. However, the temperature increases very quickly in an explosive fashion. It is not clear if the reactions continue within the site because of the high temperature, but at the beginning of the shock wave expansion phase, the temperature is so high that any ordered arrangement of atoms can no longer exist.

Further investigations are suggested in order to clarify several aspects:

- Is there a clear relationship between excess heat, LENR phenomena and the presence of craters (as supposed here) , or is excess heat obtained without observation of craters?
- The explosions responsible for the craters must be accompanied by flashes of visible light which may be detected using appropriate experimental setups.
- Metallographic studies on cuts made perpendicular to the cathode surface could show remnants of LENR sites near the bottom of craters. This would give the possible dimension of the LENR sites at the origin of the crater, and hence the maximum temperature reached
- Similar investigations could reveal reactions which occurred deep below the surface without cratering. Their presence would reinforce some theories, and their absence others.

References

[1] D. Cirillo and V. Iorio, Transmutation of metal at low energy in a confined plasma in water, in *Eleventh Int. Conf. on Condensed Matter Nucl. Sci*., 2004, Marseille, France. http://www.lenr-canr.org/acrobat/CirilloDtransmutat.pdf

[2] Y. Toriyabe, T. Mizuno, T. Ohmori and Y. Aoki, Elemental analysis of palladium electrodes after Pd/Pd light water critical electrolysis *, Proc. ICCF12 (2005),* www.icmns.org/iccf12/ToriyabeY.pdf.

[3] S. Szpak, P.A. Mosier-Boss and F.E. Gordon, Experimental evidence for LENR in a polarized Pd/D lattice, *NDIA 2006 Naval S&T Partnership Conference,* Washington DC, http://lenr-canr.org/acrobat/SzpakSexperiment.pdf.

[4] W. Zhang and J. Dash, Excess heat reproducibility and evidence of anomalous elements after electrolysis in Pd/D_2O + H_2SO_4 electrolysis cells,13^{th} *International Conference on Condensed Matter Nuclear Science,* Sochi, 2007.

[5] I. Dardik, T. Zilov, H. Branover, A. El-Boher, E. Greenspan, B. Khachaturov, V. Krakov, S.Lesin, A. Shapiro and M. Tsirlin, Ultrasonically-excited electrolysis experiments at energetics technologies, In *ICCF-14 International Conference on Condensed Matter Nuclear Science,* Washington, DC, 2008.

[6] David J. Nagel, Characteristics and energetics of craters in LENR experimental materials, *J. Condensed Matter Nucl. Sci.* **10** (2013) 1–14.

[7] Y. E. Kim, Theory of Bose–Einstein condensation mechanism for deuteron-induced nuclear reactions in micro/nano-scale metal grains and particles, *Naturwissenschaften, Published online 14 May 2009, DOI 10.1007/s00114-009-0537-6.*

[8] C. Cagran and G. Pottlacher, Thermophysical properties of palladium, *Platinum Metals Rev.* ***50*** (3) (2006) 144–149, DOI 10.1595/147106706X129079.

[9] F.A. Lewis, The hydrides of palladium and palladium alloys, *Platinum Metals Rev.* **4** (4) (1960) 132–137.

[10] J.P. Biberian, Unexplained explosion during an electrolysis experiment in an open cell mass flow calorimeter, *J. Condensed Matter Nucl. Sci.* **2** (2009) 1—6.

[11] M. Swartz, G. Verner and A. Weinberg, Non-thermal near-IR emission linked with excess power gain in high impedance and codeposition PHUSOR-LANR devices, *ICCF 14 International Conference on Condensed Matter Nuclear Science,* 10-15 – August 2008, Washington, DC.

J. Condensed Matter Nucl. Sci. 12 (2013) 69–104

Research Article

Born–Oppenheimer and Fixed-point Models for Second-order Phonon Exchange in a Metal

Peter L. Hagelstein *

Research Laboratory of Electronics, Massachusetts Institute of Technology, Cambridge, MA 02139, USA

Irfan U. Chaudhary

Department of Computer Science and Engineering, University of Engineering and Technology. Lahore, Pakistan

Abstract

We have been interested in the development of a model for anomalies in condensed matter nuclear science, and over the past few years we have developed new models that describe coherent phonon exchange between a highly-excited vibrational mode and nuclei under conditions of fractionation. When we modeled collimated X-ray emission in the Karabut experiment, we found that the conditions required by the model did not match the conditions of the experiment. One possible reason for this might be the neglect of phonon fluctuations due to coupling with conduction electrons. We would like to add a description of this effect to our phonon–nuclear model; however, models normally used for electron–phonon interactions in metals are based on the Bloch picture, and we were concerned that it may not be well suited to the problem. This has motivated us to develop a new model for phonon fluctuations in a metal that is based on the Born–Oppenheimer picture, within the context of a Brillouin–Wigner formulation. The Born–Oppenheimer results are complicated, so we have reduced them in a simpler fixed-point picture (which is based on a Taylor series expansion of the Born–Oppenheimer approximation around fixed nuclear equilibrium points). In order to verify the resulting formalism, we constructed a simplified model for the monatomic crystal phonon dispersion relation, which is well known in the Bloch picture literature. From this model we are able to extract the longitudinal dielectric constant. We find that the fixed-point dielectric constant at second order is more accurate than the Bloch picture equivalent, and that it includes dynamic corrections that match the result from field theory up to $O(\omega^2)$. This model is used in a subsequent paper for the development of phonon fluctuation models, where it is found that the Bloch picture is appropriate when the metal sample is micron scale or larger, and that the Born–Oppenheimer picture is appropriate for nano-scale samples.
 ISSN 2227-3123

Keywords: Phonon theory, Born-Oppenheimer approximation, phonon fluctuations, fractionation

*E-mail: plh@mit.edu

© 2013 ISCMNS. All rights reserved. ISSN 2227-3123

1. Introduction

We remain interested in the theoretical problem associated with how excess heat in the Fleischmann–Pons experiment [1–4] works. The key problem for us is the absence of energetic nuclear radiation in amounts commensurate with the energy produced [5], in experiments where the origin of the energy is thought to be nuclear. More than a decade ago we found that coherent energy exchange between two-level systems and a highly excited oscillator could occur efficiently when the characteristic energies were highly mismatched [6], in the lossy spin-boson boson model. In this case, energy conservation required that an (odd) integer number of oscillator quanta were needed to make up a large two-level system quantum. Coherent energy exchange in this situation in the spin-boson model is a very weak effect [7,8]; but when the model is augmented with loss, the destructive interference which hinders energy exchange can be eliminated, resulting in efficient coherent energy exchange in the lossy version of the spin–boson model [9–15].

More recently, we have developed a new physical model that is closely related to the lossy spin–boson model [16–18], and which implements the same mechanism for efficient coherent energy exchange under conditions where a large quantum is fractionated. In a sense, the new model is just the direct generalization of the nonrelativistic solid state Hamiltonian to include a relativistic description of nuclei as relativistic composite particles. In the relativistic version of the problem there is a strong coupling between the lattice vibrations and the internal nuclear degrees of freedom. Under conventional conditions, a generalized Foldy–Wouthuysen transformation rotates out this strong first-order coupling, resulting in a relativistic model not very different from the nonrelativistic one (in which the coupling between vibrations and internal nuclear degrees of freedom is very weak). The situation is very much analogous to the spin–boson model, where the first-order coupling between the oscillator and two-level systems can be removed with a Foldy–Wouthuysen type of transformation. However, when the loss is sufficiently strong to modify the occupation of the off-resonant states, then the transformation becomes unhelpful, and the model is best analyzed by brute force in the unrotated frame. The relativistic generalization of the condensed matter Hamiltonian is closely related, so when loss becomes important we propose that the Foldy–Wouthuysen transformation similarly becomes unhelpful. In this case the strong first-order coupling is available to mediate coherent dynamics on low-loss transitions. This in our view is the origin of the anomalies in condensed matter nuclear science [18].

Over the past year or two we have accumulated some experience with this new physical model. It is very interesting, in that it seems to predict anomalies very much like those seen in experiment (at least qualitatively). Since this model is capable of fractionating large quanta, it can be used to model coherent deuteron-deuteron reactions going to ^{4}He, with energy going into vibrations. Low-level gamma emission, and also transmutation effects, follow naturally as a result of coupling to internal nuclear excited state [19,20]. In our view, the simplest of the anomalies is direct vibrationally induced nuclear excitation [17], which we have proposed as responsible for collimated X-ray emission in the Karabut experiment [21–26]; this effect is also predicted by the new model. However, for all of its good things about the new theory that we have enumerated here, it is offset by the difficulty that the theory, particular model, and interpretation of the Karabut experiment are not in agreement yet quantitatively [18]. Our conclusion given this situation is that we are "close;" but some issue remains either with the theory, the model, or the interpretation.

The motivation for this work is the possibility that the theory is deficient in the case of metals generally, because coupling between vibrations and conduction electrons has not been included. We are interested in developing a model for phonon fluctuations due to this coupling to see whether it impacts, and perhaps increases, the ability of the coupled phonon–nuclear system to fractionate a large quantum.

The argument is subtle, and perhaps worth some thought here. In the lossy spin–boson model, the coupling between the two-level systems and oscillator produces a mixing between states that are far apart in energy. This coupling with off-resonant states produces a second-order indirect coupling between neighboring phonon basis states with the same two-level excitation, but different by two phonons. In the lossy spin–boson model it is this second-order interaction that determines how fast coherent energy exchange occurs under conditions of fractionation. It is no accident that

the relevant dimensionless coupling strength for coherent energy exchange goes like $g/\Delta n^2$, since the second-order indirect coupling between phonon states different by two is what produces this coupling strength [13].

Consequently, we might expect that the lossy spin–boson model will be sensitive to the addition of mechanisms which produce a coupling between neighboring phonon states. And because the new physical model is so closely related to the lossy spin–boson model, we would expect the same to be true for it as well. The coupling between vibrations and conduction electrons in a metal results ultimately in fluctuations in the phonon distribution. These fluctuations cause a spreading of the phonon distribution, caused by indirect coupling between phonon states different by two phonons, very similar to the indirect coupling resulting from the phonon–nuclear interaction. Consequently, we would expect the rate at which energy exchange occurs between phonons and nuclei under conditions of fractionation would depend on the amount of fluctuations induced in the phonon system by coupling to conduction electrons.

If so, then all that remains is to include phonon fluctuations due to phonon–electron coupling into the model. Our goal seems clear, and one might expect that all we need to do is to apply some analysis to the problem and we should be able to obtain a resolution. After all, electron–phonon coupling in metals is one problem that has been worked on a great deal over many decades. There is more than enough literature available to make clear the models and approaches available. However, amazingly enough some technical issues arise which are subtle, and these have motivated us to review the formulation of the problem.

The issue concerns two different physical pictures that appear in the literature to model phonon exchange. The leading formalism is of course the Bloch picture [27,28], which is based on periodic Bloch electron waves, and their interaction with phonons. The great majority of all calculations involve electron–phonon coupling has been done in the Bloch picture. A different approach altogether is available in the Born–Oppenheimer picture [29,30]. In this case, electrons are described using more general adiabatic wavefunctions, and phonon exchange is computed using the non-adiabatic terms in the Born–Oppenheimer Hamiltonian. Now, one might hope that the same physics is described in both cases. Most of the calculations that involve the electron–phonon interaction in metals is centered on the problem of electron screening. A much smaller number of papers are concerned with phonon decay rates resulting from resonant absorption by conduction electrons. For these problems, good answers are obtained in the Bloch picture.

But in our model, we are concerned with the coupled phonon–nuclear problem, in which states that are very much off of resonance are important. In this case it is important for us to work with a formulation that is well suited to the problem (and also which we can understand intuitively). For example, it can be shown that the phonon exchange matrix element in the Bloch picture and in the Born–Oppenheimer picture coincide when the phonon energy matches the difference in the electron energies [29]. However, we are interested in phonon fluctuations induced by the coupling with electrons, which involves off-resonant interactions. In this case, it seems we should want to use the Born–Oppenheimer picture (since there are no issues for off-resonant states). Unfortunately, we were not aware of anyone pursuing this kind of problem in a Born–Oppenheimer picture previously when we started (the formal development given by Sham and Ziman [27] covers many of the issues); so when we began it wasn't clear that a suitable foundation was available in the literature that we could use for phonon fluctuations. It seems in the literature that the two pictures are considered to be essentially equivalent, and results known so far are essentially the same in both (we will pursue this question in a following work).

Consequently, one task will be to examine the development of a suitable formulation for electron–phonon interactions in a metal that we can use to evaluation phonon fluctuations. In principle the starting place for our model is pretty clear. There is a strong electron–phonon interaction present initially, which we would like to rotate out in order to recover a model for dressed phonons that don't interact at first order. Unfortunately we do not have available an exact transformation that can do this. So instead we will work with an algebraic Brillouin–Wigner type of formulation which is well adapted to second-order models of this type, and which is also consistent with our formulation of the coupled phonon–nuclear problem. We can use it to obtain a version of the rotated problem that is good to second order, and which we could improve further later on if we wished.

With a suitable starting place and approach to follow, there is no particular difficulty in the development that follows. Unfortunately, since the Born–Oppenheimer picture describes very general configurations, the resulting formulas are quite complicated. We are able to develop a reduced version of this model in which we expand the Born–Oppenheimer wavefunctions around equilibrium positions; the model that results is a fixed-point approximation. We might consider this fixed-point model as constituting an important picture in its own right; it might be thought of as a Born–Oppenheimer version of the Bloch picture.

The development involves a fair number of pages and lots of formulas, so some effort is needed to determine whether we might have confidence in the results. For example, we would like to be able to make a connection with some known problem where the answer is available from previous work. In this case we can extract a result from the longitudinal dielectric constant directly from the model, and compare it with known results from the Bloch picture. We find that our second-order formulation results in a model for the longitudinal dielectric constant which includes frequency-dependent terms up to second order in ω, and which we are able to verify is in agreement with literature results.

In the end, we have a Born–Oppenheimer based model that allows us to specify the coupling matrix elements that describe phonon fluctuations due to coupling with conduction electrons. These matrix elements can be evaluated then in order to develop a model for phonon–nuclear coupling that includes fluctuations due to phonon–electron coupling. Such a model is analyzed in a following paper.

2. Basic Model and Sector Decomposition

The tasks that lie before us are at the same time easy (since the basic problem of electrons and nuclei is well known, and since the Born–Oppenheimer formalism is also well known) and hard (since there are some subtleties, a great many issues, and since the Brillouin–Wigner formalism is not as well known in the literature as it might otherwise be). Unfortunately, the path forward in the development that follows is not linear. Linear steps that are well motivated in each case are preferred, but in what follows we consider two independent paths that converge only after a fair amount of development and discussion.

The headache is that the separation of the phonon and electron degrees of freedom that we desire can be done effectively within the Brillouin–Wigner formalism; but sadly, the Brillouin–Wigner formalism requires a fair amount of structure within the model in order to make use of it. In particular, we need a definition of the phonon modes in order to make sense of the Brillouin–Wigner construction; but the relevant phonon mode structure can only be determined after we have made use of the Brillouin–Wigner construction.

On the other hand, electron–phonon coupling in metals is a very well known problem that has been worked over in the literature for more than 80 years. Given this, we know from earlier work that there are phonons; there are conduction electrons; they couple together; phonon exchange occurs; there is screening by conduction electrons; and we could make use of previous work to write down already a constraint for the phonon modes that would be quite close to what we will eventually arrive at. Because of this, working with a development that is not linear in what follows will cause us very little difficulty. We already know pretty much how things work and what to expect. At issue here then are the interactions that produce phonon fluctuations within the Born–Oppenheimer formalism; and the construction of the machinery that we need to describe the problem generally, and to carry out detailed calculations in particular.

This motivates us here to focus on the two ares that make up our two starting places. One is the basic physical model, which basically involves a metal lattice with interacting electrons and nuclei. The other is the basic Brillouin–Wigner separation of phonon and electron degrees of freedom.

2.1. Basic physical model

Our starting place is the specification of a model for nuclei and electrons in a metal lattice with Coulomb interactions

$$\hat{H} = \hat{H}_{\rm N} + \hat{H}_{\rm e} + \hat{V}_{\rm eN}. \tag{1}$$

The nuclear Hamiltonian is

$$\hat{H}_{\rm N} = \sum_j \frac{|\hat{\mathbf{P}}_j|^2}{2M_j} + \sum_{j<k} \frac{Z_j Z_k e^2}{4\pi\epsilon_0 |\mathbf{R}_k - \mathbf{R}_j|} \tag{2}$$

and the Hamiltonian for the electrons is

$$\hat{H}_{\rm e} = \sum_\alpha \frac{|\hat{\mathbf{p}}_\alpha|^2}{2m} + \sum_{\alpha<\beta} \frac{e^2}{4\pi\epsilon_0 |\mathbf{r}_\beta - \mathbf{r}_\alpha|}. \tag{3}$$

Coupling between electrons and the nuclei is described by

$$\hat{V}_{\rm eN} = -\sum_{j,\alpha} \frac{Z_j e^2}{4\pi\epsilon_0 |\mathbf{R}_j - \mathbf{r}_\alpha|}. \tag{4}$$

This Hamiltonian describes the same basic model as has been used in the literature for many decades (see e.g. Eq. (3.1) in [27]), and as such is well known. Our interest ultimately is in a somewhat more sophisticated model that will involve phonon–nuclear coupling, so our intention then is to take the results that we obtain for the simpler problem considered in this paper, and adapt them to the phonon–nuclear problem in a following paper.

2.2. Sector decomposition

There are a variety of mathematical techniques that are available to us to analyze this problem, along with a vast literature since our starting place is so general. In what follows we will make use of a sector decomposition approach, which is not so often used in the modern literature. It offers a number of advantages for our purposes here: the approach is relatively simple; it is easy to develop approximations in which different degrees of freedom are separated; we can work with resonant and off-resonant situations in a straightforward way; we can develop results for loss mechanisms simply; and the approach is consistent generally with the formulation that we are using for the phonon–nuclear models. It has the disadvantage of being relatively unfamiliar in this day and age, and it involves intermediate steps which are easy to specify formally but which imply projection operator constructions that are inconvenient.

In a sector decomposition generally we split the relevant Hilbert space into different pieces (which are the sectors), and then carry out our analysis on the individual sectors subsequently (this approach was used in times past in nuclear physics [31], and is discussed briefly in Appendix A of [9]). We are ultimately interested in working with a lattice in which a single-phonon mode is highly excited, so that the different sectors will correspond to the number of phonons in the highly excited mode. However, initially we will be working with more general vibrational states similar to the vibrational states of a molecule. Nevertheless, even in this case of a complicated molecule with many vibrational modes, it may be that one of the modes in particular is highly excited, so that the basic notion underlying our sector decomposition can be well defined. To accomplish this we write

$$\Psi = \Psi_0 + \Psi_1 + \Psi_2 + \cdots, \tag{5}$$

where Ψ_n is the sector that contains n phonons in the highly excited mode.

As remarked upon above, we are able to specify sectors here in the formalism which at this point in the analysis are inconvenient to specify since as yet we do not even have a specification of what constitutes a vibrational mode. Since a great deal of work has preceded our effort, much is known about the problem generally, and we know that there are vibrational modes in molecules, metals, and semiconductors. After further analysis we will be able to develop a constraint within the formalism that will determine the vibrational modes.

2.3. Sector eigenvalue equations

We are interested in the coupling of the vibrational degrees of freedom with the electronic degrees of freedom, and once again based on previous work we know that in a metal the electron–phonon coupling is dominated by single-phonon exchange interactions. If we start with the time-independent Schrödinger equation for the electrons and nuclei

$$E\Psi = \hat{H}\Psi \tag{6}$$

then we can develop coupled sector equations generally of the form

$$E\Psi_n = \hat{H}_{n,n}\Psi_n + \hat{H}_{n,n-1}\Psi_{n-1} + \hat{H}_{n,n+1}\Psi_{n+1}, \tag{7}$$

where the off-diagonal terms describe single-phonon exchange.

2.4. Second-order sector equations

It is possible to eliminate the first-order coupling by solving formally for the intermediate sectors; for example, in the case of one such intermediate sector we may write

$$\Psi_n = \left[E - \hat{H}_{n,n}\right]^{-1}\left(\hat{H}_{n,n-1}\Psi_{n-1} + \hat{H}_{n,n+1}\Psi_{n+1}\right). \tag{8}$$

Upon substituting back we obtain coupled second-order sector equations of the form

$$\begin{aligned} E\Psi_n =& \hat{H}_{n,n}\Psi_n + \hat{H}_{n,n-1}\left[E - \hat{H}_{n-1,n-1}\right]^{-1}\hat{H}_{n-1,n-2}\Psi_{n-2} \\ &+ \hat{H}_{n,n-1}\left[E - \hat{H}_{n-1,n-1}\right]^{-1}\hat{H}_{n-1,n}\Psi_n + \hat{H}_{n,n+1}\left[E - \hat{H}_{n+1,n+1}\right]^{-1}\hat{H}_{n+1,n}\Psi_n \\ &+ \hat{H}_{n,n+1}\left[E - \hat{H}_{n+1,n+1}\right]^{-1}\hat{H}_{n+1,n+2}\Psi_{n+2}. \end{aligned} \tag{9}$$

Even though the implementation of the required projection operators needed for these equations at this point remains formidable, we have achieved a suitable starting place for our investigations. We see that when first-order interactions are eliminated, we end up with diagonal and off-diagonal second-order interaction terms as a direct consequence of the basic assumptions that we have made so far (that phonons will exist in the system, and the first-order interactions are dominant).

3. Born–Oppenheimer Approximation and Phonon Exchange

Phonon exchange in metals is usually described within the framework of a Bloch picture, rather than within the framework of a Born–Oppenheimer picture. It will be useful here to pursue the development within the context of the more general Born–Oppenheimer picture here for the reasons already mentioned: the Bloch picture is thought to work well for resonant single-phonon exchange, but there are issues when we consider virtual processes; there is a close connection between the Born–Oppenheimer formulation and the Bloch formulation that will help to guide us in the development; and in process we will have developed a more general formulation (than the Bloch picture) that we can use if we like later on in connection with non-periodic systems.

Within the Born–Oppenheimer both adiabatic and non-adiabatic contributions to the Hamiltonian are recognized. For most problems the adiabatic Hamiltonian is sufficient, and the non-adiabatic Hamiltonian discarded because the associated effects are small. However, it is the non-adiabatic terms which mediate phonon exchange, so we will keep them and make use of them in what follows.

3.1. The Born–Oppenheimer approximation

In the Born–Oppenheimer approximation we separate the wavefunction into electronic and nuclear pieces [27]

$$\Psi(\{\mathbf{r}\},\{\mathbf{R}\}) = \Psi(\{\mathbf{R}\})\Phi(\{\mathbf{r}\};\{\mathbf{R}\}). \tag{10}$$

The idea is that the electronic motion is much faster than the ion motion, so the electronic wavefunction is defined assuming fixed nuclei according to

$$E_{\rm e}(\{\mathbf{R}\})\Phi(\{\mathbf{r}\};\{\mathbf{R}\}) = \left[\hat{H}_{\rm e} + \hat{V}_{\rm eN}\right]\Phi(\{\mathbf{r}\};\{\mathbf{R}\}). \tag{11}$$

The nuclear wavefunction in the adiabatic approximation is determined from

$$E\Psi(\{\mathbf{R}\}) = \left[\hat{H}_{\rm N} + E_{\rm e}(\{\mathbf{R}\})\right]\Psi(\{\mathbf{R}\}). \tag{12}$$

3.2. Isolation of the vibrational degrees of freedom

We can isolate the vibrational degrees of freedom by taking advantage of the Brillouin–Wigner formalism. To proceed we write the sector wavefunction in the form

$$\Psi_n(\{\mathbf{r}\},\{\mathbf{R}\}) = \Psi_n(\{\mathbf{R}\})\Phi_0(\{\mathbf{r}\};\{\mathbf{R}\}). \tag{13}$$

In writing this we are requiring the electronic wavefunction to be the same in the different vibrational sectors that we work with, which means that no electronic excitation is allowed in the model in association to transitions between neighboring sectors. Electronic excitation is possible in the intermediate sectors; and since electronic excitation is not permitted in the sectors that we keep we see that the part of the Hilbert space is then eliminated from further consideration (which simplifies the problem, but which we recognize is an approximation that we make). In this case, all of the outlying sectors that we do keep for our analysis will be off resonance; a situation which is consistent with the phonon–nuclear coupling problem (which is why we are interested in it), but qualitatively different from normal molecular or solid state problems (which tend to focus on the on-resonance part of the problem).

We project out the electronic degrees of freedom formally to obtain

$$\begin{aligned} E\Psi_n(\{\mathbf{R}\}) =& \langle\Phi_0|\hat{H}_{n,n}|\Phi_0\rangle\Psi_n(\{\mathbf{R}\}) \\ &+ \left\langle \Phi_0 \middle| \hat{H}_{n,n-1}\left[E - \hat{H}_{n-1,n-1}\right]^{-1}\hat{H}_{n-1,n-2}\middle|\Phi_0\right\rangle \Psi_{n-2}(\{\mathbf{R}\}) \\ &+ \left\langle \Phi_0 \middle| \hat{H}_{n,n-1}\left[E - \hat{H}_{n-1,n-1}\right]^{-1}\hat{H}_{n-1,n}\middle|\Phi_0\right\rangle \Psi_{n}(\{\mathbf{R}\}) \\ &+ \left\langle \Phi_0 \middle| \hat{H}_{n,n+1}\left[E - \hat{H}_{n+1,n+1}\right]^{-1}\hat{H}_{n+1,n}\middle|\Phi_0\right\rangle \Psi_{n}(\{\mathbf{R}\}) \\ &+ \left\langle \Phi_0 \middle| \hat{H}_{n,n+1}\left[E - \hat{H}_{n+1,n+1}\right]^{-1}\hat{H}_{n+1,n+2}\middle|\Phi_0\right\rangle \Psi_{n+2}(\{\mathbf{R}\}). \end{aligned} \tag{14}$$

By isolating the vibrational degrees of freedom, we are now much closer to being able to specify the phonon modes, and to being able to implement the projection operators implied by the formalism.

We might have reason to be concerned with not including the possibility of additional electronic excitation within this restricted version of the problem that we have kept. We note that the strong first-order phonon–electron coupling has been removed in the formalism, so that in a sense we are now dealing with phonon states which act as "dressed" (as if we had succeeded in rotating out the first-order interaction). The residual interactions are much weaker, and these are often neglected in conventional models for phonon dynamics. There is no obvious effect in the problems of interest to us that would suggest that it would not be reasonable to neglect electronic excitation in connection with phonon fluctuations. Should we wish, we could add electronic excitation as a loss later on.

Note however that we are keeping some of the second-order interactions to describe indirect coupling between phonon states differing by two; these will give rise to phonon fluctuations that are of interest for including electron–phonon coupling effects in the phonon–nuclear model.

3.3. Diagonal electronic matrix element

Within the Born–Oppenheimer approximation we can write for the expectation value of the Hamiltonian over the electronic degrees of freedom

$$\begin{aligned} \langle\Phi_0|\hat{H}|\Phi_0\rangle &= \langle\Phi_0|\hat{H}_{\rm N} + \hat{H}_{\rm e} + \hat{V}_{\rm eN}|\Phi_0\rangle \\ &= \sum_j \frac{|\hat{\mathbf{P}}_j|^2}{2M_j} + \sum_{j<k}\frac{Z_j Z_k e^2}{4\pi\epsilon_0|\mathbf{R}_k - \mathbf{R}_j|} + E_e(\{\mathbf{R}\}) \\ &\quad \sum_j \frac{1}{2M_j}\left(\langle\Phi_0|\ |\hat{\mathbf{P}}_j|^2|\Phi_0\rangle - |\hat{\mathbf{P}}_j|^2\right). \end{aligned} \tag{15}$$

We recognize adiabatic (second line) and non-adiabatic (third line) terms arising from electronic matrix elements of the Hamiltonian.

We can use this to isolate the lowest-order contribution to the diagonal sector Hamiltonian

$$\langle\Phi_0|\hat{H}_{n,n}|\Phi_0\rangle = \left|n\right\rangle\left\langle n\middle|\langle\Phi_0|\hat{H}|\Phi_0\rangle\middle|n\right\rangle\left\langle n\right|. \tag{16}$$

In this notation we will use the large $|n\rangle$ notation to refer to the complicated Born–Oppenheimer vibrational states with n phonons in the highly excited mode (the details of the rest of the vibrational wavefunction is not focused on, other than we presume that it remains unchanged in this model). In doing so, we have made our first significant connection between the Born–Oppenheimer part of the problem, and our Brillouin–Wigner formalism.

3.4. The first-order non-adiabatic term

The electronic matrix elements of the non-adiabatic part of the Born–Oppenheimer Hamiltonian can be thought of as being made up of first-order and second-order contributions. If the initial and final electronic states are different, then the non-adiabatic terms can be evaluated as

$$\langle \Phi_X | \, |\hat{\mathbf{P}}_j|^2 |\Phi_Y\rangle = 2\langle \Phi_X | (\hat{\mathbf{P}}_j \Phi_Y)\rangle \cdot \hat{\mathbf{P}}_j + \langle \Phi_X | (|\hat{\mathbf{P}}_j|^2 \Phi_Y)\rangle. \tag{17}$$

The first term on the RHS is expected to be dominated by single-phonon exchange, while the second is dominated by two-phonon exchange interactions.

It is possible to develop an estimate for the first-order non-adiabatic contribution by following an argument similar to that of Ziman [29]; this will lead to a slight generalization of Ziman's formula, which is a connection between the first-order non-adiabatic interaction and the gradient of the nuclear Coulomb potential. We recall that the electronic wavefunction in the Born–Oppenheimer approximation is determined from

$$E_Y(\{\mathbf{R}\})\Phi_Y(\{\mathbf{r}\};\{\mathbf{R}\}) = \left[\hat{H}_{\rm e} + \hat{V}_{\rm eN}\right]\Phi_Y(\{\mathbf{r}\};\{\mathbf{R}\}). \tag{18}$$

Multiplying by Φ_X and integrating over electronic coordinates leads to

$$E_Y\langle \Phi_X|\Phi_Y\rangle = \langle \Phi_X|\hat{H}_{\rm e} + \hat{V}_{\rm eN}|\Phi_Y\rangle. \tag{19}$$

We can take the gradient ∇_j of this expression to obtain

$$\begin{aligned}(\nabla_j E_Y)\langle \Phi_X|\Phi_Y\rangle + E_Y\langle \nabla_j\Phi_X|\Phi_Y\rangle + E_Y\langle \Phi_X|\nabla_j\Phi_Y\rangle \\ = \langle \nabla_j\Phi_X|\hat{H}_{\rm e} + \hat{V}_{\rm eN}|\Phi_Y\rangle + \langle \Phi_X|\nabla_j\hat{V}_{\rm eN}|\Phi_Y\rangle + \langle \Phi_X|\hat{H}_{\rm e} + \hat{V}_{\rm eN}|\nabla_j\Phi_Y\rangle \\ = E_Y\langle \nabla_j\Phi_X|\Phi_Y\rangle + \langle \Phi_X|(\nabla_j\hat{V}_{\rm eN})|\Phi_Y\rangle + E_X\langle \Phi_X|\nabla_j\Phi_Y\rangle.\end{aligned} \tag{20}$$

This reduces to

$$(\nabla_j E_Y)\langle \Phi_X|\Phi_Y\rangle + (E_Y - E_X)\langle \Phi_X|\nabla_j\Phi_Y\rangle = \langle \Phi_X|(\nabla_j\hat{V}_{\rm eN})|\Phi_Y\rangle. \tag{21}$$

When $Y \neq X$ we obtain

$$\langle \Phi_X|\nabla_j\Phi_Y\rangle = -\frac{\langle \Phi_X|(\nabla_j\hat{V}_{\rm eN})|\Phi_Y\rangle}{E_X - E_Y}. \tag{22}$$

If $Y = X$ we may write

$$\nabla_j E_X = \langle \Phi_X|(\nabla_j\hat{V}_{\rm eN})|\Phi_X\rangle. \tag{23}$$

In addition we have an orthogonality relation

$$\nabla_j \langle \Phi_X | \Phi_X \rangle = \langle \nabla_j \Phi_X | \Phi_X \rangle + \langle \Phi_X | \nabla_j \Phi_X \rangle = 0. \tag{24}$$

3.5. Connection between momentum and position matrix elements

According to Ehrenfest's theorem the evolution equations for the expectation values of position and momentum satisfy Newton's laws; in particular, we may write

$$\frac{\mathrm{d}}{\mathrm{d}t} \langle \mathbf{R}_j \rangle = \frac{\langle \hat{\mathbf{P}} \rangle}{M_j}. \tag{25}$$

For this to be true for the isolated system (with no external force) the associated matrix elements must satisfy

$$-i \left(\frac{E_\mathrm{f} - E_\mathrm{i}}{\hbar} \right) \langle f | \mathbf{R}_j | i \rangle = \frac{\langle f | \hat{\mathbf{P}} | i \rangle}{M_j}. \tag{26}$$

The first-order nonadiabatic Hamiltonian can be written as

$$\sum_j \frac{1}{M_j} \langle \Phi_X | \hat{\mathbf{P}}_j \Phi_Y \rangle \cdot \hat{\mathbf{P}}_j = -i\hbar \sum_j \langle \Phi_X | \nabla_j \Phi_Y \rangle \cdot \frac{\hat{\mathbf{P}}_j}{M_j}. \tag{27}$$

3.6. Generalized Ziman relation

We can use this to write

$$\begin{aligned}
&\left\langle \Psi_f(\{\mathbf{R}\}) \left| -i\hbar \sum_j \langle \Phi_X | \nabla_j \Phi_Y \rangle \cdot \frac{\hat{\mathbf{P}}_j}{M_j} \right| \Psi_i(\{\mathbf{R}\}) \right\rangle \\
&\quad = \sum_l \left\langle \Psi_f(\{\mathbf{R}\}) \right| - i\hbar \sum_j \langle \Phi_X | \nabla_j \Phi_Y \rangle \left| \Psi_l(\{\mathbf{R}\}) \right\rangle \cdot \left\langle \Psi_l(\{\mathbf{R}\}) \left| \frac{\hat{\mathbf{P}}_j}{M_j} \right| \Psi_i(\{\mathbf{R}\}) \right\rangle \\
&\quad = \sum_l \left\langle \Psi_f(\{\mathbf{R}\}) \left| i\hbar \sum_j \frac{\langle \Phi_X | (\nabla_j \hat{V}_\mathrm{eN}) | \Phi_Y \rangle}{E_X - E_Y} \right| \Psi_l(\{\mathbf{R}\}) \right\rangle \\
&\qquad \times \left\langle \Psi_l(\{\mathbf{R}\}) \left| -i \left(\frac{E_l - E_i}{\hbar} \right) \mathbf{R}_j \right| \Psi_i(\{\mathbf{R}\}) \right\rangle.
\end{aligned} \tag{28}$$

It seems useful to recast this as

$$\left\langle \Psi_f(\{\mathbf{R}\}) \left| -i\hbar \sum_j \langle \Phi_X | \nabla_j \Phi_Y \rangle \cdot \frac{\hat{\mathbf{P}}_j}{M_j} \right| \Psi_i(\{\mathbf{R}\}) \right\rangle$$
$$= \sum_l \left\langle \Psi_f(\{\mathbf{R}\}) \left| \frac{E_l - E_i}{E_X(\{\mathbf{R}\}) - E_Y(\{\mathbf{R}\})} \sum_j \langle \Phi_X | (\nabla_j \hat{V}_{\mathrm{eN}}) | \Phi_Y \rangle \right| \Psi_l(\{\mathbf{R}\}) \right\rangle$$
$$\times \left\langle \Psi_l(\{\mathbf{R}\}) \left| \mathbf{R}_j \right| \Psi_i(\{\mathbf{R}\}) \right\rangle. \tag{29}$$

In a general Born–Oppenheimer setting we would expect both operators in the first matrix element to have the potential to produce a transition, while the $\mathbf{R}_j$ operator will predominantly exchange a single phonon (but can also mediate higher-order phonon exchange).

In the Bloch picture we take the nuclear positions to be the periodic equilibrium positions, so $E_X - E_Y$ will be constant; also we work with phonon modes instead of more general vibrational states, so we can expect single-phonon exchange from the $\mathbf{R}_j$ operator. When the phonon energy is not matched to the transition energy we would expect differences between the Born–Oppenheimer transition matrix element and the Bloch picture transition matrix element.

3.7. Screening effects

We would expect that when a nucleus moves, the tightly bound electrons will follow. Consequently, interactions between a nucleus and distant electrons should be screened by the tightly bound electrons. Discussion of this issue has appeared previously in the literature; see for example Refs. [32,33]. This effect should be in the formulas; however, as yet it does not seem very obvious how this screening comes about within the formalism.

To proceed, we focus our attention on a particular example in order to clarify how this works. Because the formalism focuses on the electronic wavefunction, we have the freedom to work with a classical description of the nuclear motion that we can visualise, in order to help understand the quantum mechanics of the electronic wavefunction. We consider two snapshots in time; including t_0 and t_1; where the difference between the two times is presumed to be small.

We begin by writing the time independent Schrödinger equation associated with the initial state wavefunction at $t = t_1$ as

$$E_1 \Phi_1 = \hat{H}_1 \Phi_1. \tag{30}$$

The final state wavefunction at $t = t_0$ satisfies

$$E_X \Phi_X = \hat{H}_0 \Phi_X. \tag{31}$$

Overlap matrix elements then satisfy

$$E_1 \langle \Phi_X | \Phi_1 \rangle = \langle \Phi_X | \hat{H}_1 | \Phi_1 \rangle, \tag{32}$$

$$E_X \langle \Phi_1 | \Phi_X \rangle = \langle \Phi_1 | \hat{H}_0 | \Phi_X \rangle. \tag{33}$$

We can subtract one with the complex conjugate of the other to obtain

$$(E_1 - E_X)\langle\Phi_X|\Phi_1\rangle = \langle\Phi_X|\hat{H}_1|\Phi_1\rangle - \langle\Phi_1^*|\hat{H}_0|\Phi_X^*\rangle. \tag{34}$$

Next, we would like to relate the initial state wavefunction Φ_1 to basis states defined at t_0. Since the difference between the two times is presumed to be small (so that the nuclei have not moved very far), we assume that it is possible to expand according to

$$\Phi_1 = \Phi_0 + \sum_j \left(\mathbf{R}_j^{(1)} - \mathbf{R}_j^{(0)}\right) \cdot \nabla_j \Phi_0 + \cdots \tag{35}$$

Since Φ_0 and Φ_X are now defined at the same time (with identical nuclear positions) they are orthogonal

$$\langle\Phi_X|\Phi_0\rangle = 0 \tag{36}$$

and we end up with

$$(E_1 - E_X)\sum_j \left(\mathbf{R}_j^{(1)} - \mathbf{R}_j^{(0)}\right) \cdot \langle\Phi_X|\nabla_j\Phi_0\rangle + \cdots = \langle\Phi_X|\hat{H}_1|\Phi_1\rangle - \langle\Phi_1^*|\hat{H}_0|\Phi_X^*\rangle. \tag{37}$$

It may be useful to expand the Hamiltonians to obtain

$$\begin{aligned}
&(E_1 - E_X)\sum_j \left(\mathbf{R}_j^{(1)} - \mathbf{R}_j^{(0)}\right) \cdot \langle\Phi_X|\nabla_j\Phi_0\rangle + \cdots \\
&\quad = \left\langle \Phi_X \left| \sum_\alpha \frac{|\hat{\mathbf{p}}_\alpha|^2}{2m} + \sum_{\alpha<\beta} \frac{e^2}{4\pi\epsilon_0|\mathbf{r}_\beta - \mathbf{r}_\alpha|} - \sum_{j,\alpha} \frac{Z_j e^2}{4\pi\epsilon_0|\mathbf{R}_j^{(1)} - \mathbf{r}_\alpha|} \right| \Phi_1 \right\rangle \\
&\qquad - \left\langle \Phi_1^* \left| \sum_\alpha \frac{|\hat{\mathbf{p}}_\alpha|^2}{2m} + \sum_{\alpha<\beta} \frac{e^2}{4\pi\epsilon_0|\mathbf{r}_\beta - \mathbf{r}_\alpha|} - \sum_{j,\alpha} \frac{Z_j e^2}{4\pi\epsilon_0|\mathbf{R}_j^{(0)} - \mathbf{r}_\alpha|} \right| \Phi_X^* \right\rangle.
\end{aligned} \tag{38}$$

We see that the transition matrix elements written in this form involves contributions from nuclear Coulomb, electronic Coulomb, and electronic potential energy terms in the Hamiltonian.

It is the case that a mathematical cancellation occurs for the contributions to the transition matrix element; for example

$$\begin{aligned}
&(E_1 - E_X)\sum_j \left(\mathbf{R}_j^{(1)} - \mathbf{R}_j^{(0)}\right) \cdot \langle\Phi_X|\nabla_j\Phi_0\rangle + \cdots \\
&\quad = \langle\Phi_X|\hat{H}_1 - \hat{H}_0|\Phi_0\rangle \\
&\quad = \left\langle \Phi_X \left| -\sum_{j,\alpha} \frac{Z_j e^2}{4\pi\epsilon_0|\mathbf{R}_j^{(1)} - \mathbf{r}_\alpha|} \right| \Phi_1 \right\rangle - \left\langle \Phi_X \left| -\sum_{j,\alpha} \frac{Z_j e^2}{4\pi\epsilon_0|\mathbf{R}_j^{(0)} - \mathbf{r}_\alpha|} \right| \Phi_1 \right\rangle.
\end{aligned} \tag{39}$$

We see that the relation including screening evaluates to one that involves the bare nuclear charge, and that this connects with the result above in Eq. (22). However, given this situation it seems that the better way to think about the transition matrix element might be to make use of the Hamiltonians including electronic contributions for each term individually as in Eq. (38), so that the subtraction will involve matrix elements referenced to effective (screened) nuclear charges instead of bare nuclear charges.

3.8. Effective charge parameterization

We are interested in the computation of an electronic matrix element of the form

$$\hat{\mathcal{M}}_{X,0} = \sum_j \frac{\hbar}{M_j} \langle \Phi_X | \nabla_j \Phi_0 \rangle \cdot \hat{\mathbf{P}}_j . \tag{40}$$

Probably the place to start is by making a connection with the classical version of the problem, where for small $t_1 - t_0$ we have

$$\mathbf{R}_j^{(1)} - \mathbf{R}_j^{(0)} = \frac{\mathbf{P}_j^{(0)}}{M_j}(t_1 - t_0) + \cdots \tag{41}$$

Consequently, we might write

$$\begin{aligned}
&\frac{(E_1 - E_X)(t_1 - t_0)\mathcal{M}_{X,0}}{\hbar} \\
&\quad = \sum_j (\mathbf{R}_j^{(1)} - \mathbf{R}_j^{(0)}) \cdot \langle \Phi_0 | \nabla_j \Phi_X \rangle \\
&\qquad \rightarrow \left\langle \Phi_X \left| \sum_\alpha \frac{|\hat{\mathbf{p}}_\alpha|^2}{2m} + \sum_{\alpha<\beta} \frac{e^2}{4\pi\epsilon_0 |\mathbf{r}_\beta - \mathbf{r}_\alpha|} - \sum_{j,\alpha} \frac{Z_j e^2}{4\pi\epsilon_0 |\mathbf{R}_j^{(1)} - \mathbf{r}_\alpha|} \right| \Phi_1 \right\rangle \\
&\qquad - \left\langle \Phi_1^* \left| \sum_\alpha \frac{|\hat{\mathbf{p}}_\alpha|^2}{2m} + \sum_{\alpha<\beta} \frac{e^2}{4\pi\epsilon_0 |\mathbf{r}_\beta - \mathbf{r}_\alpha|} - \sum_{j,\alpha} \frac{Z_j e^2}{4\pi\epsilon_0 |\mathbf{R}_j^{(0)} - \mathbf{r}_\alpha|} \right| \Phi_X^* \right\rangle .
\end{aligned} \tag{42}$$

In essence, this gives a practical way to evaluate the classical part of the matrix element in a modern computation, such as a density functional calculation.

In the event that the electronic kinetic energy is ineffective in mediating a transition, we parameterize this as

$$\frac{(E_0 - E_X)(t_1 - t_0)\mathcal{M}_{X,0}}{\hbar} \rightarrow \sum_j (\mathbf{R}_j^{(1)} - \mathbf{R}_j^{(0)}) \cdot \left\langle \Phi_X \left| \left(-\nabla_j \sum_\alpha \frac{Z_j^* e^2}{4\pi\epsilon_0 |\mathbf{R}_j - \mathbf{r}_\alpha|} \right)_{\mathbf{R}_j^{(0)}} \right| \Phi_0 \right\rangle \tag{43}$$

since E_1 is very close to E_0. The matrix element with this parameterization becomes

$$\hat{\mathcal{M}}_{X,0} \rightarrow \frac{1}{E_0 - E_X} \sum_j \frac{\hbar}{M_j} \left\langle \Phi_X \left| \left(-\nabla_j \sum_\alpha \frac{Z_j^* e^2}{4\pi\epsilon_0 |\mathbf{R}_j - \mathbf{r}_\alpha|} \right)_{\mathbf{R}_j^{(0)}} \right| \Phi_0 \right\rangle \cdot \hat{\mathbf{P}}_j . \tag{44}$$

3.9. A sector reduction in the Born–Oppenheimer approximation

We can now return to the sector Hamiltonian and interactions with other sectors in the framework of the Born–Oppenheimer approximation. The diagonal electronic matrix element of the Hamiltonian is

$$\hat{H}_{n,n} = \langle\Phi_0|\hat{H}|\Phi_0\rangle = \sum_j \frac{\langle\Phi_0|\,|\hat{\mathbf{P}}_j|^2|\Phi_0\rangle}{2M_j} + \sum_{j<k} \frac{Z_j Z_k e^2}{4\pi\epsilon_0|\mathbf{R}_k - \mathbf{R}_j|} + E_0(\{\mathbf{R}\}), \tag{45}$$

where we have included the non-adiabatic contribution. This sector Hamiltonian with no further modification could be used to define general vibrational states (as are used in molecular problems). Later on, we will develop a second-order correction to this that gives the leading order correction due to phonon exchange

Since the non-adiabatic part of the Born–Oppenheimer Hamiltonian mediates phonon exchange in this formalism, we can write generally for $n' \neq n$

$$\begin{aligned}\hat{H}_{n,n'} &= \Big|n\Big\rangle \left\{ \sum_{Y\neq X} |\Phi_X\rangle\Big\langle n\Big|\langle\Phi_X|\hat{H}|\Phi_Y\rangle\Big|n'\Big\rangle\langle\Phi_Y| \right\} \Big\langle n'\Big| \\ &= \Big|n\Big\rangle \left\{ \sum_{Y\neq X} |\Phi_X\rangle\Big\langle n\Big| \sum_j \frac{\langle\Phi_X|\,|\hat{\mathbf{P}}|^2|\Phi_Y\rangle}{2M_j}\Big|n'\Big\rangle\langle\Phi_Y| \right\} \Big\langle n'\Big|. \end{aligned} \tag{46}$$

In the event that a phonon mode basis is defined consistent with this diagonal sector Hamiltonian, then the second-order sector-changing interaction for indirect coupling between $|n\rangle$ and $|n+2\rangle$ can be written as

$$\begin{aligned}&\Big\langle\Phi_0\Big|\hat{H}_{n,n+1}\Big[E - \hat{H}_{n+1,n+1}\Big]^{-1}\hat{H}_{n+1,n+2}\Big|\Phi_0\Big\rangle \\ &\quad\rightarrow \Big|n\Big\rangle \sum_{X\neq 0}\Big\langle n\Big|\sum_j \frac{\langle\Phi_0|\,|\hat{\mathbf{P}}_j|^2|\Phi_X\rangle}{2M_j}\Big|n+1\Big\rangle\Big[E - \hat{H}_{n+1,n+1}\Big]^{-1} \\ &\qquad \Big\langle n+1\Big|\sum_j \frac{\langle\Phi_X|\,|\hat{\mathbf{P}}_j|^2|\Phi_0\rangle}{2M_j}\Big|n+2\Big\rangle\Big\langle n+2\Big|. \end{aligned} \tag{47}$$

A similar expression can be developed for the other second-order interaction Hamiltonian.

It will become clear later on that the diagonal sector Hamiltonian here is dynamic. If we would like to make use of the static part of the Hamiltonian to define a reference, then the dynamic part of what is in the diagonal sector Hamiltonian above would contribute to the off-diagonal interaction.

3.10. Discussion

We see that phonon exchange arises from the non-adiabatic part of the Hamiltonian in the Born–Oppenheimer approximation, as has been noted in previous work. The development in this section revisits some of the ideas put forth by Ziman [29], who was interested in the connection between phonon exchange in the Bloch picture and in the Born–Oppenheimer picture.

In the Born–Oppenheimer picture the phonon exchange operator is a bit more complicated. In the reduction above we identified terms that could be identified as first-order and second-order in the reduction of the non-adiabatic

Hamiltonian. The strongest effect is due to single-phonon exchange, as expected and as known in the literature. Two-phonon exchange is clearly present, and since there are nonlinearities present in the interaction operator as a function of nuclear coordinates, we would expect higher-order phonon exchange processes as well (but of course these we expect to constitute smaller effects).

At this point we have sufficient development of the Born–Oppenheimer picture that we are able to make a more complete connection with the Brillouin–Wigner formalism. If we adopt the diagonal sector Hamiltonian (without any higher-order corrections) then we have a definition of the vibrational states, which allows us to construct the projection operator machinery required by the Brillouin–Wigner formalism. The model that results is very powerful, but has probably not seen much use (since it is a bit complicated).

4. Second-order Interactions

At this point we encounter a subtle technical issue in connection with the second-order interactions (recall here Eq. (14)). As a practical matter this technical issue involves only a minor difference in the answers we end up with later on (and as such may be more important as a philosophical issue). It concerns a differentiation between the static and dynamic parts of the second-order interaction, and is motivated by how we intend to use the model later on.

At issue is the origin of the phonon fluctuations under consideration here, which are to be used in the phonon–nuclear model. For example, in general we have some freedom in the definition of the phonon mode structure mathematically, and we know that our answers for the electron–phonon part of the problem will be the same independent of what phonon mode basis we use as long as we include all terms to all orders in the calculation. The same is true for the more complicated coupled phonon–nuclear–electron problem that motivates our analysis here. However, because this latter problem is so complicated, we are not intending to include terms to all orders (fluctuations will be described only at second order), which means that our model will definitely depend on our definition of the phonon modes.

The issue then is which definition is likely to give us the best results later on (and this is where the argument is likely to seem more philosophical than mathematical). We know that there is a static screening effect in which the conduction electrons screen the Coulomb interactions between the metal ions. Now, if this were all there was to the problem, then probably we would expect no fluctuation effect. The idea is that static screening acts the same as a (static) modification of the ion–ion interaction. Which means that we could include the effect completely just by adjusting the phonon modes and frequencies when we analyze the phonon–nuclear problem.

The intuition then is that when we consider electron–phonon interactions, the parts of the interaction that lead to simple static corrections to the ion-ion potential we know cannot produce the fluctuations we are interested in for the phonon–nuclear problem. On the other hand, the interactions that could only be accounted for by an additional dynamical degree of freedom in the problem will produce the fluctuations that we are interested in. Consequently, our attention is focused on sorting out the static and dynamic parts of the second-order interaction. Most importantly, we need to make sure that the phonon mode definitions include all of the static part of the second-order interaction (and none of the dynamic part).

The program in what follows then is to identify the part of the second-order interaction which constitutes the static part, and then to isolate it from the dynamic part of the interaction. Once this is done, we can use the dynamic part of the interaction to model the phonon fluctuations of interest.

4.1. Static part of the second-order interaction, resonant sector

To proceed, we need to isolate the static part of the interaction. The issues are simplest in the case of the resonant sector, so we begin our discussion focusing on this case. We consider one of the second-order interaction terms, and write (assuming that the n_0 sector is the one on resonance)

$$\left\langle \Phi_0 \left| \hat{H}_{n_0,n_0+1} \left[E - \hat{H}_{n_0+1,n_0+1} \right]^{-1} \hat{H}_{n_0+1,n_0} \right| \Phi_0 \right\rangle$$
$$\rightarrow \left| n_0 \right\rangle \sum_{X \neq 0} \left\langle n_0 \left| \sum_j \frac{\langle \Phi_0 | \, |\hat{\mathbf{P}}_j|^2 | \Phi_X \rangle}{2M_j} \right| n_0 + 1 \right\rangle \frac{1}{-\hbar\omega_0 + F_0 - F_X}$$
$$\left\langle n_0 + 1 \left| \sum_k \frac{\langle \Phi_X | \, |\hat{\mathbf{P}}_k|^2 | \Phi_0 \rangle}{2M_j} \right| n_0 \right\rangle \left\langle n_0 \right|, \tag{48}$$

where in the denominator $\hbar\omega_0$ is the phonon energy associated with phonon exchange of the highly excited mode. The difference between the (vibration-averaged) electronic state energies is $F_X - F_0$; for example, in the Born–Oppenheimer approximation the eigenvalues for the electronic Hamiltonian $E_0(\{\mathbf{R}\})$ and $E_X(\{\mathbf{R}\})$ depend on the nuclear positions, and here we need these to be averaged in the $n_0 + 1$ sector.

The static part of this interaction for this term can be extracted by taking

$$\left(\frac{1}{-\hbar\omega_0 + F_0 - F_X} \right)_{\text{static}} = \frac{1}{F_0 - F_X}. \tag{49}$$

The elimination of the phonon frequency in the second-order terms generally in the resonant sector allows us to extract the static part of this second-order interaction.

4.2. Static part of the interaction in other sectors

In the off-resonant sectors, things are a bit more complicated, and we probably need to think about it some. The basic issue is that the second-order interactions in general come with off-resonant denominators of the form

$$\frac{1}{E - \hat{H}_{n',n'}}. \tag{50}$$

As we consider sectors that are further and further off of resonance, the corresponding diagonal sector energy will be increasingly different from E. The simplest approach is to retain the resonant sector definition for the off-resonant sectors. The associated physical statement is that the screening in the off-resonant sectors is assumed at lowest order to be the same as in the resonant sector. Such a scheme would be most consistent with the basic Born–Oppenheimer picture, and should be effective if the system is not far off of resonance (although it is not obvious at this point, in a subsequent paper we will find that it is difficult to push a highly excited phonon mode sufficiently off of resonance to cause a significant reduction in screening).

Nonetheless, there is some freedom in the choice of the diagonal sector Hamiltonian off of resonance, which could be exploited to simplify the overall calculation. The issue is that if we decide to fix the phonon mode definitions and operators based on the resonant sector, then as we go further off of resonance there will be an increasing difference between the on-resonance phonon mode definitions and operators and their off-resonant counterparts. Much later on (in a following paper) we will find it to be advantageous to use these off-resonant phonon mode definitions. Consequently, it makes sense to examine briefly here how it works for a diagonal sector Hamiltonian off of resonance. One of the terms contributing to the second-order phonon exchange interaction in this case is

$$\left\langle \Phi_0 \left| \hat{H}_{n,n+1} \left[E - \hat{H}_{n+1,n+1} \right]^{-1} \hat{H}_{n+1,n} \right| \Phi_0 \right\rangle$$
$$= \left| n \right\rangle \sum_{X \neq 0} \left\langle n \left| \sum_j \frac{\langle \Phi_0 | \, |\hat{\mathbf{P}}_j|^2 | \Phi_X \rangle}{2M_j} \right| n+1 \right\rangle \frac{1}{-(n-n_0+1)\hbar\omega_0 + F_0 - F_X}$$
$$\left\langle n+1 \left| \sum_j \frac{\langle \Phi_X | \, |\hat{\mathbf{P}}_j|^2 | \Phi_0 \rangle}{2M_j} \right| n \right\rangle \left\langle n \right|. \tag{51}$$

The generalization of the static approximation in this case involves

$$\frac{1}{-(n-n_0+1)\hbar\omega_0 + F_0 - F_X} \;\rightarrow\; \frac{1}{-(n-n_0)\hbar\omega_0 + F_0 - F_X}. \tag{52}$$

In this kind of a picture the mode frequency changes off of resonance, so strictly speaking the off resonant energy will no longer be $(n-n_0)\hbar\omega_0$. To account for this, we will write

$$(n-n_0)\hbar\omega_0 \;\rightarrow\; \hat{E}_{\rm off}. \tag{53}$$

In the resonant sector, $\hat{E}_{\rm off}$ is zero; if we use the resonant sector static interaction off of resonance, then we would take $\hat{E}_{\rm off}$ to be zero; if there is negligible frequency shift, then $\hat{E}_{\rm off}$ will be replaced by $(n-n_0)\hbar\omega_0$; and finally, if the frequency shifts are important off of resonance then we can account for it by using a more accurate estimate $[n\hbar\omega(\hat{E}_{\rm off}) - n_0\hbar\omega_0]$.

4.3. Specification of the vibrational states

Now we come back to the problem of the definition of the vibrational states. We focus first on the second-order contribution. When we use the static approximation, or its off-resonant generalization above, we end up with equivalent weights from the case where a phonon is created, and from the case when a phonon is destroyed. Because of this we are able to simplify things by making use of the identity

$$\sum_{n'} \left| n \right\rangle \left\langle n \left| \hat{A} \right| n' \right\rangle \left\langle n' \left| \hat{B} \right| n \right\rangle \left\langle n \right| = \left| n \right\rangle \left\langle n \left| \hat{A}\hat{B} \right| n \right\rangle \left\langle n \right| \tag{54}$$

and write the diagonal sector Hamiltonian as

$$\hat{H}_n^{\rm diagonal} = \sum_j \frac{\langle \Phi_0 | \, |\hat{\mathbf{P}}_j|^2 | \Phi_0 \rangle}{2M_j} + \sum_{j<k} \frac{Z_j Z_k e^2}{4\pi\epsilon_0 |\mathbf{R}_k - \mathbf{R}_j|} + E_0(\{\mathbf{R}\})$$
$$+ \sum_{X \neq 0} \left(\sum_j \frac{\langle \Phi_0 | \, |\hat{\mathbf{P}}_j|^2 | \Phi_X \rangle}{2M_j} \right) \frac{1}{-\hat{E}_{\rm off} + F_0 - F_X} \left(\sum_k \frac{\langle \Phi_X | \, |\hat{\mathbf{P}}_k|^2 | \Phi_0 \rangle}{2M_k} \right). \tag{55}$$

This is an interesting result (good for both on resonance and off-resonance), and also a useful one. If we define the vibrational states in any sector from the eigenfunctions of this Hamiltonian, then by definition no transitions between vibrational states occur (which is why no projection operators are needed).

4.4. Off-diagonal sector Hamiltonians

If we follow the general line of argument from above, then in a model where we use phonon modes defined in the resonant sector we would write

$$\begin{aligned}
&\left\langle \Phi_0 \middle| \hat{H}_{n,n\pm1} \left[E - \hat{H}_{n\pm1,n\pm1} \right]^{-1} \hat{H}_{n\pm1,n\pm2} \middle| \Phi_0 \right\rangle \\
&\quad \rightarrow \left| n \right\rangle \sum_{X\neq 0} \left\langle n \middle| \sum_j \frac{\langle \Phi_0 | \, |\hat{\mathbf{P}}_j|^2 | \Phi_X \rangle}{2M_j} \middle| n \pm 1 \right\rangle \\
&\qquad \left[\frac{1}{-\hat{E}_{off} \mp \hbar\hat{\omega}_0 + F_0 - F_X} - \frac{1}{F_0 - F_X} \right] \\
&\qquad \left\langle n \pm 1 \middle| \sum_k \frac{\langle \Phi_X | \, |\hat{\mathbf{P}}_k|^2 | \Phi_0 \rangle}{2M_k} \middle| n \pm 2 \right\rangle \left\langle n \pm 2 \right|
\end{aligned} \tag{56}$$

as the contribution arising from two-phonon exchange.

However, we can develop a more general result. Suppose that choose part of the Hamiltonian of Equation (55) in the resonant sector for the construction of the reference problem against which to define phonon fluctuations (call this $\hat{H}_0$), then in general we can develop relevant expressions for both diagonal and sector-changing interactions through

$$\begin{aligned}
\hat{H} =& \hat{H}_0 + \sum_n \left\{ \left| n \right\rangle \left\langle n \middle| \hat{H}(E) - \hat{H}_0 \middle| n \right\rangle \left\langle n \right| + \left| n \right\rangle \left\langle n \middle| \hat{H}(E) - \hat{H}_0 \middle| n+2 \right\rangle \left\langle n+2 \right| \right. \\
&\left. + \left| n \right\rangle \left\langle n \middle| \hat{H}(E) - \hat{H}_0 \middle| n-2 \right\rangle \left\langle n-2 \right| \right\},
\end{aligned} \tag{57}$$

where $\hat{H}(E)$ stands in the for the Hamiltonian of Eq. (55) taken at the appropriate off-resonant energy. What is interesting about this approach is that the kinetic energy term

$$\sum_j \frac{\langle \Phi_0 | \, |\hat{\mathbf{P}}_j|^2 | \Phi_0 \rangle}{2M_j}$$

in the Born–Oppenheimer approximation can be defined to contain a static part and a dynamic part. The more general definition will pick up sector-changing transitions beyond those due to second-order phonon exchange.

4.5. Discussion

At this point we have achieved a convergence of the Born–Oppenheimer line of development, and the Brillouin–Wigner line of development. We are now in a position to develop useful specifications of the vibrational modes as we like systematically in both resonant and off-resonant sectors. One of our goals in this work was to develop expressions that we could use to compute phonon fluctuations to add to our phonon–nuclear model. We now have Eqs. (56) and (57) for the associated off-diagonal sector Hamiltonians in the Born–Oppenheimer approximation. This was one of our goals in this work.

5. Fixed Basis Model for Phonon Modes

We have succeeded now in making the connection between the Born–Oppenheimer picture and the Brillouin–Wigner formalism, and in constructing formulas for the specification of the vibrational modes and fluctuations. However, because the model is so general it is inconvenient to evaluate them (without having a set of wavefunctions from a density functional calculation). What is needed is a model something like the Bloch picture, but which is referenced to the Born–Oppenheimer approximation.

The motivates our interest first in a fixed basis model, and then in the following section a fixed basis crystal model. In the fixed basis model of this section, the idea is to use perturbation theory to develop an approximate version of the Born–Oppenheimer formulation that assumes slow variations around the fixed-point reference. In this sense the fixed-point model is an approximation to the Born–Oppenheimer picture; however, it may be better to think of it as a fixed-point picture in the same sense as the Born–Oppenheimer picture or Bloch picture. We can develop it directly from the Born–Oppenheimer picture, but because it is referenced to a fixed-point wavefunction, it is strictly no longer the Born–Oppenheimer picture. An important issue for us is that phonon exchange in this fixed-point model is consistent with Born–Oppenheimer phonon exchange (which is different from Bloch picture phonon exchange).

5.1. First-order interaction with a fixed basis

The first order of business then is to develop suitable expansions for the Born–Oppenheimer wavefunction in terms of fixed basis states, which are made up of the Born–Oppenheimer states with nuclei fixed at their equilibrium positions

$$\Phi(\{\mathbf{r}\};\{\mathbf{R}\}) = \Phi(\{\mathbf{r}\};\{\mathbf{R}^{(0)}\}) + \sum_j (\mathbf{R}_j - \mathbf{R}_j^{(0)}) \cdot \left[\nabla_j \Phi(\{\mathbf{r}\};\{\mathbf{R}\})\right]_{\{\mathbf{R}^{(0)}\}} + \cdots \tag{58}$$

The electronic transition matrix element in the Born–Oppenheimer picture can be written in terms of fixed basis wavefunctions as

$$\begin{aligned}
&\langle \Phi_X(\{\mathbf{r}\};\{\mathbf{R}\})|\ |\hat{\mathbf{P}}_j|^2 |\Phi_Y(\{\mathbf{r}\};\{\mathbf{R}\})\rangle \\
&\quad = \left\langle \Phi_X(\{\mathbf{r}\};\{\mathbf{R}^{(0)}\}) + \sum_k (\mathbf{R}_k - \mathbf{R}_k^{(0)}) \cdot \left[\nabla_k \Phi_X(\{\mathbf{r}\};\{\mathbf{R}\})\right]_{\{\mathbf{R}^{(0)}\}} + \cdots \right| |\hat{\mathbf{P}}_j|^2 \\
&\qquad \left| \Phi_Y(\{\mathbf{r}\};\{\mathbf{R}^{(0)}\}) + \sum_k (\mathbf{R}_k - \mathbf{R}_k^{(0)}) \cdot \left[\nabla_k \Phi_Y(\{\mathbf{r}\};\{\mathbf{R}\})\right]_{\{\mathbf{R}^{(0)}\}} + \cdots \right\rangle.
\end{aligned} \tag{59}$$

Since we are interested in matrix elements where $Y \neq X$, the lowest-order contribution vanishes

$$\begin{aligned}
&\langle \Phi_X(\{\mathbf{r}\};\{\mathbf{R}^{(0)}\})|\ |\hat{\mathbf{P}}_j|^2 |\Phi_Y(\{\mathbf{r}\};\{\mathbf{R}^{(0)}\})\rangle \\
&\qquad = |\hat{\mathbf{P}}_j|^2 \langle \Phi_X(\{\mathbf{r}\};\{\mathbf{R}^{(0)}\})|\Phi_Y(\{\mathbf{r}\};\{\mathbf{R}^{(0)}\})\rangle \\
&\qquad = 0.
\end{aligned} \tag{60}$$

For the first-order contributions we may write

$$\sum_k (\mathbf{R}_k - \mathbf{R}_k^{(0)})|\hat{\mathbf{P}}_j|^2 \cdot \langle \nabla_k \Phi_X | \Phi_Y \rangle_0 + \sum_k |\hat{\mathbf{P}}_j|^2 (\mathbf{R}_k - \mathbf{R}_k^{(0)}) \cdot \langle \nabla_k \Phi_X | \Phi_Y \rangle_0$$
$$= \sum_k (\mathbf{R}_k - \mathbf{R}_k^{(0)})|\hat{\mathbf{P}}_j|^2 \cdot \left(\langle \nabla_k \Phi_X | \Phi_Y \rangle_0 + \langle \Phi_X | \nabla_k \Phi_Y \rangle_0 \right) - 2i\hbar \langle \Phi_X | \nabla_j \Phi_Y \rangle_0 \cdot \hat{\mathbf{P}}_j, \tag{61}$$

where the notation $\langle \cdots | \cdots \rangle_0$ here means that the wavefunction and the gradient of the wavefunction involve a fixed basis (and hence no dependence on $\{\mathbf{R}\}$). Since the Born–Oppenheimer wavefunctions satisfy

$$\nabla_j \langle \Phi_X | \Phi_Y \rangle = \langle \nabla_j \Phi_X | \Phi_Y \rangle + \langle \Phi_X | \nabla_j \Phi_Y \rangle = 0, \tag{62}$$

we end up with

$$\langle \Phi_X(\{\mathbf{r}\};\{\mathbf{R}\})| \, |\hat{\mathbf{P}}_j|^2 | \Phi_Y(\{\mathbf{r}\};\{\mathbf{R}\})\rangle = -2i\hbar \langle \Phi_X | \nabla_j \Phi_Y \rangle_0 \cdot \hat{\mathbf{P}}_j + \cdots \tag{63}$$

We can generate higher-order interactions in this way systematically; however, for what follows we will be satisfied working with the first-order interaction.

5.2. Diagonal second-order interaction

We can make use of this result for single-phonon exchange to evaluate the lowest-order contribution to the diagonal part of the second-order interaction

$$\sum_{X \neq 0} \left(\sum_j \frac{\langle \Phi_0 | \, |\hat{\mathbf{P}}_j|^2 | \Phi_X \rangle}{2M_j} \right) \frac{1}{-\hat{E}_{\rm off} + F_0 - F_X} \left(\sum_k \frac{\langle \Phi_X | \, |\hat{\mathbf{P}}_k|^2 | \Phi_0 \rangle}{2M_k} \right)$$
$$\rightarrow \quad -\sum_j \sum_k \hat{\mathbf{P}}_j \cdot \left\{ \sum_{X \neq 0} \frac{\hbar^2}{M_j M_k} \frac{\langle \Phi_0 | \nabla_j \Phi_X \rangle_0 \langle \Phi_X | \nabla_k \Phi_0 \rangle_0}{-\hat{E}_{\rm off} + F_0 - F_X} \right\} \cdot \hat{\mathbf{P}}_k. \tag{64}$$

5.3. Non-adiabatic contribution

The part of the non-adiabatic interaction that does not involve electronic excitation can be written as

$$\sum_j \frac{\langle \Phi_0 | \, |\hat{\mathbf{P}}_j|^2 \, | \Phi_0 \rangle - |\hat{\mathbf{P}}_j|^2}{2M_j}$$
$$= \sum_j \left(-\frac{i\hbar}{M_j} \right) \langle \Phi_0 | \nabla_j \Phi_0 \rangle_0 \cdot \hat{\mathbf{P}}_j$$
$$+ \sum_{j,k} \left(-\frac{i\hbar}{2M_j} \right) \left\{ (\mathbf{R}_j - \mathbf{R}_j^{(0)}) \cdot \langle \nabla_j \Phi_0 | \nabla_k \Phi_0 \rangle_0 \cdot \hat{\mathbf{P}}_k + \hat{\mathbf{P}}_j \cdot \langle \nabla_j \Phi_0 | \nabla_k \Phi_0 \rangle_0 \cdot (\mathbf{R}_k - \mathbf{R}_k^{(0)}) \right\}$$
$$+ \sum_j \frac{\hbar^2}{2M_j} \left(\langle \nabla_j \Phi_0 | \nabla_j \Phi_0 \rangle_0 - \langle \Phi_0 | \nabla_j^2 \Phi_0 \rangle \right). \tag{65}$$

The first term on the right-hand side describes a residual single-phonon interaction, which might be connected with current-induced phonon generation. The second term on the right-hand side will later on result in a first-order dynamical correction to the screening. Were we to adopt a strict static Hamiltonian in the resonant sector for the definition of the phonon modes, this term would likely not be included, but instead by thought of as a kind of two-phonon exchange term similar to the second-order phonon exchange interaction we have considered explicitly. The interpretation of the last term on the right-hand side is less clear; however, we might expect second-order coupling if a strong electrical current is present that may be significant if the current is strong.

5.4. Electronic energy

We found previously that the diagonal sector Hamiltonian including the second-order interaction in the static approximation could be used to define the vibrational states. With a fixed electronic basis we no longer have a convenient specification of the dependence of the electronic energy on the nuclear positions, which motivates us here to consider expanding it out to second order around the equilibrium positions. We may write

$$\begin{aligned} E_0(\{\mathbf{R}\}) &= \langle \Phi_0(\{\mathbf{r}\};\{\mathbf{R}\})|\hat{H}_{\rm e}+\hat{V}_{\rm eN}|\Phi_0(\{\mathbf{r}\};\{\mathbf{R}\})\rangle \\ &= E_0(\{\mathbf{R}^{(0)}\}) + \sum_j (\mathbf{R}_j-\mathbf{R}_j^{(0)})\cdot(\nabla_j E_0)_0 + \frac{1}{2}\sum_{j,k}(\mathbf{R}_j-\mathbf{R}_j^{(0)})\cdot(\nabla_j\nabla_k E_0)_0\cdot(\mathbf{R}_k-\mathbf{R}_k^{(0)})+\cdots \end{aligned} \tag{66}$$

From the discussion above we know that

$$\nabla_j E_0 = \langle \Phi_0|\nabla_j \hat{V}_{\rm eN}|\Phi_0\rangle. \tag{67}$$

We can use a similar approach for $\nabla_j\nabla_k E_0$; we begin with

$$E\Phi = (\hat{H}_{\rm e}+\hat{V}_{\rm eN})\Phi$$

and differentiate twice to obtain

$$\begin{aligned} &(\nabla_j\nabla_k E)\Phi + (\nabla_j E)(\nabla_k\Phi) + (\nabla_k E)(\nabla_j\Phi) + E\nabla_j\nabla_k\Phi \\ &\quad = (\nabla_j\nabla_k\hat{V}_{\rm eN})\Phi + (\nabla_j\hat{V}_{\rm eN})(\nabla_k\Phi) + (\nabla_k\hat{V}_{\rm eN})(\nabla_j\Phi) + (\hat{H}_{\rm e}+\hat{V}_{\rm eN})\nabla_j\nabla_k\Phi. \end{aligned} \tag{68}$$

We use this to compute

$$\begin{aligned} &\nabla_j\nabla_k E + (\nabla_j E)\langle\Phi|\nabla_k\Phi\rangle + (\nabla_k E)\langle\Phi|\nabla_j\Phi\rangle + E\langle\Phi|\nabla_j\nabla_k\Phi\rangle \\ &\quad = \langle\Phi|(\nabla_j\nabla_k\hat{V}_{\rm eN})|\Phi\rangle + \langle\Phi|(\nabla_j\hat{V}_{\rm eN})|\nabla_k\Phi\rangle + \langle\Phi|\nabla_k\hat{V}_{\rm eN}|\nabla_j\Phi\rangle + \langle\Phi|\hat{H}_{\rm e}+\hat{V}_{\rm eN}|\nabla_j\nabla_k\Phi\rangle. \end{aligned} \tag{69}$$

We can simplify this to obtain

$$\begin{aligned} \nabla_j\nabla_k E = {}& \langle\Phi|(\nabla_j\nabla_k\hat{V}_{\rm eN})|\Phi\rangle + \langle\Phi|(\nabla_j\hat{V}_{\rm eN})|\nabla_k\Phi\rangle + \langle\Phi|\nabla_k\hat{V}_{\rm eN}|\nabla_j\Phi\rangle \\ &- (\nabla_j E)\langle\Phi|\nabla_k\Phi\rangle - (\nabla_k E)\langle\Phi|\nabla_j\Phi\rangle. \end{aligned} \tag{70}$$

Since $\nabla_j\nabla_k E$ is real, we can write

$$\nabla_j \nabla_k E = \langle \Phi | (\nabla_j \nabla_k \hat{V}_{\rm eN}) | \Phi \rangle + \langle \nabla_k \Phi | (\nabla_j \hat{V}_{\rm eN}) | \Phi \rangle + \langle \nabla_j \Phi | \nabla_k \hat{V}_{\rm eN} | \Phi \rangle - (\nabla_j E) \langle \nabla_k \Phi | \Phi \rangle - (\nabla_k E) \langle \nabla_j \Phi | \Phi \rangle. \quad (71)$$

These can be combined to produce

$$\nabla_j \nabla_k E = \langle \Phi | (\nabla_j \nabla_k \hat{V}_{\rm eN}) | \Phi \rangle + \frac{1}{2} \langle \Phi | (\nabla_j \hat{V}_{\rm eN}) | \nabla_k \Phi \rangle + \frac{1}{2} \langle \Phi | \nabla_k \hat{V}_{\rm eN} | \nabla_j \Phi \rangle + \frac{1}{2} \langle \nabla_k \Phi | (\nabla_j \hat{V}_{\rm eN}) | \Phi \rangle + \frac{1}{2} \langle \nabla_j \Phi | \nabla_k \hat{V}_{\rm eN} | \Phi \rangle. \quad (72)$$

We can make use of

$$\nabla_j \Phi = \left[E(\mathbf{R}) - \hat{H}_{\rm e} - \hat{V}_{\rm eN} \right]^{-1} \Big(\nabla_j [\hat{V}_{\rm eN} - E(\mathbf{R})] \Big) \Phi,$$

which leads to

$$\nabla_j \nabla_k E = \langle \Phi | (\nabla_j \nabla_k \hat{V}_{\rm eN}) | \Phi \rangle + \frac{1}{2} \left\langle \Phi \left| (\nabla_j \hat{V}_{\rm eN}) \left[E(\mathbf{R}) - \hat{H}_{\rm e} - \hat{V}_{\rm eN} \right]^{-1} (\nabla_k [\hat{V}_{\rm eN} - E(\mathbf{R})]) \right| \Phi \right\rangle + \frac{1}{2} \left\langle \Phi \left| (\nabla_k \hat{V}_{\rm eN}) \left[E(\mathbf{R}) - \hat{H}_{\rm e} - \hat{V}_{\rm eN} \right]^{-1} (\nabla_j [\hat{V}_{\rm eN} - E(\mathbf{R})]) \right| \Phi \right\rangle + \frac{1}{2} \left\langle \Phi \left| (\nabla_k [\hat{V}_{\rm eN} - E(\mathbf{R})]) \left[E(\mathbf{R}) - \hat{H}_{\rm e} - \hat{V}_{\rm eN} \right]^{-1} (\nabla_j \hat{V}_{\rm eN}) \right| \Phi \right\rangle + \frac{1}{2} \left\langle \Phi \left| (\nabla_j [\hat{V}_{\rm eN} - E(\mathbf{R})]) \left[E(\mathbf{R}) - \hat{H}_{\rm e} - \hat{V}_{\rm eN} \right]^{-1} (\nabla_k \hat{V}_{\rm eN}) \right| \Phi \right\rangle. \quad (73)$$

Finally, we can expand in terms of electronic basis states to obtain

$$(\nabla_j \nabla_k E_0)_0 = \langle \Phi | (\nabla_j \nabla_k \hat{V}_{\rm eN}) | \Phi \rangle_0 + \sum_{X \neq 0} \frac{\langle \Phi_0 | (\nabla_j \hat{V}_{\rm eN}) | \Phi_X \rangle_0 \langle \Phi_X | (\nabla_k \hat{V}_{\rm eN}) | \Phi_0 \rangle_0}{E_0 - E_X} + \sum_{X \neq 0} \frac{\langle \Phi_0 | (\nabla_k \hat{V}_{\rm eN}) | \Phi_X \rangle_0 \langle \Phi_X | (\nabla_j \hat{V}_{\rm eN}) | \Phi_0 \rangle_0}{E_0 - E_X}. \quad (74)$$

5.5. Coulomb interaction between nuclei and equilibrium

The Coulomb interaction between the nuclei can be expanded as well; we write

$$V_{NN}(\{\mathbf{R}\}) = \sum_{j'<k'} \frac{Z_{j'} Z_{k'} e^2}{4\pi\epsilon_0 |\mathbf{R}_{k'} - \mathbf{R}_{j'}|}$$
$$= V_{NN}(\{\mathbf{R}^{(0)}\}) + \sum_j (\mathbf{R}_j - \mathbf{R}_j^{(0)}) \cdot (\nabla_j V_{NN})_0$$
$$+ \frac{1}{2} \sum_j \sum_k (\mathbf{R}_j - \mathbf{R}_j^{(0)}) \cdot (\nabla_j \nabla_k V_{NN})_0 \cdot (\mathbf{R}_k - \mathbf{R}_k^{(0)}) + \cdots \quad (75)$$

Since the second-order contribution to the total energy in this model involves both nuclear position and momentum variables, the equilibrium positions are determined only from forces associated with the electronic energy and nuclear Coulomb interaction. We may write

$$(\nabla_j E_0)_0 + (\nabla_j V_{NN})_0 = 0. \quad (76)$$

5.6. Harmonic approximation for the diagonal sector Hamiltonian

We can expand the diagonal sector Hamiltonian (in the absence of current) to second-order to obtain

$$\hat{H}_n^{\text{diagonal}} \rightarrow \sum_j \frac{|\hat{\mathbf{P}}_j|^2}{2M_j} + V_{NN}(\{\mathbf{R}^{(0)}\}) + E_0(\{\mathbf{R}^{(0)}\}) + \sum_j \frac{\hbar^2}{2M_j} \left(\langle \nabla_j \Phi_0 | \nabla_j \Phi_0 \rangle_0 - \langle \Phi_0 | \nabla_j^2 \Phi_0 \rangle \right)$$
$$+ \frac{1}{2} \sum_j \sum_k (\mathbf{R}_j - \mathbf{R}_j^{(0)}) \cdot (\nabla_j \nabla_k V_{NN})_0 \cdot (\mathbf{R}_k - \mathbf{R}_k^{(0)})$$
$$+ \frac{1}{2} \sum_j \sum_k (\mathbf{R}_j - \mathbf{R}_j^{(0)}) \cdot (\nabla_j \nabla_k E_0)_0 \cdot (\mathbf{R}_k - \mathbf{R}_k^{(0)})$$
$$+ \sum_{j,k} \left(-\frac{i\hbar}{2M_j} \right) \left\{ (\mathbf{R}_j - \mathbf{R}_j^{(0)}) \cdot \langle \nabla_j \Phi_0 | \nabla_k \Phi_0 \rangle_0 \cdot \hat{\mathbf{P}}_k + \hat{\mathbf{P}}_j \cdot \langle \nabla_j \Phi_0 | \nabla_k \Phi_0 \rangle_0 \cdot (\mathbf{R}_k - \mathbf{R}_k^{(0)}) \right\}$$
$$- \sum_j \sum_k \hat{\mathbf{P}}_j \cdot \left\{ \sum_{X \neq 0} \frac{\hbar^2}{M_j M_k} \frac{\langle \Phi_0 | \nabla_j \Phi_X \rangle_0 \langle \Phi_X | \nabla_k \Phi_0 \rangle_0}{-\hat{E}_{off} + F_0 - F_X} \right\} \cdot \hat{\mathbf{P}}_k. \quad (77)$$

We can simplify this by defining the classical energy at equilibrium according to

$$H_0 = V_{NN}(\{\mathbf{R}^{(0)}\}) + E_0(\{\mathbf{R}^{(0)}\}) + \sum_j \frac{\hbar^2}{2M_j} \left(\langle \nabla_j \Phi_0 | \nabla_j \Phi_0 \rangle_0 - \langle \Phi_0 | \nabla_j^2 \Phi_0 \rangle \right). \quad (78)$$

We can define force constants through

$$\mathbf{K}_{jk} = (\nabla_j \nabla_k V_{NN})_0 + (\nabla_j \nabla_k E_0)_0. \quad (79)$$

Further simplification can be obtained by defining a matrix associated with the inverse mass according to

$$\frac{1}{2}\mathbf{L}_{jk} = \frac{1}{2M_j}\mathbf{I}\delta_{jk} - \sum_{X\neq 0}\frac{\hbar^2}{M_j M_k}\frac{\langle\Phi_0|\nabla_j\Phi_X\rangle_0\langle\Phi_X|\nabla_k\Phi_0\rangle_0}{-\hat{E}_{\rm off}+F_0-F_X}. \tag{80}$$

The Hamiltonian in the harmonic approximation becomes

$$\begin{aligned}\hat{H}_n^{\rm diagonal} \;\rightarrow\; & H_0 + \frac{1}{2}\sum_{j,k}\hat{\mathbf{P}}_j\cdot\mathbf{L}_{jk}\cdot\hat{\mathbf{P}}_k + \frac{1}{2}\sum_{j,k}(\mathbf{R}_j-\mathbf{R}_j^{(0)})\cdot\mathbf{K}_{jk}\cdot(\mathbf{R}_k-\mathbf{R}_k^{(0)}) \\ & + \frac{1}{2}\sum_{j,k}\left[(\mathbf{R}_j-\mathbf{R}_j^{(0)})\cdot\mathbf{J}_{jk}\cdot\hat{\mathbf{P}}_k + \hat{\mathbf{P}}_j\cdot\mathbf{J}_{kj}\cdot(\mathbf{R}_k-\mathbf{R}_k^{(0)})\right],\end{aligned} \tag{81}$$

where

$$\mathbf{J}_{jk} = \left(-\frac{i\hbar}{M_j}\right)\langle\nabla_j\Phi_0|\nabla_k\Phi_0\rangle_0. \tag{82}$$

5.7. Off-diagonal interaction

We can write for the phonon exchange contribution to the off-diagonal interaction in a similar picture

$$\begin{aligned}&\left\langle\Phi_0\left|\hat{H}_{n,n\pm1}\left[E-\hat{H}_{n\pm1,n\pm1}\right]^{-1}\hat{H}_{n\pm1,n\pm2}\right|\Phi_0\right\rangle \\ &\quad\rightarrow\; -\sum_j\sum_k\left|n\right\rangle\left\langle n\left|\hat{\mathbf{P}}_j\right|n\pm1\right\rangle\cdot\sum_{X\neq0}\frac{\hbar^2}{M_jM_k}\langle\Phi_0|\nabla_j\Phi_X\rangle_0\langle\Phi_X|\nabla_k\Phi_0\rangle_0 \\ &\qquad\times\left[\frac{1}{-\hat{E}_{\rm off}\mp\hbar\hat{\omega}_0+F_0-F_X}-\frac{1}{F_0-F_X}\right]\left\langle n\pm1\left|\hat{\mathbf{P}}_k\right|n\pm2\right\rangle\left\langle n+2\right|.\end{aligned} \tag{83}$$

Since phonon modes can be defined for this problem, we can express the vibrational states now as

$$\left|n\right\rangle \;\rightarrow\; |n\rangle\overline{\Psi}, \tag{84}$$

where $|n\rangle$ is a number state of the highly excited phonon mode, and where $\overline{\Psi}$ is made up of all the other modes. Since we are focused only on phonon exchange with the highly excited mode we may write

$$\left\langle n\left|\hat{\mathbf{P}}_j\right|n\pm1\right\rangle \;\rightarrow\; \langle n|\hat{\mathbf{P}}_j|n\pm1\rangle. \tag{85}$$

For the phonon exchange contribution to the off-diagonal sector Hamiltonian we have

$$\left\langle \Phi_0 \left| \hat{H}_{n,n\pm1} \left[E - \hat{H}_{n\pm1,n\pm1} \right]^{-1} \hat{H}_{n\pm1,n\pm2} \right| \Phi_0 \right\rangle$$
$$\rightarrow \; - \sum_j \sum_k |n\rangle\langle n|\hat{\mathbf{P}}_j|n\pm1\rangle \cdot \sum_{X\neq 0} \frac{\hbar^2}{M_j M_k} \langle\Phi_0|\nabla_j \Phi_X\rangle_0 \langle\Phi_X|\nabla_k \Phi_0\rangle_0$$
$$\times \left[\frac{1}{-\hat{E}_{\rm off} \mp \hbar\hat{\omega}_0 + F_0 - F_X} - \frac{1}{-F_0 - F_X} \right] \langle n\pm1|\hat{\mathbf{P}}_k|n\pm2\rangle\langle n+2|. \quad (86)$$

In addition, if we work with a strict static phonon basis, then one of the terms that we encountered in the reduction of the non-adiabatic interaction will contribute to the off-diagonal interaction. In this case, the associated interaction will take the form

$$|n\rangle\langle n| \sum_{j,k} \left(-\frac{i\hbar}{2M_j} \right) \Big\{ (\mathbf{R}_j - \mathbf{R}_j^{(0)}) \cdot \langle\nabla_j \Phi_0|\nabla_k \Phi_0\rangle_0 \cdot \hat{\mathbf{P}}_k$$
$$+ \hat{\mathbf{P}}_j \cdot \langle\nabla_j \Phi_0|\nabla_k \Phi_0\rangle_0 \cdot (\mathbf{R}_k - \mathbf{R}_k^{(0)}) \Big\} |n\pm2\rangle\langle n\pm2|. \quad (87)$$

This sector-changing interaction will then be the lowest-order interaction in this kind of model.

5.8. Discussion

As mentioned above the fixed-point model developed here constitutes a picture in its own right on the same basic footing as the Born–Oppenheimer picture and Bloch picture. It is much simpler than the Born–Oppenheimer picture, and nearly as powerful. We have not seen much in the way of application of this model in the literature; in times past it was occasionally mentioned in discussions about the connection between the Born–Oppenheimer approximation and Bloch picture. This seems unfortunate as the fixed-point model looks like it could be very useful.

In any case, we have succeeded in making a connection now between the fixed-point model and the Brillouin–Wigner formalism. This gives us basic formulas for determining the phonon modes (including the static part of the second-order interaction), and for evaluating the off-diagonal sector Hamiltonian which determine the phonon fluctuations at second order. In the fixed-point picture based on a strict static resonant sector definition of the phonon modes, the lowest-order contribution to the phonon fluctuations arises from the non-adiabatic interaction; second-order phonon exchange contributes at the next order.

6. Longitudinal Dielectric Constant from Phonon Dispersion

In the previous section we developed relations for the fixed-point picture from the Born–Oppenheimer picture. In the special case that the fixed-point model is evaluated for a periodic lattice, we end up with an interesting picture in which phonon exchange works the same as in the Born–Oppenheimer approximation. We can make use of this model now to describe phonon fluctuations in our phonon–nuclear model.

However, the amount of development that has led up to this point is considerable. It would be nice if we were able to use the formalism to compute some interesting result that has been obtained previously, in order to gain confidence generally in the results obtained so far. To this end we consider the development of the phonon dispersion relation for a metal crystal. This problem seems of interest because it has received so much attention previously in the literature in the context of the Bloch picture.

The issue that we will focus on here in particular is the establishment of a connection with the longitudinal dielectric constant. For example, the problem of phonon dispersion in metals involves many different issues. We will oversimplify things in our treatment here in order to focus on the longitudinal dielectric constant. When done, we will find that our second-order formalism leads to a dielectric model consistent with the field theory version of the result good to ω^2. It makes clear how phonon exchange in a Born–Oppenheimer based model contributes to the dielectric constant; and finally it provides an important check on the consistency of the fixed-point model against known results in the literature.

6.1. Secular equation in general

Usually the phonon modes are determined from an eigenvalue equation that comes from Newton's laws. In this case we may write

$$\frac{\mathrm{d}}{\mathrm{d}t}(\mathbf{R}_j - \mathbf{R}_j^{(0)}) = \sum_k \mathbf{L}_{jk}\mathbf{P}_k + \sum_k \mathbf{J}_{kj} \cdot (\mathbf{R}_k - \mathbf{R}_k^{(0)}),$$

$$\frac{\mathrm{d}}{\mathrm{d}t}\mathbf{P}_j = -\sum_k \mathbf{K}_{jk} \cdot (\mathbf{R}_k - \mathbf{R}_k^{(0)}) - \sum_k \mathbf{J}_{jk} \cdot \mathbf{P}_k. \tag{88}$$

The phonon frequencies can then be determined in general from

$$-i\omega \begin{pmatrix} \mathbf{R}_j - \mathbf{R}_j^{(0)} \\ \mathbf{P}_j \end{pmatrix} = \sum_k \begin{pmatrix} \mathbf{J}_{kj} & \mathbf{L}_{jk} \\ -\mathbf{K}_{jk} & -\mathbf{J}_{jk} \end{pmatrix} \begin{pmatrix} \mathbf{R}_k - \mathbf{R}_k^{(0)} \\ \mathbf{P}_k \end{pmatrix}, \tag{89}$$

which requires solving for all of the atomic displacements simultaneously. This result is appropriate for a general fixed-point picture model; we have as yet not taken advantage of periodicity in the metal crystal.

6.2. Secular matrix for a monatomic crystal

Much of the relevant literature is concerned with the case of a monatomic metal crystal, where the basic formulas are simplest. It is possible within the framework of the approach that we have taken to develop results for the secular equation. We begin by asserting that the classical position and momentum vectors can be obtained from the real part of the complex versions given by

$$\mathbf{R}_j(t) = \mathbf{R}_j^{(0)} + \mathbf{u}_\mathbf{q} \mathrm{e}^{-i\omega t} \mathrm{e}^{i\mathbf{q}\cdot\mathbf{R}_j^{(0)}}, \tag{90}$$

$$\mathbf{P}_j(t) = \mathbf{v}_\mathbf{q} \mathrm{e}^{-i\omega t} \mathrm{e}^{i\mathbf{q}\cdot\mathbf{R}_j^{(0)}}. \tag{91}$$

The associated mode eigenvalue equation is then

$$-i\omega \begin{pmatrix} \mathbf{u}_\mathbf{q} \\ \mathbf{v}_\mathbf{q} \end{pmatrix} = \begin{pmatrix} \mathbf{J}^{\mathrm{T}}(\mathbf{q}) & \mathbf{L}(\mathbf{q}) \\ -\mathbf{K}(\mathbf{q}) & -\mathbf{J}(\mathbf{q}) \end{pmatrix} \begin{pmatrix} \mathbf{u}_\mathbf{q} \\ \mathbf{v}_\mathbf{q} \end{pmatrix}, \tag{92}$$

where

$$\mathbf{J}(\mathbf{q}) = \sum_k \mathbf{J}_{jk} \mathrm{e}^{i\mathbf{q}\cdot(\mathbf{R}_k^{(0)} - \mathbf{R}_j^{(0)})}, \tag{93}$$

$$\mathbf{K}(\mathbf{q}) = \sum_k \mathbf{K}_{jk} \mathrm{e}^{i\mathbf{q}\cdot(\mathbf{R}_k^{(0)} - \mathbf{R}_j^{(0)})}, \tag{94}$$

$$\mathbf{L}(\mathbf{q}) = \sum_k \mathbf{L}_{jk} \mathrm{e}^{i\mathbf{q}\cdot(\mathbf{R}_k^{(0)} - \mathbf{R}_j^{(0)})}. \tag{95}$$

Note that these secular equations are more complicated than what is usually used in Bloch picture models. Our definition for the transformed force constant matrix is the same as the Bloch picture version (we have the freedom to take the reference site $\mathbf{R}_j^{(0)}$ as the origin), but we require in addition $\mathbf{J}(\mathbf{q})$ and $\mathbf{L}(\mathbf{q})$ matrices which do not show up in the normal Bloch picture model.

6.3. Transformed force matrix

We can split the $\mathbf{K}(\mathbf{q})$ matrix into two parts; one due to interactions between the nuclei; and one due to the electronic energy

$$\mathbf{K}(\mathbf{q}) = \mathbf{K}^{(\mathrm{N})}(\mathbf{q}) + \mathbf{K}^{(\mathrm{e})}(\mathbf{q}). \tag{96}$$

The force constant associated with ion–ion interactions is

$$\mathbf{K}_{jk}^{(\mathrm{N})} = (1 - \delta_{j,k}) \left(\nabla_j \nabla_k \frac{(Ze)^2}{4\pi\epsilon_0 |\mathbf{R}_k - \mathbf{R}_j|} \right)_{\mathbf{R}_j^{(0)}, \mathbf{R}_k^{(0)}}, \tag{97}$$

so we may write

$$\mathbf{K}^{(\mathrm{N})}(\mathbf{q}) = \sum_k (1 - \delta_{j,k}) \left(\nabla_j \nabla_k \frac{(Ze)^2}{4\pi\epsilon_0 |\mathbf{R}_k - \mathbf{R}_j|} \right)_{\mathbf{R}_j^{(0)}, \mathbf{R}_k^{(0)}} \mathrm{e}^{i\mathbf{q}\cdot(\mathbf{R}_k^{(0)} - \mathbf{R}_j^{(0)})}. \tag{98}$$

The force constant associated with the electronic energy is

$$\mathbf{K}_{j,k}^{(\mathrm{e})} = \sum_{X \neq 0} \frac{\langle \Phi_0 | (\nabla_j \hat{V}_{\mathrm{eN}}) | \Phi_X \rangle_0 \langle \Phi_X | (\nabla_k \hat{V}_{\mathrm{eN}}) | \Phi_0 \rangle_0}{E_0 - E_X} + \frac{\langle \Phi_0 | (\nabla_k \hat{V}_{\mathrm{eN}}) | \Phi_X \rangle_0 \langle \Phi_X | (\nabla_j \hat{V}_{\mathrm{eN}}) | \Phi_0 \rangle_0}{E_0 - E_X}, \tag{99}$$

which leads to

$$\mathbf{K}^{(\mathrm{e})}(\mathbf{q}) = \sum_k \sum_{X \neq 0} \left(\frac{\langle \Phi_0 | (\nabla_j \hat{V}_{\mathrm{eN}}) | \Phi_X \rangle_0 \langle \Phi_X | (\nabla_k \hat{V}_{\mathrm{eN}}) | \Phi_0 \rangle_0}{E_0 - E_X} + \frac{\langle \Phi_0 | (\nabla_k \hat{V}_{\mathrm{eN}}) | \Phi_X \rangle_0 \langle \Phi_X | (\nabla_j \hat{V}_{\mathrm{eN}}) | \Phi_0 \rangle_0}{E_0 - E_X} \right) \mathrm{e}^{i\mathbf{q}\cdot(\mathbf{R}_k^{(0)} - \mathbf{R}_j^{(0)})}. \tag{100}$$

6.4. Transformed inverse mass matrix

We can similarly decompose the inverse mass matrix $\mathbf{L}(\mathbf{q})$ into two pieces; one associated with the physical inverse mass; and one associated with the non-adiabatic second-order interaction

$$\mathbf{L}(\mathbf{q}) = \mathbf{L}^{(\mathrm{M})}(\mathbf{q}) + \mathbf{L}^{(\mathrm{eN})}(\mathbf{q}). \tag{101}$$

For the physical inverse mass contribution, we may write

$$\mathbf{L}^{(\mathrm{M})}(\mathbf{q}) = \frac{\mathbf{I}}{M}. \tag{102}$$

For the second-order contribution due to electron–phonon interactions, in the resonant sector we have

$$\mathbf{L}^{(\mathrm{eN})}(\mathbf{q}) = -\sum_k \sum_{X\neq 0} \frac{2\hbar^2}{M^2} \frac{\langle\Phi_0|\nabla_j\Phi_X\rangle_0\langle\Phi_X|\nabla_k\Phi_0\rangle_0}{E_0 - E_X} \mathrm{e}^{i\mathbf{q}\cdot(\mathbf{R}_k^{(0)}-\mathbf{R}_j^{(0)})}. \tag{103}$$

We recall that

$$\langle\Phi_X|\nabla_j\Phi_Y\rangle = -\frac{\langle\Phi_X|(\nabla_j\hat{V}_{\mathrm{eN}})|\Phi_Y\rangle}{E_X - E_Y},$$

so that we may write the second-order contribution to the transformed inverse mass matrix as

$$\mathbf{L}^{(\mathrm{eN})}(\mathbf{q}) = \sum_k \sum_{X\neq 0} \frac{2\hbar^2}{M^2} \frac{\langle\Phi_0|(\nabla_j\hat{V}_{\mathrm{eN}})|\Phi_X\rangle_0\langle\Phi_X|(\nabla_k\hat{V}_{\mathrm{eN}})|\Phi_0\rangle_0}{(E_0 - E_X)^3} \mathrm{e}^{i\mathbf{q}\cdot(\mathbf{R}_k^{(0)}-\mathbf{R}_j^{(0)})}. \tag{104}$$

6.5. Transformation of the **J** matrix

We may write

$$\begin{aligned}\mathbf{J}(\mathbf{q}) &= \sum_k \left(-\frac{i\hbar}{M}\right) \langle\nabla_j\Phi_0|\nabla_k\Phi_0\rangle_0 \, \mathrm{e}^{i\mathbf{q}\cdot(\mathbf{R}_k^{(0)}-\mathbf{R}_j^{(0)})} \\ &= \sum_k \sum_{X\neq 0} \left(-\frac{i\hbar}{M}\right) \frac{\langle\Phi_0|(\nabla_j\hat{V}_{\mathrm{eN}})|\Phi_X\rangle_0\langle\Phi_X|(\nabla_k\hat{V}_{\mathrm{eN}})|\Phi_0\rangle_0}{(E_0 - E_X)^2} \, \mathrm{e}^{i\mathbf{q}\cdot(\mathbf{R}_k^{(0)}-\mathbf{R}_j^{(0)})}.\end{aligned} \tag{105}$$

Now we have a complete set of definitions for the transformed matrices of the fixed-point model which can be used for detailed calculations (we will ultimately require further results for the electronic matrix elements in order to evaluate numerically).

6.6. Simplified ion model

Almost all of the literature on electron–phonon coupling makes the assumption that the core electrons follow the nucleus, and focuses on the resulting interactions between ions and conduction electrons. We can implement this model within the formalism above through the replacements

$$\hat{V}_{\rm eN} \;\rightarrow\; \hat{V}_{\rm ei} = \sum_{j,k} U(|\mathbf{r}_j - \mathbf{R}_k|), \tag{106}$$

$$\frac{Z_j Z_k e^2}{4\pi\epsilon_0 |\mathbf{R}_k - \mathbf{R}_j|} \;\rightarrow\; V_{j,k}(|\mathbf{R}_k - \mathbf{R}_j|), \tag{107}$$

where

$$\lim_{|\mathbf{R}_k - \mathbf{R}_j| \rightarrow \infty} V_{j,k}(|\mathbf{R}_k - \mathbf{R}_j|) = \frac{Z_j^* Z_k^* e^2}{4\pi\epsilon_0 |\mathbf{R}_k - \mathbf{R}_j|}. \tag{108}$$

However, in what follows we will pursue an even simpler version of the model in which

$$\hat{V}_{\rm ei} \;\rightarrow\; -\sum_{j,k} \frac{Z_k^* e^2}{4\pi\epsilon_0 |\mathbf{R}_k - \mathbf{r}_j|} \tag{109}$$

and

$$V_{j,k}(|\mathbf{R}_k - \mathbf{R}_j|) \;\rightarrow\; \frac{Z_j^* Z_k^* e^2}{4\pi\epsilon_0 |\mathbf{R}_k - \mathbf{R}_j|}. \tag{110}$$

This will reduce the complexity of the calculations to follow. It is of course well known that the electron–ion potential is softer than a Coulomb potential, and there is no difficulty with replacing this Coulomb model with a better pseudopotential model anywhere in the calculations that follow.

6.7. Reduction of the transformed force constant matrix

In order to identify the longitudinal dielectric constant, it will be easiest to simply evaluate the different transformed matrices. To this end, we can make use of the discrete Fourier transform of the normalized Coulomb potential to write

$$\frac{1}{|\mathbf{R} - \mathbf{r}|} = \frac{1}{V} \sum_{\mathbf{K}} \frac{4\pi}{|\mathbf{K}|^2} {\rm e}^{i\mathbf{K}\cdot(\mathbf{R}-\mathbf{r})}. \tag{111}$$

The electron–ion interaction can then be written as

$$\hat{V}_{\rm ei} = -\sum_{j,k} \frac{Z_k^* e^2}{\epsilon_0 V} \sum_{\mathbf{K}} \frac{1}{|\mathbf{K}|^2} {\rm e}^{i\mathbf{K}\cdot(\mathbf{R}_k - \mathbf{r}_j)} \tag{112}$$

and the gradient becomes

$$\nabla_k \hat{V}_{\rm ei} = -i \sum_j \frac{Z_k^* e^2}{\epsilon_0 V} \sum_{\mathbf{K}} \frac{\mathbf{K}}{|\mathbf{K}|^2} e^{i\mathbf{K}\cdot(\mathbf{R}_k - \mathbf{r}_j)}. \tag{113}$$

We can use this to reduce the transformed force constant matrix

$$\begin{aligned}
\mathbf{K}^{(\rm e)}(\mathbf{q}) \;\rightarrow\; & -\sum_k \sum_{X\neq 0} \sum_{\mathbf{K}} \sum_{\mathbf{K}'} \left(\frac{Z^* e^2}{\epsilon_0 V}\right)^2 \frac{\mathbf{K}\mathbf{K}'}{|\mathbf{K}|^2|\mathbf{K}'|^2} \frac{1}{E_0 - E_X} {\rm e}^{i\mathbf{K}\cdot\mathbf{R}_j} {\rm e}^{i\mathbf{K}'\cdot\mathbf{R}_k} \\
& \left\langle \Phi_0 \left| \sum_l {\rm e}^{-i\mathbf{K}\cdot\mathbf{r}_l} \right| \Phi_X \right\rangle \left\langle \Phi_X \left| \sum_{l'} {\rm e}^{-i\mathbf{K}'\cdot\mathbf{r}_{l'}} \right| \Phi_0 \right\rangle {\rm e}^{i\mathbf{q}\cdot(\mathbf{R}_k^{(0)} - \mathbf{R}_j^{(0)})} \\
& -\sum_k \sum_{X\neq 0} \sum_{\mathbf{K}} \sum_{\mathbf{K}'} \left(\frac{Z^* e^2}{\epsilon_0 V}\right)^2 \frac{\mathbf{K}\mathbf{K}'}{|\mathbf{K}|^2|\mathbf{K}'|^2} \frac{1}{E_0 - E_X} {\rm e}^{i\mathbf{K}\cdot\mathbf{R}_k} {\rm e}^{i\mathbf{K}'\cdot\mathbf{R}_j} \\
& \left\langle \Phi_0 \left| \sum_l {\rm e}^{-i\mathbf{K}\cdot\mathbf{r}_l} \right| \Phi_X \right\rangle \left\langle \Phi_X \left| \sum_{l'} {\rm e}^{-i\mathbf{K}'\cdot\mathbf{r}_{l'}} \right| \Phi_0 \right\rangle {\rm e}^{i\mathbf{q}\cdot(\mathbf{R}_k^{(0)} - \mathbf{R}_j^{(0)})}.
\end{aligned} \tag{114}$$

We can take advantage of the random phase approximation; to proceed we split this into coherent and incoherent pieces

$$\mathbf{K}^{(\rm e)}(\mathbf{q}) = \mathbf{K}^{(\rm e)}_{\rm coh}(\mathbf{q}) + \mathbf{K}^{(\rm e)}_{\rm inc}(\mathbf{q}), \tag{115}$$

where the coherent part is

$$\begin{aligned}
\mathbf{K}^{(\rm e)}_{\rm coh}(\mathbf{q}) = & \sum_k \sum_{X\neq 0} \sum_{\mathbf{K}} \left(\frac{Z^* e^2}{\epsilon_0 V}\right)^2 \frac{\mathbf{K}\mathbf{K}}{|\mathbf{K}|^4} \frac{1}{E_0 - E_X} \\
& \left[{\rm e}^{i(\mathbf{q}-\mathbf{K})\cdot(\mathbf{R}_k^{(0)} - \mathbf{R}_j^{(0)})} + {\rm e}^{i(\mathbf{q}+\mathbf{K})\cdot(\mathbf{R}_k^{(0)} - \mathbf{R}_j^{(0)})} \right] \\
& \left\langle \Phi_0 \left| \sum_l {\rm e}^{-i\mathbf{K}\cdot\mathbf{r}_l} \right| \Phi_X \right\rangle \left\langle \Phi_X \left| \sum_{l'} {\rm e}^{i\mathbf{K}\cdot\mathbf{r}_{l'}} \right| \Phi_0 \right\rangle.
\end{aligned} \tag{116}$$

Note that

$$\begin{aligned}
& \left\langle \Phi_0 \left| \sum_l {\rm e}^{-i\mathbf{K}\cdot\mathbf{r}_l} \right| \Phi_X \right\rangle \left\langle \Phi_X \left| \sum_{l'} {\rm e}^{i\mathbf{K}\cdot\mathbf{r}_{l'}} \right| \Phi_0 \right\rangle \\
& \quad = \left\langle \Phi_0 \left| \sum_l {\rm e}^{i\mathbf{K}\cdot\mathbf{r}_l} \right| \Phi_X \right\rangle \left\langle \Phi_X \left| \sum_{l'} {\rm e}^{-i\mathbf{K}\cdot\mathbf{r}_{l'}} \right| \Phi_0 \right\rangle,
\end{aligned} \tag{117}$$

so we may write

$$\mathbf{K}^{(\mathrm{e})}_{\mathrm{coh}}(\mathbf{q}) = \sum_k \sum_{X\neq 0} \sum_{\mathbf{K}} 2\left(\frac{Z^* e^2}{\epsilon_0 V}\right)^2 \frac{\mathbf{K}\mathbf{K}}{|\mathbf{K}|^4} \frac{1}{E_0 - E_X} \mathrm{e}^{i(\mathbf{q}-\mathbf{K})\cdot(\mathbf{R}^{(0)}_k - \mathbf{R}^{(0)}_j)} \left\langle \Phi_0 \left| \sum_l \mathrm{e}^{-i\mathbf{K}\cdot\mathbf{r}_l} \right| \Phi_X \right\rangle \left\langle \Phi_X \left| \sum_{l'} \mathrm{e}^{i\mathbf{K}\cdot\mathbf{r}_{l'}} \right| \Phi_0 \right\rangle. \tag{118}$$

6.8. Reduction of the transformed inverse mass matrix

A similar computation can be done for the electron–ion part of the transformed inverse mass matrix; we may write

$$\begin{aligned}\mathbf{L}^{(\mathrm{ei})}(\mathbf{q}) &= \sum_k \sum_{X\neq 0} \frac{2\hbar^2}{M^2} \frac{\langle\Phi_0|(\nabla_j \hat{V}_{\mathrm{ei}})|\Phi_X\rangle_0 \langle\Phi_X|(\nabla_k \hat{V}_{\mathrm{ei}})|\Phi_0\rangle_0}{(E_0 - E_X)^3} \mathrm{e}^{i\mathbf{q}\cdot(\mathbf{R}^{(0)}_k - \mathbf{R}^{(0)}_j)} \\ &\rightarrow -\sum_k \sum_{X\neq 0} \sum_{\mathbf{K}} \sum_{\mathbf{K}'} \frac{2\hbar^2}{M^2} \left(\frac{Z^* e^2}{\epsilon_0 V}\right)^2 \frac{\mathbf{K}\mathbf{K}'}{|\mathbf{K}|^2|\mathbf{K}'|^2} \frac{1}{(E_0 - E_X)^3} \mathrm{e}^{i\mathbf{K}\cdot\mathbf{R}^{(0)}_j} \mathrm{e}^{i\mathbf{K}'\cdot\mathbf{R}^{(0)}_k} \\ &\quad \left\langle \Phi_0 \left| \sum_l \mathrm{e}^{-i\mathbf{K}\cdot\mathbf{r}_l} \right| \Phi_X \right\rangle \left\langle \Phi_X \left| \sum_{l'} \mathrm{e}^{-i\mathbf{K}'\cdot\mathbf{r}_{l'}} \right| \Phi_0 \right\rangle \mathrm{e}^{i\mathbf{q}\cdot(\mathbf{R}^{(0)}_k - \mathbf{R}^{(0)}_j)}. \end{aligned} \tag{119}$$

We can divide this into coherent and incoherent parts

$$\mathbf{L}^{(\mathrm{ei})}(\mathbf{q}) = \mathbf{L}^{(\mathrm{ei})}_{\mathrm{coh}}(\mathbf{q}) + \mathbf{L}^{(\mathrm{ei})}_{\mathrm{inc}}(\mathbf{q}). \tag{120}$$

The coherent part involves terms where $\mathbf{K} + \mathbf{K}' = 0$

$$\mathbf{L}^{(\mathrm{ei})}_{\mathrm{coh}}(\mathbf{q}) = \sum_k \sum_{X\neq 0} \sum_{\mathbf{K}} \frac{2\hbar^2}{M^2} \left(\frac{Z^* e^2}{\epsilon_0 V}\right)^2 \frac{\mathbf{K}\mathbf{K}}{|\mathbf{K}|^4} \frac{1}{(E_0 - E_X)^3} \mathrm{e}^{i(\mathbf{q}-\mathbf{K})\cdot(\mathbf{R}^{(0)}_k - \mathbf{R}^{(0)}_j)} \left\langle \Phi_0 \left| \sum_l \mathrm{e}^{-i\mathbf{K}\cdot\mathbf{r}_l} \right| \Phi_X \right\rangle \left\langle \Phi_X \left| \sum_{l'} \mathrm{e}^{i\mathbf{K}\cdot\mathbf{r}_{l'}} \right| \Phi_0 \right\rangle. \tag{121}$$

We assume the coherent part dominates, and that the residual incoherent part can be neglected, consistent with the random phase approximation.

6.9. Reduction of the transformed **J** matrix

Due to the similarity between these different transformed matrices, we can write directly

$$\mathbf{J}(\mathbf{q}) = \mathbf{J}_{\mathrm{coh}}(\mathbf{q}) + \mathbf{J}_{\mathrm{inc}}(\mathbf{q}), \tag{122}$$

where

$$\mathbf{J}_{\rm coh}(\mathbf{q}) = -\sum_k \sum_{X\neq 0} \sum_{\mathbf{K}} \frac{i\hbar}{M} \left(\frac{Z^* e^2}{\epsilon_0 V}\right)^2 \frac{\mathbf{K}\mathbf{K}}{|\mathbf{K}|^4} \frac{1}{(E_0 - E_X)^2} e^{i(\mathbf{q}-\mathbf{K})\cdot(\mathbf{R}_k^{(0)} - \mathbf{R}_j^{(0)})} \left\langle \Phi_0 \left| \sum_l e^{-i\mathbf{K}\cdot\mathbf{r}_l} \right| \Phi_X \right\rangle \left\langle \Phi_X \left| \sum_{l'} e^{i\mathbf{K}\cdot\mathbf{r}_{l'}} \right| \Phi_0 \right\rangle. \tag{123}$$

6.10. Transformed ion-ion part of the force matrix

The transformed ion–ion part of the force matrix in this model is

$$\begin{aligned}\mathbf{K}^{(\rm i)}(\mathbf{q}) &= \sum_k (1-\delta_{j,k}) \left(\nabla_j \nabla_k \frac{(Z^* e)^2}{4\pi\epsilon_0 |\mathbf{R}_k - \mathbf{R}_j|}\right)_{\mathbf{R}_j^{(0)}, \mathbf{R}_k^{(0)}} e^{i\mathbf{q}\cdot(\mathbf{R}_k^{(0)} - \mathbf{R}_j^{(0)})} \\ &= \sum_k \sum_{\mathbf{K}} (1-\delta_{j,k}) \frac{(Z^* e)^2}{\epsilon_0 V} \frac{\mathbf{K}\mathbf{K}}{|\mathbf{K}|^2} e^{i(\mathbf{q}-\mathbf{K})\cdot(\mathbf{R}_k^{(0)} - \mathbf{R}_j^{(0)})}.\end{aligned} \tag{124}$$

6.11. Connection with literature longitudinal dielectric constant

It seems useful to make a connection with the literature, which focuses on the longitudinal dielectric constant. Perhaps the most straightforward way to do this is to make use of

$$\mathbf{P}_j \;\rightarrow\; -i\omega M_j (\mathbf{R}_j - \mathbf{R}_j^{(0)}) \tag{125}$$

and write the model in terms of a frequency-dependent force model

$$\begin{aligned}&\frac{1}{2}\sum_{j,k} \hat{\mathbf{P}}_j \cdot \mathbf{L}_{jk} \cdot \hat{\mathbf{P}}_k + \frac{1}{2}\sum_{j,k} (\mathbf{R}_j - \mathbf{R}_j^{(0)}) \cdot \mathbf{K}_{jk} \cdot (\mathbf{R}_k - \mathbf{R}_k^{(0)}) \\ &\quad + \frac{1}{2}\sum_{j,k} \left[(\mathbf{R}_j - \mathbf{R}_j^{(0)}) \cdot \mathbf{J}_{jk} \cdot \hat{\mathbf{P}}_k + \hat{\mathbf{P}}_j \cdot \mathbf{J}_{kj} \cdot (\mathbf{R}_k - \mathbf{R}_k^{(0)}) \right] \\ &\qquad \rightarrow\; \frac{1}{2}\sum_j \frac{|\hat{\mathbf{P}}_j|^2}{2M} + \frac{1}{2}\sum_{j,k} (\mathbf{R}_j - \mathbf{R}_j^{(0)}) \cdot \left[\mathbf{K}_{jk} - iM\omega[\mathbf{J}_{jk} + \mathbf{J}_{jk}^{\rm T}] - M^2\omega^2 \mathbf{L}_{jk}^{(\rm ei)} \right] \cdot (\mathbf{R}_k - \mathbf{R}_k^{(0)}).\end{aligned} \tag{126}$$

The idea here is to view the various **J** and **L** matrices as providing dynamical corrections to the force constant matrix. From such a perspective it would make sense to define a dynamical version of the transformed force matrix from the coherent parts of the $\mathbf{J}(\mathbf{q})$, $\mathbf{K}(\mathbf{q})$ and $\mathbf{L}(\mathbf{q})$ transformed matrices according to

$$\mathbf{K}^{(\rm eff)}(\mathbf{q},\omega) \;\rightarrow\; \sum_k \sum_{\mathbf{K}} \left\{ \frac{1-\delta_{j,k}}{\epsilon_0} + \left[\frac{1}{\epsilon(\mathbf{K},\omega)} - \frac{1}{\epsilon_0} \right] \right\} \frac{(Z^* e)^2}{\epsilon_0 V} \frac{\mathbf{K}\mathbf{K}}{|\mathbf{K}|^2} e^{i(\mathbf{q}-\mathbf{K})\cdot(\mathbf{R}_k^{(0)} - \mathbf{R}_j^{(0)})}, \tag{127}$$

where

$$\frac{1}{\epsilon(\mathbf{K},\omega)} = \frac{1}{\epsilon_0} + \sum_{X\neq 0} \frac{2e^2}{\epsilon_0^2 V|\mathbf{K}|^2} \left[\frac{1}{E_0 - E_X} - \frac{\hbar\omega}{(E_0 - E_X)^2} - \frac{(\hbar\omega)^2}{(E_0 - E_X)^3} \right] \left\langle \Phi_0 \left| \sum_l \mathrm{e}^{-i\mathbf{K}\cdot\mathbf{r}_l} \right| \Phi_X \right\rangle \left\langle \Phi_X \left| \sum_{l'} \mathrm{e}^{i\mathbf{K}\cdot\mathbf{r}_{l'}} \right| \Phi_0 \right\rangle . \tag{128}$$

This suggests that the model which we are working with involves dynamical terms which match up to second order a more sophisticated model based on

$$\frac{1}{\epsilon(\mathbf{K},\omega)} = \frac{1}{\epsilon_0} + \sum_{X\neq 0} \frac{2e^2}{\epsilon_0^2 V|\mathbf{K}|^2} \frac{1}{\hbar\omega + E_0 - E_X} \left\langle \Phi_0 \left| \sum_l \mathrm{e}^{-i\mathbf{K}\cdot\mathbf{r}_l} \right| \Phi_X \right\rangle \left\langle \Phi_X \left| \sum_{l'} \mathrm{e}^{i\mathbf{K}\cdot\mathbf{r}_{l'}} \right| \Phi_0 \right\rangle . \tag{129}$$

The static limit of this dielectric constant is consistent with Nozieres and Pines [34]. The explicit frequency dependence of this model is similar to that appearing in the model of Ehrenreich and Cohen [35]. We might expect that if we were to include higher-order dynamical terms that more terms in the associated geometric series would be generated, resulting ultimately in this full dynamical longitudinal dielectric model.

6.12. Discussion

We have succeeded in this section of implementing a fixed-point picture model for the phonon dispersion relation of a monatomic metal crystal, and we have evaluated it in the special case of a simple Coulomb interaction for the electron-ion interaction in order to extract the associated longitudinal dielectric model. We find that the resulting dielectric model matches the literature result from field theory up to and including second-order (ω^2), which helps to verify the model, and also to clarify how things work. For example, we can see that it is the second-order phonon-exchange interaction in the fixed-point model that produces the ω^2 term. The discussions in [36,37] may be relevant here. We note that there was other earlier work in which the dispersion relation and the longitudinal dielectric constant have been studied within the Born–Oppenheimer approximation [38].

7. Summary and Conclusions

In earlier work we have developed a model that describes coherent energy exchange under conditions of fractionation between nuclei and a highly excited phonon mode. To compare with experiment, we begin with the basic theory described in [18], we make use of the interpretation (based on coherent energy exchange between acoustic vibrations and excitation of the lowest nuclear level in ^{201}Hg) described in [17], and a specific model consistent with this interpretation. What we found was a substantial disagreement between the resulting model and experimental observations.

The resulting disagreement could be due to a problem with the underlying theory, issues with our proposed interpretation, or errors in the model and/or model parameters. We were motivated in this work by a concern that the problem might be in the basic theory; in particular we had neglected phonon fluctuations due to coupling with conduction electrons. Our interest in modeling the effect ultimately resulted in this study. The problem that we encountered is that electron–phonon interactions in metals is usually formulated in the Bloch picture, but there are differences between how phonon exchange works in the Bloch picture and in the Born–Oppenheimer picture. We are interested in models that involve off-resonant interactions, and the equivalence of the two pictures has been argued for on-resonance; consequently, we are interested in phonon exchange in a Born–Oppenheimer picture to describe phonon fluctuations.

It seemed ultimately to be simplest just to start from scratch, and follow the development of the Born–Oppenheimer approximation in a Brillouin–Wigner formulation that is well matched to other models we have been constructing. The Brillouin–Wigner formalism is suited to taking into account the strong first-order interaction, and otherwise separating the phonon and electron degrees of freedom. In the end we have a model that describes the second-order coupling of equivalent "dressed" phonons (in the Brillouin–Wigner sense) which gives rise to the fluctuations of interest in the phonon–nuclear model.

However, in the process we have covered a lot of developmental ground, so there is reason to be concerned as to whether the fixed-point model we are working with is free of errors. In order to test this, we decided to develop relations that describe the phonon dispersion relation for a monatomic metal crystal, which is probably the best known relevant problem from Bloch picture models in the literature. The longitudinal dielectric constant consistent with this model results in the same static model as is obtained from the Bloch picture, and gives results up to second order that are in agreement with literature results from field theory. This provides confidence in the preceding development.

We have made use of simple Coulomb potentials for the electron-ion interaction, which is appropriate for long wavelength vibrations. For computations involving shorter wavelength phonons we would need to make use of better electron-ion potentials. This is discussed extensively in the literature, and the modification of the formulas for this case is straightforward. The reduction of the many-electron matrix elements into simpler models is also straightforward, and will have to be addressed in using these results for detailed calculations.

A reviewer noted that this paper seems to lack a major punchline. In response it seems useful to spell out the major punchlines for this paper, and for what we found subsequently when we made use of it. The first is that there does not exist in the literature a systematic treatment of Born–Oppenheimer and related approximations adapted for the case of a metal, which in our view is suitable for the development of a fluctuation model; the biggest contribution of this paper then is to provide a useful foundation in a relevant language. Another significant result is the clarification of how the longitudinal dielectric constant of a metal comes about in the lowest orders of perturbation theory in a Born–Oppenheimer approximation. Although it is mentioned in a few works that such a result was known previously, we have not found a clear discussion of it. Another important result which we found when we used the model described here to develop a fluctuation model is that the results from the Born–Oppenheimer picture are very different from what we get with a Bloch picture model. In the literature the two pictures are largely viewed as equivalent in connection with describing phonon exchange in metals; while perhaps true for screening and for lowest-order phonon exchange, this is certainly not the case for phonon fluctuations. And finally, we will discuss in a following publication that a fluctuation model based on the Born–Oppenheimer picture is inappropriate above a certain size scale, so that a fluctuation model based on the Bloch picture must be used. On the other hand, fluctuations for a nano-scale metal sample should be treated using a Born–Oppenheimer model.

References

[1] M. Fleischmann, S. Pons and M. Hawkins, *J. Electroanal. Chem.* **201** (1989) 301; errata **263** (1990) 187.
[2] M. Fleischmann, S. Pons, M.W. Anderson, L.J. Li and M. Hawkins, *J. Electroanal. Chem.* **287** (1990) 293.
[3] E. Storms, *Science of Low Energy Nuclear Reaction: A Comprehensive Compilation of Evidence and Explanations about Cold Fusion*, World Scientific, New Jersey (2004).
[4] P.L. Hagelstein, M.C.H. McKubre, D.J. Nagel, T.A. Chubb and R.J. Hekman, *Proc. ICCF11* (2004) 23.
[5] P.L. Hagelstein, Constraints on energetic particles in the Fleischmann– Pons experiment, *Naturwissenschaften* **97** (2010) 345.
[6] P.L. Hagelstein, A unified model for anomalies in metal deuterides, *Proc. ICCF9* (2002) 121.
[7] P.L. Hagelstein and I.U. Chaudhary, Level splitting in association with the multiphoton Bloch—Siegert shift, *J. Phys. B: At. Mol. Phys.* **41** (2008) 035601.
[8] P.L. Hagelstein and I.U. Chaudhary, Models relevant to excess heat production in Fleischmann–Pons experiments, *Low-energy Nuclear Reactions Sourcebook, ACS Symposium Series* **998** (2008) 249.

[9] P.L. Hagelstein and I.U. Chaudhary, Energy exchange in the lossy spin–boson model, *J. Cond. Mat. Nucl. Sci.* **5** (2011) 52.
[10] P.L. Hagelstein and I.U. Chaudhary, Dynamics in the case of coupled degenerate states, *J. Cond. Mat. Nucl. Sci.* **5** (2011) 72.
[11] P.L. Hagelstein and I.U. Chaudhary, Second-order formulation and scaling in the lossy spin–boson model, *J. Cond. Mat. Nucl. Sci.* **5** (2011) 87.
[12] P.L. Hagelstein and I.U. Chaudhary, Local approximation for the lossy spin—boson model, *J. Cond. Mat. Nucl. Sci.* **5** (2011) 102.
[13] P.L. Hagelstein and I.U. Chaudhary, Coherent energy exchange in the strong coupling limit of the lossy spin–boson model, *J. Cond. Mat. Nucl. Sci.* **5** (2011) 116.
[14] P.L. Hagelstein and I.U. Chaudhary, Generalization of the lossy spin-–boson model to donor and receiver systems, *J. Cond. Mat. Nucl. Sci.* **5** (2011) 140.
[15] P.L. Hagelstein and I.U. Chaudhary, Errata and comments on a recent set of papers in Journal of Condensed Matter in Nuclear Science, *J. Cond. Mat. Nucl. Sci.* **7** (2012) 1.
[16] P.L. Hagelstein and I.U. Chaudhary, Including nuclear degrees of freedom in a lattice hamiltonian, *J. Cond. Mat. Nucl. Sci.* **7** (2011) 35.
[17] P.L. Hagelstein and I.U. Chaudhary, A model for collimated emission in the Karabut experiment, *Proc. ICCF17*, in press.
[18] P.L. Hagelstein and I.U. Chaudhary, Phonon–nuclear coupling for anomalies in condensed matter nuclear science, *J. Cond. Mat. Nucl. Sci.* , submitted.
[19] P.L. Hagelstein, Bird's Eye View of Phonon Models for Excess Heat in the Fleischmann–Pons Experiment, *J. Cond. Mat. Nucl. Sci.* **6** (2011) 169.
[20] P.L. Hagelstein and I.U. Chaudhary, Models for excess heat in PdD and NiH, *Proc. ICCF17*, in press.
[21] A.B. Karabut, Research into powerful solid X-ray laser (wave length is 0.8–1.2 nm) with excitation of high current glow discharge ions, *Proc. 11th Int. Conf. on Emerging Nuclear Energy Systems*, 29 September–4 October 2002, Albuquerque, New Mexico, USA, pp. 374–381.
[22] A.B. Karabut, Experimental research into characteristics of X-ray emission from solid-state cathode medium of high-current glow discharge, *Proc. 10th Int. Conf. on Cold Fusion*, August 24–29, 2003, Cambridge, MA, USA.
[23] A.B. Karabut, Research into characteristics of x-ray emission laser beams from solid-state cathode medium of high current glow discharge, *Proc. 11th Int. Conf. on Cold Fusion*, 31 October-–5 November, 2004, France, pp. 253–257.
[24] A.B. Karabut, Study of energetic and temporal characteristics of x-ray emission from solid state cathode medium of high current glow discharge, *Proc. 12th Int. Conf. on Cold Fusion*, December 2-–7, 2006, Japan, pp. 344-–350.
[25] A.B. Karabut and E.A. Karabut, Research into energy spectra of X-ray emission from solid cathode medium during the high current glow discharge operation and after the glow discharge current switch off, *Proc. 14th Int. Conf. on Cold Fusion*, August 10-–15, 2008, USA.
[26] A.B. Karabut, E.A. Karabut and P.L. Hagelstein, Spectral and temporal characteristics of X-ray emission from metal electrodes in a high-current glow discharge, *J. Cond. Mat. Nucl. Sci.* **6** (2012) 217.
[27] L.J. Sham and J.M. Ziman, The electron–phonon interaction, *Solid State Phys.* **15** (1963) 221.
[28] S.K. Joshi and A.K. Rajagopa, Lattice dynamics of metals, *Solid State Phys.* **22** (1969) 159.
[29] J.M. Ziman, The electron–phonon interaction, according to the adiabatic approximation, *Math. Proc. Cambridge Philos. Soc.* **51** (1955) 707.
[30] J. C. Taylor, The electron–phonon interaction, according to the adiabatic approximation, *Math. Proc. Cambridge Philos. Soc.* **52** (1956) 693.
[31] H. Feshbach, A unified theory of nuclear reactions, II *Ann. Phys.* **19** (1962) 287.
[32] R.A. Deegan, electron–phonon interaction in the tight-binding approximation: Validity of the Bloch formulation, *Phys. Rev. B 5* (1972) 1183.
[33] J. Ashkenazi, M. Dacorogna and M. Peter, On the equivalence of the Frolich and Bloch approaches to the electron–phonon coupling, *Sol. State Comm.* **29** (1979) 181.
[34] P. Nozieres and D. Pines, A dielectric formulation of the many body problem: Application to the free electron gas, *Il Nuovo Cimento* **9** (1958) 470.
[35] H. Ehrenreich and M.L. Cohen, Self-consistent field approach to the many-electron problem, *Phys. Rev.* **115** (1959) 786.
[36] E.G. Brovman and Yu. Kagan, The phonon spectrum of metals, *Sov. Phys. JETP* **25** (1967) 364.

[37] B.T. Geilikman, The adiabatic approximation and Fröhlich model in the theory of metals, *J. Low. Temp. Phys.* **4** (1971) 189 .
[38] R. M. Pick, M.H. Cohen and R. M. Martin, Microscopic theory of force constants in the adiabatic approximation, *Phys. Rev. B* **1** (1970) 910.

J. Condensed Matter Nucl. Sci. 12 (2013) 105–142

Research Article

Phonon–nuclear Coupling for Anomalies in Condensed Matter Nuclear Science

Peter L. Hagelstein *

Research Laboratory of Electronics, Massachusetts Institute of Technology, Cambridge, MA 02139, USA

Irfan U. Chaudhary

Department of Computer Science and Engineering, University of Engineering and Technology. Lahore, Pakistan

Abstract

Excess heat in the Fleischmann–Pons experiment is thought to have a nuclear origin, yet there are no energetic particles observed in amounts commensurate with the energy produced. This in our view is the most fundamental issue in connection with theory. In earlier work we developed a mathematical model (the lossy spin–boson model) which shows coherent energy exchange between two-level systems and an oscillator under conditions of fractionation. Recently, we have found an interesting physical model that is closely connected, and which is capable of coherent energy exchange with fractionation; this model is based on a relativistic description of composite nuclei in a lattice. In this work we present a much stronger development of the model directly from field theory than given previously. In the lossy spin–boson model, the ability of the model to fractionate a large quantum depends on the presence of suitable loss mechanisms; the same is true in the case of the new physical model. The new model predicts anomalies such as excess heat without energetic nuclear radiation, ^{4}He production, low-level gamma emission, and collimated X-ray emission in the Karabut experiment; however, as yet we have not demonstrated agreement between theory and experiment. Last summer we concluded (erroneously) that coupling with strong static transitions might impact the fractionation power of the model on dynamic transitions, and the resulting model appeared to be in agreement with our interpretation of the experiment. Here we review this kind of model more carefully, and find that no such enhancement is present. Our conclusion in the end is that the theory, model, and interpretation are "close" to the experimental results in the case of the Karabut experiment, but some problem remains.
 ISSN 2227-3123

Keywords: Phonon theory, fractionation, Fleischmann-Pons experiment, Karabut experiment, fundamental Hamiltonian

1. Introduction

Excess heat in the Fleischmann–Pons experiment [1,2] is an effect that should probably not occur, at least according to how nuclear physics and condensed matter physics are currently understood in text books and in the literature.

*E-mail: plh@mit.edu

 ISSN 2227-3123

Nevertheless, there are a sufficient number of experiments showing positive results [3,4] that we consider the effect to be very real, and very much worth understanding theoretically. How many positive confirmation experiments will be required in order to convince the scientific community generally to take an interest is one of the imponderable questions in the field. The situation at this time is almost beyond comprehension, as experiments in the case of the Piantelli group and the Swartz effort have reached the point where the possible commercialization of the associated technology could be contemplated [and other groups (Rossi, and Defkalion) are currently claiming to have already made substantial progress toward the commercialization of relevant technology].

The amount of excess energy produced in the Fleischmann–Pons experiment is prodigious, yet there is no commensurate level of chemical products observed. This observation led Fleischmann to conjecture that the origin of the energy might be nuclear. In the case of PdD experiments, ^{4}He has been observed in amount commensurate with the energy produced, and correlated with energy production (the effect was first studied by Bush, Miles, and coworkers [5–8]). Unfortunately, no similar results are available for the NiH experiments (where ^{3}He measurements are badly needed). Measurements of the amount of ^{4}He produced to energy generated are consistent with the 24 MeV mass difference between two deuterium atoms and ^{4}He [3], but further measurements are needed to be sure.

In normal nuclear reactions, the energy produced is expressed through energetic nuclear particles. If this were the case in the Fleischmann–Pons experiment, we would be able to study the reaction mechanism using conventional nuclear techniques. For example, fusion between two deuterons leads to p+t and n+^{3}He as energetic products in roughly equal amounts; but as is well known neither channel occurs in amounts commensurate with the energy produced in Fleischmann–Pons experiment. Since ^{4}He is considered to be a product in the case of PdD experiments, we might expect it to carry away some fraction of the reaction energy in a Rutherford scenario. If we consider the PdD itself to constitute a nuclear detector, then from a theoretical calibration we conclude that it is an exquisitely sensitive detector of fast alphas [9,10]. From data reported for simultaneous neutron and excess power production, we conclude that the alphas are born confidently with an energy less than 20 keV [10,11], under conditions where the reaction energy is thought to be 24 MeV. This is inconsistent with any sensible Rutherford picture reaction mechanism.

Huizenga considered the absence of 24 MeV gammas in connection with ^{4}He as a product to be one of his three "miracles" [12]. From our perspective Huizenga did not come close to capturing what is really significant in connection with this "hidden product miracle;" instead of focusing on the absence of gamma emission, the real headache in these experiments is the complete absence of any energetic nuclear emission at a level commensurate with the energy produced. For example, if energetic electrons or gammas were present at the watt level, then it would be obvious (as a health hazard if for no other reason); and if energetic neutrons, protons, alphas, or other low-mass nuclei were present there would be a corresponding large penetrating neutron signal (which is not seen). We note that there have been a very large number of theoretical mechanisms put forth over the years to account for excess energy in the Fleischmann–Pons experiment. Since the vast majority of these are based ultimately on Rutherford picture reaction mechanisms (that is, that the reaction energy comes out as energetic nuclear radiation in amounts commensurate with the energy produced), we can conclude that nearly all of these theoretical proposals can be discounted as being inconsistent with experiment (because nuclear radiation at levels commensurate with the energy produced is not seen in the PdD experiments). This point has generally not been appreciated within the condensed matter nuclear science community, as new proposals and models continue to be put forth which would ultimately lead to orders of magnitude more nuclear radiation than is observed in experiment.

If the energy produced does not go into the generation of energetic nuclear radiation, then we might reasonably ask: where does it go? For example, one can see in Schwinger's ICCF4 paper his focus on this problem, which he recognized as perhaps the most significant theoretical issue [13]. Preparata was of the opinion that the nuclear energy coupled to plasmons [14] or various low energy channels [15]. The focus of our efforts for a great many years now has centered on the possibility that the nuclear energy is coupled into vibrations.

Although this has clearly been the key theoretical issue in our view since the beginning, there is very little in the

way of experimental measurements that shed light on how it works. The singular exception is in the case of the Letts two-laser experiment [16,17]. In this experiment, excess heat is triggered when two weak laser beams at different wavelengths overlap in p-polarization on the surface of a Fleischmann–Pons cathode held just below threshold for excess heat production. The excess power produced is seen to be largest at three resonances; the lower two of which correspond to the Γ-point and L-point of the optical phonon mode dispersion relation (which are points where the group velocity for the compressional optical phonon modes go to zero). By itself, this implicates the participation of these optical phonon modes in excess heat production. In single-laser experiments [18–23] excess heat is also triggered by a weak laser beam; however, in this case it goes away when the laser is turned off. In the two-laser experiment, the excess heat is observed to persists after the lasers are switched off. It has been argued [17] that this provides indirect evidence that the nuclear energy is going into these vibrational modes to sustain them (an argument that has not been universally accepted). In a more recent report [24], the excess heat in at least one case was seen to die off slowly after the lasers are switched off.

Of course, once one goes down this particular road, the immediate issue that arises has to do with how a very large MeV quantum gets split up into the large number of low-energy quanta associated with a condensed matter degree of freedom. Up-conversion from the optical regime to the X-ray regime is known in high-harmonic generation [25], where several thousand low-energy quanta are combined to make a more energetic X-ray quantum. However, for the Fleischmann–Pons experiment, the conversion of a 24 MeV quantum into optical phonons near 8 THz would require a fractionation of the large nuclear quantum into roughly 7×10^8 phonons. No mechanism is recognized in physics that is capable of this level of fractionation. It was this problem that we expect motivated Schwinger's early exploratory phonon models; and the somewhat smaller number of plasmons (in the vicinity of a few million) for Preparata's model for multi-photon exchange [14].

In the first several years of our efforts in the field we pursued all manner of schemes, in an effort on the one hand seeking an understanding of the lay of the theoretical landscape, and on the other hand looking for a mechanism that could fractionate a large quantum. After a very large number of failures (most not published), we decided to focus on the fractionation mechanism as a mathematical problem divorced from any physical scheme. To be honest, things were sufficiently discouraging at this point in the research effort that the problem had boiled down to determining whether fractionation was possible with any kind of model, with the expectation that it could be shown to be impossible. In this kind of analysis, the nuclei were reduced to equivalent two-level systems, and the modes of the condensed matter system were turned into linear and nonlinear oscillators. The models at the outset showed some weak ability to fractionate a large quantum, but resisted efforts generally to try to make the effect stronger. Ultimately, the question came down to what prevented the models from fractionating more effectively (since at the nuts and bolts level it seemed that it should have been possible to do better).

We found that the issue was destructive interference. This could be seen most readily in perturbation theory, where the problem of coherent energy exchange under conditions of fractionation was found to be equivalent to that of indirect coupling between distant states that were degenerate. In general there are a large number of paths connecting the two states, and to within near precision the contributions from all the different paths cancelled out. Hence, the only way to increase the fractionation power of the models was to find a mechanism that distinguished broadly between the paths that contributed with a positive sign from those that contributed with a negative sign. In the end, it became clear that loss mechanisms were the most likely candidate. Sure enough, when models were constructed which were augmented with loss (which was discussed at ICCF9 in 2002 [26]), the resulting rate of coherent energy exchange under conditions of fractionation showed orders of magnitude increase. These results were discussed in conference proceedings; however it took many years before a systematic exposition of the new model was published [27–33]. Although the mathematical models focused on coherent energy exchange between sets of two-level systems and an oscillator, the basic mechanism is sufficiently general that it would also apply in the case of two-level systems (or more level systems) coupling to an oscillator, or to other two-level systems (or more level systems).

However, being able to demonstrate coherent energy exchange under conditions of fractionation in a mathematical model is not the same as having a physical model. For example, it is a straightforward calculation to determine the parameters in the mathematical model that would allow fractionation, but it is another thing altogether to specify a physical system in which those parameters can be obtained. We know this well, since over the course of a decade we made several major attempts to identify the physical system in terms of energy levels and coupling mechanism. In all cases, we met with nothing but failure when we carried out calculations with the candidate physical systems. Ultimately we put together a computer code to carry out a systematic evaluation of the important parameters relevant to the system including several hundred candidate transitions, pretty much including all which might conceivably be relevant; and in less than a second the program reported back that none of them calculated out to be suitable candidates. In essence, we could eliminate every atomic, molecular and nuclear transition that we tried as being a suitable receiver transition the donor–receiver model of Ref. [32].

The basic problem in all cases was that the coupling was too weak to do the job. For the requirements of the donor–receiver model to be satisfied, the strength of the coupling for a particular transition to a vibrational mode of the lattice had to be very strong. Meanwhile, all the different coupling mechanisms that we identified, and developed estimates for the coupling strength, resulted in coupling orders of magnitude too weak give sufficient fractionation power. This was very discouraging.

Keep in mind that just because we were not able to make a connection with the existing experimental results with these models, they described effects qualitatively very similar to experiment. For example, we could model excess heat production from deuterons reacting to make ^{4}He, with the energy going into optical phonon modes; however, the conditions required within the model to make it work involved orders of magnitude more deuterons, and orders of magnitude more phonon excitation, than could possible be present in the experiments. In a sense, the models worked and predicted anomalies similar to what was seen in experiment, except that the numbers were all wrong.

We decided to calculate out a model for excitation transfer between vibrations and the lowest energy nuclear transition from the ground state of a stable nucleus (1565 eV transition in ^{201}Hg). The idea here was that according to the models this should be one of the easiest anomalies to implement experimentally. For example, we could design an experiment to demonstrate coherent energy exchange of this kind based on couplings that are understood; the presumption is that if some additional coupling existed that we didn't understand, it should only make the experiment work better. At the end of this exercise, the design required very strong optical phonon excitation over square meters of surface area, but suggested that we should be able to excite the ^{201}Hg nuclei. Ultimately we understood that if it worked we would expect collimated X-ray emission normal from the surface if optical phonon excitation at the Γ-point were used.

At this point we recognized that the effect under consideration would be consistent with collimated emission near 1.5 keV in Karabut's high-current density glow discharge experiment [34–39] . We could use our model to analyze Karabut's data, and we should be able to extract information about the coupling strength directly from the experiment. When we did so, the coupling strength that resulted was enormous. And it was immediately clear that only direct phonon-nuclear coupling could produce such a large coupling strength.

Note that we had considered direct phonon-nuclear coupling over the years (it seems like a dozen times), and each time we concluded that such an effect was impossible. The basic issue is that there is a clean separation of the center of mass motion of a composite (which would be involved in the vibrations), and the internal relative degrees of freedom of a composite (which would be involved in the internal nuclear transition) in nonrelativistic mechanics. The relativistic problem is more complicated, but our understanding was that the separation was equally clean in the relativistic problem (otherwise there should be sections in the text books explaining the consequences of such a coupling).

A lot of thought went into this problem (over a decade altogether, since this problem had been on the radar screen for years prior to the connection with the Karabut experiment). There is a very strong coupling initially in the relativistic model between the center of mass motion and internal transitions. This coupling disappears when we take the nonrelativistic limit, but we know that it was there initially in the relativistic version of the problem. For an isolated

composite, we know that a generalized Foldy–Wouthuysen transformation eliminates this strong first-order coupling, which then allows us to take the nonrelativistic limit. Our interpretation of the Karabut experiment then directly points to issues involved with the generalized Foldy–Wouthuysen transformation.

It seems useful here to summarize the resulting situation. We have mathematical models that describe coherent energy exchange under conditions of fractionation, and these models point to the Karabut collimated X-ray experiment as perhaps the most fundamental experiment in the field. From a comparison of the model and experiment, we are forced to conclude that transitions are mediated by very strong direct phonon-nuclear coupling. Coupling that is of sufficient strength is present initially in the relativistic version of the problem. But we know that a generalized Foldy–Wouthuysen transformation eliminates this coupling (and hence the game is over). But collimated X-rays are seen in Karabut's experiment! You might predict the outcome if you suggest to your colleagues that the generalized Foldy–Wouthuysen transformation breaks (this is not a good way to impress one's physics colleagues!).

After some reflection, we realized that we have encountered a very similar situation previously. If we go back to our mathematical model for two-level systems coupled to an oscillator, we find an analogy. In the lossless version of the spin–boson model, we can apply a generalized Foldy–Wouthuysen transformation, which eliminates the first-order coupling. A weak higher-order coupling remains in the rotated version of the problem, and we found that matrix elements of this residual coupling describes coherent energy exchange in the multi-phonon version of the problem accurately [40]. However, when the model is augmented with loss the resulting behavior of the model changes qualitatively; the rate for coherent energy exchange is increased by many orders of magnitude. In this case the strong first-order coupling which is normally rotated out by the Foldy–Wouthuysen transformation seems to stick around to mediate coherent energy exchange under conditions of fractionation. Conclusions in this case that we might make based on the Foldy–Wouthuysen rotated version of the lossless version of the problem just do not match with the results of direct calculations in the presence of loss. It is as if the Foldy–Wouthuysen transformation "breaks." Note that it is impossible for a unitary transformation to "break" in that it is just a change of basis. However, it is very much possible for a change of basis to be unhelpful in the analysis of a problem. And this seems to be the situation here.

In what follows, we consider a fundamental relativistic model for condensed matter nuclear science (see [41] for our earlier effort), and examine the model under conditions where the generalized Foldy–Wouthuysen transformation is unhelpful. Not long ago we were convinced that the resulting model could account for the anomalies, and that we finally had a model relevant to experiment. For example, last year we discussed results from a version of this model, where we found that the model seemed to be consistent quantitatively with the experimental parameters in the Karabut experiment [42,43]. We also found a degree of consistency with gamma emission, and with rates for energy generation and ^{4}He production in the Letts experiment.

Unfortunately, while documenting the model of last summer, we found an error (which we explain and correct in this work). At issue was the question of whether the presence of a large number of very strong static transitions impacts the dynamics on a weak low-energy transition which undergoes coherent dynamics. In the model of last summer, we concluded that there was a very strong impact. With the error corrected, the conclusion now is that there is essentially no impact. This is important, since it means that when we analyze coherent dynamics on a single transition, we know that all of the other transitions act as if the generalized Foldy–Wouthuysen transformation had been successful (in essence, they are decoupled). Rather than having to re-analyze the entire system with all possible transitions each time, we can focus only on those transitions likely to exhibit coherent dynamics.

2. Dirac Model for Interacting Protons

The issues that we must deal with in the development of our model are subtle, so it makes sense to begin with an introductory example that focuses on a particularly simple version of the problem. As it turns out, our intuition about the nonrelativistic limit of a relativistic problem depends critically on the Foldy–Wouthuysen transformation [44] in

the case of Dirac particles. Even though the Foldy–Wouthuysen transformation is usually thought of as providing for the nonrelativistic limit of the Dirac model, what it actually does is to rotate out the strong first-order coupling with the proton momentum. This produces a transformed model in which this first-order interaction has been removed, which then allows an easy development of the nonrelativistic approximation subsequently.

Since this example is so simple, we are able to construct the rotation explicitly; we can see clearly how things work in every step of the computation; and we see that this coupled lattice and Dirac proton model has a mathematical structure very closely related to the spin–boson model. Unfortunately, the analogy in this case is not quite as close as we might like, as the negative energy states are mathematical states and not physical states in this example; however, in the more general case to be considered later on, coupling to physical states does occur. By laying out the development explicitly for this simple version of the model, we can see how things work, and we can understand how fundamental the Foldy–Wouthuysen transformation is in this development.

2.1. Idealized model for a lattice made of Dirac protons

We begin with an idealized lattice model with relativistic protons described using a Dirac Hamiltonian

$$\hat{H} \;=\; \sum_j \left(\boldsymbol{\alpha}_j \cdot c\hat{\mathbf{P}}_j + \beta_j Mc^2 \right) + \sum_{j<k} V(|\mathbf{R}_j - \mathbf{R}_k|), \tag{1}$$

where a Born–Oppenheimer approximation has been adopted for the electrons resulting in an effective proton-proton potential. Such a model can of course be criticized since at low pressure hydrogen crystallizes into an HCP lattice of H_2 molecules, and at high pressure it is expected to form more complicated lattice structures [45]; which would require a more complicated effective proton–proton potential than are included here. We are interested here in an idealized model in which the Dirac protons make up a simple crystal lattice, rather than a molecular solid. Nevertheless, although its applicability to a physical system is limited, this simple model is useful to us since we can use it to study the reduction of the relativistic model to a nonrelativistic one.

It will be convenient to rewrite the Hamiltonian in the form

$$\hat{H} \;=\; \sum_j \left\{ \begin{pmatrix} 1 & 0 \\ 0 & -1 \end{pmatrix}_j Mc^2 + \begin{pmatrix} 0 & 1 \\ 1 & 0 \end{pmatrix}_j (\boldsymbol{\sigma} \cdot c\hat{\mathbf{P}})_j \right\} + \sum_{j<k} V(|\mathbf{R}_j - \mathbf{R}_k|). \tag{2}$$

Doing so brings out the coupling between the large and small components, and provides us with a notation that we can take advantage of in connection with the unitary operator for the transformation which follows.

2.2. Foldy–Wouthuysen rotation and nonrelativistic limit

As discussed above, the Foldy–Wouthuysen transformation was introduced to address the reduction of the relativistic Dirac electron problem to obtain the nonrelativistic limit; however, from our perspective the critical issue is that it removes a strong first-order coupling term. We make use of the Foldy–Wouthuysen transform to write

$$\hat{H}' \;=\; \hat{\mathcal{U}}^\dagger \hat{H} \hat{\mathcal{U}} \;=\; \sum_j \begin{pmatrix} 1 & 0 \\ 0 & -1 \end{pmatrix}_j \sqrt{(Mc^2)^2 + c^2|\hat{\mathbf{P}}_j|^2} + \sum_{j<k} V(|\hat{\mathbf{R}}'_j - \hat{\mathbf{R}}'_k|), \tag{3}$$

where the unitary transformation is given explicitly by

$$\hat{\mathcal{U}} \;=\; \exp\frac{i}{2}\left\{\sum_j \mathrm{Arctan}\left(\frac{(\boldsymbol{\sigma}\cdot c\hat{\mathbf{P}})_j}{Mc^2}\right)\begin{pmatrix}0 & -i\\ i & 0\end{pmatrix}_j\right\}. \tag{4}$$

The rotated position operator is

$$\hat{\mathbf{R}}'_j \;=\; \hat{\mathcal{U}}^\dagger\hat{\mathbf{R}}_j\hat{\mathcal{U}} \;=\; \mathbf{R}_j + \begin{pmatrix}0 & -i\\ i & 0\end{pmatrix}_j \frac{(Mc^2)^2}{(Mc^2)^2 + c^2|\hat{\mathbf{P}}_j|^2}\frac{\hat{\mathbf{s}}_j}{Mc}. \tag{5}$$

In the rotated version of the problem the strong first-order $\boldsymbol{\alpha}\cdot c\mathbf{P}$ interaction has been eliminated.

2.3. Nonrelativistic limit and discussion

It is possible to recover the nonrelativistic limit by retaining lowest order terms in the momentum, while at the same time eliminating the negative energy sector; this leads to

$$\hat{H}' \;\rightarrow\; \sum_j\left(Mc^2 + \frac{|\hat{\mathbf{P}}_j|^2}{2M}\right) + \sum_{j<k} V(|\mathbf{R}_j - \mathbf{R}_k|). \tag{6}$$

This simple example is important because it makes explicit the arguments and steps that take us from an idealized relativistic model to a rotated version of the model, and then to the nonrelativistic limit. It makes clear just how central the Foldy–Wouthuysen transformation itself is in connection with the discussion. In this idealized model there is a strong relativistic coupling between the proton momentum and internal degrees of freedom (in this case, a positive to negative energy state transition); which is eliminated by the rotation. We see that the Foldy–Wouthuysen transformation (and later on its generalization) provides the foundation generally upon which our intuition of how the world works rests.

3. Lattice Model with Dirac Protons

The next step in this introductory discussion is to revisit the Foldy–Wouthuysen rotation under conditions where the protons interact harmonically, so that the associated position and momentum variables become operators of the lattice problem. We encounter this situation in the more general version of the problem to follow, so it is worth studying here in the context of the simpler idealized proton model where we can construct the rotation explicitly.

3.1. Harmonic lattice with Dirac protons

For a displacement around the equilibrium position of a proton $\mathbf{R}_j^{(0)}$ we write

$$\mathbf{R}_j \;=\; \mathbf{R}_j^{(0)} + \mathbf{r}_j. \tag{7}$$

With this notation the potential can be expanded in the vicinity of equilibrium

$$V_{jk} \;=\; V_{jk}^{(0)} + (\mathbf{r}_j - \mathbf{r}_k)\cdot\mathbf{K}_{jk}\cdot(\mathbf{r}_j - \mathbf{r}_k) + \cdots \tag{8}$$

where $\mathbf{K}_{jk}$ is the associated force constant matrix. Keeping only the second order terms, we may write

$$\hat{H} \;=\; \sum_j \left(\boldsymbol{\alpha}_j \cdot c\hat{\mathbf{P}}_j + \beta_j Mc^2 \right) + V_0 + \sum_{j<k} (\mathbf{r}_j - \mathbf{r}_k) \cdot \mathbf{K}_{jk} \cdot (\mathbf{r}_j - \mathbf{r}_k). \tag{9}$$

We would expect that this model would behave very nearly like a conventional harmonic lattice model since we recognize that the protons should act nonrelativistically in a lattice setting. However, instead of carrying out a Foldy–Wouthuysen transformation here, we would like instead to first develop a description of the problem in terms of phonon modes prior to the rotation.

3.2. Hamiltonian written in terms of phonon modes

To carry out the approach mentioned above, we make use of a mathematical device that allows us to develop a harmonic lattice while keeping the Dirac proton description intact; we add and subtract nonrelativistic kinetic energy terms to obtain

$$\begin{aligned} \hat{H} = & \sum_j \frac{|\hat{\mathbf{P}}_j|^2}{2M} + V_0 + \sum_{j<k} (\mathbf{r}_j - \mathbf{r}_k) \cdot \mathbf{K}_{jk} \cdot (\mathbf{r}_j - \mathbf{r}_k) \\ & + \sum_j \left(\boldsymbol{\alpha}_j \cdot c\hat{\mathbf{P}}_j + \beta_j Mc^2 \right) - \sum_j \frac{|\hat{\mathbf{P}}_j|^2}{2M}. \end{aligned} \tag{10}$$

Written in this form, we see a harmonic lattice model, and the relativistic part of the Hamiltonian appears separately, augmented with a counter term. We recast the harmonic lattice part of the problem into phonon mode operators

$$\sum_j \frac{|\hat{\mathbf{P}}_j|^2}{2M} + \sum_{j<k} (\mathbf{r}_j - \mathbf{r}_k) \cdot \mathbf{K}_{jk} \cdot (\mathbf{r}_j - \mathbf{r}_k) = \sum_i \hbar\omega_i \left(\hat{a}_i^\dagger \hat{a}_i + \frac{1}{2} \right). \tag{11}$$

In what follows we will need to make use of proton position and momentum operators written in terms of phonon mode creation and annihilation operators; the relations will be written as

$$\hat{\mathbf{R}}_j = \mathbf{R}_j^{(0)} + \sum_\mu \frac{\mathrm{d}\mathbf{R}_j}{\mathrm{d}a_\mu} (\hat{a}_\mu + \hat{a}_\mu^\dagger), \tag{12}$$

$$\hat{\mathbf{P}}_j = \sum_\mu \frac{\mathrm{d}\mathbf{P}_j}{\mathrm{d}a_\mu} \left(\frac{\hat{a}_\mu - \hat{a}_\mu^\dagger}{i} \right), \tag{13}$$

where the derivatives $\mathrm{d}\mathbf{R}_j/\mathrm{d}a_\mu$ and $\mathrm{d}\mathbf{P}_j/\mathrm{d}a_\mu$ here are intended as a kind of shorthand to keep track of different terms which make up the mode operators. With these relations we can write the model as

$$\hat{H} = \sum_{\mu} \hbar\omega_{\mu} \left(\hat{a}_{\mu}^{\dagger} \hat{a}_{\mu} + \frac{1}{2} \right) + Mc^2 \sum_j \begin{pmatrix} 1 & 0 \\ 0 & -1 \end{pmatrix}_j + V_0$$
$$+ \sum_j \sum_{\mu} \begin{pmatrix} 0 & 1 \\ 1 & 0 \end{pmatrix}_j \boldsymbol{\sigma}_j \cdot c \frac{\mathrm{d}\,\hat{\mathbf{P}}_j}{\mathrm{d}a_{\mu}} \left(\frac{\hat{a}_{\mu} - \hat{a}_{\mu}^{\dagger}}{i} \right) - \sum_j \frac{|\hat{\mathbf{P}}_j|^2}{2M}. \tag{14}$$

We have succeeded in implementing a harmonic lattice model for the interacting protons, while retaining the strong first-order relativistic coupling between the proton momentum (now written in terms of phonon operators) and internal transitions between the large and small Dirac components. As a result of the mathematical device mentioned above, we retain a counter term for the Dirac mass and kinetic energy terms. The problem is now set up so that we can examine cleanly the implementation of a Foldy–Wouthuysen transformation.

3.3. Foldy–Wouthuysen rotation for the spin–boson problem

It probably comes as no surprise that we are able to carry out a Foldy–Wouthuysen transformation in this case as well, since this new model can be thought of as a special case of the more general version of the model discussed above. In fact, the unitary transformation that eliminates the linear coupling term is formally the same is in the case above, although we write it now in terms of the phonon mode operators

$$\hat{\mathcal{U}} = \exp \left\{ \frac{i}{2} \sum_j \mathrm{Arctan} \left(\sum_i \frac{1}{Mc} \boldsymbol{\sigma}_j \cdot \frac{\mathrm{d}\mathbf{P}_j}{\mathrm{d}a_i} (\hat{a}_i + \hat{a}_i^{\dagger}) \right) \begin{pmatrix} 0 & -i \\ i & 0 \end{pmatrix}_j \right\}. \tag{15}$$

The rotated Hamiltonian can be written as

$$\hat{H}' = \hat{\mathcal{U}}^{\dagger} \hat{H} \hat{\mathcal{U}}$$
$$= \sum_j \begin{pmatrix} 1 & 0 \\ 0 & -1 \end{pmatrix}_j \sqrt{(Mc^2)^2 + c^2 |\hat{\mathbf{P}}_j|^2} - \sum_j \frac{|\hat{\mathbf{P}}_j|^2}{2M} + \sum_{\mu} \hbar\omega_{\mu} \left(\hat{a}_{\mu}^{\dagger} \hat{a}_{\mu} + \frac{1}{2} \right)$$
$$+ V_0 + \sum_{j<k} (\hat{\mathbf{r}}'_j - \hat{\mathbf{r}}'_k) \cdot \mathbf{K}_{jk} \cdot (\hat{\mathbf{r}}'_j - \hat{\mathbf{r}}'_k) - \sum_{j<k} (\mathbf{r}_j - \mathbf{r}_k) \cdot \mathbf{K}_{jk} \cdot (\mathbf{r}_j - \mathbf{r}_k), \tag{16}$$

where the transformed position operators are

$$\hat{\mathbf{r}}'_j = \hat{\mathcal{U}}^{\dagger} \hat{\mathbf{r}}_j \hat{\mathcal{U}}$$
$$= \mathbf{r}_j + \begin{pmatrix} 0 & -i \\ i & 0 \end{pmatrix}_j \frac{(Mc^2)^2}{(Mc^2)^2 + c^2 \left| \sum_{\mu} \frac{\mathrm{d}\mathbf{P}_j}{\mathrm{d}a_{\mu}} \left(\frac{\hat{a}_{\mu} - \hat{a}_{\mu}}{i} \right) \right|^2} \frac{\hat{\mathbf{s}}_j}{Mc}. \tag{17}$$

Similar to the case considered earlier, the Foldy–Wouthuysen transformation in this case has eliminated the first-order coupling between the phonon and internal Dirac degrees of freedom. We see that the Foldy–Wouthuysen transformation that we have used in the two different examples is essentially the same; working in the context of a lattice with phonon modes has not impeded our ability to implement the rotation.

3.4. Nonrelativistic limit

Taking the nonrelativistic limit now becomes straightforward; we may write

$$\hat{H}' \rightarrow \sum_j \begin{pmatrix} 1 & 0 \\ 0 & -1 \end{pmatrix}_j (Mc^2)^2 + \sum_\mu \hbar\omega_\mu \left(\hat{a}_\mu^\dagger \hat{a}_\mu + \frac{1}{2} \right) + V_0$$

$$+ \sum_{j<k} (\hat{\mathbf{r}}'_j - \hat{\mathbf{r}}'_k) \cdot \mathbf{K}_{jk} \cdot (\hat{\mathbf{r}}'_j - \hat{\mathbf{r}}'_k) - \sum_{j<k} (\mathbf{r}_j - \mathbf{r}_k) \cdot \mathbf{K}_{jk} \cdot (\mathbf{r}_j - \mathbf{r}_k), \tag{18}$$

where we recognize the residual nuclear spin interactions denoted by the second line of the rotated Hamiltonian to be small. The kinetic energy counter term in this case has eliminated the second-order kinetic energy contribution from the expansion of the relativistic energy; and we have dropped higher-order terms.

3.5. Discussion

There are a variety of issues to consider in this discussion, and we have made some progress in providing some illumination with these idealized example models. We have seen that in both cases that there appears a first-order coupling between proton momentum and internal Dirac degrees of freedom; and we recognize that the problems would be much more difficult to solve and understand if we had to work with this first-order coupling in place. From these examples, we view the Foldy–Wouthuysen transformation as most importantly removing this first-order coupling; the problem that we end up with in both cases has a nearly clean separation between proton momentum and internal Dirac degrees of freedom. We see additionally that the Foldy–Wouthuysen transformation is effective in both examples on equal footing; when the momentum to be made up of phonon mode operators there is no fundamental difference in the associated unitary operator, or in the rotated version of the problem.

When the interacting protons in this model are worked into a harmonic lattice description, the resulting problem is closely related mathematically (but not so closely related physically) to the spin–boson model. As mentioned above, we are able to make use of the Foldy–Wouthuysen transformation in the spin–boson model in the same way as done here, which allows us to eliminate the first-order coupling (and the residual high-order coupling gives rise to known results for coherent energy exchange when many quanta are exchanged) [40]. Also as discussed above, the spin–boson model behaves very differently in regard to coherent energy exchange when substantial loss is present (since loss removes the destructive interference that inhibits energy exchange) [27–31].

This motivates us to consider what the idealized Dirac proton lattice model might look like if augmented with loss. Note that protons cannot have real occupation of the negative energy state, so there are some differences with the lossy spin-boson problem. The idea here is to examine briefly here the situation that would result in this idealized problem if the Foldy-Wouthusyen transformation were to become unhelpful due to the inclusion of a strong loss model.

The Hamiltonian for the lossy spin–boson model can be written as

$$\hat{H} = \hbar\omega_0 \hat{a}^\dagger \hat{a} + \frac{\Delta E}{2} \sum_j \begin{pmatrix} 1 & 0 \\ 0 & -1 \end{pmatrix}_j + V \sum_j \begin{pmatrix} 0 & 1 \\ 1 & 0 \end{pmatrix}_j (\hat{a} + \hat{a}^\dagger) - i \frac{\hbar \hat{\Gamma}(E)}{2}. \tag{19}$$

There is no problem in using a Foldy–Wouthuysen type of transformation as a mathematical operation for such a model; and by doing so one eliminates the first-order coupling between the oscillator and two-level system, similar to the situation above. However, the loss operator in this case is transformed as well, and the rotated version of the loss

operator is nearly impossible to work with. We have found that for this kind of problem we are much better off simply working with the unrotated version of the model.

As commented upon previously, the lossy spin–boson model is closely related to the lattice and Dirac proton model discussed above, and we expect an analogous situation if the model is similarly augmented with loss. In this case we might write

$$\begin{aligned}\hat{H} \;\rightarrow\; & \sum_\mu \hbar\omega_\mu \left(\hat{a}_\mu^\dagger \hat{a}_\mu + \frac{1}{2}\right) + Mc^2 \sum_j \begin{pmatrix} 1 & 0 \\ 0 & -1 \end{pmatrix}_j + V_0 \\ & + \sum_j \sum_\mu \begin{pmatrix} 0 & 1 \\ 1 & 0 \end{pmatrix}_j \boldsymbol{\sigma}_j \cdot c \frac{\mathrm{d}\hat{\mathbf{P}}_j}{\mathrm{d}a_\mu} \left(\frac{\hat{a}_\mu - \hat{a}_\mu^\dagger}{i}\right) - \sum_j \frac{|\hat{\mathbf{P}}_j|^2}{2M} - i\frac{\hbar\hat{\Gamma}(E)}{2}, \end{aligned} \tag{20}$$

then we would encounter the same difficulty. In this case, under the Foldy–Wouthuysen transformation we would be able to write down a nonrelativistic limit for the basic model

$$\begin{aligned}\hat{H}' \;\rightarrow\; & \sum_\mu \hbar\omega_\mu \left(\hat{a}_\mu^\dagger \hat{a}_\mu + \frac{1}{2}\right) + V_0 + \sum_j \begin{pmatrix} 1 & 0 \\ 0 & -1 \end{pmatrix}_j (Mc^2)^2 \\ & + \sum_{j<k} (\hat{\mathbf{r}}'_j - \hat{\mathbf{r}}'_k) \cdot \mathbf{K}_{jk} \cdot (\hat{\mathbf{r}}'_j - \hat{\mathbf{r}}'_k) - \sum_{j<k} (\mathbf{r}_j - \mathbf{r}_k) \cdot \mathbf{K}_{jk} \cdot (\mathbf{r}_j - \mathbf{r}_k) - i\frac{\hbar\hat{\Gamma}'(E)}{2}, \end{aligned} \tag{21}$$

However, the loss is also transformed under the Foldy–Wouthuysen transformation

$$\hat{\Gamma}'(E) = \hat{\mathcal{U}}^\dagger \hat{\Gamma}(E) \hat{\mathcal{U}}. \tag{22}$$

Under conditions where the loss is extremely fast in accessible regimes, then the rotated version of the loss operator becomes extremely difficult to work with; in such cases we are much better off analyzing the problem in the original frame. Strong loss in accessible regimes can produce a modification of the phonon distribution which ruins the entanglement between the phonon and nuclear degrees of freedom that the Foldy–Wouthuysen rotation seeks to simplify.

4. Coupling between Momentum and Internal Nuclear Degrees of Freedom

By now we have made several attempts at specifying a fundamental Hamiltonian that we might be able to use as a starting point for modeling the new effects [46,41,42], and in each case the resulting Hamiltonian could be criticized for one reason or another. In [46] we worked with nonrelativistic models (where the first-order coupling under discussion is eliminated); in [41] we proposed using a many-particle Dirac Hamiltonian for nucleons, which is not covariant; and in [42] we discussed a Dirac Hamiltonian for quarks, where such a model does not provide even a useful starting place for nucleons, much less nuclei made up of several nucleons. This motivates us to return once again to this problem, and to try to develop an improved foundation for the model.

4.1. The problem of the basic description

We might consider adopting as a starting point QED to describe electrons and the electromagnetic field, and QCD to describe quarks and gluons; in this case our fundamental Hamiltonian takes the form

$$\hat{H} = \hat{H}_{\rm QED} + \hat{H}_{\rm QCD}. \tag{23}$$

Surely such a starting place must be free of all such criticisms. Such a model would be appropriately relativistically covariant; we would now have a useful starting point capable at least in principle of describing nucleons appropriately and leading ultimately to compound nuclei.

Even so, we still recognize deficiencies. We need to make sure that our QCD Hamiltonian has photon exchange so that interactions between nuclei and other nuclei or electrons is included. Eventually we will want to describe weak interactions, so perhaps only a standard model Hamiltonian will do the job. On the practical side, now that we have decided on a sufficiently general Hamiltonian, we have little hope of carrying out specific calculations, in part because we have now enlarged our model to include pretty much everything. We inherit the headache that bound state QCD has not yet reached the stage that it can be used routinely for nuclei with many nucleons.

In light of this, it may be time to adopt a different strategy altogether for the problem. Since the effects that we are interested in depend only on the changes in the relativistic nuclear wavefunction when it moves (slowly), it might be better to start over and to focus on the modification of the internal nuclear that occurs in connection with motion, and recast the problem in terms of the associated coupling matrix elements. In this way we might better focus attention on the part of the problem most relevant to the model, and by doing so cast the relevant coupling matrix elements into a form that might allow for suitable approximations later on. In what follows this is the approach that we will take.

4.2. Rest frame basis states

We begin then by presuming the existence of a complete set of rest frame basis states for a compound nucleus that are eigenfunctions of a relevant relativistic Hamiltonian

$$M_j c^2 \Phi_j = \hat{H}_{\rm QCD} \Phi_j. \tag{24}$$

Sadly, we already run into a technical issue in such a proposition. These eigenfunctions include those we need that correspond to physical states, along with a great many solutions that involve particles in negative energy states. At this stage, formally we are going to need all of them as mathematical solutions; later we are going to have to be careful to make sure that we end up with solutions that we can identify as being in the positive energy sector, which will correspond to physical states.

4.3. Boosted wavefunctions in terms of a rest frame basis

Next, we consider boosted versions of the state constructed according to

$$\Phi'_j(\mathbf{P}) = \exp\left\{ i \frac{\mathbf{P}}{\hbar} \cdot \mathbf{R} \right\} \hat{U}(\mathbf{P}) \Phi_j(0). \tag{25}$$

The idea here is that the dependence on the center of mass coordinate $\mathbf{R}$ here is a pure plane wave $\exp\{i\mathbf{P}\cdot\mathbf{R}/\hbar\}$, which constitutes the only $\mathbf{R}$-dependence in the problem. The internal nuclear wavefunction undergoes a rearrangement relative to the rest frame in order to be consistent with relativity. Note that we are interested in stationary states in this discussion, and in what follows; hence the $\exp(-iEt/\hbar)$ terms that might appear in a space-time description is not present.

Since QCD is Lorentz invariant, we the energy of the boosted basis state satisfies

$$\sqrt{(M_j c^2)^2 + c^2|\mathbf{P}|^2}\ \Phi'_j(\mathbf{P}) = \hat{H}_{\rm QCD}\Phi'_j(\mathbf{P}). \tag{26}$$

Since we are working with a complete set of (mathematical) states, we can expand the boosted state in terms of the rest frame basis

$$\Phi'_j(\mathbf{P}) = \exp\left\{i\frac{\mathbf{P}}{\hbar}\cdot\mathbf{R}\right\}\sum_k \langle\Phi_k(0)|\Phi'_j(\mathbf{P})\rangle\Phi_k(0). \tag{27}$$

Since there is no center of mass dependence outside of the explicit plane wave dependence, it is possible to expand the rearranged internal nuclear wavefunction in terms of rest frame basis states.

4.4. Linearization around the rest frame

For nuclei in the lattice, the coherent energy transfer effects of interest to us will occur under conditions where the nuclei individually are moving slowly. Consequently, we would like to develop an approximate relativistic model that will be useful in the vicinity of the rest frame. To proceed, we probably need to extract the rest frame part of $\hat{H}_{\rm QCD}$. To do so, we can make use (at least formally) of the rest frame basis states in order to construct a rest frame version of the Hamiltonian

$$\hat{H}_0 = \sum_j |\Phi_j(0)\rangle M_j c^2 \langle\Phi_j(0)|. \tag{28}$$

Next, we assume that we can obtain a reasonable boosted wavefunction keeping terms only up to first order in the rotation

$$\Phi'_j(\mathbf{P}) = \exp\left\{i\frac{\mathbf{P}}{\hbar}\cdot\mathbf{R}\right\}\left[\Phi_j(0) + \left(\nabla_{\mathbf{P}}\hat{\mathcal{U}}\right)_{\mathbf{P}=0}\cdot\mathbf{P}\Phi_j(0) + \cdots\right]. \tag{29}$$

We would expect this approximate boost to produce an approximate solution to the Schrödinger equation (26); this we might expand as

$$\begin{aligned}&\left[M_j c^2 + \frac{|\mathbf{P}|^2}{2M_j} + \cdots\right]\exp\left\{i\frac{\mathbf{P}}{\hbar}\cdot\mathbf{R}\right\}\left[\Phi_j(0) + \left(\nabla_{\mathbf{P}}\hat{\mathcal{U}}\right)_{\mathbf{P}=0}\cdot\mathbf{P}\Phi_j(0) + \cdots\right]\\ &\quad= \left[\hat{H}_0 + \left(\nabla_{\mathbf{P}}\hat{H}_{\rm QCD}\right)_{\mathbf{P}=0}\cdot\hat{\mathbf{P}} + \cdots\right]\exp\left\{i\frac{\mathbf{P}}{\hbar}\cdot\mathbf{R}\right\}\left[\Phi_j(0) + (\nabla_{\mathbf{P}}\hat{\mathcal{U}})_{\mathbf{P}=0}\cdot\mathbf{P}\Phi_j(0) + \cdots\right].\end{aligned} \tag{30}$$

There are some subtleties associated with such an equation. Since we needed to make use of the rest frame basis functions to construct the rest frame Hamiltonian, probably we need to do something similar in order to construct the gradient of the Hamiltonian. If we begin with $\nabla_{\mathbf{P}}\hat{H}_{\rm QCD}$, then it would follow that we can develop a rest frame version of it also by taking advantage of the rest frame basis

$$\left(\nabla_{\mathbf{P}}\hat{H}_{\rm QCD}\right)_{\mathbf{P}=0} = \sum_j\sum_k |\langle\Phi_j(0)\rangle\langle\Phi_j(0)|\nabla_{\mathbf{P}}\hat{H}_{\rm QCD}|\Phi_k(0)\rangle\langle\Phi_k(0)|. \tag{31}$$

We can isolate the rest frame part of the boost operator similarly. In the end, we match terms linear in $\mathbf{P}$ to obtain a relation between the gradient of the unitary operator and the gradient of the Hamiltonian

$$\left(\nabla_{\mathbf{P}}\hat{\mathcal{U}}\right)_{\mathbf{P}=0} = \left(M_j c^2 - \hat{H}_0\right)^{-1} \left(\nabla_{\mathbf{P}}\hat{H}_{\rm QCD}\right)_{\mathbf{P}=0}. \tag{32}$$

Note that this discussion has been focused on what happens to a single basis state, so that in this equation the operator on the LHS is specific to Φ_j. We could obtain a more general version of the operator by replacing the rest frame mass M_j with the rest frame mass matrix.

4.5. Reduction to matrix form

Our discussion so far has been pretty general, but now we need to attend to the problem of developing a model that we can use in the context of a lattice Hamiltonian. In essence, the point of the development above was to achieve a separation between the center of mass dynamics and the internal dynamics in a way that will be useful in what follows. The linearized Hamiltonian is now expressed completely in terms of rest frame basis states and the center of mass momentum operator. It will be convenient to write this as

$$\begin{aligned}\hat{H}_0 + \left(\nabla_{\mathbf{P}}\hat{H}_{\rm QCD}\right)_{\mathbf{P}=0} \cdot \hat{\mathbf{P}} + \cdots \\ = \sum_j |\Phi_j(0)\rangle M_j c^2 \langle\Phi_j(0)| + \sum_{j,k} |\Phi_j(0)\rangle\langle\Phi_j(0)|\nabla_{\mathbf{P}}\hat{H}_{\rm QCD}\cdot\hat{\mathbf{P}}|\Phi_k(0)\rangle\langle\Phi_k(0)| + \cdots\end{aligned} \tag{33}$$

It will be convenient to define the vector $\mathbf{a}_{jk}$ according to

$$\mathbf{a}_{jk} = \frac{1}{c}\langle\Phi_j(0)|\nabla_{\mathbf{P}}\hat{H}_{\rm QCD}|\Phi_k(0)\rangle. \tag{34}$$

This allows us to recast the Hamiltonian as

$$\hat{H}_0 + \left(\nabla_{\mathbf{P}}\hat{H}_{\rm QCD}\right)_{\mathbf{P}=0} \cdot \hat{\mathbf{P}} + \cdots = \sum_j |\Phi_j(0)\rangle M_j c^2 \langle\Phi_j(0)| + \sum_{j,k} |\Phi_j(0)\rangle \mathbf{a}_{jk}\cdot c\hat{\mathbf{P}}\langle\Phi_k(0)| + \cdots \tag{35}$$

Since we have made use of the rest frame basis in the construction of the rest frame Hamiltonian, as well as for isolating the linear part, we can make use of a basis expansion in terms of rest frame states to construct a solution

$$\Psi = \exp\left\{i\frac{\mathbf{P}}{\hbar}\cdot\mathbf{R}\right\}\sum_j c_j\Phi_j(0). \tag{36}$$

The expansion coefficients satisfy a matrix version of the Schrödinger equation

$$i\hbar\frac{\partial}{\partial t}\mathbf{c}(t) = \mathbf{H}\cdot\mathbf{c}(t) \tag{37}$$

with

$$\mathbf{H} = \mathbf{M}c^2 + \mathbf{a} \cdot c\hat{\mathbf{P}} + \cdots \tag{38}$$

Note that there are an infinite number of rest frame basis states, so these matrices are correspondingly infinitely large. It may be that a reasonable approximation can be developed in principle with a finite number of basis states; adopting a matrix form is convenient for such a finite basis approximation.

4.6. Quadratic relation

We can square the matrix version of the Hamiltonian operator to write

$$\hat{\mathbf{H}}^2 = (\mathbf{M}c^2)^2 + (\mathbf{M}c^2)(\mathbf{a} \cdot c\hat{\mathbf{P}}) + (\mathbf{a} \cdot c\hat{\mathbf{P}})(\mathbf{M}c^2) + (\mathbf{a} \cdot c\hat{\mathbf{P}})^2 + \cdots \tag{39}$$

Since the square of the total energy has no linear dependence on momentum, it follows that

$$(\mathbf{M}c^2)(\mathbf{a} \cdot c\hat{\mathbf{P}}) + (\mathbf{a} \cdot c\hat{\mathbf{P}})(\mathbf{M}c^2) = 0. \tag{40}$$

Since the square of the energy depends on the square of the momentum with no higher order terms appearing, if follows that

$$\hat{\mathbf{H}} = \mathbf{M}c^2 + \mathbf{a} \cdot c\hat{\mathbf{P}} \tag{41}$$

with no higher-order terms (the $\cdots$ above must be zero). In addition, the **a**-matrix must satisfy

$$(\mathbf{a} \cdot c\hat{\mathbf{P}})^2 = c^2|\hat{\mathbf{P}}|^2. \tag{42}$$

4.7. Dirac-like formalism for composite nuclei

In essence, the argument here is that if we work with the rest frame basis states, the the form of the associated matrix Hamiltonian must be analogous to the free-space Dirac Hamiltonian

$$\mathbf{M}c^2 + \mathbf{a} \cdot (c\hat{\mathbf{P}}) \;\leftrightarrow\; \beta Mc^2 + \boldsymbol{\alpha} \cdot (c\hat{\mathbf{P}}). \tag{43}$$

The Dirac matrices are very simple, and the mass matrix for the composite nucleus using the rest frame basis is diagonal. The **a**-matrix for the composite nucleus will be enormously complicated; fortunately we will need only a small number of matrix elements in working with the model that results.

4.8. Discussion

When we began these studies our focus was on many-nucleon Dirac models primarily because such models were the simplest one that were likely to contain the effects we sought [and these models resulted in a free composite Hamiltonian of the form $\mathbf{M}c^2 + \mathbf{a} \cdot (c\hat{\mathbf{P}})$]. Now that we have some experience working with these earlier models, the path forward to generalize the approach to more sophisticated models seems clearer.

In all cases the basic issue is that a rest frame state is modified according to relativity when boosted, although how this works is different in a Dirac model versus a Lorentz covariant model such as QCD. Now we have a better

formulation that can be used systematically for either approach, and we are able to have a consistent formulation that can be used with a covariant field theory.

There remain issues that are worth some additional thought. In view of the discussion of the previous section, we understand that the complete set of basis states includes positive energy states, as well as states in other sectors where some components involve negative energy states. This is a necessary feature of the formulation (as it was in the previous section) since in general the construction of a positive energy boosted wavefunction will require pieces that are from sectors with negative energy components in the rest frame.

5. Lattice Model with Internal Nuclear Degrees of Freedom

We now have a starting place for a general description of nuclei embedded in a lattice that takes into account changes in the internal nuclear wavefunction due to relativity when it moves. In the event that we make use of a Born–Oppenheimer approximation, we end up with a model that describes the interaction between interacting nuclei, including the coupling between the nuclear momentum and internal degrees of freedom. The resulting problem constitutes the generalization of the Dirac proton lattice model of Section 3, and the issues that arise are analogous. In this section we consider the model itself, the use of a generalized Foldy–Wouthuysen transformation for the elimination of the first-order coupling, the nonrelativistic limit of the model, and the possibility that regimes exist where the Foldy–Wouthuysen transformation is not useful.

5.1. A model for nuclei in the lattice

We make use of the matrix Hamiltonian of the previous section to construct a many-nucleon Hamiltonian that interact through effective potentials that arise from a Born–Oppenheimer treatment of the electrons

$$\hat{H} = \sum_j \left(\mathbf{M}c^2 + \mathbf{a} \cdot c\hat{\mathbf{P}} \right)_j + \sum_{j<k} V(|\mathbf{R}_j - \mathbf{R}_k|). \tag{44}$$

This model constitutes a direct generalization of the idealized model of Section 2. Once again we have adopted a simple effective potential for interactions between nuclei which is easily generalized to more complicated models which better describe physical systems.

Although this model is of the same form as earlier coupled lattice and nuclear models that we have put forth previously [41,42], this one is different. The basis states that provide the foundation for the construction of the matrices are now eigenstates of the rest frame QCD problem. We recognize now that the dominant coupling of the $\mathbf{a} \cdot c\mathbf{P}$ interaction is with states that have explicit negative energy components, generalizing the situation encounter with the Dirac phenomenology of Section 2. Although our discussion of the previous section focused on a QCD description for the nuclei, we might have used any other covariant model with similar results.

5.2. Generalized Foldy–Wouthuysen transformation

As was the case with the Dirac proton model, we see in this model a first-order coupling between the center of mass momentum of the nuclei and their internal degrees of freedom. And as before we are able to carry out a rotation that eliminates this first-order coupling which leads to

$$\hat{H}' = \hat{\mathcal{U}}^\dagger \hat{H} \hat{\mathcal{U}} = \sum_j \left(\mathbf{M}c^2 \sqrt{1 + \frac{c^2 |\hat{\mathbf{P}}|^2}{(\mathbf{M}c^2)^2}} \right)_j + \sum_{j<k} \hat{V}'_{jk}, \tag{45}$$

where

$$\hat{V}'_{jk} = \hat{\mathcal{U}}^{\dagger} V(|\mathbf{R}_j - \mathbf{R}_k|)\hat{\mathcal{U}}. \tag{46}$$

We recognize the rotation that accomplished this as a generalized Foldy–Wouthuysen transformation; one which diagonalizes in this case very large matrices, rather than simple two by two matrices of Section 2. The specific unitary operator $\hat{\mathcal{U}}$ that does this is very complicated, and can be obtained formally from rest frame matrix elements of the boost operator of the previous section. We note that generalizations of the Foldy–Wouthuysen rotation beyond the single Dirac particle have been discussed in the literature (e.g., see [47], [48,49]).

5.3. Discussion and nonrelativistic limit

In the original Hamiltonian of equation (44) we see a strong first-order $\mathbf{a} \cdot c\mathbf{P}$ coupling between the two degrees of freedom that produces mixing between the different degrees of freedom. Note that the generalized Foldy–Wouthuysen transformation has removed the first-order coupling between the momentum and internal nuclear transitions in the rotated version of the problem. In the transformed Hamiltonian, the two degrees of freedom are very nearly independent. We might think of the original Hamiltonian as describing the "physical" system, and the rotated Hamiltonian as describing a "dressed" version of the system. The "dressed" system is free of the strong coupling between the composite motion and internal degrees of freedom; it is this situation upon which our intuition about how the world works in solid state physics (that the nuclei effective don't notice lattice vibrations).

From this perspective, the situation that occurs when the generalized Foldy–Wouthuysen transform becomes inappropriate perhaps makes more sense. In both regimes there occurs strong mixing between the nuclear and vibrational system; we have grown so used to the conventional regime where the generalized Foldy–Wouthuysen transform works that the "dressed" version of the system looks like reality to us; consequently we are amazed when we see a regime where the generalized Foldy–Wouthuysen transform doesn't work and the mixing between the two degrees of freedom lead to anomalies.

As was the case previously, when the generalized Foldy–Wouthuysen transformation can be used we are able to develop the nonrelativistic approximation

$$\hat{H}' \;\rightarrow\; \sum_j \left(\mathbf{M}c^2 + \frac{|\hat{\mathbf{P}}|^2}{2\mathbf{M}} \right)_j + \sum_{j<k} \hat{V}'_{jk}. \tag{47}$$

6. Composite Nuclei in a Harmonic Lattice

At this point we have assembled a foundation sufficient to allow us to take the next step, which is to consider composite nuclei interacting in a harmonic lattice. This problem is closely related to the idealized model for Dirac protons in a harmonic lattice considered above; hence, from the discussion above we anticipate that a generalized Foldy–Wouthuysen transformation will be able to eliminate the first-order coupling between the composite center of mass momentum and internal degrees of freedom. On the other hand, we also know that the problem is also closely related to the lossy spin–boson model mentioned above and described in earlier works; consequently, we expect that under some conditions a Foldy–Wouthuysen transformation will be unhelpful.

6.1. Composite nuclei in a harmonic lattice

Composite nuclei in a harmonic lattice (again within a Born–Oppenheimer approximation) are described then by a Hamiltonian of the form

$$\hat{H} = \sum_j \left(\mathbf{M}c^2 + \mathbf{a} \cdot c\hat{\mathbf{P}} \right)_j + V_0 + \sum_{j<k} (\mathbf{r}_j - \mathbf{r}_k) \cdot \mathbf{K}_{jk} \cdot (\mathbf{r}_j - \mathbf{r}_k). \tag{48}$$

We would like to work with lattice position and momentum operators as for the Dirac proton version of the problem. For this, we make use of the same mathematical device of adding and subtracting nonrelativistic kinetic energy terms to obtain

$$\begin{aligned} \hat{H} = & \sum_j \frac{|\hat{\mathbf{P}}_j|^2}{2M_j} + V_0 + \sum_{j<k} (\mathbf{r}_j - \mathbf{r}_k) \cdot \mathbf{K}_{jk} \cdot (\mathbf{r}_j - \mathbf{r}_k) \\ & + \sum_j \left(\mathbf{M}c^2 + \mathbf{a} \cdot c\hat{\mathbf{P}} \right)_j - \sum_j \frac{|\hat{\mathbf{P}}_j|^2}{2M_j}, \end{aligned} \tag{49}$$

where we adopt ground state nuclear masses for the nonrelativistic kinetic energy terms. As before, the associated harmonic lattice problem is recast in terms of phonon mode operators

$$\sum_j \frac{|\hat{\mathbf{P}}_j|^2}{2M_j} + \sum_{j<k} (\mathbf{r}_j - \mathbf{r}_k) \cdot \mathbf{K}_{jk} \cdot (\mathbf{r}_j - \mathbf{r}_k) \;\rightarrow\; \sum_\mu \hbar\omega_\mu \left(\hat{a}_\mu^\dagger \hat{a}_\mu + \frac{1}{2} \right). \tag{50}$$

We may write for the coupled harmonic lattice and nuclei problem the Hamiltonian

$$\hat{H} = \sum_\mu \hbar\omega_\mu \left(\hat{a}_\mu^\dagger \hat{a}_\mu + \frac{1}{2} \right) + V_0 + \sum_j \left(\mathbf{M}c^2 + \mathbf{a} \cdot c\hat{\mathbf{P}} \right)_j - \sum_j \frac{|\hat{\mathbf{P}}_j|^2}{2M_j}. \tag{51}$$

6.2. Generalized Foldy–Wouthuysen transformation

In a conventional regime (where strong loss terms are absent) we can carry out a generalized Foldy–Wouthuysen transformation for this Hamiltonian leading to

$$\hat{H}' = \sum_\mu \hbar\omega_\mu \left(\hat{a}_\mu^\dagger \hat{a}_\mu + \frac{1}{2} \right) + V_0 + \sum_j \left(\mathbf{M}c^2 \sqrt{1 + \frac{c^2 |\hat{\mathbf{P}}|^2}{(\mathbf{M}c^2)^2}} \right)_j - \sum_j \frac{|\hat{\mathbf{P}}_j|^2}{2M_j} + \sum_{j<k} \Delta \hat{V}'_{jk}, \tag{52}$$

where

$$\Delta \hat{V}'_{jk} = \left[(\mathbf{r}'_j - \mathbf{r}'_k) \cdot \mathbf{K}_{jk} \cdot (\mathbf{r}'_j - \mathbf{r}'_k) \right] - \left[(\mathbf{r}_j - \mathbf{r}_k) \cdot \mathbf{K}_{jk} \cdot (\mathbf{r}_j - \mathbf{r}_k) \right]. \tag{53}$$

In this case we worked with quantized vibrations and an appropriate relativistic nuclear model, and once again we have removed the strong first-order coupling between the vibrational and internal nuclear degrees of freedom. We recognize that we must add to this the constraint that we want to take the positive energy sector states to correspond to physical nuclei; and we would like further to match the nuclear state mass to the mass used in the kinetic energy terms used for

the construction of the phonon mode. In the resulting "dressed" version of the problem, we recognize that the system is very nearly decoupled, and we would not expect to see anomalies.

We are able to develop a nonrelativistic model from this rotated Hamiltonian; we may write

$$\hat{H}' \rightarrow \sum_j M_j c^2 + \sum_\mu \hbar\omega_\mu \left(\hat{a}_\mu^\dagger \hat{a}_\mu + \frac{1}{2}\right) + V_0, \tag{54}$$

where we have eliminated higher-order terms, and further assumed (positive energy) ground state occupation of the dressed composite nuclear states.

6.3. Loss mechanisms

As discussed above, we know that in the presence of strong loss the lossy spin–boson model predicts efficient coherent energy exchange under conditions of fractionation, which is qualitatively different from what we see in the normal spin–boson model. Because of the close connection between the lossy spin–boson model, and the models under discussion here, we anticipate a similar difference for composite nuclei in a harmonic lattice when loss is present.

The issue relevant here then is what loss mechanisms should be considered in this context. Usually when loss is considered in the context of a simple harmonic oscillator, the discussion is focused on dissipation effects that provide "friction;" which is the most important loss in many applications. Here, the issue is more subtle. For example, such friction losses are hardly going to impact the utility of a generalized Foldy–Wouthuysen transformation. What would make a real difference is a massive loss of state occupation for states critical to the separation of degrees of freedom accomplished by the Foldy–Wouthuysen transformation.

In general we would not expect a significant impact on this state occupation for a thermal lattice, or even for localized excitations. The situation is different in the event that a single mode is very highly excited. For the spin–boson case the Hamiltonian provides coupling which results in massive coupling between the different unrotated states. All of this coupling is of course sorted out under the Foldy–Wouthuysen transformation. However, if fast loss channels are present then the situation changes drastically. Many of the states coupled to in the unrotated spin–boson model are basis states driven very far off of resonance, which have much less energy than the system has (as measured by the eigenvalue of the overall state under consideration). Such states might be considered to have an energy surplus, and the decay rate can become greatly enhanced on account of this energy surplus. Basis states at higher energy suffer an energy deficit, so the associated decay rate is reduced. This describes the mechanism responsible for removing destructive interference in the lossy spin–boson model, which leads to a large increase in coherent energy exchange under conditions of fractionation.

In a metal, phonon loss to electron promotion would be expected to be the dominant energy loss mechanism for the coupled phonon–nuclear system. A highly-excited vibrational mode will similarly lose energy rapidly if a strong vibrational nonlinearity is present. These are the most important loss mechanisms under consideration in this discussion.

6.4. Lossy coupled lattice–nuclear model

In light of this discussion, we might augment the model with these loss channels and write

$$\hat{H} = \sum_\mu \hbar\omega_\mu \left(\hat{a}_\mu^\dagger \hat{a}_\mu + \frac{1}{2}\right) + V_0 + \sum_j \left(\mathbf{M}c^2 + \mathbf{a}\cdot c\hat{\mathbf{P}}\right)_j - \sum_j \frac{|\hat{\mathbf{P}}|^2}{2M} - i\frac{\hbar\hat{\Gamma}(E)}{2}. \tag{55}$$

We have used such a notation in previous work to denote the augmentation of similar models with loss. We recognized the operator $\hat{\Gamma}(E)$ as a loss operator in an infinite-order Brillouin–Wigner formalism [27,50]. In such a formalism

one works with a Hermitian model, and then divides the state space into sectors. If we focus on a single sector, then interactions which couple from one sector to another appear not to be Hermitian with respect to that sector. If the associated loss produces an exponential decay of the sector probability, then such a description is very useful since one can carry out an approximate evaluation of the decay rate within the formalism to obtain the Golden Rule estimate. Consequently, we recognize this Hamiltonian as describing a relevant sector of interest, with the loss operator keeping track of the associated decay mechanisms (such as those described above).

Note that it is straightforward to write down relevant Hermitian models. For example, in the case of anharmonic coupling and atomic ejection, we could add atomic continuum states explicitly and describe the associated nonlinear coupling. Some nuclear excitation (and disintegration) in principle is already described since we have the $\mathbf{a}\cdot c\mathbf{P}$ coupling present. Coupling to electrons could be modeled using an appropriate electron Hamiltonian and adding electron-phonon interaction terms.

6.5. Discussion

As discussed above, when accessible fast loss channels are available that are sufficiently strong to impact the state occupation, then the generalized Foldy–Wouthuysen transformation becomes inappropriate. We are still able to carry out the rotation mathematically, but the implementation of the loss operator becomes problematic, and the resulting picture is not useful. In this case we need to work with unrotated problem with its strong first-order coupling and strong loss directly. In this regime the strong first-order coupling between vibrational and internal nuclear degrees of freedom (which is normally hidden from us because we are used to the rotated frame where it is eliminated) has the potential to produce anomalies observed in experiments.

Previously we would have considered the model of Eq. (55) to constitute the basic model that describes anomalies in condensed matter nuclear science. By now we know that this model is at the same time successful and unsuccessful. The model is known to be successful in that it describes new effects such as collimated X-rays in the Karabut experiment; excess heat generation and nonenergetic ^{4}He production in the Fleischmann–Pons experiment; it resolves Huizenga's three miracles; it sheds light on the origin of low-level gamma emission in the Gozzi experiment [51] and in Piantelli's experiment [52]; and it provides a basis to understand some transmutation effects. Sadly, the model is unsuccessful in that the conditions where these effects are predicted in the analysis done so far do not match with those of the experiments.

In a sense, we are close. But something is still missing from the model (and our effort to remedy this will be dealt with in following publications).

7. Lattice-induced Nuclear Excitation

As we have seen from many years of developing and analyzing models, models for excess heat production within the approach we have pursued are complicated (in that there are donor transitions and receiver transitions); there are uncertainties (we do not know from experiment in general which transitions operate as receiver transitions in the model); and in the end it is hard to be certain that the model is correct (due to the absence of relevant observables in the experiments). Much better would be a simpler effect with only one set of transitions, and even better if there was a clean diagnostic to tell from experiment what is going on in more detail.

In light of these difficulties, in recent years our focus has shifted to Karabut's collimated X-rays. These we have interpreted as due to direct excitation of the 1565 eV transition in a small number of ^{201}Hg impurities on the cathode surface. If this interpretation is correct, then the situation is very different. Instead of two transitions (donor and receiver), only one would be involved here (very much reducing the model). For completeness, we note that there is also the possibility of a donor and receiver scheme leading to excitation of the ^{201}Hg, a possibility that will be considered

in a subsequent paper. Although the identity of the transition has not been confirmed experimentally, it seems likely since it is the only nuclear transition from the ground state of a stable nucleus anywhere close to the energy observed in experiment. And finally if the 1565 eV ^{201}Hg transition is excited, we would expect electron emission, X-ray emission, and most importantly collimated X-ray emission if phase coherence is established.

7.1. Previous work

The problem of coherent energy exchange between a highly-excited oscillator and two-level systems in the lossy spin–boson model was considered as a mathematical problem in [27,29–31]. As a result, we might consider this to be a known problem that has been analyzed and solved within the framework of the lossy spin–boson model. However, as mentioned above there is a difference between the (toy) mathematical model (of the lossy spin–boson model), and a physical model (such as that of composite nuclei in a harmonic lattice as discussed above). While the mathematical model clarifies how the physical mechanism works, we expect a physical model to predict the physical conditions under which the effect should be observed.

The situation at present is then that we have relevant mathematical models based on the lossy spin–boson model that we can solve, and which give results which seem to be connected to experiment. By now we also have experience with a number of physical models, all of which we can analyze with sufficient accuracy to ascertain whether they agree with experiment or not. For models based on electron–nuclear coupling as a basis for phonon–nuclear interaction, there are orders of magnitude between the predictions and experiment. In the case of a donor and receiver model based on electron–electron coupling for fractionation, there are again orders of magnitude difference (but fewer) between the model and experiment.

Now that we have a much improved model for phonon–nuclear coupling as described by Eq. (55), which is based on a much stronger coupling between vibrations and the internal nuclear degrees of freedom, of interest is whether this model agrees with experiment. Sadly, our initial efforts at predicting the Karabut experiment with this model showed some deficiency remained, either in the fundamental theory, or else in the particular model examined for the Karabut experiment. Although collimated X-ray emission is predicted, the fractionation power in this model seems to be short of what the experiment seems to be doing by at least two orders of magnitude. While far superior to earlier models (in that the numbers are now very much closer), some problem remains.

During the summer of last year, we had a brainstorm as to how this problem might be resolved. The idea was that perhaps the transitions that are coupled to most strongly would produce additional phonon fluctuations which might make up the difference. Under the gun before the ICCF17 we analyzed a model of this kind, and found (errantly) that these additional fluctuations could provide an enhancement to the fractionation power, resulting in general agreement between our proposed model for the Karabut experiment and our interpretation of the experimental conditions. For a while things were very exciting, since we were able for the first time to work with a physical model that seemed to give good results for the Karabut experiment [42], and at the same time could make sense of excess heat experiments, and also gamma emission [43]. After the conference while writing up the model, we found the error. We now know that this approach that we had tried doesn't work.

In what follows in this section, we consider the basic arguments of last summer's model more carefully. At issue here is the question of what happens in the case of a relatively weak low-energy transitions when a great many much stronger (and lossy) high-energy transitions are present. The issue is relevant generally if we are to make use of this kind of model, and since the models are new we have little intuition *a priori*. The result of the analysis is that we would expect essentially no contribution from all of these much stronger lossy transitions. This resolves the issues raised last summer; sadly, this also takes away the good agreement between the new theory and Karabut model, and experiment, that had for a few months been elating. Even so, there is good news in the result, and that is that even when we can't use Foldy–Woutuysen transformation, the result that we obtain for all transitions not involved in the coherent

dynamics is the same as if we had been able to use the transformation. This means that we are free to focus on those transitions involved in phonon-nuclear coherent dynamics, which simplifies what we need to do when analyzing the model considerably.

However, in spite of all that is good about it, the new theory and our particular Karabut model is still not in agreement with our interpretation of the experiment. This will motivate us to re-examine the theory, the model, and the interpretation of the experiment, in following works.

7.2. The model

We are interested then in a model for lattice-induced nuclear excitation relevant to collimated X-ray emission in the Karabut experiment. Our starting place for this analysis will be the fundamental phonon–nuclear Hamiltonian developed in the last section

$$\hat{H} = \sum_\mu \hbar\omega_\mu \left(\hat{a}_\mu^\dagger \hat{a}_\mu + \frac{1}{2} \right) + V_0 + \sum_j \left(\mathbf{M}c^2 + \mathbf{a}\cdot c\hat{\mathbf{P}} \right)_j - \sum_j \frac{|\hat{\mathbf{P}}|^2}{2M} - i\frac{\hbar\hat{\Gamma}(E)}{2}.$$

Here, all the phonon modes and all transitions in all nuclei are accounted for. Our job in what follows will be to bring out the dynamics associated with the highly excited phonon mode and preferred nuclear transition.

7.3. The coupled lattice-nuclear problem

We assume that the sufficiently fast decay channels restrict us from using a generalized Foldy–Wouthuysen transformation, in which case we need to pursue solutions for the coupled lattice and nuclear problem. The strongest coupling occurs with basis states that have negative energy components, and also with internal nucleon degrees of freedom (isobars). Consequently, we would like to deal with the coupling with these degrees of freedom first.

In previous work we proposed to make up separate $\mathbf{M}c^2$ and $\mathbf{a}\cdot c\mathbf{P}$ terms for the preferred transitions, and for all other transitions. Such an approach has the advantage that it is conceptually easy to explain and to work with; but it has the disadvantage that it doesn't provide such a good match to the physical system. Here we will use a different approach where we work with the Hamiltonian as given rather than splitting it up. Instead here we split up the transition matrix into separate parts

$$\left(\mathbf{a}\cdot c\hat{\mathbf{P}} \right)_j = \left(\overline{\mathbf{a}}\cdot c\hat{\mathbf{P}} \right)_j + \left(\mathbf{a}_{\text{preferred}}\cdot c\hat{\mathbf{P}} \right)_j, \tag{56}$$

where the preferred transition is separated from all others. The idea is that we are interested in describing coherent dynamics on the preferred transition, while conditions on the other transitions are more nearly static. If we wish to be precise, we should also extract the contribution of this transition from the counter term, and write

$$\sum_j \frac{|\hat{\mathbf{P}}_j|^2}{2M_j} = \overline{\sum_j \frac{|\hat{\mathbf{P}}_j|^2}{2M_j}} + \left(\sum_j \frac{|\hat{\mathbf{P}}_j|^2}{2M_j} \right)_{\text{preferred}}. \tag{57}$$

In practice the contribution of the preferred transition to the counter term is trivially small (e.g., in the case of nonlinear Rabi oscillations), so that we might reasonably make use of the full kinetic energy counter term for the rest of the

problem. Also, from previous work we know that the counter term plays very little role under conditions where coherent dynamics occurs, so that it could be neglected away from threshold.

In light of these comments we seek eigenfunctions and eigenvalues of the coupled lattice and nuclear problem (in the absence of the preferred transition) given by

$$E\Upsilon = \left\{ \sum_\mu \hbar\omega_\mu \left(\hat{a}_\mu^\dagger \hat{a}_\mu + \frac{1}{2} \right) + V_0 + \sum_j \left(\mathbf{M}c^2 + \overline{\mathbf{a}} \cdot c\hat{\mathbf{P}} \right)_j - \sum_j \frac{|\hat{\mathbf{P}}|^2}{2M} - i\frac{\hbar\hat{\Gamma}(E)}{2} \right\} \Upsilon. \tag{58}$$

The eigenfunctions that result from this calculation are very close to the states of the transformed system (but expressed in the unrotated frame) were we able to make use of the Foldy–Wouthuysen transformation. If there were no preferred transition and we used the full transition matrix **a** (instead of the reduced $\overline{\mathbf{a}}$), and if loss could be neglected, then the eigenfunctions are the same (to within a unitary transformation) as the states of the separated problem following the Foldy–Wouthuysen transformation. In the unconventional regime where the Foldy–Wouthuysen transformation is not helpful, this calculation takes its place in the description of most of the coupled system.

We have recently studied a similar model in which a highly excited mode is coupled to N-level transitions initially in the ground state, with highly unstable excited states [50]. Our present model is different in that there are many states at lower energy that involve negative energy components. However, since these cannot have real occupation, the extension of the model to such states involves no modifications that will end up producing a different answer in interactions with the highly excited mode. We found that approximate product solutions gave results very similar to exact numerical solutions for a highly excited oscillator as long as the coupling is strong.

Interactions with unexcited modes or thermal modes produces mixing which matches the contribution to the counter term to second order exactly on a mode by mode basis. The detailed analysis of this problem would require a minor modification of the approach used in [50] to adapt it to low n, but essentially the same product state approximation would be effective.

7.4. Finite basis expansion for the low-energy dynamic transition

Next we focus on the coupling between the preferred low-energy nuclear transition and the highly excited mode. In previous work we found that we could develop good estimates for the rate of coherent energy exchange by working with a finite basis expansion for product states of the oscillator number states and two-level system Dicke states. Unfortunately in this problem the oscillator is now strongly-coupled to the internal nuclear transitions, and this needs to be taken into account in our analysis.

In view of these comments, we adopt a global solution of the form

$$\Psi = \sum_j c_j \Upsilon_j, \tag{59}$$

where the coupled nuclear and lattice states Υ_j includes excitations of the lattice, the preferred transition, as well as all other states. In general these states are too complicated to work with, so we need to simplify things to proceed. Since our focus is on the dynamics of the the preferred transition, and on energy exchange with the highly excited phonon mode, it seems sensible to bring out the associated indices of these systems and suppress those not immediately involved. To accomplish this we adopt the notation

$$\Upsilon_j \;\rightarrow\; \Upsilon_{m,n}, \tag{60}$$

where n is essentially the number of oscillator quanta in the highly excited mode, and where m is a Dicke index associated with the Dicke states $|S,m\rangle$ of the two-level system. It may not be obvious that such a notation is appropriate, given that we are dealing with a system that involves substantial coupling between the vibrational and nuclear degrees of freedom. These states are complicated, so we might expect that more is needed to describe them.

However, we recall that the coupled vibrational and nuclear system we are dealing with would be described by

$$E\Upsilon' = \left\{ \sum_\mu \hbar\omega_\mu \left(\hat{a}_\mu^\dagger \hat{a}_\mu + \frac{1}{2} \right) + V_0 + \sum_j \left(\mathbf{M}c^2 \sqrt{1 + \frac{c^2|\hat{\mathbf{P}}|^2}{(\mathbf{M}c^2)^2}} \right)_j - \sum_j \frac{|\hat{\mathbf{P}}_j|^2}{2M_j} + \sum_{j<k} \Delta\hat{V}'_{jk} \right\} \Upsilon' \tag{61}$$

if we could make use of the Foldy–Wouthuysen transformation. In the unconventional regime we cannot make use of the transformation, but nonetheless the coupled lattice and nuclear states are, for the most part, not very different from what we would compute in the conventional regime. Since there is no difficulty with the assignment of n or m for the conventional regime, it should probably not be surprised that the same indices are appropriate in the unconventional regime.

It will be useful to take another step along these lines. In the conventional regime we would have no difficulty in using a product wavefunction for the highly excited mode and Dicke system

$$\Upsilon_{m,n} \;\rightarrow\; \overline{\Upsilon}|n\rangle|S,m\rangle. \tag{62}$$

For the unconventional regime we can reasonably separate out the Dicke system, but for now we will keep the background coupled vibrational and nuclear states together keeping in mind the mixing; in this case we write

$$\Upsilon_{m,n} \;\rightarrow\; \overline{\Upsilon}_n|S,m\rangle \qquad \text{(conventional)}. \tag{63}$$

In the end our finite basis expansion is of the form

$$\Psi = \sum_m \sum_n c_{m,n} \overline{\Upsilon}_n |S,m\rangle. \tag{64}$$

7.5. Resonant versus off-resonant states

Before continuing there remains on last issue to address; this involves whether the basis states are resonant (real) or off-resonant (virtual) states. It is this issue which led to problems in our earlier analysis of lattice-induced nuclear excitation in Refs. [42,43], so we are motivated to focus some attention on the issue here.

The case of real states probably corresponds best to our intuition, so this would be the place to start. The issue here is that the energy we would use to evaluate the loss operator would be the same as the energy eigenvalue; we might denote this situation as

$$E_{m,n}\Upsilon_{m,n} = \left\{ \sum_\mu \hbar\omega_\mu \left(\hat{a}^\dagger_\mu \hat{a}_\mu + \frac{1}{2} \right) + V_0 + \sum_j \left(\mathbf{M}c^2 + \overline{\mathbf{a}} \cdot c\hat{\mathbf{P}} \right)_j - \sum_j \frac{|\hat{\mathbf{P}}|^2}{2M} - i\frac{\hbar\hat{\Gamma}(E_{m,n})}{2} \right\} \Upsilon_{m,n} \qquad \text{(real)}. \tag{65}$$

Alternatively, we might be interested in the computation of the coupled lattice and nuclear states in the off-resonant case. For example, in a finite basis calculation we might have basis states of the coupled lattice and nuclear problem for which the part of the system energy available is very different than the basis state energy. In this case, we might indicate this as

$$E_{m,n}\Upsilon_{m,n} = \left\{ \sum_\mu \hbar\omega_\mu \left(\hat{a}^\dagger_\mu \hat{a}_\mu + \frac{1}{2} \right) + V_0 + \sum_j \left(\mathbf{M}c^2 + \overline{\mathbf{a}} \cdot c\hat{\mathbf{P}} \right)_j - \sum_j \frac{|\hat{\mathbf{P}}|^2}{2M} - i\frac{\hbar\hat{\Gamma}(E)}{2} \right\} \Upsilon_{m,n} \qquad \text{(virtual)}. \tag{66}$$

These two problems are very different, especially since the unconventional regime is one where the loss is presumed to be extremely fast for some of the accessible states. As we are using state exclusion as a way to take into account the very fast loss, a different set of states would be excluded in the two calculations. We need to make sure that the correct ones are used in for the computations that follow.

7.6. Eigenvalue equation for the expansion coefficients

We can take our finite basis expansion and insert into the model to obtain an eigenvalue equation for the expansion coefficients; this produces

$$\begin{aligned} Ec_{m,n} =& E_{m,n}c_{m,n} \\ & - i\left(\mathbf{a}_0 \cdot c\frac{\mathrm{d}\hat{\mathbf{P}}}{\mathrm{d}a} \right) \sqrt{(S-m)(S+m+1)} \sum_{\Delta n_1} \langle \overline{\Upsilon}_{m,n} | \hat{a} | \overline{\Upsilon}_{m+1,n+\Delta n_1} \rangle c_{m+1,n+\Delta n_1} \\ & + i\left(\mathbf{a}_0 \cdot c\frac{\mathrm{d}\hat{\mathbf{P}}}{\mathrm{d}a} \right) \sqrt{(S-m)(S+m+1)} \sum_{\Delta n_1} \langle \overline{\Upsilon}_{m,n} | \hat{a}^\dagger | \overline{\Upsilon}_{m+1,n+\Delta n_1} \rangle c_{m+1,n+\Delta n_1} \\ & - i\left(\mathbf{a}_0 \cdot c\frac{\mathrm{d}\hat{\mathbf{P}}}{\mathrm{d}a} \right) \sqrt{(S+m)(S-m+1)} \sum_{\Delta n_1} \langle \overline{\Upsilon}_{m,n} | \hat{a} | \overline{\Upsilon}_{m-1,n+\Delta n_1} \rangle c_{m-1,n+\Delta n_1} \\ & + i\left(\mathbf{a}_0 \cdot c\frac{\mathrm{d}\hat{\mathbf{P}}}{\mathrm{d}a} \right) \sqrt{(S+m)(S-m+1)} \sum_{\Delta n_1} \langle \overline{\Upsilon}_{m,n} | \hat{a}^\dagger | \overline{\Upsilon}_{m-1,n+\Delta n_1} \rangle c_{m-1,n+\Delta n_1}. \end{aligned} \tag{67}$$

As in our previous work, we implement loss through the removal of highly unstable states. The idea is that when the associated decay rate of a state is fast in a sector Hamiltonian, faster than can be replenished by transitions to that state,

then the occupation of the state is reduced. We have found in previous work that only minor differences in the coherent energy exchange rate occur between models with accurate loss models and those where the unstable states are removed.

7.7. Approximate eigenvalue equation

It will be convenient to take the limit where S is large, but where $|m|$ is not close to S; in this case we approximate

$$\sqrt{(S-m)(S+m+1)} \;\rightarrow\; \sqrt{S^2-m^2},$$

$$\sqrt{(S+m)(S-m+1)} \;\rightarrow\; \sqrt{S^2-m^2}. \tag{68}$$

Under conventional conditions where the Foldy–Wouthuysen transformation can be used, we can write for the phonon exchange matrix elements

$$\langle\overline{\Upsilon}_{m,n}|\hat{a}|\overline{\Upsilon}_{m\pm1,n+\Delta n_1}\rangle \;\rightarrow\; \sqrt{n_0}\,\delta_{\Delta n_1,1} \qquad \text{(conventional)},$$

$$\langle\overline{\Upsilon}_{m,n}|\hat{a}^\dagger|\overline{\Upsilon}_{m\pm1,n+\Delta n_1}\rangle \;\rightarrow\; \sqrt{n_0}\,\delta_{\Delta n_1,-1} \qquad \text{(conventional)}, \tag{69}$$

where we have assumed that the oscillator is highly excited, so that n_0 is very large, and n is near n_0. In the unconventional regime this remains the case for the majority of the n states; because of this, it is convenient to write the eigenvalue equation as

$$\begin{aligned} Ec_{m,n} =& E_{m,n}c_{m,n} - i\left(\mathbf{a}_0\cdot c\frac{\mathrm{d}\hat{\mathbf{P}}}{\mathrm{d}a}\right)\sqrt{n_0}\sqrt{S^2-m^2} \\ &\times\left\{\sum_{\Delta n_1}\frac{\langle\overline{\Upsilon}_{m,n}|\hat{a}-\hat{a}^\dagger|\overline{\Upsilon}_{m+1,n+\Delta n_1}\rangle}{\sqrt{n_0}}\,c_{m+1,n+\Delta n_1}\right. \\ &\left.+\sum_{\Delta n_1}\frac{\langle\overline{\Upsilon}_{m,n}|\hat{a}-\hat{a}^\dagger|\overline{\Upsilon}_{m-1,n+\Delta n_1}\rangle}{\sqrt{n_0}}\,c_{m-1,n+\Delta n_1}\right\}. \end{aligned} \tag{70}$$

We now have an eigenvalue equation that is similar to eigenvalue equations that we have encountered previously, and which we can analyze using the same methods as before. What is different here is that the energies of the basis states are not equi-spaced in n, and the coupling between the different states is now more complicated.

7.8. Periodic approximation

We found in previous work that we could reduce the two-dimensional problem down to a one-dimensional problem by taking advantage of the fact that when the resonance condition is satisfied

$$\Delta E = \Delta n\hbar\omega_0, \tag{71}$$

the system is nearly periodic for large S away from the boundaries (where $|m|$ is close to S). In this case

$$\left(\mathbf{a}_0 \cdot c\frac{\mathrm{d}\hat{\mathbf{P}}}{\mathrm{d}a}\right)\sqrt{n_0}\sqrt{S^2-m^2} \;\rightarrow\; g_v\hbar\omega_0 = \text{constant}. \tag{72}$$

We can construct approximate eigenfunctions of the locally periodic model using

$$c_{m,n} = \mathrm{e}^{im\phi}v_{n-m\Delta n}(\phi). \tag{73}$$

The v expansion coefficients then satisfy

$$E(\phi)v_n \;=\; E_n v_n - i\hbar\omega_0 g_v \left\{ \mathrm{e}^{i\phi}\sum_{\Delta n_1}\frac{\langle\overline{\Upsilon}_{m,n}|\hat{a}-\hat{a}^\dagger|\overline{\Upsilon}_{m+1,n+\Delta n_1}\rangle}{\sqrt{n_0}}\,v_{n+\Delta n_1-\Delta n}\right.$$

$$\left. -i\mathrm{e}^{-i\phi}\sum_{\Delta n_1}\frac{\langle\overline{\Upsilon}_{m,n}|\hat{a}-\hat{a}^\dagger|\overline{\Upsilon}_{m-1,n+\Delta n_1}\rangle}{\sqrt{n_0}}\,v_{n+\Delta n_1+\Delta n}\right\}, \tag{74}$$

where we implement loss through the elimination of states for negative n

$$v_n = 0 \quad \text{for } n < 0. \tag{75}$$

The index n is incremental in this case. The matrix elements for the $\overline{\Upsilon}$ states of the underlying coupled lattice nuclear problem is analyzed as in Ref. [50], and we take g_u for the associated dimensionless coupling constant.

From previous work we know that for large Δn we can estimate the indirect coupling matrix element from the difference between the energy eigenvalue for two phases

$$V_{\text{eff}} \;\rightarrow\; \frac{E(0)-E(\pi)}{4}. \tag{76}$$

7.9. Results

We have obtained numerical solutions for this model for representative cases, with the result that the model is only weakly dependent on the coupling strength associated with the mixed lattice and nuclear system. Results from a calculation with $\Delta n = 41$ are shown in Fig. 1. In essence the indirect matrix element depends only on g_v unless g_u gets to be sufficiently large that the underlying coupled lattice and nuclear system has the strength to fractionate the quantum by itself. This behavior is consistent between many computations we have done with various different values of Δn.

This means that it is a reasonable approximation to replace the complicated eigenvalue equation for the locally periodic approximation with a much simpler model

$$\frac{E(\phi)}{\hbar\omega_0}v_n = nv_n - ig_v\left\{\mathrm{e}^{i\phi}\left[v_{n+\Delta n-1}-v_{n+\Delta n+1}\right]+\mathrm{e}^{-i\phi}\left[v_{n-\Delta n-1}-v_{n-\Delta n+1}\right]\right\}. \tag{77}$$

The indirect coupling matrix element that results is

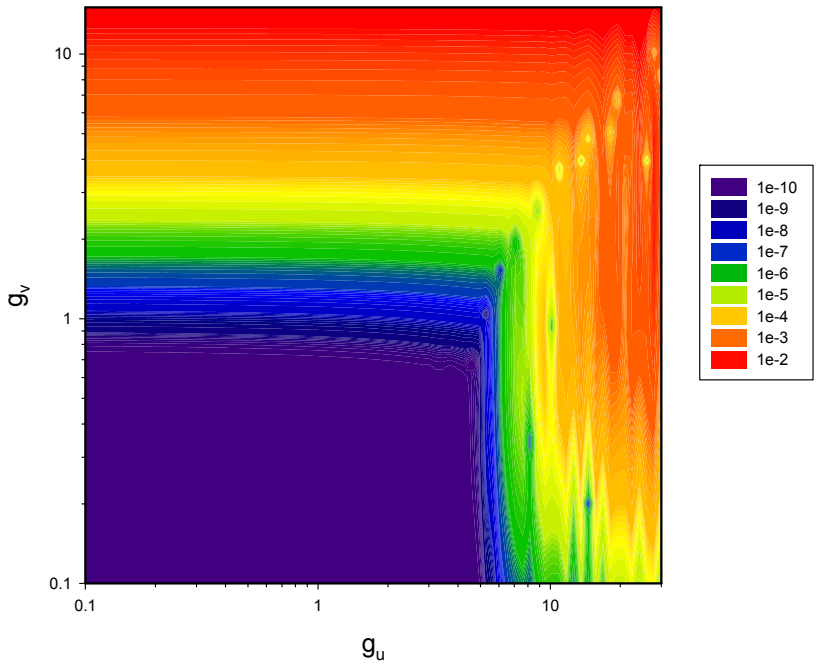

Figure 1. Indirect coupling strength $V_{\rm eff}/\Delta E$ as a function of the two dimensionless coupling strengths g_u and g_v, for $\Delta n = 41$.

$$\frac{V_{\rm eff}}{\Delta E} = 4 g_v \Phi(g_v), \tag{78}$$

where $\Phi(g)$ has been calculated, discussed, and fitted in Ref. [31].

7.10. Discussion

There are a number of conclusions that we can draw from this result. Perhaps the most important is that we seem to be getting pretty much the same result for the indirect coupling matrix element as we would have if the lattice and nuclear problem for all the other transitions were rotated using a Foldy–Wouthuysen transformation. This is important since it provides a major simplification for the analysis of indirect coupling matrix elements and the associated dynamics within the theory.

Another result from this is that our earlier analysis of this problem [42,43] which gave an enhancement in the indirect coupling matrix element is in error. In the earlier analysis we made use of intermediate states calculated as real states, instead of calculating them as virtual states. When done correctly (as in this section) the problems noted in the earlier calculation are resolved.

8. Summary and Conclusions

Accounting for excess heat in the Fleischmann–Pons experiment has proven to be a tough theoretical problem over the years. By now a very large number of theoretical proposals have been put forward, but even more than 24 years after the effect was first announced there is no consensus within the community as to how it might work.

From our perspective the biggest theoretical issue has to do with where the energy goes, since energetic nuclear particles are not present in amounts commensurate with the energy produced. For example, if coherent energy exchange could proceed efficiently under conditions where the large (MeV) nuclear quantum is fractionated into small (eV) quanta of the condensed matter system, then there would be no difficulty in accounting for the anomalies. In earlier work we showed that the lossy spin–boson model as a toy mathematical model describes exactly such an effect. The difficulty has been in the identification of a relevant physical model which makes use of this mechanism.

From a comparison of different models with experiment in the case of Karabut's collimated X-ray emission, we have evolved to focus now on a model for phonon–nuclear coupling mediated by relativistic coupling (under conditions where the Foldy–Wouthuysen transformation is unhelpful). From the discussion of Sections 2–4 in this work, we have argued that the new model is on a solid theoretical foundation. We know that it implements coherent energy exchange under conditions of fractionation based on the same mechanism demonstrated previously in the lossy spin–boson model; and in addition it has the strongest phonon–nuclear coupling possible (stronger by orders of magnitude than indirect coupling mechanisms).

The new model is in addition elegant, in that it describes a straightforward relativistic generalization of the condensed matter system to include coupling with internal nuclear degrees of freedom in a very fundamental and obvious formulation. In a Born–Oppenheimer picture, we can describe physical systems now using a Hamiltonian of the form

$$\hat{H} = \sum_j \left(\mathbf{M}c^2 + \mathbf{a} \cdot c\hat{\mathbf{P}} \right)_j + \sum_{j<k} V(|\mathbf{R}_j - \mathbf{R}_k|) - i\frac{\hbar}{2}\hat{\Gamma}(E). \tag{79}$$

There is no difficulty in working with a more fundamental version of the problem where the electrons are included explicitly, as in

$$\begin{aligned} \hat{H} = &\sum_j \left(\mathbf{M}c^2 + \mathbf{a} \cdot c\hat{\mathbf{P}} \right)_j + \sum_k \frac{|\hat{\mathbf{p}}_k|^2}{2m} + \sum_{j<j'} \frac{Z_j Z_{j'} e^2}{4\pi\epsilon_0 |\mathbf{R}_{j'} - \mathbf{R}_j|} \\ &+ \sum_{k<k'} \frac{e^2}{4\pi\epsilon_0 |\mathbf{r}_{k'} - \mathbf{r}_k|} - \sum j, k \frac{Z_j e^2}{4\pi\epsilon_0 |\mathbf{r}_k - \mathbf{R}_j|}. \end{aligned} \tag{80}$$

In this case, electron loss would emerge in a systematic treatment, so that we no longer would have to include a loss Hamiltonian explicitly. In the case of a highly excited phonon mode, we would expect this model to describe coherent energy exchange under conditions of fractionation.

This is interesting for many reasons. These new models under discussion constitute a clear improvement over text book models, since they greatly extend the realm of physics under discussion, while retaining (including) a basic description of known results in both condensed matter physics and in nuclear physics. In addition we are able to work with the new models, and carry out calculations without undo heroics. These models describe coupling of vibrational energy to the nuclear system, qualitatively consistent with collimated X-ray emission in the Karabut experiment; excess heat in PdD with ^{4}He production; and low-level gamma emission effects. In all cases the effects predicted are qualitatively very much like experiment.

Unfortunately, in our use of the models we have as yet not obtained quantitative agreement between theory and experiment. For example, if we make use of a result from the lossy spin–boson model [31], we obtain an approximate constraint for coherent energy exchange which should give us a threshold for nuclear excitation in the Karabut experiment; this constraint can be written as

$$\frac{g}{\Delta n^2} \;\rightarrow\; \frac{1}{\Delta n^2}\left(\frac{acP\sqrt{S^2-m^2}}{\Delta E}\right) \;>\; 5\times 10^{-4}, \tag{81}$$

where g is the dimensionless coupling constant, Δn is the number of phonons exchanged, a is the coupling matrix element for the $\Delta E = 1565$ eV transition, P is the Hg atom momentum matrix element, and where $\sqrt{S^2-m^2}$ is the Dicke number. We have so far been unable to find model parameters for the Karabut experiment consistent with our interpretation of the experiment which allow this constraint to be satisfied.

Our conclusion then is that we are in a sense "close," in that we have new models which have a good physical basis, which describe the phenomena observed in experiment, and which can fractionate a large quantum. But because we do not obtain consistency so far with the experimental parameters of our interpretation of the Karabut experiment, we know that something important is missing. There is a problem either in the theory, in the particular model, or in the interpretation.

We have understood within the past year that in metals that electron-phonon coupling can lead to phonon fluctuations, and that these phonon fluctuations have the potential for increasing the fractionation power in the phonon–nuclear problem. This effect would be included in the model of Eq. (80) ([ut not in models of the form of Eq. (79)). Our efforts over the past several months have been focused on the analysis of this problem; we will describe our efforts in a forthcoming paper.

Appendix A.

A thoughtful reviewer has taken the time to read some of our papers, and offer a criticism which in our view gets at some key issues that are important. This is the case in our model, and also in other models that seek to account for excess heat in the Fleischmann–Pons experiment based on deuteron-deuteron fusion reactions. Because of this, we felt that it would be of interest to others to include some of the reviewer's comments in this Appendix, and to provide a response in what follows.

Appendix A.1. Reviewer's argument

The main assumption of this and other papers in this rather extensive line of research by the authors is that there is direct coupling at the Hamiltonion level between the nuclear states and various oscillatory modes (phonons, plasmons, etc.) of a condensed matter system. Let us refer to these oscillatory modes as simply phonons. This assumption then allows the authors to examine different forms of coupling and loss mechanisms, and to seek ways to explain "fractionation" of a nuclear reaction like a fusion event's Q energy into a large number ($\sim 7\times 10^8$) of small quanta of these phonons. They are also interested in explaining X-ray production in the Karabut experiment. The key assumption is that a Hamiltonian of this form, which directly couples phonons to the nuclear states, is a valid theory. There are two ways to look at this. First, the authors have in mind that the standard model of particle physics lies at the basis of the nuclear structure and reactions, and that their Hamiltonian is an effective Hamiltonian which will ultimately be found to be compatible with the standard model, and hopefully can be derived from it. The second possibility is that the authors may wish to imply that the standard model is simply wrong, and does not apply to the nuclear structure or reactions that have been observed in LENR expreriments.

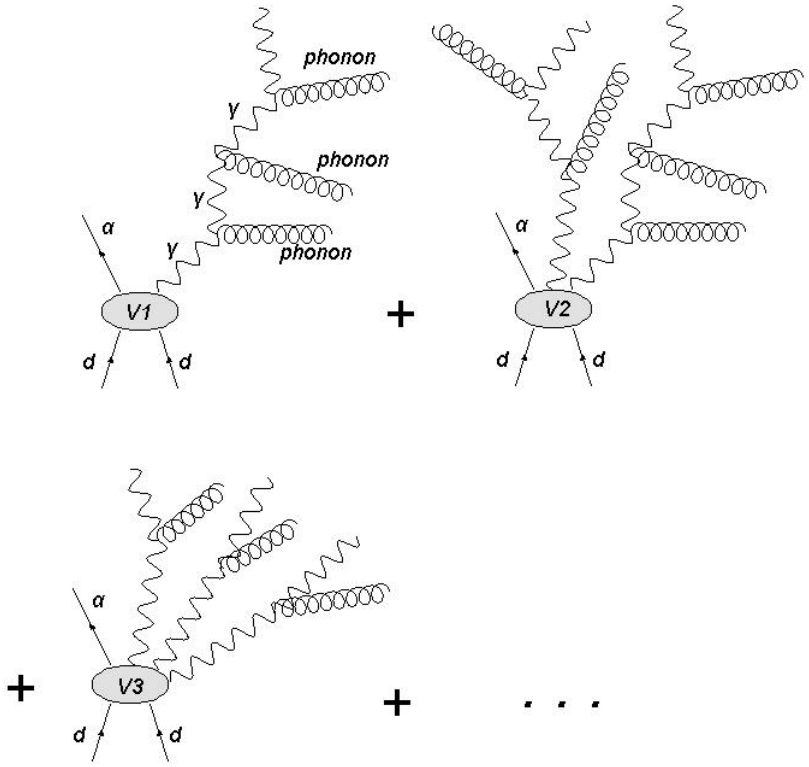

Figure 2. Feynman diagrams for phonon excitation in a standard model description of d + d + phonons + photons. The phonons are produced when the photon lines interact with charged particles (not shown) in the lattice.

If the authors wish to present a theory which does not contradict the standard model of particle physics, then I believe the basic assumption that a Hamiltonian which directly couples phonons to nuclear states is not plausible, at least for deuterium cold fusion. The reason is that the standard model requires that a nuclear fusion event that couples fusion with the lattice when ^{4}He is being produced should be mediated by the electromagnetic force, ie. by photons. The principle coupling in the standard model (or in just plain QED for that matter) between a fusion reaction and phonons in a solid is via photon exchange. The photons are exchanged between the fusion event and various charged particles in the solid. The following Feynman diagrams illustrate this situation for the production of ^{4}He.

Each photon emitted from the vertex brings a factor of the fine structure constant to the probability of the diagrams in Figure 1. So, the probability of emitting a large number of photons is vanishingly small, unless the vertex functions Vn were to have anomalous behavior for large number of photons n, which has not been observed in other fusion experiments. We must therefore limit the number of photons being emitted. So each photon emitted would be expected to be a gamma ray, and the largest contribution should come from single photon emission. But then we know from many experiments how a gamma ray will react with a solid. Yes, they will produce some phonons, but they will also have a range of motion, and many should be observed in the LENR experiments that have been performed. So these

Feynman diagrams would seem to rule out the possibility that a direct Hamiltonian coupling between the nuclear state and phonons is a good approximation to the standard model in the case of deuterium fusion. You need to have photons to transfer energy from the nuclear event to the lattice, and this system does not seem to be well approximated by any direct phonon to nuclear state coupling.

The time reverse situation is also in effect. In order for a phonon to excite a nucleus, it must do so by causing a virtual photon be be created in the lattice which can then be absorbed by the nucleus. There is expected to be a factor of α (fine structure constant) for each such photon. Although this situation might be better approximated by a direct nuclear–phonon interaction in the standard model or in QED, it's not clear from the current paper how to justify this or to justify the magnitude of the coupling constant needed for appreciable fractionation.

The standard model also predicts the reactions

$$\mathrm{d} + \mathrm{d} \rightarrow \mathrm{t} + \mathrm{p}$$

and

$$\mathrm{d} + \mathrm{d} \rightarrow \mathrm{n} + {}^{3}\mathrm{He}.$$

Although the energetic charged particles produced could produce some phonons, it is very hard to see how these channels might be suppressed to the rates observed in LENR experiments which would be required in order for a direct phonon-nucleus interaction to be a good approximation.

So, if we then assume that the standard model is inconsistent with direct phonon coupling, and we still insist that we will consider a direct coupling of phonons to nuclear states, then that begs the question how exactly does the energy from the nuclear event get communicated to the charged particles of the lattice which is the only mechanism to excite a phonon. There needs to be some local but long range field that mediates this force. The only fundamental long range forces in nature are electromagnetism and gravitation. It we eliminate gravity due to its extremely weak coupling, then electromagnetism is the only known way for a force to be communicated from the nuclear event to the charge particles of the solid (including electrons). But we must avoid photons in order to avoid gamma rays (in some reactions at least). One possibility that might be considered is action at a distance theory, like that of Fokker–Tetrode–Wheeler–Feynman for the electromagnetic force [53]. But these theories can violate causality and are a "hard sell" to most physicists. Moreover, they are difficult to solve as the Cauchy problem is non trivial for them. Still, it might be the only way for a direct nuclear-phonon interaction Hamiltonian to fit into "conventional" theoretical physics.

Appendix A.2. Response

We are generally of the opinion that if a model (for excess heat in the Fleischmann–Pons experiment, or for other anomalies) is inconsistent with the standard model in the area that the standard model applies, then it will likely have issues being consistent with the large body of conventional experimental results. Having the standard model in this sense is a good thing, since it gives a starting place that we and others can have some confidence in. We are of the opinion that our model lies within the standard model generally.

From the reviewer's comments it might seem that if we would like ^{4}He as a reaction product from a deuteron-deuteron fusion reaction (which is the subject of other papers, but not so much this one), then we are stuck with an electromagnetic interaction, and will have to face the consequences of producing an energetic gamma. According to the reviewer, "*The reason is that the standard model requires that a nuclear fusion event that couples fusion with the lattice when ^{4}He is being produced should be mediated by the electromagnetic force, ie. by photons.*" Seemingly it could not be any simpler; if a model is to be consistent with the standard model, then it must be an electromagnetic interaction that mediates the deuteron-deuteron to ^{4}He reaction. If the interaction is not mediated by electromagnetic interaction, then it lies outside of the standard model (by this criterion). What follows from this argument is a highly

unlikely picture in which phonon emission comes about from subsequent interactions involving the gamma; a picture that we are in complete agreement with the reviewer has sufficient associated headaches that there is little chance things actually could work this way.

On the other hand, a deuteron–deuteron reaction leading to ^{4}He mediated by phonon exchange as we have proposed is not something that you see every day in nuclear physics texts. If we make use of the requirement put forth by the reviewer, that the reaction must be mediated by photon exchange in order to be consistent with the standard model, then it is hard to see how a phonon-mediated version of the reaction could be consistent. This then is what we need to think about, and to address here, in response to the reviewer's comments.

In a sense, the resolution is pretty simple; in our view it has to do with the difference between the viewpoint taken in particle physics or nuclear physics, and the viewpoint taken in condensed matter physics. For example, suppose we think about a QHD type of model (plausibly derivable from the standard model) in which nucleons interact with each other through pion exchange and photon exchange; then we envision a Hamiltonian of the general form

$$\hat{H} = \hat{H}_{\rm nucleon} + \hat{H}_{\pi} + \hat{H}_{\rm EM} + \hat{V}_{\pi-{\rm n}} + \hat{V}_{\rm phot\text{-}n} \tag{A.1}$$

except that a particle physicist would work with a Lagrangian instead of a Hamiltonian. In such a model we have Dirac nucleons, Hamiltonians for pions and photons, with single pion exchange and single photon exchange terms. If we start with two deuterons in free space, and hope to end up with a ^{4}He in free space, then the lowest-order interaction that is going to make it work is single photon exchange. If there happen to be other atoms around, then they are far away, and we expect little impact from them. Any residual interactions in such a view can be dealt with through perturbation theory.

Next, a particle physicist would begin writing out Feynman diagrams, since the mathematical machinery for computations with this kind of model have all been automated. However, here we will adopt a much more pedestrian approach and focus on how photon exchange comes into the problem in the case of a single nucleon that we focus on; the relevant Hamiltonian for this part of the problem might be written as

$$\hat{H} = \boldsymbol{\alpha}\cdot c[\hat{\mathbf{p}} - q\hat{\mathbf{A}}(\mathbf{r})] + \beta Mc^2 + \sum_j \hat{V}_{\pi}(\mathbf{r}-\mathbf{r}_j) + \sum_j \frac{qq_j}{4\pi\epsilon_0|\mathbf{r}-\mathbf{r}_j|}. \tag{A.2}$$

Pion exchange here is accounted for through an equivalent nuclear potential as was done in years past (since our focus is on the electromagnetic interaction and not on pion exchange). In this kind of model, the only relevant propagating degree of freedom capable of dealing with the relevant large energy quantum is electromagnetic. We can expand out the vector potential operator

$$\hat{A}(\mathbf{r}) = \sum_{\mathbf{k},\sigma} \hat{\mathbf{i}}_{\sigma} \sqrt{\frac{\hbar}{2\omega_{\mathbf{k}}\epsilon_0 L^3}} \left[\frac{\hat{a}_{\mathbf{k},\sigma} {\rm e}^{i\mathbf{k}\cdot\mathbf{r}} - \hat{a}^{\dagger}_{\mathbf{k},\sigma} {\rm e}^{-i\mathbf{k}\cdot\mathbf{r}}}{i} \right] \tag{A.3}$$

and see creation and annihilation operators for the photons appearing explicitly. The construction of the theory itself helps us keep track of photon creation as an independent quantum degree of freedom.

Phonon exchange was not important in nuclear reactions generally historically, so we have no phonon modes in this kind of formulation. Since phonons in a metal come about due in part to Coulomb interactions between the nucleons, and in part due to the electronic degrees of freedom, one knows that they are described within a sufficiently general Hamiltonian (the standard model includes electrons and photon exchange, so phonons are consistent with the standard model). Phonon exchange comes into this kind of picture after the fact; either as a result of interactions with the gamma

as proposed by the reviewer, or perhaps as a consequence of soft photon exchange with the lattice as an external system, in which case one could argue that in this picture the associated perturbation is small.

Now let us consider the problem from a condensed matter viewpoint. In this case, the deuterons are presumed to be inside the solid, and the lattice vibrations which we are interested in (for thinking about phonon exchange) include the deuterons of the initial state, and the ^{4}He of the final state. As such, the center of mass position and momentum of the nuclei are now lattice operators. In general the lattice is disordered, so that the vibrational modes are a mess; we might write in this case

$$\hat{\mathbf{R}}_j = \mathbf{R}_j^{(0)} + \sum_\mu \frac{d\mathbf{R}_j}{da_\mu}\left[\hat{a}_j + \hat{a}_j^\dagger\right], \tag{A.4}$$

$$\frac{\hat{\mathbf{P}}_j}{m_j} = \sum_\mu \frac{d\mathbf{P}_j}{da_\mu}\left[\frac{\hat{a}_j - \hat{a}_j^\dagger}{i}\right], \tag{A.5}$$

where the capital position and momentum operators refer to the nuclear center of mass degrees of freedom. In place of the QHD-type of Hamiltonian, we will have a new one which looks like

$$\hat{H} = \hat{H}_{\rm vib} + \hat{H}'_{\rm nucleon} + \hat{H}_\pi + \hat{H}_{\rm EM} + \hat{V}_{\pi-{\rm n}} + \hat{V}_{\rm phot\text{-}n}, \tag{A.6}$$

where we now have a vibrational Hamiltonian to keep track of the relevant lattice degrees of freedom. Since the nuclear center of mass coordinates are now part of the vibrational Hamiltonian, we have to remove them from the nucleon Hamiltonian, which is indicated by $\hat{H}_{\rm nucleon} \rightarrow \hat{H}'_{\rm nucleon}$. On the face of it, there seems to be little change in the nucleon interactions, since we have not added any distinct phonon interaction terms. However, there are now all kinds of places where phonon exchange comes in, primarily since the nucleon positions and momenta have acquired phonon operator components. To see this, we revisit the simple one-nucleon Hamiltonian

$$\hat{H} = \boldsymbol{\alpha}\cdot c[\hat{\mathbf{p}} - q\hat{\mathbf{A}}(\hat{\mathbf{r}})] + \beta Mc^2 + \sum_j \hat{V}_\pi(\hat{\mathbf{r}} - \hat{\mathbf{r}}_j) + \sum_j \frac{qq_j}{4\pi\epsilon_0|\hat{\mathbf{r}} - \hat{\mathbf{r}}_j|} \tag{A.7}$$

and view it with new eyes. Since the nucleon position operators now include phonon operators, we find that phonon exchange can occur in connection with Coulomb interactions, transverse photon exchange, and with the strong-force interaction (however, phonon exchange in the latter case requires the nucleons to be associated with different nuclei, so we can get phonon exchange when one nucleus tunnels close to another).

Having spent time analyzing phonon exchange in all of these cases, we can conclude that phonon exchange generally is a very small effect for these terms, which can be treated as minor perturbations consistent with the view described above. However, there remains the $\boldsymbol{\alpha}\cdot c\hat{\mathbf{p}}$ term which is now in part a phonon operator, and which can mediate phonon exchange now. Normally this operator is rotated out in a Foldy–Wouthuysen transformation, where it loses whatever teeth it had. However, under conditions where a Foldy–Wouthuysen transformation is unhelpful, then the associated interaction strength is quite large. In this simple example, we can think of transverse photon exchange for a single nucleon as mediated by the interaction

$$\hat{h}_{\rm int}^{\rm (photon)} = -\boldsymbol{\alpha}\cdot cq\hat{\mathbf{A}}(\hat{\mathbf{r}}), \tag{A.8}$$

We can relate the nucleon momentum operator to the center of mass operator according to

$$\hat{\mathbf{p}} = \frac{\hat{\mathbf{P}}}{N} + \hat{\boldsymbol{\pi}}, \tag{A.9}$$

where N is the number of nucleons in the nucleus, and where $\hat{\boldsymbol{\pi}}$ is relative momentum operator. Because of this, the $\boldsymbol{\alpha} \cdot \hat{\mathbf{p}}$ operator contains a part that is a roughly equivalent phonon operator

$$\hat{h}_{\rm int}^{\rm (phonon)} = \boldsymbol{\alpha} \cdot c\frac{\hat{\mathbf{P}}}{N}. \tag{A.10}$$

Perhaps in this context it is useful to examine phonon exchange and photon exchange in the context of the idealized relativistic composite model discussed in the text. In this case we may write

$$\hat{H} = \sum_j \left(\mathbf{M}c^2 + \mathbf{a}_M \cdot c\hat{\mathbf{P}} - q\mathbf{a}_q \cdot c\hat{\mathbf{A}} \right)_j + \sum_{j<k} V(\mathbf{R}_j - \mathbf{R}_k). \tag{A.11}$$

This corrects an error in [54] where we followed the suggestion of a reviewer that we make use of the formulation to add the coupling to the electromagnetic field by analogy with the electron case (we note in addition that the model in [54] suffers additionally from the problem that nucleons are not Dirac particles, and that the matrix element is too low by more than an order of magnitude as a direct result of this approximation). However, in general the mass weighted $\mathbf{a}$-matrix ($\mathbf{a}_M$) is different than the charge weighted $\mathbf{a}$-matrix ($\mathbf{a}_q$); so in writing this we have distinguished between the two. So, if we wished to describe deuteron–deuteron fusion mediate by photon exchange within this formalism, the interaction would be

$$\hat{h}_{\rm int}^{\rm (photon)} = -q\mathbf{a}_q \cdot c\hat{\mathbf{A}}, \tag{A.12}$$

which is similar in form to the equivalent phonon interaction

$$\hat{h}_{\rm int}^{\rm (phonon)} = \mathbf{a}_M \cdot c\hat{\mathbf{P}}. \tag{A.13}$$

Some modification of the photon exchange interaction in this form would be required for interactions beyond the dipole interaction, since the relativistic composite operators deal with transitions appropriate for long wavelength radiation; new operators will be needed to deal with higher multipoles where the wavelength is on the order of the nuclear size.

Consistent with the discussion here, there is no reason to exclude phonon exchange from interactions within the standard model; for interactions between nuclei embedded in a lattice, working with position and momentum operators that are phonon operators is the more natural and more useful description. Unfortunately, in general the problem becomes more complicated when this is done, so one gives up some of the advantage that the simpler free-space formalism provides for computations.

The assertion of the reviewer that phonon exchange cannot mediate an electromagnetic transition and remain within the standard model is simply incorrect (although a very understandable misconception). It is true that one cannot satisfy energy and momentum conservation for the deuteron–deuteron to ^{4}He transition, since there is no way a single phonon can take away 24 MeV. This is why we have explored alternative schemes in which the 24 MeV excitation is transferred elsewhere to a different system capable of fractionating the large quantum. In this kind of scheme, we require a single phonon exchange interaction to mediate the $D_2/^4$He virtual transition, and then deal with the fractionation as a separate part of the problem.

References

[1] M. Fleischmann, S. Pons and M. Hawkins, *J. Electroanal Chem.* **201** (1989) 301; errata **263** (1990) 187.
[2] M. Fleischmann, S. Pons, M.W. Anderson, L.J. Li and M. Hawkins, *J. Electroanal. Chem.* **287** (1990) 293.
[3] P.L. Hagelstein, M.C.H. McKubre, D.J. Nagel, T.A. Chubb and R.J. Hekman, *Proc. ICCF11* (2004) 23.
[4] E. Storms, *Science of Low Energy Nuclear Reaction: A Comprehensive Compilation of Evidence and Explanations about Cold Fusion* (World Scientific, New Jersey, 2004).
[5] B.F. Bush, J.J. Lagowski, M.H. Miles and G.S. Ostrom, Helium production during the electrolysis of D_2O in cold fusion, *J. Electroanal. Chem.* **304** (1991) 271.
[6] M.H. Miles and B. Bush, Search for anomalous effects during D_2O electrolysis using palladium cathodes, *Proc. ICCF3* (1992) 189.
[7] M.H. Miles, R.A. Hollins, B.F. Bush, J.J. Logowski and R.E. Miles, Correlation of excess power and helium production during D_2O and H_2O electrolysis using palladium cathodes, *J. Electroanal. Chem.* **346** (1993) 99.
[8] M.H. Miles, B. Bush and J.J. Lagowski, Anomalous effects involving excess power, radiation and helium production during D2O electrolysis using palladium cathodes, *Fusion Technol.* **25** (1994) 478.
[9] P.L. Hagelstein, Neutron yield for energetic deuterons in PdD and in D_2O, *J. Cond. Mat. Nucl. Sci.* **3** (2010) 35.
[10] P.L. Hagelstein, Secondary neutron yield in the presence of energetic alpha particles in PdD, *J. Cond. Mat. Nucl. Sci.* **3** (2010) 41.
[11] P.L. Hagelstein, Constraints on energetic particles in the Fleischmann– Pons experiment, *Naturwissenschaften* 97 (2010) 345.
[12] J.R. Huizenga, *Cold Fusion: The Scientific Fiasco of the Century* (University of Rochester Press, Rochester, New York, 1993).
[13] J. Schwinger, *Proc. ICCF4* EPRI Report TR-104188 **4** (1994) 1-1.
[14] G. Preparata, *QED Coherence in Matter* (World Scientific, Singapore, 1995).
[15] G. Preparata, Setting cold fusion in context: a reply, *Proc. ICCF5* (1995) 265.
[16] D. Letts, D. Cravens and P.L. Hagelstein, Dual laser stimulation and optical phonons in palladium deuteride, in low-energy nuclear reactions and new energy technologies, *Low-Energy Nuclear Reactions Sourcebook*, Vol. 2 (American Chemical Society: Washington DC, 2009) pp. 81–93.
[17] P.L. Hagelstein, D. Letts and D. Cravens, Terahertz difference frequency response of PdD in two-laser experiments, *J. Cond. Mat. Nucl. Sci.* **3** (2010) 59.
[18] D. Letts, D. Cravens, Laser stimulation of deuterated palladium: past and present, *10th Int. Conf. on Cold Fusion, Condensed Matter Nuclear Science*, Cambridge, MA, P.L. Hagelstein and S.R. Chubb (Eds.) (World Scientific, New Jersey, 2003) p. 159.
[19] D. Cravens, D. Letts, Practical techniques in CF research: triggering methods, *10th Int. Conf. on Cold Fusion, Condensed Matter Nuclear Science*, Cambridge, MA, P.L. Hagelstein and S. R. Chubb (Eds.) (World Scientific, New Jersey, 2003) p. 171.
[20] E. Storms, Use of a very sensitive Seebeck calorimeter to study the Pons–Fleischmann and Letts effects, *10th Int. Conf. on Cold Fusion, Condensed Matter Nuclear Science*, Cambridge, MA, P.L. Hagelstein and S. R. Chubb (Eds.), (World Scientific, New Jersey, 2003) p. 183.
[21] M. McKubre, F. Tanzella, P.L. Hagelstein, K. Mullican, M. Trevithick The need for triggering in cold fusion reactions, *10th Int. Conf. on Cold Fusion, Condensed Matter Nuclear Science*, Cambridge, MA, P.L. Hagelstein and S. R. Chubb (Eds.) (World Scientific, New Jersey, 2003) p. 199.
[22] M.R. Swartz, Photo-induced excess heat from laser-irradiated electrically polarized palladium cathodes in D_2O, *10th Int. Conf. on Cold Fusion, Condensed Matter Nuclear Science*, Cambridge, MA, P.L. Hagelstein and S. R. Chubb (Eds.) (World Scientific, New Jersey, 2003) p. 213.
[23] M. Apicella, E. Castagna, L. Capobianco, L. D'Aulerio, G. Mazzitelli, F. Sarto, A. Rosada, E. Santoro, V. Violante, M. McKubre, F. Tanzella, C. Sibilia, Some recent results and ENEA, *12th Int. Conf. on Cold Fusion, Condensed Matter Nuclear Science*, Yokohama, A. Takahashi, K.-I. Ota and Y. Iwamura (Eds.) (World Scientific, Singapore, 2005) p. 117.
[24] P.L. Hagelstein and D.L. Letts, Temperature dependence of excess power in two-laser experiments, *Proc. ICCF17* (in press).
[25] B. Dromey, S. Kar, C. Bellei, D.C. Carroll, R.J. Clarke, J.S. Green, S. Kneip, K. Markey, S.R. Nagel, P.T. Simpson, L. Willingale, P. McKenna, D. Neely, Z. Najmudin, K. Krushelnick, P.A. Norreys and M. Zepf, Bright multi-keV harmonic generation from

relativistically oscillating plasma surfaces, *Phys. Rev. Lett.* **99** (2007) 085001.
[26] P.L. Hagelstein, A unified model for anomalies in metal deuterides, *Proc. ICCF9* (2002) 121.
[27] P.L. Hagelstein and I.U. Chaudhary, Energy exchange in the lossy spin–boson model, *J. Cond. Mat. Nucl. Sci.* **5** (2011) 52.
[28] P.L. Hagelstein and I.U. Chaudhary, Dynamics in the case of coupled degenerate states, *J. Cond. Mat. Nucl. Sci.* **5** (2011) 72.
[29] P.L. Hagelstein and I.U. Chaudhary, Second-order formulation and scaling in the lossy spin–boson model, *J. Cond. Mat. Nucl. Sci.* **5** (2011) 87.
[30] P.L. Hagelstein and I.U. Chaudhary, Local approximation for the lossy spin–boson model, *J. Cond. Mat. Nucl. Sci.* **5** (2011) 102.
[31] P.L. Hagelstein and I.U. Chaudhary, Coherent energy exchange in the strong coupling limit of the lossy spin–boson model, *J. Cond. Mat. Nucl. Sci.* **5** (2011) 116.
[32] P.L. Hagelstein and I.U. Chaudhary, Generalization of the lossy spin–boson model to donor and receiver systems, *J. Cond. Mat. Nucl. Sci.* **5** (2011) 140.
[33] P.L. Hagelstein and I.U. Chaudhary, Errata and comments on a recent set of papers in Journal of Condensed Matter in Nuclear Science, *J. Cond. Mat. Nucl. Sci.* **7** (2012) 1.
[34] A. B. Karabut, Research into powerful solid X-ray laser (wave length is 0.8–1.2 nm) with excitation of high current glow discharge ions, *Proc. 11th Int. Conf. on Emerging Nuclear Energy Systems*, 29 September–4 October 2002, Albuquerque, New Mexico, USA, pp. 374–381.
[35] A.B. Karabut, Experimental research into characteristics of X-ray emission from solid-state cathode medium of high-current glow discharge, *Proc. 10th Int. Conf. on Cold Fusion*, August 24–29, 2003, Cambridge, MA, USA.
[36] A.B. Karabut, Research into characteristics of X-ray emission laser beams from solid-state cathode medium of high current glow discharge, *Proc. 11th Int. Conf. on Cold Fusion*, 31 October-–5 November, 2004, France, pp. 253–257.
[37] A.B. Karabut, Study of energetic and temporal characteristics of x-ray emission from solid state cathode medium of high current glow discharge, *Proc. 12th Int. Conf. on Cold Fusion*, December 2-–7, 2006, Japan, pp. 344-–350.
[38] A.B. Karabut, E. A. Karabut, Research into energy spectra of X-ray emission from solid cathode medium during the high current glow discharge operation and after the glow discharge current switch off, *Proc. 14th Int. Conf. on Cold Fusion*, August 10-–15, 2008, USA.
[39] A.B. Karabut, E.A. Karabut and P.L. Hagelstein, Spectral and temporal characteristics of X-ray emission from metal electrodes in a high-current glow discharge, *J. Cond. Mat. Nucl. Sci.* **6** (2012) 217.
[40] P.L. Hagelstein and I.U. Chaudhary, Level splitting in association with the multiphoton Bloch-–Siegert shift, *J. Phys. B: At. Mol. Phys.* **41** (2008) 035601.
[41] P.L. Hagelstein and I.U. Chaudhary, Including nuclear degrees of freedom in a lattice hamiltonian, *J. Cond. Mat. Nucl. Sci.* **7** (2011) 35.
[42] P.L. Hagelstein and I.U. Chaudhary, A model for collimated emission in the Karabut experiment, *Proc. ICCF17* (in press).
[43] P.L. Hagelstein and I.U. Chaudhary, Models for excess heat in PdD and NiH, *Proc. ICCF17* (in press).
[44] L.L. Foldy and S.A. Wouthuysen, On the Dirac theory of spin 1/2 particles and the nonrelativistic limit, *Phys. Rev.* **78** (1950) 29.
[45] J.M. McMahon and D.M. Ceperley, Ground state structures of atomic metallic hydrogen, *Phys. Rev. Lett.* **106** (2011) 165302.
[46] P. Hagelstein, I. Chaudhary, M. Melich and R. Johnson, A theoretical formulation for problems in condensed matter nuclear science, *Proc. ICCF14* (2008) 596.
[47] K.M. Case, Some generalizations of the Foldy–Wouthuysen transformation, *Phys. Rev.* **95** (1954) 1323.
[48] A. Wolf, M. Reiher and B.A. Hess, The generalized Douglas–Kroll transformation, *J. Chem. Phys.* **117** (2002) 9215.
[49] T. Nakajima and K. Hirao, Extended Douglas–Kroll transformations applied to the relativistic many-electron Hamiltonian, *J. Chem. Phys.* **119** (2003) 4105.
[50] P.L. Hagelstein and I.U. Chaudhary, Lossy spin–boson model with an unstable upper state and extension to N-level models, *J. Cond. Mat. Nucl. Sci.* (in press).
[51] D. Gozzi, F. Cellucci, P.L. Cignini, G. Gigli, M. Tomellini, E. Cisbani, S. Frullani, G.M. Urciuoli, X-ray, heat excess and ^{4}He in the D:Pd system, *J. Electroanal. Chem.* **452** (1998) 253.

[52] S. Focardi, V. Gabbani, V. Montalbano, F. Piantelli and S. Veronesi, Evidence of electromagnetic radiation from Ni–H systems, *Proc. ICCF11* 70 (2004).
[53] J.A. Wheeler and R.P. Feynman, Classical dynamics in terms if direct interparticle action, *Rev. Mod. Phys.* **21** (1949) 425.
[54] P.L. Hagelstein and I.U. Chaudhary, Central and tensor contributions to the phonon-exchange matrix element for the $D_2/^4$He transition, *J. Cond. Mat. Nucl. Sci.* **11** (2012) 15.

J. Condensed Matter Nucl. Sci. 12 (2013) 143–157

Research Article

The Fleischmann–Pons Effect: Reactions and Processes

Stanislaw Szpak *,† and Frank Gordon‡

SPAWAR Systems Center, San Diego, CA 92152. USA

Abstract

A selected group of experimental evidence indicates that the Pd/D–D_2O system can be put in its nuclear active state. This is done by negatively polarizing the system which (i) starts the process of self-organization, i.e. development of coherent processes involving protons/deuterons and lattice defects to produce the pre-nuclear active state and (ii) creates conditions for the electron capture by proton/deuteron reaction to occur. The low energy neutrons transform the pre-nuclear active state into an active state, i.e. display of features such as hot spots, transmutation and particle emission which, in turn, yields information on participating reactions and processes.
 ISSN 2227-3123

Keywords: Hot spots, Modeling, Particle emission, Transmutation

1. Introduction

Shortly after the ICCF–2 meeting Fleischmann was asked by the Royal Society to give an account of the status of research in cold fusion. In his address he stated that *In the development of any area of research (and especially in one likely to arouse controversy) it is desirable to achieve first of all a qualitative demonstration of the phenomena invoked in the explanation of the observations. It is the qualitative demonstrations which are unambiguous: the quantitative analyses of the experimental results can be the subject of debate but if these quantitative analyses stand in opposition to the qualitative demonstration then these methods of analysis must be judged to be incorrect* [1]. Two of such phenomena are observed in operating cells Pd/D_2O,Li^+,OD^-/Pt employing massive Pd cathodes namely (i) excess enthalpy generation and (ii) time separating complete saturation and the onset of thermal activities, the incubation time. The first was examined in great detail [2,3]. It is the second that can be explained only through the participation of processes that put the system in its pre-nuclear active state.

Fleischmann et al. [4], noted that, in this time period, nuclear reactions in a host lattice are affected by coherent processes, and that ... *there are appropriate thermodynamic conditions for the formation of large large clusters of hydrogen nuclei or of regions of the lattice containing ordered arrays of hydrogen nuclei at high H/Pd ratios*, resulting

*Present address: 3498 Conrad Ave, San Diego, CA 92117, USA.
†Retired.
‡E-mail: dr.frank.gordon@gmail.com

 ISSN 2227-3123

in the *. . . formation of clusters of deuterons dispersed in palladium lattice that would lead to the formation of ordered domains having high D/Pd ratios*. The formation of clusters of deuterons suggests that excess enthalpy generation is localized and can be displayed by infrared photography [5].

The thermodynamic arguments may be extended by the teachings of the non-equilibrium thermodynamics. To start, an equilibrium is defined as a state generated by the balance between operating forces. Mathematically it is expressed by a minimum of the free energy (thermodynamic interpretation) or by the equality of forward and reverse velocities (kinetic interpretation), As the departure from equilibrium is increased, the system becomes unstable and evolves to form new structures exhibiting coherent behavior [4]. The system undergoes "self-organization", the process of formation of new structures, which is complex [6]. It is quite accurately described by an interplay of kinetic and thermodynamic quantities. The interaction between them takes the form of a struggle – some are eliminated others are formed, i.e. there exists a state of dynamic equilibrium.

1.1. Scope and order of presentation

A single observation, that of the incubation time, has led to conclusions which, in turn, opened a way to explore the meaning and content of other characteristic features such as hot spots, transmutation and particle emission. Here, we limit our remarks to behavior of cells employing cathodes prepared by *an interesting new variant of the electrochemical method* [1], which eliminates the incubation time. In our interpretation we employ terminology that is common in chemical research. However, to remove ambiguity we define what is meant by certain terms (cf. Sections 2.1–2.5).

In what follows, we argue that a lot can be learned about the nuclear events when three key observations (i) hot spots, (ii) transmutations and (iii) particle emission are interpreted using the concept of self-organization and accepting that the electron capture by a proton/deuteron starts a set of nuclear reactions.

2. Background Information

A general observation: The system is not in equilibrium, consequently, methods of non-equilibrium thermodynamics are an indispensable tool to examine the nature of the F-P effect. Furthermore, the mini-explosions recorded as a function of time, yield information from which one can speculate on the kinetics of formation of domains and their stability. To avoid miss-interpretation we define (i) molecule, (ii) chemical reaction, (iii) interphase, (iv) self-organization and (v) co-deposition. To prevent misunderstanding, terminology common in chemical research is employed.

2.1. Molecule, aggregate, cluster and domain

A molecule is defined as an assembly of two or more atoms bound together to form a structure with sufficient stability to consider it as an identifiable specie [6]. As used here, an aggregate is an assembly of molecules, a cluster is an assembly of aggregates held together by forces operating in chemical systems. A domain denotes a volume containing one or more clusters interacting with lattice defects.

2.2. Chemical reaction

A chemical reaction is usually described by either (i) $aA + bB \rightarrow cC + dD + Q$ or (ii) $A + a \rightarrow B + b + Q$ where the heat of reaction $Q > 0$ denotes an exothermic and $Q < 0$ an endothermic reaction. As written, only limited information is provided, viz conservation of matter and charge, i.e. the system consists of unbounded particles in the sense that there is a continuous range of possible energies. In reality, the initial state in both cases is controlled by experimental protocol and the final state by energy considerations.

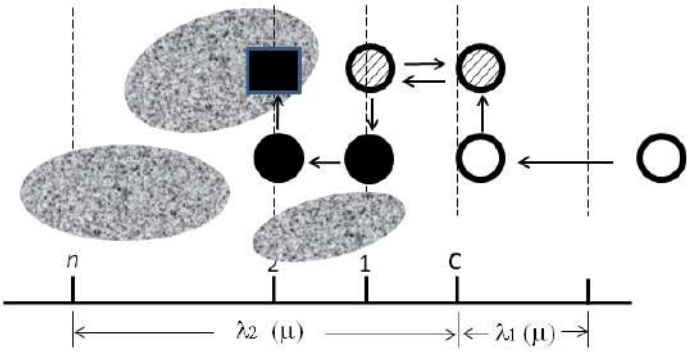

Figure 1. Structure of the interphase. c - contact surface, 1, 2, . . . , n - atomic layers, λ - thickness of the interphase, $\lambda_2(\tau)$ - thickness of the time dependent metal side layer, λ_1 thickness of the solution side layer, τ - relaxation time of the dominant process(es). open circle - H^+ ion. shaded – H in atomic state, solid - proton, square - lattice defect, shaded areas location of clusters.

2.3. Interphase

Chemical reactions rarely occur in an ideal environment, i.e. at constant temperature in time and space and at constant concentration in space. In the present case additional difficulties arise from the structural aspects of the solid phase.

These considerations lead to recognition that to uncover the true mechanism one must consider (i) conditions of an experiment, (ii) problems arising from transport of energy (heat) and matter and (iii) structural factors of the solid phase. Within the metal side of the interphase, hydrogen isotopes are distributed as follows: the sub-surface hydrogen, in the top-most layer of Pd atoms provides link between the adsorbed and dissolved atomic hydrogen, with the latter interacting with the lattice, yielding protons. With adsorption there is associated surface reconstruction but, because the surface processes are faster than bulk processes, only the hydrogen in the top-most Pd layer is responsible for its maintenance [7]. That is to say, within the interphase exists a state of dynamic equilibrium which governs the distribution of hydrogen interacting with the palladium lattice.

2.4. Self-organization

The self-organization denotes a set of processes putting the system in its nuclear active state. These processes are due to the change in the energy stored in the electric double layer, i.e. the change in its value is the driving force that generates the domains containing Pd lattice defects and deuterons. That is to say: Self-organization promotes the formation of a volume element within the system having dimensions much larger than the molecular dimensions but smaller than the volume of the system. It can occur only if the system is able to exchange part of its energy with the outside world [8].

2.5. Co-deposition

Co-deposition refers to production of electrodes by simultaneous reduction of palladium and hydrogen ions.

3. Key Features: Experimental Protocol

Characteristic features selected to identify chemical aspects of the Fleischmann–Pons effect are: (i) thermal effects, (ii) mechanical effects, (iii) transmutation and (iv) particle emission. A detailed protocol is provided only for experiments that have not been described previously.

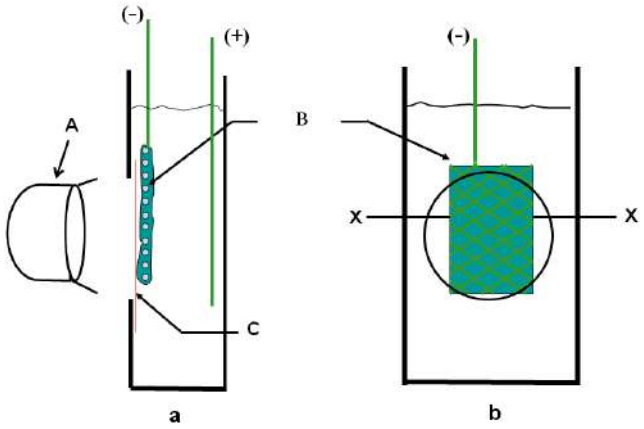

Figure 2. Experimental set-up for display of thermal activities.

3.1. Thermal effects

3.1.1. *Experimental*

One method to examine thermal behavior of the polarized Pd/D–D_2O system is to view the electrode surface using an infra-red camera. Experimentally the IR camera A, Fig. 2(a), views the surface of an active negative electrode B placed next to the thin Mylar sheet C, affixed to the wall of a rectangular cell made of clear plastic. Two conditions must be met for a successful monitoring of the thermal behavior, viz. (i) the amount of the D_2O between the electrode surface and the IR camera must be minimal (in order to avoid the attenuation of the signal), and (ii) the electrode surface facing the IR camera must be open (in a sense that the electrode processes are accessible to viewing by the IR camera). These conditions are met by co-depositing the Pd/D film on an open substrate, e.g. on a Ni screen placed in close proximity to the thin wall (made of Mylar). The IR camera can be operated in two modes: (i) to monitor temperature distribution on the electrode surface and (ii) to measure the cell temperature across the cell (i.e. along the *X*–*X* line), Fig. 2(b).

Results of IR viewing the surface of an active cathode are summarized in Fig. 3.

The negatively polarized Pd/D–D_2O system shows the development of short lived "hot spots". These thermal activities, illustrated in Fig. 3(a) are observed early during the Pd+D co-deposition and during electrolysis. Temperature

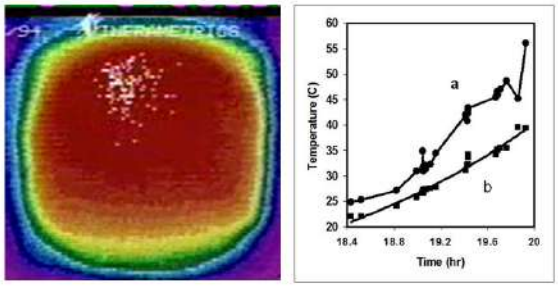

Figure 3. Thermal activities recorded by an IR camera. (a) hot spots and (b) temperature profile.

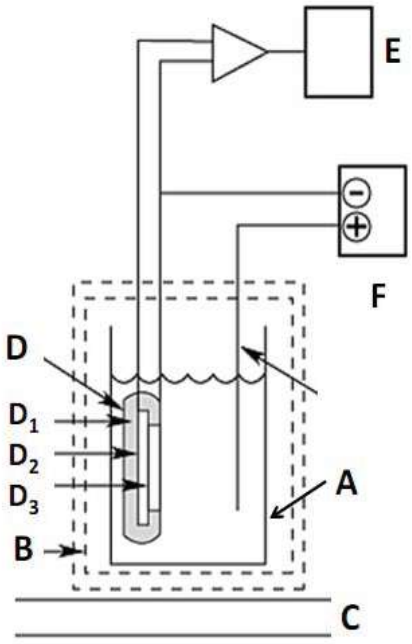

Figure 4. Recording thermal effects by an IR camera 14 Electrochemical cell designed for recording mechanical effects due to hot spots. Fig. 2b 0-0 A – electrochemical cell, B – Faraday case, C –shock absorbing pad, D – cathode assembly, D_1 – insulator, D_2 – piezoelectric disc, D_3 – Pd/D film, F – power source, E – recorder|.

profile recorded across the electrode surface when the IR camera was operated in the second mode is shown in Fig. 3(b). The cell temperature profile was taken periodically during electrolysis. The difference between surface temperature and that of solution increases with time, being initially at ca 2°C and reaching a value as high as 17°C, two hours later.

3.2. Mechanical effects

A fast exothermic reaction causes deformation of the electrode structure and the rise in temperature, thus sending pressure and temperature waves away from the source. Such waves were detected when co-deposited films were placed in contact with a piezoelectric substrate. An experimental arrangement to record their occurrence is shown in Fig. 4.

3.2.1. *Experimental*

Electrochemical cell, **A**, is placed in a Faraday cage, **B** (to prevent external noise) and the whole assembly is placed on a shock absorbing pad, **C**. The key part for the successful display of mini-explosions is the construction of the cathode, **D**. Here, a thin circular slice, in the form of a disk ($r = 1.143 \times 10^{-2}$m, $l = 2.0 \times 10^{-3}$ m of the piezoelectric material (lead–zirconium–titanate) with a conductor, e.g. (Ag) deposited on parallel surfaces was connected to an oscilloscope, **E**, and a power source, **F**, in a manner indicated. The Pd/D film was deposited onto one side a piezoelectric substrate. The characteristic feature of a piezoelectric material is the one-to-one correspondence of direct and reverse effect, e.g. compression develops a potential shift and a shift in the potential produces compression.

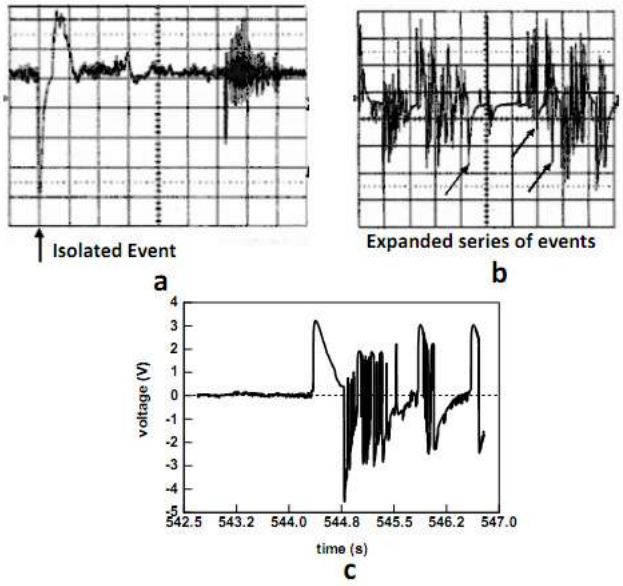

Figure 5. (a) hot spots, (b) System's response to mini-explosions. a – single event, b– burst of events. (c) *Effect of solution temperature.

As a rule, a single event, Fig. 5(a), occurs rarely. A burst of events, Fig. 5(b), is the common occurrence. Here, we see clearly a single spike which, in the negative direction corresponds to the pressure pulse. Using a simple

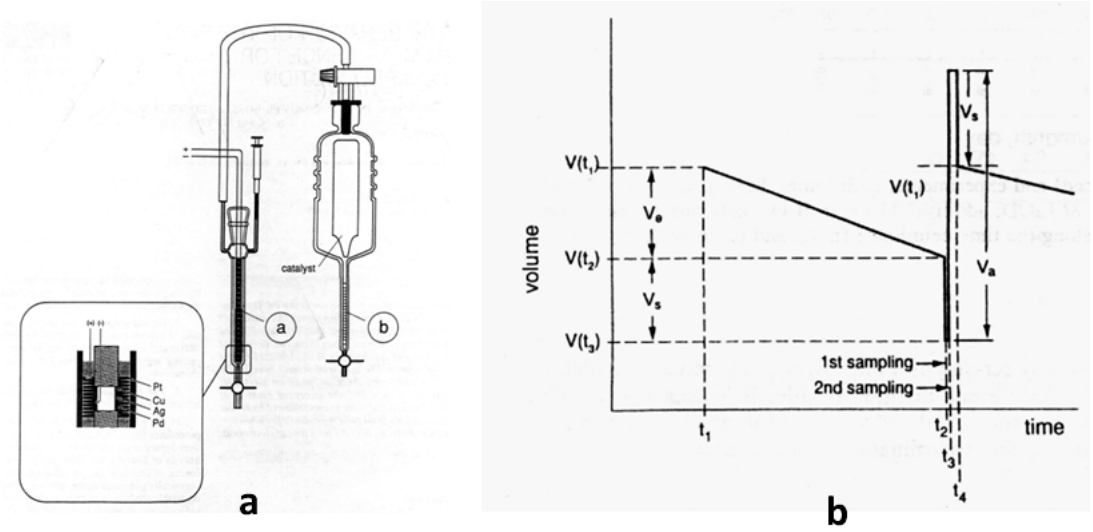

Figure 6. Cell design (a) and sampling procedure (b). 1 — cell with graduated wall a, 2 – recombiner. (b) – sampling sequence.

model, e.g. that of a spherical reaction space, one could, from the magnitude of the voltage spike and the Δt, reach some conclusion concerning the position and strength of the heat source which is temperature dependent. This strong temperature dependence is illustrated in Fig. 5, where spike of 30°C are measured in mV while at solution temperature 80°C, the spikes are measured in volts.

3.3. Transmutation

In support of conclusions reached by Fleischmann and Pons that the excess enthalpy is of nuclear origin, a search for other manifestation of nuclear activity was initiated. In the SPAWAR laboratory we selected the production of tritium. This was based on the belief that the governing reaction is $d^+ + d^+ \rightarrow He^*$ in which the highly excited He^* atom decays into tritium and proton. Somewhat later it was demonstrated that transmutation to other elements is common [9].

3.3.1. *The $d^+ \rightarrow t^+$ transmutation*

The cell with graduated walls to provide check on the volume of electrolyte, was connected to another cell containing a catalyst with sufficiently large surface area to assure complete recombination of evolving gases, Fig. 6(a). Detailed description of sampling procedure, Fig.6(b), and analysis can be found in [10,11].

Two examples of tritium production are illustrated in Fig. 7, viz. the sporadic production, Fig. 7(a) and a massive short time production, Fig. 7(b).

3.3.2. *Transmutation – production of new elements*

The production of new elements in cells using co-deposited cathodes is insignificant. However, if these cells are placed in an external electrostatic or magneto-static field, then the rate of new elements production is markedly enhanced [12]. An external electrostatic field changes conditions at the contact surface and, only via the relaxation mechanisms, extends them into the interphase. An external magneto-static field affects not only the conditions at the interphase (via Lorentz forces) but penetrates the interphase where the gradient forces and, to a lesser degree the Lorentz forces, are

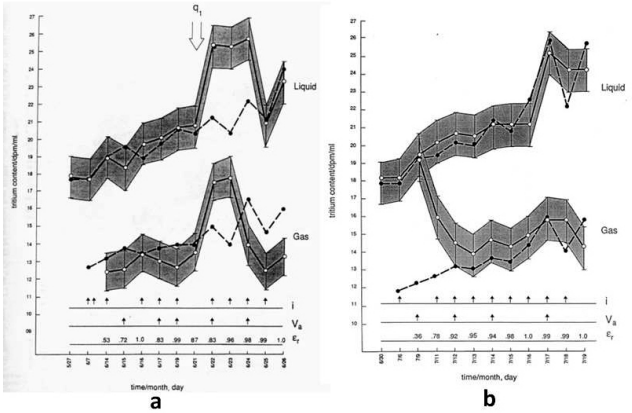

Figure 7. Experimental and calculated rates of tritium production.

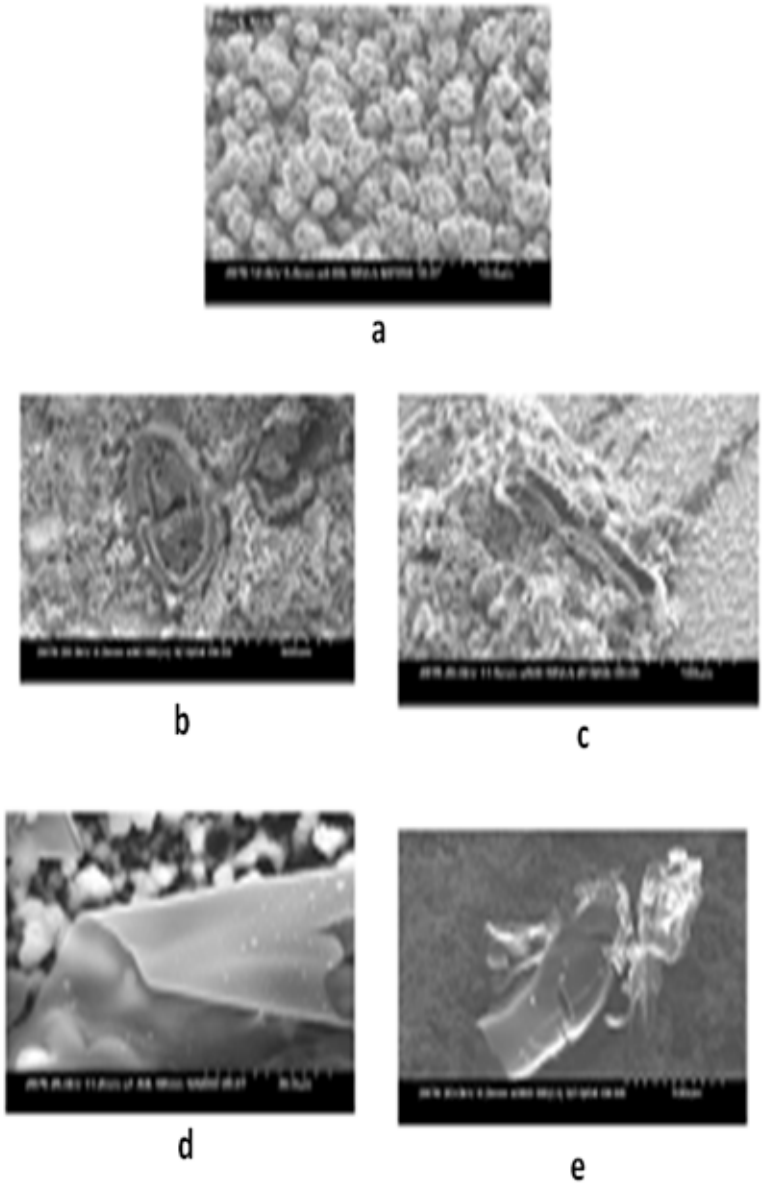

Figure 8. The almost spherical globules, (a) were re-arranged to produce a layered structure, (b) chaotic placement of small thin fragments, (c) a bent large thin plate (foil?) with, what appears to be, branches of wires attached to its surface, (d) and a violent event resembling explosion.

active. Hence, it is not surprising that magnetic field would affect both the Pd/D structure and the reaction products in different way.

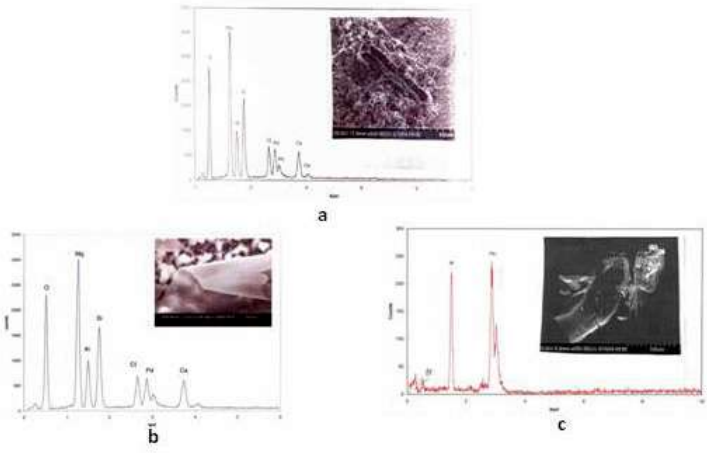

Figure 9. Selected examples of transmutation and associated morphology in external electric field.

3.3.3. *Electrostatic field*

The set of SEM photographs, assembled in Fig. 8, shows shapes which are difficult to explain, except that their formation would require substantial energy expenditure. Even a cursory examination leads to a conclusion that the energy required to produce such changes is far in excess of that which, under the conditions of experiment, could be extracted from the external field at the required rate and intensity.

The selected examples show that the number of transmutations to new elements varies from a single element, Fig. 9(a), to multiple elements, Fig. 9(b),(c). The number of new elements does not depend on the strength of applied field. Also, there are no recognizable distinct morphological features that would indicate the number or the identity of new element(s). Note that oxygen, chlorine and Pd are not new elements since they are cell components.

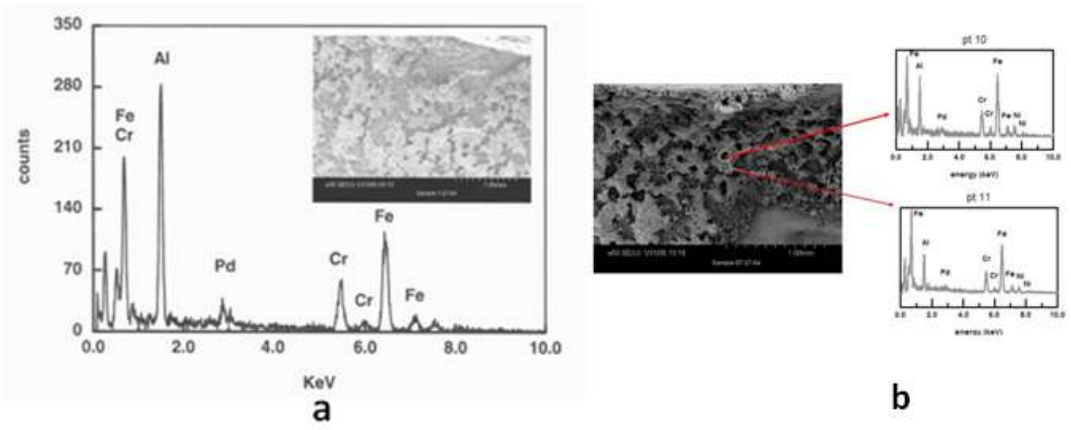

Figure 10. Selected examples of transmutation and associated morphology in external magnetic field.

3.3.4. *Magnetic field*

The shape change of the co-deposited film when placed in an external magnetic field is somewhat different from that associated with the electric field. The distinct morphological features, e.g. boulders and craters, are replaced by "pancake-like" structures, Fig. 10(a). To emphasize the difference, we selected examples that show production of new elements (transmutation) not seen in electric field. The EDX analysis of selected sites shows production of Fe, Cr in addition to Al, Figs. 10(a), (b). Elements such as Mg, Si were found in other samples. As a rule, the number of new elements found is larger than that observed in an electric field.

3.4. Particle emission

The detection and identification of particles emitted from polarized Pd/D films, when such films were placed in an external field, yields significant information about the chemistry and physics of the nuclear processes occurring within these films.

3.4.1. *Detection of emitted particles*

If CR-39 chips are used to display the particle emission, then an appropriate procedure must be developed that would exclude misinterpretation. One such procedure involves Pd+D co-deposition on an open metallic substrate, e.g. a screen or a single wire, placed in contact with the CR-39 chip. The detection and identification of particles emitted from polarized Pd/D films, when such films were placed in an external field, yields significant information about the chemistry and physics of the nuclear processes occurring within these films. If the emission of particles from the Pd/D film occurs, then they could be detected only along the electrode edge, as illustrated in Fig. 11(a). The bright line along the peripheries of a single eyelet is, in fact, an overlap of hundreds of impingement tracks, as displayed in Fig. 11(b) which represents an expanded area indicated by an arrow. Clearly, the bright line represents a set of impingement tracks next to each other while an arrow points to an area of numerous tracks. The images in Fig. 11(c) show double and triple tracks implying that there are reactions emitting two or three particles having approximately the same mass and energy.

4. Conclusions

Conclusions that are derived from the examination of an observation are either (i) certain, (ii) probable or (iii) speculative and presented in the following order: (I) the starting point, (II) hot spots, (III) transmutation and (IV) particle emission.

4.1. The starting point

The hydrogen isotope, when in palladium lattice, exists in form of protons, deuterons or tritons interacting with the lattice defects and free electrons, i.e. electrons whose chemical potential, when electric field, is $\mu(e^-) = \mu(e^-)_{\phi=0} + e^-\phi$ [14]. When polarized and, in particular, with hydrogen evolution taking place, there is re-arrangement of absorbed deuterium and lattice defects and, if the conditions are right [15], the reaction $e^- + d^+ \rightarrow 2n$ occurs. Upon completion of the self-organization the system is in the pre-nuclear active state and transits into the nuclear active state via reactions involving neutrons. In co-deposited electrodes the self-organization is an integral part of the co-deposition process.

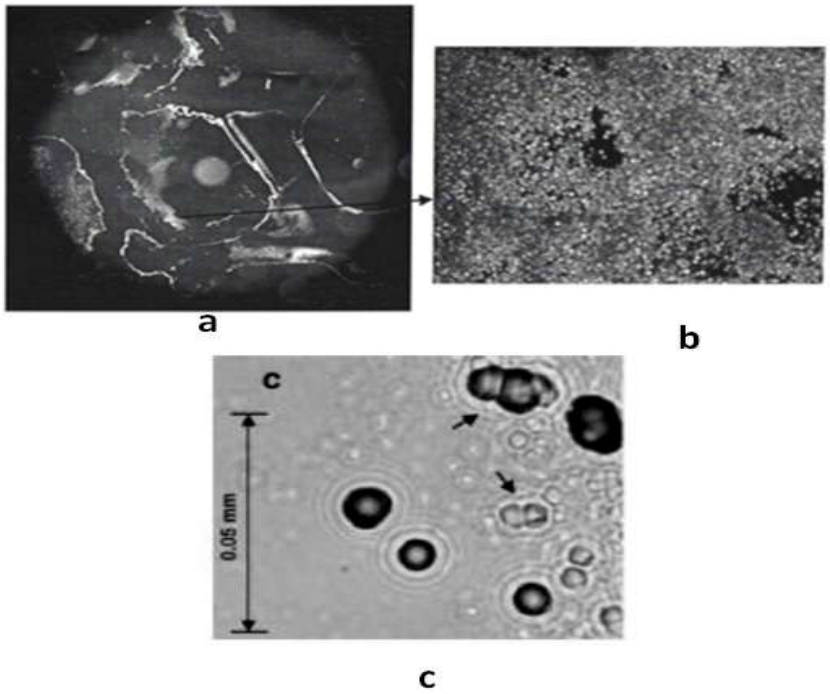

Figure 11. Impingement tracks generated by particle emission.

4.2. Hot spots

4.2.1. *Certain*

(a) Hot spots represent a situation where a microscopically large, but macroscopically small domains absorb large quantities of deuterium in lattice defects. In order to observe hot spots, it is necessary to confine a large number of reacting particles within a small volume. Thus, there are certain locations where (i) the concentration of reactant(s) is very large, (ii) reactions are fast and (iii) they occur during early stages of co-deposition,

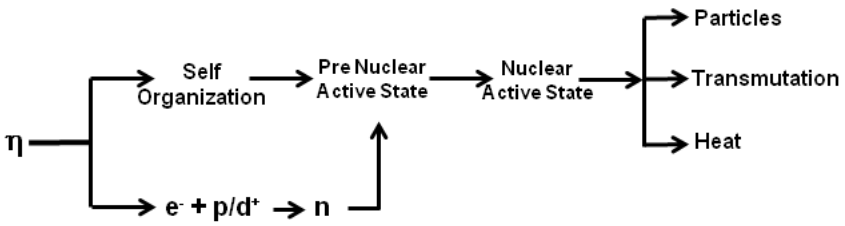

Figure 12. Sequence of events preceding initiation of nuclear activity.

cf. Fig. 5(a), (b).

(b) One characteristic feature is an increase in the piezoelectric sensor response to change in the solution temperature. As the solution temperature of 30°C approaches its boiling point, e.g. at 80°C, there is a significant change in the sensor response, cf. Fig. 5(a), (c). The several orders of magnitude in the sensor response indicates that an increase in solution temperature produces a significant increase in the hot spot's intensity, cf. Fig. 5(c) and Section 3.1.2.

4.2.2. *Probable*

(a) *Origin.* Nuclear reactions are not affected by solution temperatures. Consequently, an increase in the reaction intensity is because (i) domains contain a significantly larger number of active species, or (ii) the rate constants of the participating processes depend strongly on temperature. The reaction mechanism(s) is (are) not known but could be either chain reactions or "collapse" of aggregates as visualized by, e.g. Adamenko [17] who postulated *... evolution of self-organized and self-supported collapse of electronic-nuclear plasma of initial solid-state density under the action of coherent electronic driver up to a state of large non-stationary electronic-molecular clusters with density close to that of nuclear substance*.

(b) *Location*. The temperature difference measured at the front side, cf. Fig. 3(b) and that at the back-side, cf. [16], indicates that the reaction yielding excess power is located close to the electrode/solution contact surface.

4.3. Speculative

(a) *Size*. After viewing the recorded hot spots data Chubb [18] concluded that $10^4 - 10^9$ is the number of single events within a sphere having $r = 100$Å).

(b) *Safety of operation*. Catastrophic thermal run-a-ways occur very seldom in cells employing either solid or co-deposited cathodes which indicates that the heat source(s) is (are) located near the surface because, if the heat sources were throughout the bulk, then the positive feed-back would cause the temperature to rise exponentially, This model is supported by the increased frequency of thermal-run-a-ways when the cell placed in an external magnetic field, cf. [15].

4.4. Transmutation

4.4.1. *Certain*

(a) *Tritium production*. Tritium production via reaction $n + d^+ \rightarrow t^+$.

(b) *Tritium production*. Intermittent production, cf. Fig. 7(a) with occasional "massive" production, cf. Fig. 7(b).

(c) *Location*. Tritium production occurs within the interphase. This conclusion is based on the following: Tritium is absent in the bulk except when Al^{3+} is added to electrolyte which changes the interphase dynamics and effectively slows the desorption process, cf. [10].

(d) *Clusters composition*. Clusters of different composition of aggregates, yielding single or multiple new elements.

4.4.2. *Probable*

(a) *"Massive" production of tritium*. On several occasions tritium was produced at much higher rates, cf Fig.7(b). One possible mechanism is shown in Fig. 13 where electron capture by a deuteron produces two neutrons of which one reacts with deuteron yielding tritium. Assuming that electron capture by triton can occur, i.e. that $\mu(n) - \frac{1}{3}\mu(t^+) + \epsilon > 0$, three additional neutrons are produced which, by reacting with deuterons yield tritons.

(b) *Transmutation path*. The multiple new elements suggests that the stable new elements are the result of a series of reactions of the type $n + {}^{A}(X) \rightarrow {}^{A+1}(X) - [p^{+}, \alpha^{2+}, n, \gamma] \rightarrow {}^{A_1}_{Z_1}X$).

4.5. Particle emission

4.5.1. *Certain*

(a) *Location of nuclear reactions*. Nuclear reactions take place within the interphase region, cf. Fig. 11(a).
(b) *Type of emitted particles*. Emission of two or three particles having approximately the same mass and energy, cf. Fig. 11(c).

5. Reformulation

The reported reactions, processes, and conclusions are re-arranged to make them useful to experimenters. Evidently, (i) the bulk of activities, if not all, occur within the inhomogeneous region, the interphase, (ii) they are assembled in groups that identify their principal functions and (iii) they provide rationale for the choice of approach to discussion of the system's behavior.

5.1. Reactions/processes in Group I

Reactions within the first group are: (i) ionization of absorbed deuterium – $D \rightarrow D^{+} + e^{-}$, (ii) production of molecule-ions $D + D^{+} \rightarrow D_2^{+}$ [10,13], (iii) production of hybrid molecule-ion $n + D_2^{+} \rightarrow D^{+}T^{+}$, (iv) self-organization leading to the formation of clusters of aggregates $Pd^{*} + nD^{+} \rightarrow Pd^{*}\ldots D_n^{+}$, (v) production of neutrons $e^{-} + D^{+} \rightarrow 2n$. Reactions (i)–(iv) are typical chemical reactions while (v) is treated as a chemical reaction within the context of nuclear chemistry.

Function: The system is in the state of dynamic equilibrium established through the order–disorder activity at the contact surface. Its principal activity is to provide, via self-organization, reactants that produce excess power and new elements (transmutation). These are essentially chemical processes and could be either exo- or endothermic.

Useful information: Chemical processes are affected by the structure (morphology and formation of mobile lattice defects) of an interphase which, in turn, is affected by the cell current profile and external fields; Methods of non-equilibrium thermodynamics and non-linear chemical kinetics would have to be applied to fully describe the formation of domains associated with production of localized hot spots.

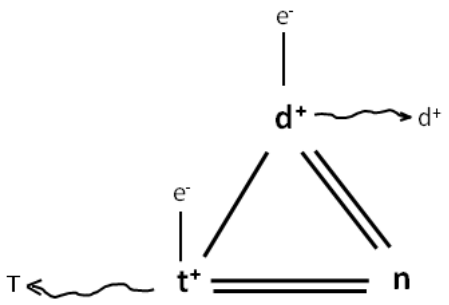

Figure 13. Coupled reactions leading to tritium production.

5.2. Reaction/processes in Group II

Reactants entering Group II are the products of self-organization. These reactants can interact with electrons (electron capture) or with neutrons. In either case, the dynamic equilibrium of stable aggregates generated by self-organization, is disturbed and the affected aggregates can either collapse or explode, depending on the type of interaction with environment. There is (i) self-organization, (ii) dense plasma corresponding to clusters interacting with the Pd lattice defects, e.g. mobile dislocations, (iii) "of solid-state density" corresponding to the action of the $F\Delta\Phi$ and asymmetric stress field and (iv) "coherent electronic driver. . . ," is equivalent to the formation of new structures on the "super-molecular" level.

Function: The reaction/processes in Group II provide the principal production of excess power via an unspecified set of nuclear processes, except for the electron capture by deuteron.

Useful information: There are many possible theories dealing with the nature of nuclear processes responsible for both production of excess enthalpy, transmutation, radiation and particle emission. So far as we were able to understand, none of the proposed theories meet all of the conditions stated by Chubb [18], namely: *for the model driven research, four conditions must be evaluated: (i) Is it applicable? (ii) Does it violate the second law of thermodynamics? (iii) Is it physically and mathematically complete? (iv) is it reducible to mathematical expressions that are useful to experimenters.*.

5.3. Reactions/processes in Group III

While the processes in Groups I and II can be treated in terms of chemical concepts, those in Group III involve system stabilization via the transition from unstable nuclei to stable ones by various decay processes. A very general picture is as follows: The first step, in stage I, is the production of neutrons *via* the electron capture process: $e^- + D^+ \rightarrow 2n$. Stage II is the seat for nuclear reaction of the type $n + \Sigma_Z^A X_i \rightarrow \Sigma_Z^{A+1} X_j$. Here the reaction product, entering stage III, is a set of new unstable nuclei ${}_Z^{A+1}X_j^*$ which undergo process of "stabilization" by fusion, fission, particle emission and electromagnetic radiation: $\Sigma_Z^{A+1} X_j^* - [p^+, \alpha^{2+}, n, \gamma, X] \rightarrow \Sigma_{Z+1}^{A_1} X_j$.

Function: Production of new elements via the various decay paths leading to the formation of stable elements such as Ca, Al, Si, etc.

Useful information: Although the transition from unstable to stable nuclei is highly exothermic, its contribution to the cell power output is minimal (basis - miss-match, amount of nuclear products and excess enthalpy He + transmutation).

6. Concluding Remarks

Nearly a quarter century ago, a new phenomenon – the room temperature nuclear reaction in a test tube – was disclosed by Fleischmann and Pons. Since this effect was discovered by two professors of chemistry – one would expect that methods and reasoning of chemistry would be helpful in the interpretation and further development of the understanding of this phenomenon. But such has not been the case. The chemical aspects were replaced by topics of interest to physicists. Theories based on specific assumptions elegantly executed, were followed by a search for the predicted behavior. Here, we propose another approach, that advocated by Born [19], who wrote *"My advice to those who wish to learn the art of scientific prophesy is not to rely on abstract reason, but to decipher the secret language of Nature from Nature's documents,the facts of experience."*

In following this advise we relied on two observations, viz. hot spots and production of new elements, and drew conclusions based on chemical reasoning. The conclusions reflect our current understanding of the F–P effect. We conclude this communication with a statement that a lot can be gained by examining the chemical aspects of the polarized Pd/d–D_2O system.

References

[1] M. Fleischmann, The present status of research in cold fusion, *ICCF 2*, p. 475.
[2] M. Fleischmann An overview of cold fusionb phenomena, *ICCF 1*, p. 344.
[3] S. Szpak, P.A. Mosier-Boss, M.Miles and M. Fleischmann, *Thermochim. Acta* **410** (2004) 101.
[4] M. Fleischmann, S. Pons and G. Preparata, *Il Nuovo Cimento* **107 A** (1994) 143.
[5] S. Szpak and P.A. Mosier-Boss, *Phys. Lett.* A **221** (1996) 141.
[6] L. Pauling, *The Nature of Chemical Bond* (Cornell University Press, Ithaca, New York, 1960).
[7] J. Behm, *J. Chem. Phys.* **78** (1983) 7496.
[8] G. Nicolis, *Self-organization in Non-equilibrium Systems* (Wiley Interscience, Hoboken, New Jersey, 1977).
[9] S. Szpak, P.A. Mosier-Boss, C. Young and F.E. Gordon, *Naturwissenschaften* **92** (2005) 384.
[10] S. Szpak, P.A. Mosier-Boss, R.D. Boss and J.J. Smith, *J. Elecroanal. Chem.* **373** (1994) 1.
[11] S. Szpak, P.A. Mosier-Boss, R.D. Boss and J.J. Smith, *Fusion Technol.* **33** (1998) 38.
[12] S. Szpak, P.A. Mosier-Boss, C. Young and F.E. Gordon, *Naturwissenschaften* **92** (2005) 384.
[13] P.A. Mosier-Boss, *Eur. Phys. J.* **40** (2007) 293.
[14] J.R. Hwews and C.J. Hwang, *J. Chem. Phys.* **54** (1971) 3263.
[15] S. Szpak and J. Dea, *J. Cond. Mat. Nucl. Sci.* **9** (2012) 21.
[16] S. Szpak, P.A. Mosier-Boss and J.J. Smith, *J. Electroanal. Chem.* **302** (1991) 255.
[17] S. Adamenko, *ICCF 10*, Cambridge, MA, 2003.
[18] S.R. Chubb, Private communication, 1994.
[19] S.R. Chubb, An overview of cold fusion theory, in thermal and nuclear aspects of the Pd/D_2O system, SPAWAR Technical report 1862, 2002.
[20] M. Born, *Experiment and Theory in Physics* (Dover, Mineola, New York, 1943).